

UCSF

UC San Francisco Electronic Theses and Dissertations

Title

Design and Characterization of Novel Thyroid Hormone Receptor Alpha Specific Ligands

Permalink

<https://escholarship.org/uc/item/4xq7175j>

Author

Ocasio, Cory Antonio

Publication Date

2007-07-24

Peer reviewed|Thesis/dissertation

**Design and Characterization of Novel Thyroid
Hormone Receptor Alpha Specific Ligands**

by

Cory Antonio Ocasio

DISSERTATION

Submitted in partial satisfaction of the requirements for the degree of

DOCTOR OF PHILOSOPHY

in

Chemistry and Chemical Biology

in the

GRADUATE DIVISION

of the

UNIVERSITY OF CALIFORNIA, SAN FRANCISCO

© 2007

by

Cory Antonio Ocasio

ACKNOWLEDGMENTS

I dedicate this thesis to my grandmother, Senora Marino, whose love and guidance was a constant source of motivation and support throughout my personal and professional/academic life. My grandmother instilled in me qualities that every student and researcher needs in order to meet the demands of a constantly changing and technically innovative career. This coupled with my own innate curiosity of the natural world is the perfect formula for fostering success in the multidisciplinary field of chemical biology. Additionally, she taught me to aim high, work hard, make goals, and never waiver when hardships arise. My drive to make her proud, impress her, and make her happy through my own success was a major source of inspiration in my academic and scientific pursuits. It is well known that academia is highly competitive and my grandmother prepared me for this as well. I would like to thank my grandmother for teaching me not only ambition, the value of a strong work ethic, and the importance of education and knowledge, but for teaching me the importance of family, friends, and being fair to everyone. I believe that positive reinforcement, sharing knowledge, and communication and honesty should never be sacrificed at the expense of personal gain; hence, I move forward eager to learn and share what I know and what I do not know in hopes of making advancements in medicine, drug discovery, and build upon the basic science of chemical biology.

This thesis is also dedicated to my mother, Diane Marino, sisters, Desiree and Brandina, my brother Emmanuel, and my niece Nyell. They are a constant

source of inspiration and support and I thank them for making my life a happier one. My partner Isaac Benjamin Atal made my time at UCSF much more enjoyable by providing me an outlet away from academia and science to explore the wonderful city of San Francisco, travel, and enjoy our lives together. His love and support is greatly appreciated and I thank him for his patience, encouragement, and for showing me how to enjoy and balance all aspects of my life; from work to recreation and the dark days of graduate school to the successful bright ones.

Chapter 3 is adapted with the permission of the American Chemical Society from the manuscript of: Ocasio, C.A. and Scanlan, T.S. (2006) Design and characterization of a thyroid hormone receptor alpha (α)-specific agonist. *ACS Chem. Biol.*, 1, pp. 585-593. I designed and synthesized CO23, the first potent TR α -specific agonist to show TR α -specificity *in vitro* and *in vivo*.

I would like to thank my colleagues and members of the UCSF community who have contributed to my development as a scientist. I received a great deal of guidance and advice these past six years and would not have had the same graduate experience without them. I am particularly grateful to Ha Nguyen, Mathew Hart, and Hikari Yoshihara who supported me not only in terms of technical training in synthetic chemistry and for laying the ground work for my project, but for their scientific discussions and challenging me to think about my project and thyroid hormone analogue design in a creative and multidisciplinary

manner. Edwin Tan, my classmate, friend, and colleague, has been an invaluable resource for the past six years who provided healthy competition which spurred me on to make more compounds and constructive criticism regarding my project and presentations. I am grateful to him for our brainstorming sessions, helpful intellectual discussions, and the camaraderie we shared during our time at UCSF.

I am grateful to members of the lab of R. Kiplin Guy and to Kip Guy himself for providing many resources. Also, I thank Leggy Arnold for helping me to address a major question that arose during my research. He provided invaluable coactivator peptides, SRC2-2 and SRC3-3, which were used to explore the mechanism behind CO23 specificity.

I owe a great debt of gratitude to mentors Kevan Shokat and Pam England whose support during my last year of graduate school was invaluable. I also thank the Shokat and England labs for their interesting discussions, their interest in my project, which was evident in their suggestions, friendship, and welcoming me into their labs. As a result of their magnanimity, I was able to pursue my research goals without interruption.

I would like to thank mentors Paul Ortiz de Montellano and Robert Fletterick who served on my orals committee. Their questions, suggestions, and encouragement were greatly appreciated. Holly Ingraham and Kevan Shokat,

who served on my orals and thesis committees, have been just as supportive and encouraging as well.

Susana Cuhna-Lima from the Baxter lab was very welcoming when I approached her to request training on how to perform an ^{125}I -T₃ competitive binding assay. She went above and beyond her role as a collaborator. With her help, I was able to successfully perform binding experiments against thyroid hormone receptors, thereby determining their binding affinities and subtype selectivity.

The Furlow lab at the University of California-Davis was extremely helpful in terms of sharing their expertise and knowledge of the complex molecular events that govern amphibian metamorphosis. Particularly, how different TR subtypes act separately and in unison to regulate different sets of morphological changes. I am extremely grateful to Professor J. David Furlow, Eric Neff, and Cindy Chen for their advice, guidance, and taking time to critically analyze the *Xenopus laevis* induced metamorphosis experiments.

I also have to give a special thanks to the bay area screening center. Prior to graduate school, I worked in industry and focused on the design of high-throughput assays for screening compounds against various enzymatic targets like amidotransferase. This experience allowed me to take advantage of the resources provided by the bay area screening center. In addition, I am extremely grateful to the UCSF community for sharing their resources and for maintaining

the center. I am particularly grateful to the Yamamoto lab for sharing their DNA Engine Opticon 2 real-time PCR machine, which allowed me to investigate CO23 induced gene expression in various amphibian tissues such as head, tail, and hind legs.

My graduate advisor Tom Scanlan was an exceptional mentor and I am in awe of his vast knowledge of endocrinology, molecular biology, chemistry, and physiology and his ability to integrate all of this knowledge for the purpose of understanding the “big picture,” as he would put it. These past years have been challenging and exciting in part due to the enthusiasm that I share with my advisor regarding drug design and selective thyroid hormone modulation. He allowed me to express my ideas and carry out most of them, because at the same time he taught me the importance of patience and to think through my ideas in order to cull the good ones from the ones that pose the greatest risk of being inconclusive. I am certain that without Professor Scanlan’s Nuclear Hormone Receptor acumen, synthetic astuteness, and encouraging and enthusiastic take on teaching and research, I would not have experienced the same level of success today.

Chris Olson is an ever present source of encouragement, guidance, support, and friendship as she is more than a program director; she genuinely cares about my progress and for me as a person. I thank her for taking time out of her extremely busy schedule to listen to me, providing a source of strength during the hard

times, and for being firm. I was taught that you know someone cares when they are firm, incessant, and driven to see that I excel. Even the best scientists need a little prodding, and her presence and friendship was reassuring and invaluable to my graduate experience.

Valerie Ohman has been an incredibly helpful and kind figure throughout my graduate tenure. She played an important role in helping me receive funding from UCSF during my first year of graduate school and is an incredible assistant to Kevan Shokat. I appreciate the time she took out of her busy schedule to help me schedule meetings with Kevan, provide support in the form of ordering research supplies and taking care of many administrative matters, and taking time out of her day to have a friendly conversation.

Lastly, I would like to thank the following for their financial support: UCSF for awarding me the Eugene Cota-Robles fellowship which funded my graduate education for the first two years, the Ford Foundation for awarding me a three-year fellowship, and to the NIH for providing supplemental funding as well (R01-DK52798).

ABSTRACT

Design and Characterization of Novel Thyroid Hormone Receptor Alpha Specific Ligands

Cory Antonio Ocasio

Thyroid hormone orchestrates a multifarious set of physiological activities ranging from fetal, brain, and skeletal maturation to improving vascular tone and controlling cardiac output. Thyroid hormone elicits its effects by binding to the ligand binding domain of the thyroid hormone receptor (TR) for which there are two subtypes for two isoforms: TR α 1, TR α 2, TR β 1, and TR β 2. Although TR isoforms, with the exception of TR β 2 which is mainly expressed in the pituitary, are ubiquitously expressed, these isoforms are expressed in different ratios in different tissues giving rise to tissue-specific isoform action. Selective thyroid hormone analogues, or selective thyromimetics, that discriminate between these two subtypes would serve as useful chemical tools to gain or refine our understanding of the physiological effects of thyroid hormone. These compounds may also prove useful in the clinic as known thyromimetics (*i.e.* 3,5-diiodothyropropionic acid and GC-1) show promise in treating cardiac related diseases and metabolic disorders. One way to generate selective thyromimetics with unique pharmacological profiles is to synthesize a small panel of compounds by employing a bioisosteric replacement strategy. This method entails derivatizing one region of the thyronine backbone, the C₁ region, by incorporation of various heterocycles or carbocycles. This strategy led to the production of a small panel of ligands which were screened in ¹²⁵I-T₃ competitive binding and transactivation assays. After this screen, the TR α -specific ligand CO22 was

identified; however, it demonstrated poor binding and potency. Replacing the inner-ring methyl groups of CO22 with iodides led to CO23, the first potent thyromimetic to show TR α -specificity *in vitro* and *in vivo*. CO23 showed specificity in TR α -mediated transcription in U2OS and HeLa cells and caused *Xenopus laevis* tadpoles to experience more extensive and rapid hind leg growth, less larval tissue resorption, greater induction of TR α early genes, and less induction of TR β early and late genes. It was surmised that the imidazolidinedione moiety of the inner-ring confers TR α -specificity; therefore, to engender ligands with improved specificity the 3' outer-ring position was derivatized. This led to several analogues with less potency than CO23, but with a gain in specificity of up to 2-fold.

TABLE OF CONTENTS

List of Figures.....	xvii
List of Tables.....	xix
List of Schemes.....	xx

Chapter 1: Introduction to Thyroid Hormone Endocrinology and the Molecular Basis of Thyroid Hormone Action

1.1 Overview.....	2
1.2 Thyroid Hormone Endocrinology.....	3
1.2.1 The Discovery of the Thyroid Gland.....	3
1.2.2 The Discovery of Thyroid Hormone.....	3
1.2.3 Thyroid Hormone Biosynthesis.....	7
1.2.4 Thyroid Hormone Metabolism.....	9
1.2.4.1 Selenodeiodinases.....	9
1.2.4.1.1 Regulation of Thyroid Hormone by Deiodinases.....	10
1.2.4.1.2 Deiodination of Thyroid Hormone.....	12
1.2.4.2 Thyronamines.....	14
1.2.5 The Hypothalamic-Pituitary-Thyroid Axis.....	15
1.2.6 Thyroid Hormone Physiology.....	16
1.2.6.1 Target Genes in the Heart and Physiologic Outcome.....	17
1.2.6.2 Target Genes in the Liver and Physiologic Outcome.....	19
1.2.6.3 Other Target Genes and Their Physiologic Outcome.....	20

1.2.6.3.1	Pituitary.....	20
1.2.6.3.2	Brain.....	21
1.2.6.3.3	Bone.....	22
1.2.7	Pathophysiology of Thyroid Hormone Related Diseases.....	24
1.2.7.1	Hyperthyroidism.....	24
1.2.7.2	Hypothyroidism.....	25
1.3	Molecular Basis of Thyroid Hormone Action.....	26
1.3.1	Thyroid Hormone Transport and Uptake.....	26
1.3.2	Thyroid Hormone Receptor Mediated Transcription.....	28
1.3.2.1	TR Functional Domains.....	29
1.3.2.2	Structure of the TR Ligand Binding Domain.....	31
1.3.2.3	Molecular Basis of TR Mediated Transcription.....	32
1.3.2.3.1	TR and 9- <i>cis</i> -Retinoic Acid Receptor (RXR) Dimerization.....	33
1.3.2.3.2	TR Response Elements.....	34
1.3.2.3.3	TR Coregulators.....	35
1.4	Nongenomic Effects.....	37
1.5	References.....	39
Chapter 2: Rationale and Bioisosteric Replacement Strategy for the Development of Thyroid Hormone Analogues with Novel Pharmacology		
2.1	Overview.....	50
2.2	Tissue-Specific TR Isoform Action.....	51

2.2.1	Murine “Knockout/Knock-In” Studies of TR.....	52
2.2.2	Selective Thyromimetics as Probes of TR Biology.....	54
2.2.2.1	TR β - and Liver-Selective Thyromimetics.....	55
2.2.2.1.1	Prototypical Thyromimetics: Triac and 3,5-Diiodothyronine.....	56
2.2.2.1.2	SFK-94901.....	56
2.2.2.1.3	Oxamic and Malonamic Acid Derivatives.....	57
2.2.2.1.4	Azauracil and Bicyclic Inner- and Outer-Ring Derivatives.....	58
2.2.2.1.5	Thyromimetics with A Novel Phenyl-Naphthylene Core.....	60
2.2.2.1.6	GC-1 and KB-141.....	61
2.2.2.1.7	Second Generation TR β -Selective Thyromimetics.....	63
2.2.2.1.8	TR β -Selective Antagonists and Indirect Antagonists.....	63
2.2.2.2	Cardiac- and TR α -Selective Thyromimetics.....	66
2.2.2.2.1	DITPA: A Thyromimetic with Cardiac-Selective Effects.....	66
2.2.2.2.2	Dronedarone.....	68
2.3	Rationale Behind Modifying the C ₁ Moiety: Bioisosteric Replacement.....	69
2.4	Synthesis of Thyromimetics with Heterocycles or Carbocycles in the C ₁ Region (CO1 – CO22).....	75

2.5	<i>In vitro</i> Analysis of Selected C ₁ Derivatized Thyromimetics.....	80
2.5.1	¹²⁵ I-T ₃ Competitive Binding Analysis.....	83
2.5.2	Transactivation Analysis.....	85
2.6	Conclusion.....	88
2.7	References.....	89

Chapter 3: Design and Characterization of CO23 - The First Thyromimetic with TR α -Specific Effects *In vitro* and *In vivo*

3.1	Overview.....	102
3.2	Design and Synthesis of CO23.....	103
3.2.1	Replacement of Inner-Ring Methyl Groups with Iodides.....	104
3.2.2	Synthesis of CO23.....	105
3.3	<i>In vitro</i> Analysis of CO23: Binding and Transactivation Against Human and <i>Xenopus</i> TRs.....	106
3.4	A High-Throughput <i>In vitro</i> Binding Assay for Recruitment of Coregulator Peptides.....	110
3.5	<i>In vivo</i> Analysis of CO23.....	112
3.5.1	<i>Xenopus laevis</i> Tadpole Metamorphosis.....	112
3.5.1.1	Amphibian Metamorphosis as a Model System for A TR α -Specific Thyromimetic.....	113
3.5.1.2	Effects of CO23 on Amphibian Metamorphosis.....	114
3.5.1.3	Dose Response and Inhibition of CO23-Induced Metamorphosis.....	116

3.5.2	Hind Leg Growth.....	116
3.5.2.1	Four-Day Time Course and Hind Leg Growth.....	118
3.5.2.2	Quantification of Hind Leg Growth.....	118
3.5.3	Temporal Separation of TR Subtype Mediated Effects on Morphogenesis.....	119
3.5.4	Quantitative Real-Time PCR Analysis.....	121
3.6	Conclusion.....	123
3.7	References.....	125

Chapter 4: Novel CO₂₃ Analogues with Enhanced TR α -Specificity

4.1	Overview.....	129
4.2	Rationale Behind Expanding the SAR Data for Inner- and Outer-Ring CO ₂₃ Derivatives.....	130
4.3	Synthesis of CO ₂₃ Analogues.....	132
4.4	<i>In vitro</i> Characterization of CO ₂₃ Analogues.....	135
4.5	<i>In vivo</i> Analysis of CO ₂₄	139
4.5.1	Effects of CO ₂₄ on Amphibian Metamorphosis.....	139
4.5.2	Dose Response of CO ₂₄ Induced Metamorphosis.....	140
4.6	Conclusion and Future Directions.....	141
4.7	References.....	144

Appendix A: Experimental Procedures

A.1	Synthetic Organic Chemistry Procedures.....	147
-----	---	-----

A.1.1	General Chemical Procedures, Chapter 2.....	148
A.1.2	General Chemical Procedures, Chapter 3.....	166
A.1.3	General Chemical Procedures, Chapter 4.....	172
A.2	Preparation of Chemicals for Use <i>In vitro</i> or <i>In vivo</i>	181
A.3	¹²⁵ I-T ₃ Competitive Binding Assay.....	181
A.4	TR Transactivation Assay.....	181
A.5	High-Throughput <i>In vitro</i> Binding Assay for TR-Coregulator Interactions.....	183
A.6	<i>Xenopus Laevis</i> Induced Metamorphosis Procedures.....	184
A.6.1	General <i>X. laevis</i> Tadpole Procedures, Aquaculture and Euthanasia.....	184
A.6.2	Induced Metamorphosis Experiments.....	185
A.6.3	Quantification of Hind Leg Development.....	186
A.6.4	Temporal Separation of TR Subtype Mediated Effects on Morphogenesis.....	187
A.6.4	Quantitative Real-Time PCR.....	187
A.7	References.....	189

Appendix B: ¹H and ¹³C Nuclear Magnetic Resonance (NMR)

Characterization of Compounds

B.1	NMR Spectra of Compounds from Chapter 2.....	192
B.2	NMR Spectra of Compounds from Chapter 3.....	219
B.3	NMR Spectra of Compounds from Chapter 4.....	222

List of Figures

- 1.1 Gross anatomy of the human thyroid gland (anterior view)
- 1.2 3,5,3',5'-tetraiodo-L-thyronine (thyroxine/T₄) and 3,5,3'-triiodo-L-thyronine (T₃)
- 1.3 Biosynthesis of thyroid hormone
- 1.4 Thiocarbamide drugs
- 1.5 The hypothalamic-pituitary-thyroid axis
- 1.6 Thyroid hormone mechanism of action
- 1.7 Nuclear hormone receptor ligands
- 1.8 Modular architecture of thyroid hormone receptor isoforms
- 1.9 Structure of the TR ligand binding domain
- 1.10 Heterodimerization of TR and RXR on a DR4 TRE
- 2.1 Structures of Triac and 3,5-diiodothyronine
- 2.2 Structures of SFK-94901, DIMIT, and oxamic and malonamic acid derivatives
- 2.3 Structures of azauracil and bicyclic inner- and outer-ring analogues
- 2.4 Structure of thyromimetics with a phenyl-naphthylene core
- 2.5 GC-1, KB-141, and a second generation of TR β -selective thyromimetics
- 2.6 NH-3, prototypical TR β -selective antagonists DIBRT and GC-14, and an indirect antagonist
- 2.7 Structures of DITPA, Dronedarone, and Debutyldronedarone
- 2.8 Bioisosteric replacement of the alanine side chain with heterocycles or carbocycles
- 2.9 Structure-activity data for the TR ligand binding pocket
- 2.10 Sequence Alignment of TR α and TR β
- 2.11 Structural alignment of TR α (LBD):Triac and TR β (LBD):Triac
- 2.12 Crystal structure of the hTR β (LBD) complexed with GC-1
- 2.13 Diagram showing T₃-hormone interactions in the TR ligand binding pocket
- 2.14 Target thyroid hormone analogues with and without a linker
- 2.15 Dual-luciferase transactivation assay and dose-response curves
- 2.16 Transactivation data for CO8 and CO12
- 2.17 Transactivation data for CO10 and CO14
- 3.1 Structures of CO22 and CO23
- 3.2 *In vitro* evaluation of CO22 and CO23
- 3.3 CO23 transactivation against *Xenopus* TRs in U2OS cells
- 3.4 A high-throughput *in vitro* binding assay for recruitment of coactivator peptide SRC2-2
- 3.5 *Xenopus laevis* tadpole metamorphosis
- 3.6 Effects of CO23 on Amphibian Metamorphosis
- 3.7 Figure 3.6 Induction of metamorphosis by CO23 in a dose-dependent manner and inhibition of CO23 induced metamorphosis with NH-3
- 3.8 Progression of Induced Metamorphosis Over Four Days
- 3.9 Quantification of hind leg development

- 3.10 Temporal separation of TR subtype-mediated metamorphic effects
- 3.11 Quantitative real-time PCR of late and early TR-responsive genes in developing *X. laevis* tadpoles
 - 4.1 Optimization of the CO23 scaffold by derivatization of the 3' position
 - 4.2 Evidence that the 3' position tolerates derivatization
 - 4.3 Transactivation analysis of CO24, CO26, and CO32 in HeLa cells
 - 4.4 Transactivation analysis of CO24 in U2OS cells against xTRs
 - 4.5 *In vivo* analysis of CO24
 - 4.6 Induction of metamorphosis by CO24 in a dose-dependent manner

List of Tables

- 1.1 Target genes of thyroid hormone and physiologic outcome
- 2.1 TR knockout/knock-in mice phenotypes
- 2.2 Reaction conditions for Suzuki couplings
- 2.3 ^{125}I -T₃ competitive binding data: Screen of CO1 – CO17
- 3.1 Binding affinity and potency of CO22 and CO23
- 4.1 Binding affinity and potency of CO23 analogues

List of Schemes

- 1.1 Deiodinative pathway showing all possible thyroxine metabolites
- 1.2 Conversion of thyronines to thyronamines
- 2.1 Synthesis of ligands without a linker
- 2.2 Synthesis of ligands with an ethylene or ethyl linker
- 2.3 Synthesis of ligands with a single carbon linker
- 3.1 Synthesis of CO₂₃
- 4.1 Synthesis of boronic acids
- 4.2 Synthesis of ligands CO₂₄ and CO₂₆-CO₃₂

CHAPTER ONE

Introduction to Thyroid Hormone Endocrinology and the Molecular Mechanisms of Thyroid Hormone Action

1.1 Overview

The principal active form of thyroid hormone, 3,5,3'-triiodo-L-thyronine (T_3), is a classic endocrine signaling hormone that plays an important role in human physiology. The following introduction will highlight some important historical events in the discovery of thyroid hormone as well as describe its biosynthesis, metabolism and regulatory mechanisms, physiologic activity, pathophysiology, and the molecular level basis of its activity. The effects of T_3 range from promoting normal growth and development to regulating homeostatic processes such as energy and heat production. Thyroid hormone also plays an important role in maintaining healthy cardiac performance and lipid inventory. Thyroid hormone is actively transported into cells and exerts its effects by binding to the ligand binding domain of its cognate receptor, the thyroid hormone receptor (TR). The detailed molecular events behind TR-mediated gene expression are described as well as TR structure-function relationships. This information assists in dissecting the roles of TR subtypes, TR α and TR β , which is of critical importance as different TR subtypes confer tissue-specific action by regulating different sets of target genes, their unequal distribution in different tissues, or in other more esoteric ways such as tissue-specific uptake. Integrating TR molecular and structural biology and genetics with the design of thyromimetics having unique pharmacologic profiles provides an interdisciplinary approach to understanding TR biology and possibly correcting TR dysregulation across its full physiologic spectrum.

1.2 Thyroid Hormone Endocrinology

1.2.1 The Discovery of the Thyroid Gland

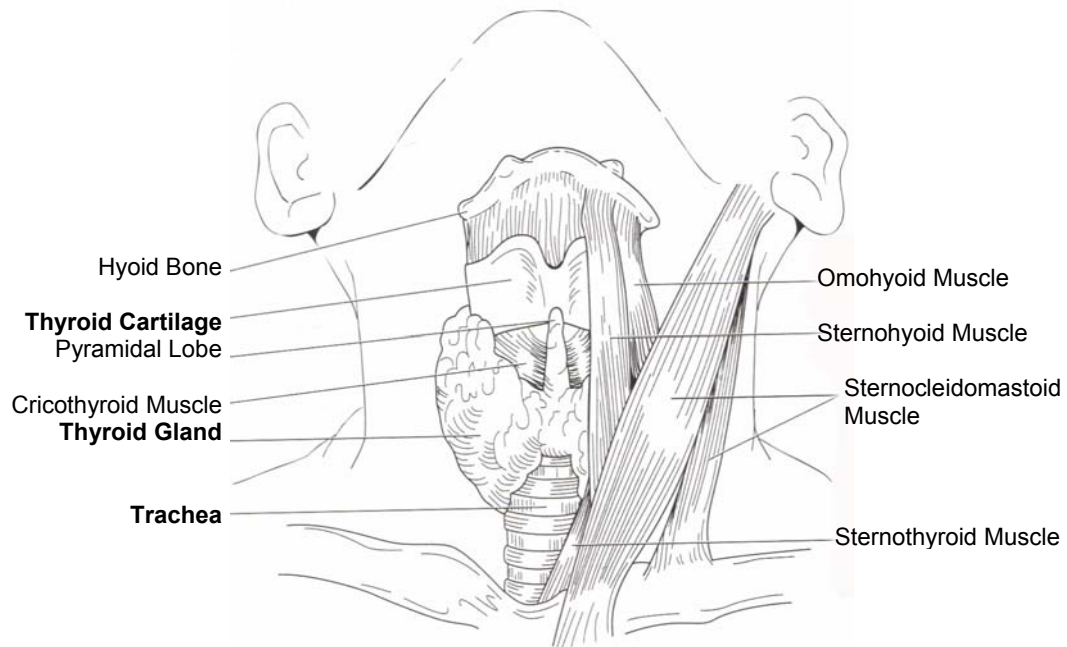
The thyroid gland was first described by Galen (130 – 200 A.D.) of Pergamum, a prominent ancient Greek physician, but was not given a name until Wharton (1656) named it “thyroid.” The name “thyroid,” Greek for shield-shaped, was given not because of the shape of the thyroid itself, but due to the shape of the nearby thyroid cartilage (1,2). The thyroid gland (Fig. 1.1) originates at the base of the pharynx and grows downward anterior to the trachea, bifurcates forming a series of cellular cords, and these cords develop into tiny balls or follicles that give rise to two lateral lobes connected by a thin isthmus (3). The sole purpose of the thyroid gland is to synthesize and secrete thyroid hormone, and thus makes it the largest organ in the human body that is specialized for endocrine function (3).

1.2.2 The Discovery of Thyroid Hormone

The discovery of thyroid hormone as the active biomolecule secreted by the thyroid gland took years of searching and was not without controversy. Not surprisingly, thyroid-linked disorders such as cretinism, goiter, and thyrotoxicosis (or hyperthyroidism) and hypothyroidism were crucial to solving this mystery.

The first observations of cretinism were made by Alpine travelers in the

Figure 1.1 Gross anatomy of the human thyroid gland (anterior view)



Reproduced with permission of The McGraw-Hill Companies: Greenspan, F.S. (2001) The Thyroid Gland. In *Basic and Clinical Endocrinology* (Greenspan, F.S. and Gardner, D.G., Eds.) 6th ed., pp. 202, Lange Medical Books/McGraw-Hill, New York.

thirteenth century; however, the first clinical descriptions were made in the sixteenth century when Paracelsus (circa 1527) and Platter (in 1562) made the connection between goiter and cretinism (4).

Until the nineteenth century, medical theories of disease causation were humorally based or attributed to an imbalance of the four humors: blood, phlegm, bile, and black bile. In fact, some thought goiter to be caused by excessive phlegm. Despite this misconception, numerous empiric remedies for goiter were proposed and usually consisted of complex mixtures of seaweed and marine sponge. These aquatic substances were well known in Europe and used to treat

goiter a thousand years earlier in China. It wasn't until 1812 that Courtois discovered iodine in the residue of burnt seaweed. In 1820, Coindet, an Edinburgh-trained physician working among goitrous patients in Geneva, Switzerland, treated goiter patients with iodine mainly in the form of the potassium salt. Although the treatment was successful in diminishing the size of the goiter, it was likely abused by many and this revealed major toxic side-effects. As a result, this treatment fell into disfavor; however, Coindet's work led to a shift in treating illness; from empiric, folk medicine to the rational treatment of a defined illness with a specific substance (4).

Unbeknownst to Coindet, his work illuminated another thyroid-linked disorder; iodine-induced thyrotoxicosis. However, it took several decades to recognize and classify this disorder. Coindet and Parry both saw signs of rapid heartbeat and goiter, and Parry also described exophthalmos. However, the term thyrotoxicosis was irrelevant until the 1890's and early 1900's, because it was not until this time that it was first realized that an excessive amount of some thyroid related substance could cause this disorder. At first the disorder was thought to be cardiac related, but Charcot emphasized the neurological nature of the disease (excess nervousness in patients) causing a more neurologic hypothesis. In the 1880's, surgeons reported a disappearance in nervousness of goiterectomized patients, and in the 1890's, it was observed that excess thyroid extract recapitulated the nervousness experienced by patients with the disorder; hence, the name thyrotoxicosis (4).

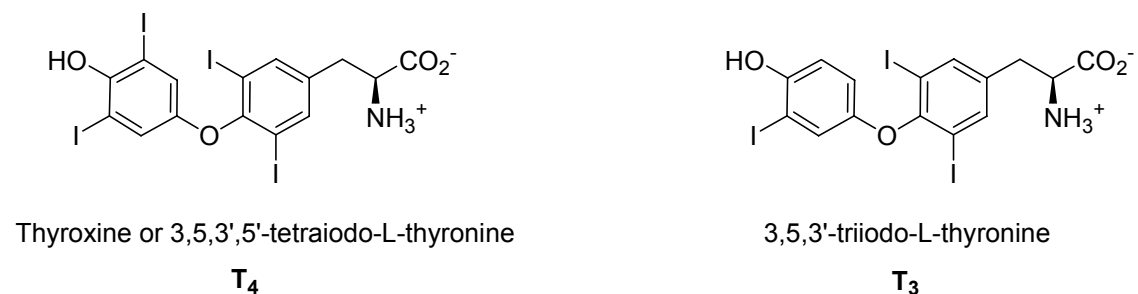
Hypothyroidism took even longer to recognize, and was initially named myxoedema due to patients' swollen skin and excess mucin. Also, the ability to safely remove the thyroid gland from thyrotoxic patients or goiters from patients who were not nervous or overactive brought to light a disastrous outcome: the patients lived, but became puffy-faced and slow of mind as a result of thyroid hormone deficiency.

Finally, due to the observation of Felix Semon that thyroidectomized Swiss patients seemed similar to English patients with myxedema, the Clinical Society of London formed a committee to investigate the link between these two types of patients. In 1888, this classic report showed that cretinism, myxedema, and the post-thyroidectomy changes all were due to the loss of function of the thyroid gland (4). This prompted a vigorous search for the active substance which was assisted in great part by Baumann who discovered that iodine existed in the thyroid gland. On Christmas day in 1914, Kendall, using iodine as a marker for the isolation of the active substance, succeeded in isolating bioactive crystalline material and named it thyroxin. In 1927, to Kendall's dismay, Harington and Barger found the correct structure of this material, noting that it has four not three iodine atoms, synthesized it, and added an 'e' to the name calling it thyroxine (Fig. 1.2) (4,5).

Kendall's extracted thyroxine was patented and commercially licensed, yet was very expensive and not as effective as desiccated thyroid. In 1949, thyroxine

was being synthesized in high yield in the form sodium L-thyroxine, improving its bioavailability compared to the free acid version originally synthesized. Years later, another more active form of thyroid hormone was found nearly simultaneously by two groups: triiodothyronine (Fig. 1.2) was discovered by Pitt-Rivers, an associate of Harington, and her postdoctoral fellow Gross; and by a group in Paris that included Roche, Lissitsky, and Michel (4).

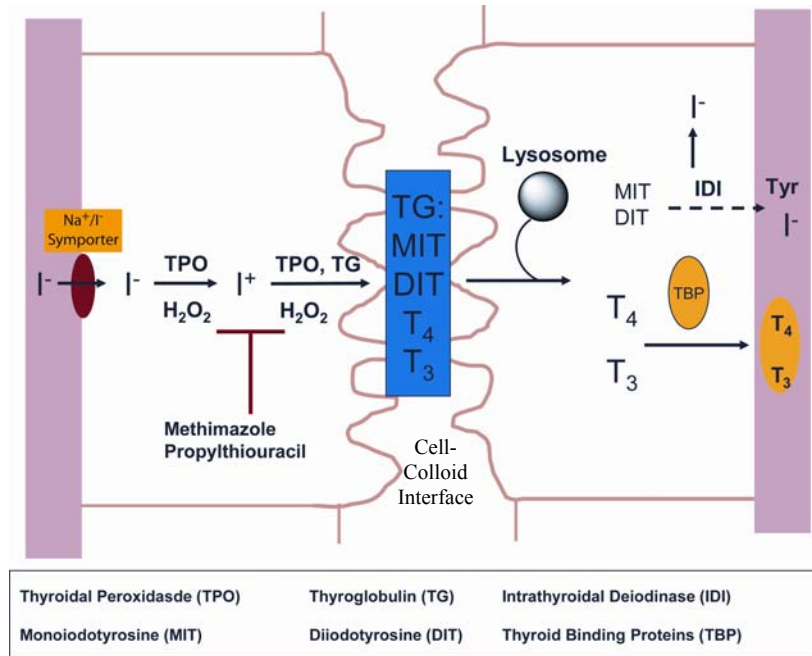
Figure 1.2 3,5,3',5'-tetraiodo-L-thyronine (Thyroxine/T₄) and 3,5,3'-triiodo-L-thyronine (T₃)



1.2.3 Thyroid Hormone Biosynthesis

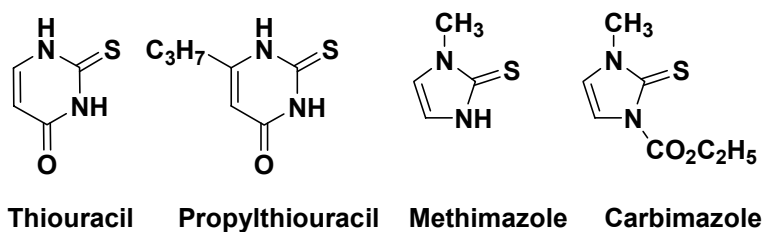
The biosynthesis of the thyroid hormone starts off with the active transport of iodide across the basement membrane of the thyroid cell by the membrane bound Na⁺/I⁻ symporter. This and activation of Na⁺-K⁺ ATPase drives the transport process and allows the thyroid gland to maintain iodide levels at a concentration 30-40 times that in plasma. Thyroidal peroxidase catalyzes the oxidation of iodide by hydrogen peroxide to its active form, I⁺. At the cell-colloid

Figure 1.3 Biosynthesis of Thyroid Hormone



interface, thyroidal peroxidase also drives the organification of I⁺ by incorporating active iodine into tyrosyl residues within thyroglobulin (Fig 1.3). Coupling of mono- and diiodinated tyrosyl residues (MIT and DIT) by thyroidal peroxidase leads to a mixture of 3,5,3',5'-tetraiodo-L-thyronine (T₄) and 3,5,3'-triiodo-L-thyronine (T₃, Fig. 1.2). This process can be impeded by thiocarbamide drugs that inhibit thyroidal peroxidase, and thus are utilized to manage hyperthyroidism (Fig. 1.4). Lysosomal processing of colloid vesicles in the cytoplasm of follicular cells leads to proteolysis of thyroglobulin and the release of T₄, T₃, MIT, and DIT. About 90% of secreted thyroid hormone is in the pro-hormone state, T₄, and after secretion both T₄ and T₃ are taken up by carrier proteins such as thyroxine-

Fig 1.4 Thiocarbamide drugs



binding globulin (TBG), prealbumin or transthyretin (TTR), and albumin, and then transported via the circulatory system. MIT and DIT are processed by intrathyroidal deiodinase in order to recycle iodide within the gland (3).

1.2.4 Thyroid Hormone Metabolism

Thyroid hormone may be metabolized in a number of ways. One way is by the deiodination of the inner- and outer-rings by deiodinases (Scheme 1.1, 6).

However, it has been proposed that the ubiquitous enzyme L-amino acid decarboxylase (AADC) may act on thyroid hormone, giving rise to thyronamines (Scheme 1.2, 3,7-9).

1.2.4.1 Selenodeiodinases

The discovery of T₃ by Gross and Pitt-Rivers raised the notion that deiodination of the 5' position of the outer-ring is the first step in activation of the thyroid pro-hormone T₄ (4,6). Following the discovery of T₃, two decades worth of work went

into documenting the presence of two different enzyme activities: that of types 1 and 2 outer-ring deiodinase (D1 and D2) (10-13). Also, an inner-ring deiodinase (D3) was discovered and can inactivate both T_4 and T_3 (14). Inhibition of D1 by propylthiouracil (PTU) was instrumental in distinguishing D1 from D2 as only D1 is sensitive to PTU, and subsequent cloning of all deiodinases revealed in all species cloned to date a selenocysteine (Sec) codon, UGA, in the region encoding the highly conserved active center (6).

1.2.4.1.1 Regulation of Thyroid Hormone by Deiodinases

The D1 monomer is a type 1 integral membrane protein, but *in situ* exists as a homodimer of about 50-60 KDa localized to the plasma membrane (15). D1 is broadly expressed in humans with notable expression in liver, kidney, thyroid, and the pituitary; it is absent in the central nervous system. Unlike other deiodinases, D1 can deiodinate the inner- and outer-rings with equal efficiency (16). D1 also undergoes substrate induced inactivation and has a half-life of about 12 hours (6).

D2 is a strict outer-ring deiodinase of 31 KDa and is an endoplasmic reticulum (ER) associated integral membrane protein localized intracellularly to the perinuclear space (6,13,17). Like D1, D2 is expressed in most tissues in humans, particularly the thyroid, heart, brain, spinal cord, skeletal muscle, and placenta, but present in low abundance in the kidney and pancreas. Another

similarity between D1 and D2 is that D2 also undergoes substrate induced inactivation. On the other hand, the half-life of D2, about 45 minutes, is significantly decreased by ER associated degradation, a ubiquitin-proteasome pathway dependent process (17).

This difference in subcellular localization allows D2 containing organs to regulate their TR occupancy independent of plasma T_3 levels. For example, in most tissues of euthyroid rats about 50% of TRs are ligand occupied; however, in tissue that express D2, a substantially higher fraction of TRs are ligand occupied: from 75% in brown adipose tissue to 97% in cerebral cortex. This extra T_3 is produced from plasma T_4 and has direct access to the nucleus, whereas D1 derived T_3 must first be exported out of the cell.

The ability to generate local hyperthyroidism is extremely important and necessary in times of duress. Small mammals such as mice rely on brown adipose tissue (BAT) to produce heat when the ambient temperature drops below a certain threshold, a process known as adaptive thermogenesis. This stimulates the sympathetic nervous system which induces uncoupling protein 1 (UCP1), and thus generates heat. Hypothyroid mice are unable to mount this response as norepinephrine and T_3 work synergistically to induce UCP1. The reason for this is that this synergism requires saturation of nuclear TRs. Under euthyroid conditions, norepinephrine via a cAMP response element induces BAT D2, and thus generates high levels of T_3 in the nucleus. Under hypothyroid

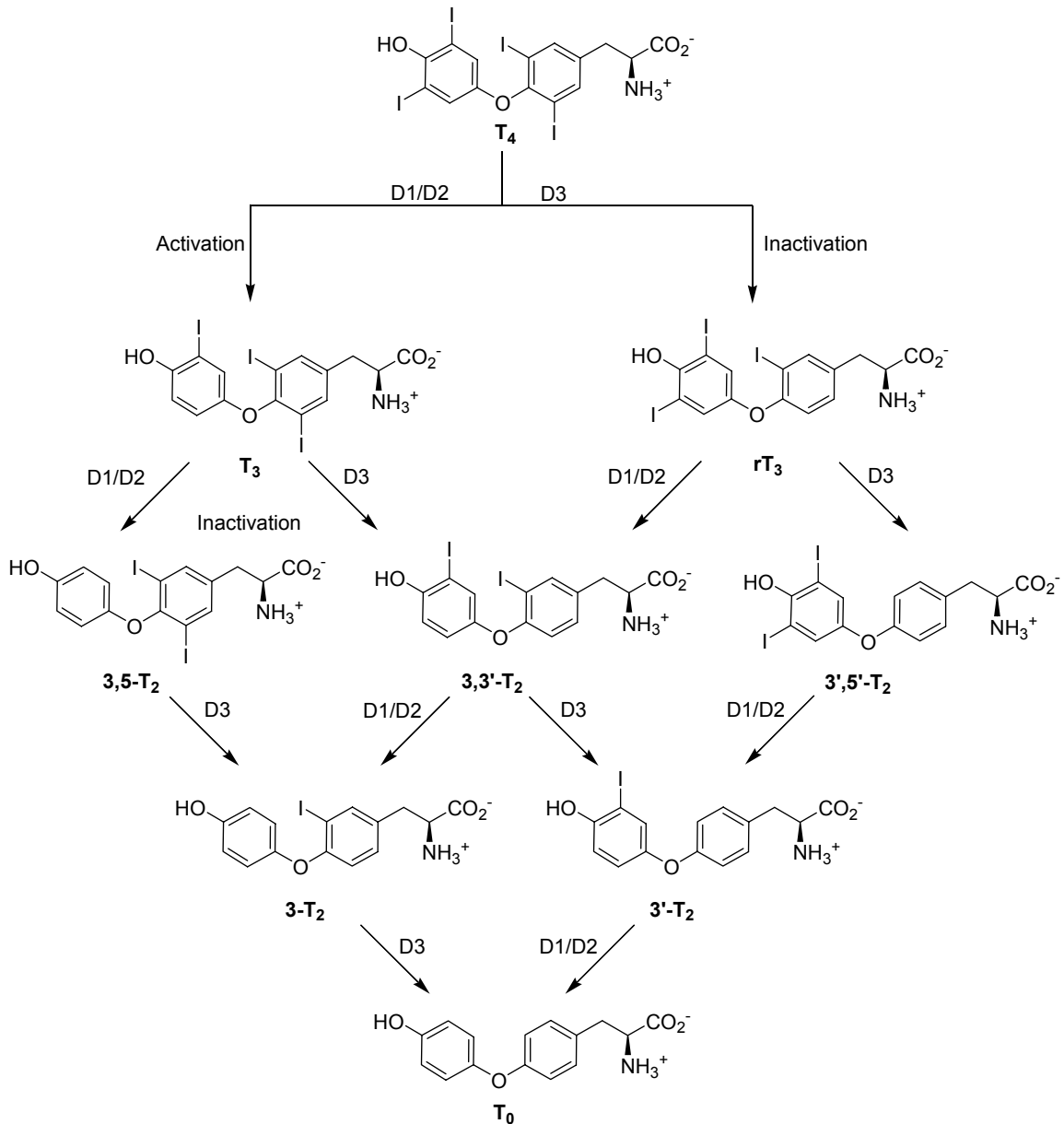
conditions, there is not enough T_4 to achieve this and the animal does not elicit an adequate BAT response (17).

The induction of D2 or any means to locally generate D2 is a means to independently regulate T_3 levels without affecting circulating levels of T_3 . Recently, it has been shown that ubiquitinated D2 circumvents proteasomal processing by interacting with von Hippel-Lindau protein-interacting deubiquitinating enzymes- 1 and -2 (VDU1 and VDU2). These interactions prolong the D2 half-life and rejuvenate enzyme activity. Therefore, VDU regulation of D2 provides another regulatory mechanism for local and peripheral thyroid hormone action (17).

1.2.4.1.2 Deiodination of Thyroid Hormone

Peripherally, T_4 is converted to its active form T_3 by types 1 and 2 deiodinase and this transformation provides the majority of active thyroid hormone in plasma (Scheme 1.1, 3,6). The biological activity of thyroid hormone is highly influenced by the position of iodine atoms on the inner- and outer-rings: positions 3, 5, 3', and 5'. Deiodination of the outer-ring yields T_3 which is about 3-8 times more potent than T_4 . On the other hand, deiodination of the inner-ring leads to reverse

Scheme 1.1 Deiodinative pathway showing all possible thyroxine metabolites



T_3 or rT_3 , which is biologically inert. About equal amounts of T_3 and rT_3 are generated from T_4 in circulation; however, under certain conditions like

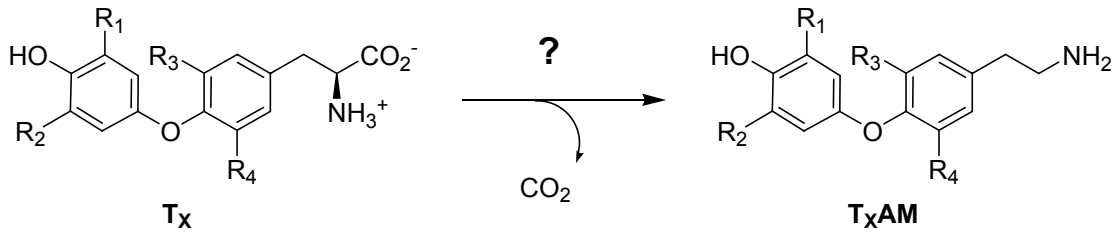
carbohydrate restriction and chronic illness, rT_3 is produced from T_4 to a greater extent in order to slow metabolic activity and conserve cellular resources. In periods of iodine deficiency, T_4 may be deiodinated by outer-ring deiodinase to T_3 in the thyroid in order to increase the efficiency of thyroid hormone action by secreting a mixture with an increased T_3 to T_4 ratio. Ultimately, deiodination of thyroxine and its metabolites can yield every possible combination of 3, 5, 3', and 5' iodinated thyronines including thyronine devoid of iodine (Scheme 1.1). The physiological significance of these metabolites is still under investigation. Other enzymatic transformation that inactive thyroid hormone are by deamination, decarboxylation, and conjugation to glucuronic acid and sulfate in the liver followed by secretion into bile (3,18).

1.2.4.2 Thyronamines

A second type of thyroid hormone metabolite that has been recently discovered is the thyronamine which is simply a decarboxylated thyronine (Scheme 1.2). Two thyronamines, T_0AM and T_1AM are present in a wide variety of mammalian tissues including the brain and in circulation (9). One of these metabolites, 3-iodothyronamine, has been shown to exert its effects in a way unlike thyroid hormone, which binds in the nucleus to its cognate receptor, by acting on the G-protein coupled trace amine receptor (7). Recently, the non-transcriptional role of thyronamines has been expanded as some act as specific dopamine and

norepinephrine reuptake inhibitors. Thyronamines also inhibit the transport of monoamines into synaptic vesicles (9).

Scheme 1.2 Conversion of thyronines to thyronamines

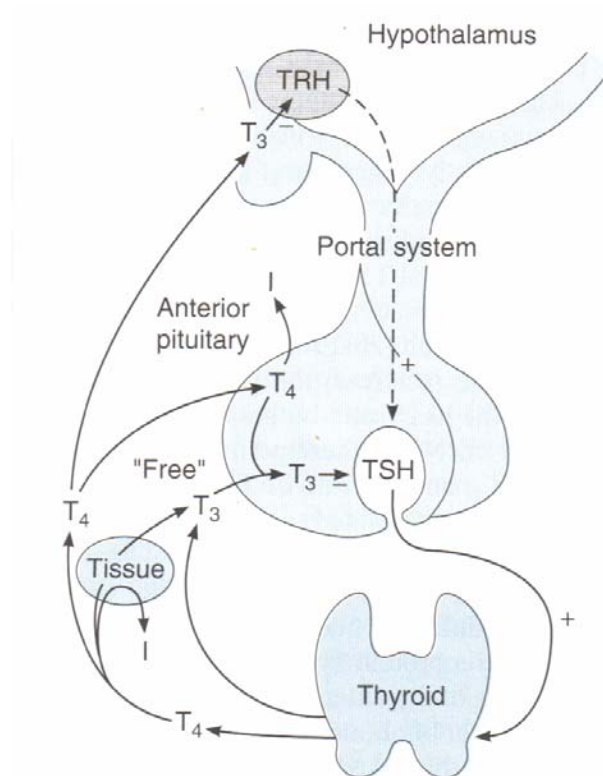


1.2.5 The Hypothalamic-Pituitary-Thyroid Axis

In addition to the autoregulation of thyroid hormone levels by the thyroid itself in response to iodide availability and regulation of thyroid hormone peripherally by deiodinases, another regulatory mechanism known as the hypothalamic-pituitary-thyroid axis acts to control the effects of thyroid hormone. This negative feedback system allows thyroid hormone to maintain the proper balance of hormones in circulation by inhibition of thyrotropin-releasing hormone (TRH) and thyroid-stimulating hormone (TSH) in the hypothalamus and anterior pituitary respectively (Fig. 1.5). TRH is a tripeptide that is synthesized by neurons in the supraoptic and supraventricular nuclei of the hypothalamus, stored in the median eminence, and then transported to the anterior pituitary where it controls synthesis and release of TSH. TSH or thyrotropin is a glycoprotein synthesized and secreted by the thyrotrophs of the anterior pituitary gland. TSH controls

thyroid cell growth and thyroid hormone synthesis and secretion by binding to the TSH receptor on the thyroid cell membrane and activating G-protein adenylyl cyclase-cAMP and phospholipase C signaling systems (3).

Figure 1.5 The hypothalamic-pituitary-thyroid axis



Reproduced with permission of The McGraw-Hill Companies: Greenspan, F.S. (2001) The Thyroid Gland. In *Basic and Clinical Endocrinology* (Greenspan, F.S. and Gardner, D.G., Eds.) 6th ed., p. 217, Lange Medical Books/McGraw-Hill, New York.

1.2.6 Thyroid Hormone Physiology

Through mediating the expression or repression of target genes, thyroid hormone regulates a number of physiological processes. These transcriptional effects

generally have a lag time of hours to days in order to reach full effect and range from effecting cardiac parameters and fetal development to setting the basal metabolic rate and regulating lipid levels (3). Table 1.1 summarizes thyroid hormone physiology and shows which genes are responsible for carrying out thyroid hormone action.

1.2.6.1 Target Genes in the Heart and Physiologic Outcome

Thyroid hormone has chronotropic and inotropic actions on the heart and increases cardiac output by decreasing systemic vascular resistance, both arterial and venous, and by decreasing venous compliance (19). The cardiac cycle is divided into two steps: systolic contraction and diastolic relaxation. Processes related to contraction are considered inotropic effects while processes related to relaxation are considered lusitropic effects (20). Thyroid hormone has several actions on the heart which improve contractility such as increasing the content of myocardial calcium cycling proteins, which stimulate calcium uptake by the sarcoplasmic reticulum. The rate of diastolic relaxation of the heart is related to intracellular Ca^{2+} concentration and sarcoplasmic reticulum Ca^{2+} -ATPase (SERCA2). SERCA is an ion pump that removes Ca^{2+} from the cytosol during systole and stores it in the sarcoplasmic reticulum. This decrease in intracellular Ca^{2+} content then triggers diastole or muscle relaxation (21). It has been shown that treatment of the hypothyroid heart with T_3 increases SERCA

and decreases its inhibitor, phospholamban (PLB). The ratio between these two proteins is a major determinant of cardiomyocyte contractility (19,20).

Myosin isozymes and myosin heavy chain isoforms are cardiac contractile proteins which are highly regulated by thyroid hormone. The myosin holoenzyme consists of two MHCs and four light chains. Myosin V1 predominates in the normal heart and consists of two MHC α s, V3 contains two MHC β s, and lastly, V2 is a heterodimer of MHC α and MHC β . The ATPase activity of these various holoenzymes vary markedly, with V1 being the most active. Thyroid hormone causes an increase in MHC α gene expression and negatively regulates MHC β gene expression, resulting in an increase in cardiac contraction (20,22).

Furthermore, several plasma membrane ion transporters such as Na⁺/K⁺-ATPase, Na⁺/Ca²⁺ exchanger, and voltage-gated potassium channels, including KCBN1, KCNA5, KCNQ1, and KCNE1, are all regulated at the transcriptional level by thyroid hormone and act to coordinate the electrochemical and mechanical responses of the myocardium (3,20,23).

The electrical activity of the heart in response to thyroid hormone treatment is not completely understood, but several changes in ion channel expression occur in response to thyroid hormone treatment. Of particular interest is hyperpolarization-activated cyclic nucleotide-gated channel 2 (HCN2), a component of the pacemaker. The heart rate is influenced by HCN gene

products in the sino atrial node, and thyroid hormone is known to positively regulate HCN2 (20-23).

1.2.6.2 Target Genes in the Liver and Physiologic Outcome

Thyroid hormone over-activity correlates with a decline in cholesterol and lipid levels. Low-density lipoprotein (LDL) cholesterol particles are associated with atherosclerotic disease and take part in shuttling cholesterol from the liver to target tissues where it is utilized for the synthesis of steroids, cell membranes, and other material. High-density lipoprotein (HDL) cholesterol is considered “good cholesterol” as it is anti-atherosclerotic. HDL cholesterol function is opposite that of LDL cholesterol in that it shuttles cholesterol from peripheral tissue to the liver, where it is metabolized (19,24).

Thyroid hormone influences cholesterol metabolism in a number of ways. Firstly, T_3 increases LDL receptors which result in an accelerated rate of LDL cholesterol clearance. It also increases apolipoprotein A1 gene expression, a major component of HDL. The enzyme 7α -hydroxylase is responsible for the conversion of cholesterol to bile acids and is also induced upon thyroid hormone administration. Paradoxically, T_3 increases 3-hydroxy-3-methylglutaryl coenzyme A (HMG-CoA), an enzyme that catalyzes the committing step of cholesterol biosynthesis by reducing HMG-CoA to mevalonate, and thus may increase plasma cholesterol levels; however, cholesterol lowering may be due to

enhanced clearance of cholesterol compared to cholesterol synthesis (19, 24-28). Another benefit of thyroid hormone action is the increased expression of lipoprotein lipase that results in lipolysis, releasing fatty acids and glycerol (19,24).

1.2.6.3 Other Target Genes and Their Physiologic Outcome

Thyroid hormone action is pervasive and affects gene transcription in the pituitary, brain, and bone as well as in other tissues (3). As discussed previously, T₃ and norepinephrine mount a synergistic response in rodent BAT upon cold exposure by stimulating UCP1 and adrenergic responsiveness (17). In all tissues except the brain, spleen, and testis, T₃ increases oxygen consumption and heat production by stimulation of Na⁺/K⁺-ATPase, thereby setting the basal metabolic rate. Counter-intuitively, superoxide dismutase decreases with increasing thyroid hormone levels, leading to an increase in superoxide anion free radical formation (3).

1.2.6.3.1 Pituitary

Thyroid hormone has two critical functions in the pituitary that include stimulation of growth hormone (GH) synthesis and the negative regulation of TSH, directly and indirectly. The effects on GH are most notable in rodents, whereas in humans, thyroid hormone deprivation does not decrease GH levels even though

growth is impaired. In human somatotrope adenomas, thyroid hormone stimulated GH release, but had variable effects on its transcription (21).

In terms of TSH, thyroid hormone has negative effects on its transcription, both directly and indirectly. Indirectly, thyroid hormone negatively regulates TRH in the hypothalamus, which decreases transcription of TSH in the pituitary. Thyroid hormone negatively regulates TSH directly by decreasing expression of the TSH α and TSH β subunits. Overall, these effects are major contributors to the hypothalamic-pituitary-thyroid axis and allow thyroid hormone to negatively regulate itself (3,21).

1.2.6.3.2 Brain

The brain is a major target of thyroid hormone action as neonatal hypothyroidism due to genetic causes or iodine deficiency in humans may lead to mental retardation and neurological defects (21, 29-31). Animal models have greatly assisted in our understanding of thyroid hormone action in the brain and although rodent neural development differs significantly than that of human, the 30 day postnatal period in rats is most comparable to the third trimester in humans. T₃ deprivation of the developing cerebellum leads to extensive defects in structure, especially abnormalities in myelination, neuronal migration, synaptogenesis, and arborization. A number of cerebellar genes such as calbindin, IP3 receptor, PCP-2, and myelin basic protein have been identified and shown to be thyroid

hormone responsive; however, their role in cerebellar development is still unknown (21,29).

1.2.6.3.3 Bone

Thyroid hormone is necessary for normal bone growth and development, especially in children (3,19,32). The effects of thyroid hormone are both direct and indirect and can cause major developmental problems such as short stature and delayed closure of the epiphyses (21,32). The direct effects include increasing osteoclast and osteoblast activity. Hydroxyproline, urinary pyridinium, and deoxypyridinium cross-links are markers of osteoclast activity and are all increased in response to high levels of T_3 . The expression of genes such as alkaline phosphatase and osteocalcin in osteoblasts serve as indicators of enhanced osteoblast activity (21,32).

Another indirect way in which thyroid hormone effects bone tissue is through stimulation of GH and insulin like growth factor I (IGF-I). The primary function of GH is to promote linear growth and does so through interaction with IGFs (3,32). As described before, T_3 induces the expression of GH and both may play key roles in maintaining healthy bones. They may also act synergistically in bone maintenance as studies show that GH without T_3 is unable to stimulate the maturation and organization of growth plate chondrocytes (32).

Table 1.1 Target genes of thyroid hormone and physiologic outcome

Organ	Gene	Physiologic Outcome	+ or - regulation	Reference
Heart	SERCA2	Diastolic relaxation	+	19-21
	Phospholamban	Phospholamban negatively regulates SERCA2	-	20
	MHC α	Regulates cardiac contractility	+	19-22
	MHC β	Regulates cardiac contractility	-	19-22
	KCBN1	Voltage-gated potassium channels, regulate electrical activity of the heart	+	23
	KCNA5		+	23
	KCNQ1		-	23
KCNE1	-		23	
HCN2	Pacemaker	+	20,21	
Liver	LDL Receptor	LDL cholesterol clearance	+	22,24-28
	Apolipoprotein A1	Component of HDL cholesterol, good cholesterol	+	21
	7 α -Hydroxylase	Secretion of cholesterol as bile acid	+	24
	HMG-CoA Reductase	Cholesterol Biosynthesis	+	24
	Lipoprotein Lipase	Lipid metabolism and clearance	+	3
Pituitary	Growth Hormone	Promotes linear growth	+	3,21
	TSH α	Thyroid hormone biosynthesis	-	21
	TSH β	Thyroid hormone biosynthesis	-	21
Brain (Cerebellum)	Myelin Basic Protein	Cerebellar Development	+	29-31
	Calbindin	Cerebellar Development	+	29
Bone	Alkaline Phosphatase	Osteoblast activity, bone formation	+	21
	Osteocalcin	Osteoblast activity, bone formation	+	21
Other	Na ⁺ /K ⁺ -ATPase	Oxygen consumption, metabolic rate	+	3
	Superoxide Dismutase	Clears free radicals	-	3

1.2.7 Pathophysiology of Thyroid Hormone Related Diseases

Thyroid hormone plays a major role in human physiology and changes in thyroid hormone levels cause a number of deleterious effects. Excess thyroid hormone causes hyperthyroidism, whereas a decline in thyroid hormone is known as hypothyroidism.

1.2.7.1 Hyperthyroidism

In the liver, T_3 stimulates lipogenesis and lipolysis, the latter more than the former, resulting in an overall decrease in serum cholesterol and triglycerides, and thus, decreases the risk of atherosclerosis and coronary artery disease (21,28,33-35). In terms of the heart, T_3 has unsafe and undesirable side-effects. Excess thyroid hormone causes tachycardia (increased heart rate), increases stroke volume and speed and force of systolic contraction, shortens the duration of diastolic relaxation, and decreases peripheral resistance. The culmination of these effects leads to an increase in cardiac output and is manifest in maladies such as arrhythmias, cardiac hypertrophy, and heart failure (20,33,34,36-39). T_3 action on skeletal remodeling leads to an increase in bone formation and resorption (3,21,24,32-35). In some patients, the net effect is a decrease in bone mineral density and this often leads to osteoporosis in hyperthyroid post-menopausal women (3). Many thyrotoxic patients also have muscle weakness

due to muscle wasting and experience nervousness, anxiety, hyperactivity, and heat sensitivity (3,21,29,33-35,40).

In the US, Grave's disease is the most common form of thyrotoxicosis and is viewed as an autoimmune disease. Grave's disease is caused when T lymphocytes become sensitized to antigens within the thyroid gland and stimulate B lymphocytes to synthesize antibodies against the antigen. One such antibody is directed against the TSH receptor site and causes the thyroid cell to function and grow uncontrollably. Besides the symptoms of hyperthyroidism already mentioned, Grave's patients also experience enlargement of the thyroid gland, also known as goiter, and ophthalmopathy. Treatment usually consists of antithyroid drug therapy, methimazole, propylthiouracil (Fig. 1.4), propranolol, or iopanoic acid, surgery, or radioactive iodine therapy (Na^{131}I) (3,41).

1.2.7.2 Hypothyroidism

Hypothyroidism causes the opposite effects seen in hyperthyroidism such as slowing down of the metabolism and bradycardia; however, due to the importance of thyroid hormone in development and growth, other effects occur. Cretinism and myxedema are the most common clinical manifestation of hypothyroidism. Cretinism is generally seen in new born infants in areas with low iodide intake and endemic goiter. Symptoms include mental retardation, short stature, a characteristic puffy appearance of the face and hands, and deaf

mutism. Adults with hypothyroidism usually develop myxedema and suffer from easy fatigability, coldness, weight gain, cool rough dry skin, puffy face and hands, and slow reflexes. In adults, these symptoms can be reversed by treatment with T_4 (3,41).

1.3 Molecular Basis of Thyroid Hormone Action

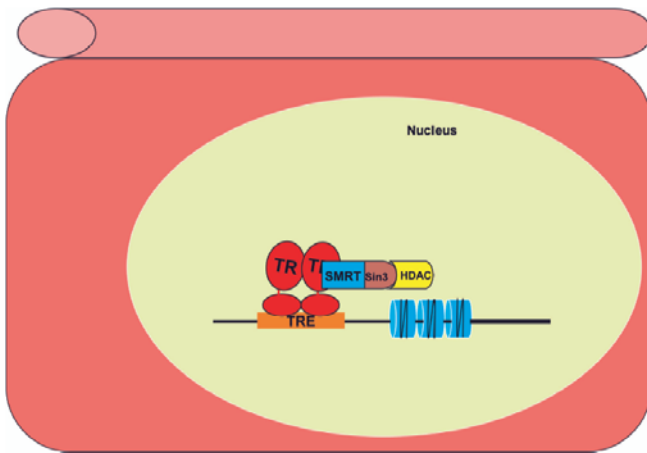
1.3.1 Thyroid Hormone Transport and Uptake

After thyroid hormone is synthesized in the thyroid gland (Fig. 1.3), it is secreted and dispersed via the circulatory system. In circulation, T_4 and T_3 are shuttled around mostly while bound to carrier proteins (Fig. 1.6). Normally, 0.04% of T_4 and 0.4% of T_3 in serum are free. The most common known binding proteins include thyroxine-binding globulin (TBG), thyroxine-binding prealbumin (TBPA), and albumin. TBG has a single high affinity binding site for T_4 and T_3 and is responsible for transporting 70% of circulating thyroid hormones. The other carrier proteins have a much lower affinity for thyroid hormones, responsible for carrying 25% of thyroid hormones in circulation collectively. Although their interaction with thyroid hormones is less avid, they are a source of free thyroid hormone to tissues as they have a high dissociation constant (3).

Upon delivery to target cells, thyroid hormones are actively transported into cells by means of the monocarboxylate transporter 8 (MCT8) thyroid hormone transporter or possibly others (42,43).

Figure 1.6 Thyroid hormone mechanism of action

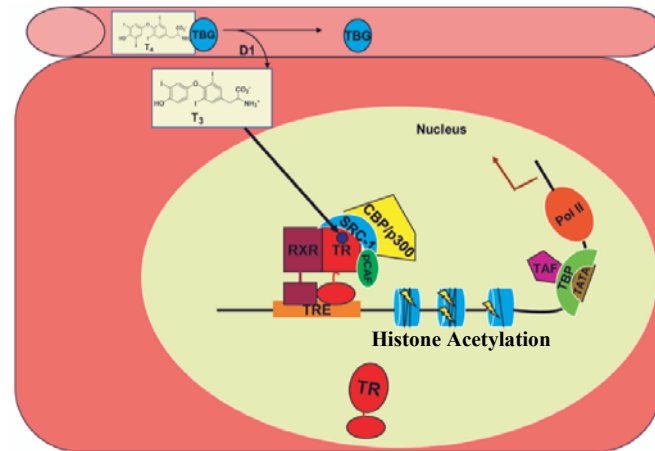
a) Inactive State



Key:

TR, thyroid hormone receptor ligand binding domain; SMRT, silencing mediator of retinoic acid and thyroid hormone receptors; Sin3, part of a nuclear corepressor complex; HDAC, histone deacetylase; TRE, thyroid hormone receptor response element

b) Active State



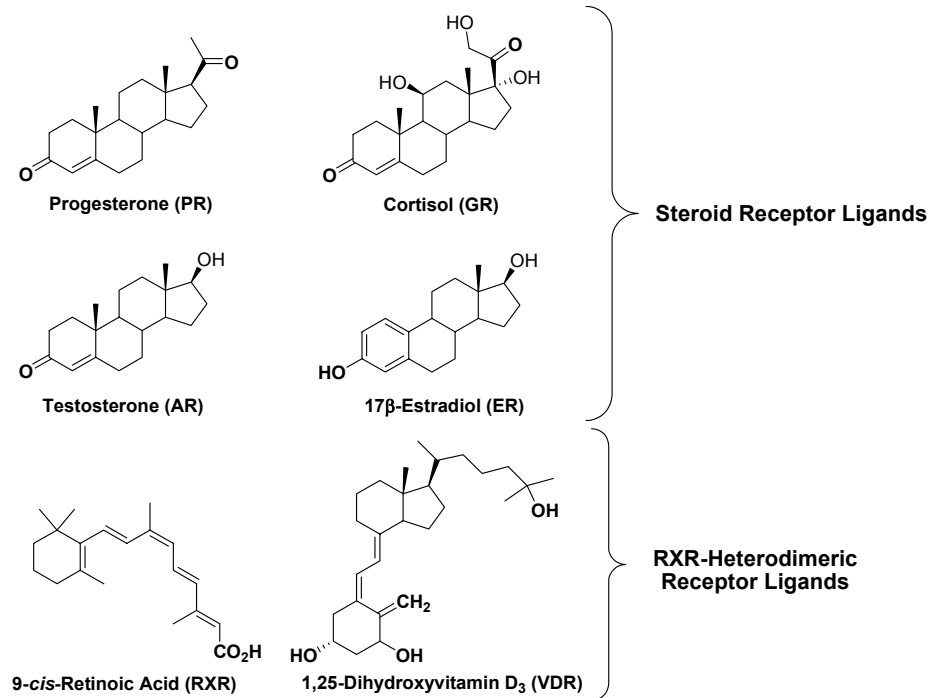
TBG, Thyroxine-binding globuline; D1, type 1 deiodinase; RXR, 9-cis-retinoic acid receptor ligand binding domain; TR, thyroid hormone receptor ligand binding domain; SRC-1, steroid receptor coactivator 1; p/CAF, p300/CBP-associated factor; CBP, cAMP response element-binding protein (CREB) binding protein; TRE, thyroid hormone receptor response element; TAF and TBP, part of the general transcription apparatus; Pol II, RNA polymerase II; TATA, a DNA sequence (cis-regulatory element) found in the promoter region of most genes

1.3.2 Thyroid Hormone Receptor Mediated Transcription

Thyroid hormone action is mediated by its cognate receptor, TR, and thus an understanding of TR structure and function is critical to understanding the molecular basis of thyroid hormone action (44,45). TR is a member of a large family of nuclear hormone receptor ligand-responsive transcription factors (48 human members) (46). This family also includes receptors for steroid hormones, non-steroidal hormones such as 1,25-dihydroxyvitamin D₃ and retinoic acid, and a host of orphan receptors for which no physiologically significant ligands have been identified (Fig. 1.7) (47,48). Like most nuclear hormone receptors, TR has a modular architecture that allows it to interact with DNA and regulatory proteins. These interactions are important as TR mediated gene transcription is orchestrated by interactions with various coregulators, DNA response elements, and auxiliary proteins such as 9-*cis*-retinoic acid receptor (RXR), and yet, this is still an over-simplification (49).

There are two genes for TR, TR α and TR β , that give rise to an ensemble of four different isoforms by means of alternative splicing and differential promoter usage: TR α_1 , TR α_2 , TR β_1 and TR β_2 (Fig. 1.8) (50). Although TR α_1 and TR α_2 differ only in their C-termini, TR α_2 contains a larger ligand binding domain (LBD) and is not ligand responsive. TR β_1 and TR β_2 are different in their N-termini, yet both respond equally well to T₃ (19,40,50).

Figure 1.7 Nuclear hormone receptor ligands



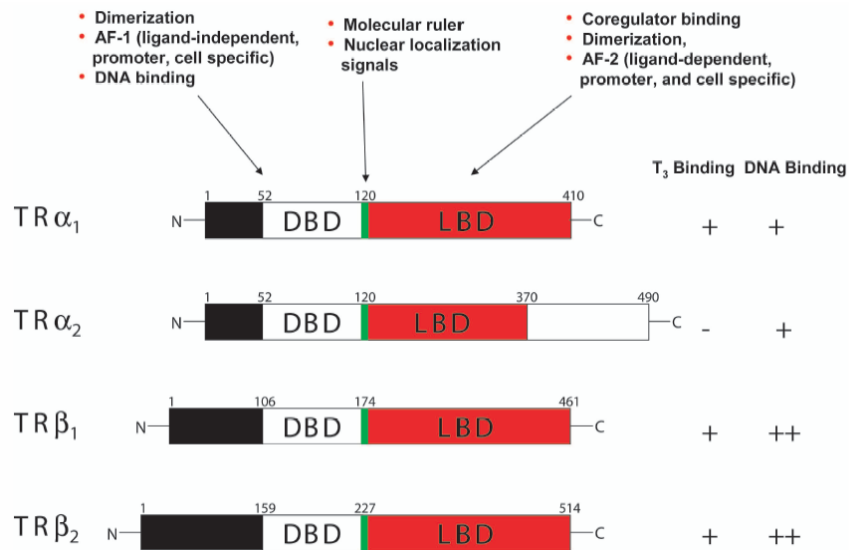
PR, Progesterone Receptor; GR, Glucocorticoid Receptor; AR, Androgen Receptor; ER, Estrogen Receptor; RXR, 9-cis-Retinoic Acid Receptor; VDR, Vitamin D Receptor

1.3.2.1 TR Functional Domains

TR contains three major domains consisting of a C-terminal LBD and an N-terminal DNA binding domain (DBD) separated by a short hinge region (Fig. 1.8) (47,49). The thyroid hormone receptor has two transcriptional activation domains. The ligand-independent activation function 1 (AF-1) region lies near the N-terminus and is responsible for the constitutive activation of the receptor. The activation function 2 (AF-2) region lies in the C-terminal LBD and requires ligand for transcriptional activation (51).

The DBD and LBD are multifunctional domains that play different roles in carrying out transcription. The DBD is the most conserved domain and is required for binding to DNA response elements. Two zinc-fingers motifs in which the zinc ion is tetrahedrally coordinated by four cysteines and an amphipathic α -helix C-terminal extension contribute to high-affinity DNA binding. The DBD,

Figure 1.8 Modular architecture of thyroid hormone receptor isoforms



when in the presence of the correct response element on DNA, also contributes to homo and heterodimerization. The LBD, in addition to containing the AF-2 region, contributes to homo and heterodimerization and interacts with coregulator and heat shock proteins (Fig. 1.8) (51,52).

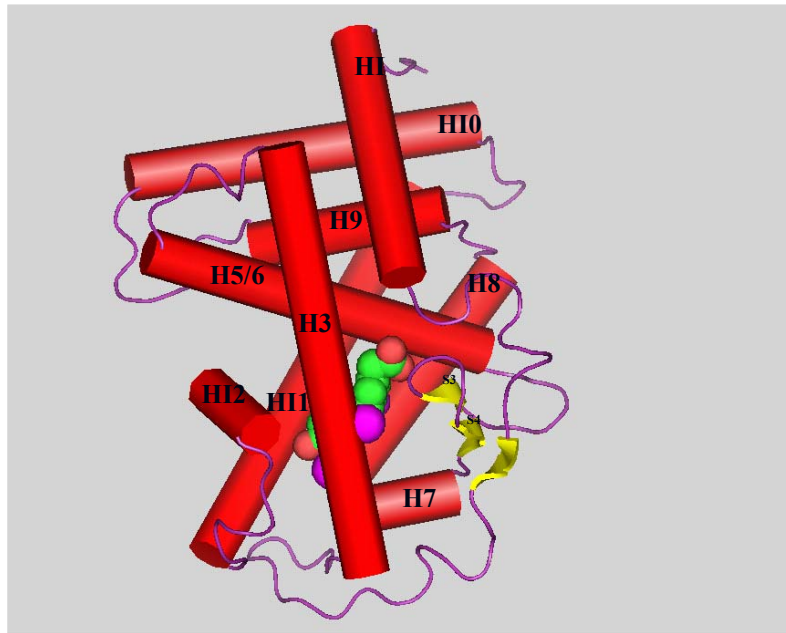
The hinge region connecting the DBD to the LBD must rotate 180° in order to properly orient the DBDs of RXR and its cognate receptor (Fig. 1.10) (53). What is known hitherto of the hinge region is that it plays an important role in ligand binding and contains a nuclear localization sequence (Fig. 1.8) (51,54). Also, in the case of TR, the hinge region forms an extended α -helix that makes significant contacts with DNA and molecular modeling suggests that it acts as a molecular ruler that directly measures the half-site spacing of the direct repeat 4 (DR-4) response element, a type of TRE, by steric exclusion (52).

1.3.2.2 Structure of the TR Ligand Binding Domain

The TR LBDs share 88% sequence identity and contain several structural features that enable it to carry out its function. Firstly, the LBD contains 12 linked α -helices and four short β strands (hTR β) (Fig. 1.9). A conserved β turn is situated between helices 5/6 and 7. The TR LBD is made up of three layers of helices, forming an anti-parallel helical sandwich. The central layer consists of helices 6 and 7, which are enriched with hydrophobic residues. The core of the LBD contains two hydrophobic helices and a small hydrophobic molecule; therefore, it is expected that the apo-receptor undergoes extensive conformational change upon hormone binding (Fig. 1.6). The AF-2 region is located on helix 12 and hormone binding causes it to undergo a conformational change that is known to be critical for coregulator recruitment. The coactivator-binding surface appears to form upon ligand binding by folding of helix 12 into a

scaffold formed by helices three, four, and five (55). Lastly, T₃ is held in place by a hydrophilic pocket formed by side chains from helices two, three, six, and sheet 3 (47,51,56).

Figure 1.9 Structure of the TR ligand binding domain



The tertiary structure of the ratTR α LBD bound to Triac was generated using Sybil (Tripos Associates). Coordinates used are from Wagner, R.L. et al. (2001) Mol. Endocrinol. 15, 398-410.

1.3.2.3 Molecular Basis of TR Mediated Transcription

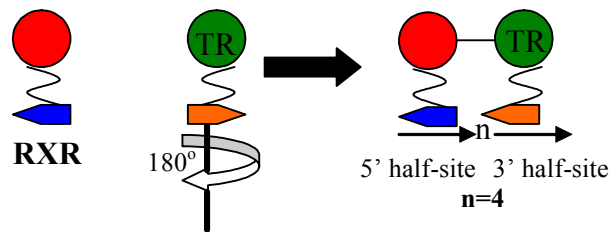
In many instances, inactive TR exists as a homodimer already associated with a TRE in the promoter region of a target gene (Fig. 1.6). A common TRE for TR consists of two direct repeats of consensus sequence AGGTCA separated by four nucleotides, also referred to as a DR-4 type TRE (52,53). Ligand binding

causes TR to heterodimerize with RXR and induces a conformational change in the LBD which allows the complex to activate or repress gene expression by interacting with corepressor and coactivator proteins (57-61). Recruitment of coactivator proteins leads to acetylation of histones and loosening of chromatin, permitting assembly of the general transcriptional apparatus and transcription of TR regulated genes (Fig. 1.6).

1.3.2.3.1 TR and 9-cis-Retinoic Acid Receptor (RXR) Dimerization

TR binds as homodimers or as heterodimers with RXR on TREs consisting of two sequences of AGGTCA with diverse orientations. It has been shown that

Figure 1.10 Heterodimerization of TR and RXR on a DR4 TRE



heterodimerization between TR and RXR LBDs are mediated through amino acids on helices 10 and 11 of the TR LBD. X-ray crystallographic studies show that residues E393 and L400 on helix 10 and P419, L422, M423, T426, and M430 on helix 11 of human TR β_1 are critical components of the heterodimerization interface. This interface is not only important for

heterodimerization, but appears to mediate formation of homodimers as well. TR-RXR heterodimers are more stable than TR homodimers due to DBD interactions between TR and RXR on various TREs. In this sense, heterodimerization is cooperative, with initial dimerization occurring via LBDs and then further stabilization occurs through DBD interactions. In terms of RXR, DNA binding induces and stabilizes the structure in a region of the second zinc-finger motif that forms the dimerization interface when RXR binds as a dimer on a DR recognition element (60,62,63). Other thyroid receptor auxiliary proteins (TRAPs), or proteins that augment TR binding to a TRE, include retinoic acid receptor (RAR) and COUP-TF (64).

1.3.2.3.2 TR Response Elements

TR positively or negatively regulates gene expression through interacting with specific sequences on DNA termed TREs upstream of the transcription start point. DNA has a polarity that gives it a sense of direction termed 5' to 3'. One type of TRE, DR4, consists of two half-sites (each site contains the hexameric sequence AGGTCA) separated by four nucleotides with one site in the 5' position and the other in the 3' position (Fig. 1.10). Other common TREs consist of half-sites arranged symmetrically as inverted (IR) or everted (ER) palindromes inseparated or separated by random nucleotides (IR0, ER6, ER8) (52,60,62). TREs play a crucial role in gene regulation as unliganded TR can repress gene expression from a positive TRE or induce it from a negative TRE (21).

1.3.2.3.3 TR Coregulators

In order to regulate gene expression, TR must interact with other proteins termed coregulators while associated with its respective TRE, RXR or other TRAPs, or other TRs. There are two classes of coregulators: coactivators and corepressors. These terms can be misleading as unliganded TR can activate transcription of genes such as TSH α , TSH β , and TRH from a negative TRE by recruitment of corepressors (65,66). TR accomplishes this by shifting the balance between histone acetylation and histone deacetylation such that chromatin is in a hyperacetylated state. This process is a protein-protein mediated event and TR is not required to bind DNA to activate or repress transcription (66). On the other hand, there is evidence for the requirement of TR to bind as either a monomer on negative TREs in the promoter regions of TSH β and TRH or as a heterodimer on an unusual element with RXR in order to activate transcription independent of ligand (59). The DNA-independent hypothesis states that while unliganded and not bound to DNA, TR recruits corepressors that carry along with it proteins with histone deacetylase activity or HDACs. This allows cAMP response element-binding protein (CREB) to bind to its DNA response element and recruit CREB-binding protein (CBP) and associated proteins with histone acetylase (HAT) activity, which then hyperacetylates histones. Histone acetylation causes chromatin to loosen up and exposes the promoter region of a target gene, which results in recruitment of

the general transcriptional apparatus and induction of genes negatively regulated by unliganded TR (65,66).

The canonical or most well understood mode of action of ligand-dependent TR induced transcription from positive TREs starts with repression of transcription when TR is bound to a TRE such as a DR4 (Fig. 1.6). While bound as a heterodimer with RXR, TR suppresses basal transcription by interacting with corepressors such as nuclear corepressor (NCoR) or silencing mediator for retinoic acid and thyroid hormone receptors (SMRT). Within the interaction domains of NCoR and SMRT are consensus sequences LXXXIXXX(I/L) where X represents any amino acid. These sequences bind to both TR and RXR heterodimers, as TR binding to RXR unmask a corepressor binding site. Transcriptional repression by corepressors is further assisted by their participation in the formation of larger complexes with histone deacetylase (HDAC) activity. Purification of NCoR from *Xenopus laevis* recovered three distinct complexes, one of which contained Sin3, histone deacetylase 1 (HDAC1), and RbAp48. Transcriptional silencing may be due to binding of components of the general transcriptional apparatus, such as TFIIB, to silencing domain 1 (SD-1) of SMRT or by packing hypoacetylated DNA to mask promoter regions (21,57,58).

Conversely, coactivators cause the transcription of genes by recruitment of a different complex with HAT activity. Upon ligand binding, corepressors

dissociate and coactivators are recruited. Coactivators interact with TR by means of LXXLL motifs, where X is any amino acid, only after hormone binding and formation of the coactivator interface by shifting helix 12. Insights into the mechanism by which coactivators are recruited came from the identification of the p160 family of nuclear receptor coactivators, two of which are referred to as steroid receptor coactivator 1 (SRC1)/nuclear coactivator (NCoA) and TIFII/glucocorticoid receptor interacting protein 1 (GRIP1). Like corepressors, these proteins are part of much larger complexes, but with opposing HAT activity. The conserved C-terminal domain of p160 family coactivators mediates interactions with CBP/p300, containing HAT activity, and CBP/p300 can recruit additional factors with HAT activity such as pCAF (57,58).

1.4 Nongenomic Effects

The classical mode of action of thyroid hormone occurs through activation of the thyroid pro-hormone by deiodination of T_4 to T_3 , the principal active form of thyroid hormone; however, much evidence over the past few years have shed light on other important roles of thyroid hormone and its metabolites. Upon treatment of 293T cells with T_4 or T_4 -agarose, the mitogen activated protein kinase (MAPK) pathway is activated, MAPK translocates into the nucleus, and active MAPK docks with the DBD of TR and phosphorylates Ser142 in the AF-1 region. Phosphorylation of TR in this region causes dissociation of TR-SMRT complexes, and may potentiate ligand-independent and –dependent TR

mediated transcription. Furthermore, it has been shown that T₄ treatment of CV-1 cells causes phosphorylation of TR by MAPK kinase 6 (MKK6), protects TR from ligand-binding induced degradation, and increases the affinity of the TR DBD for its response element (67,68). It has also been shown that T₄ treatment causes phosphorylation of TR β by a cAMP-dependent protein kinase (PKA)-dependent mechanism, indicating that T₄ may be a substrate for a G-protein coupled receptor (GPCR) or another plasma membrane associate receptor such as a receptor tyrosine kinase (60). Lastly, metabolites of T₄, termed thyronamines, have nongenomic effects through the GPCR trace amine receptor (7).

1.5 References

1. "Galen Of Pergamum." Encyclopædia Britannica. 2007. Encyclopædia Britannica Online. 9 June 2007 <<http://www.britannica.com/eb/article-9035854>>.
2. van Middlesworth, L. (1986) Thyroid Physiology. In *The Thyroid Gland* (van Middlesworth, L., Ed.), pp 1-2, Year Book Medical Publishers Inc., Chicago.
3. Greenspan, F.S. (2001) The thyroid gland. In *Basic and Clinical Endocrinology* (Greenspan, F.S. and Gardner, D.G., Eds.) 6th ed., pp. 201-271, Lange Medical Books/McGraw-Hill, New York.
4. Sawin, C.T. (2000) History, Ontogeny, and Anatomy. In *Werner & Ingbar's The Thyroid: A Fundamental and Clinical Text* (Braverman, L.E. and Utiger, R.D., Eds.) 8th ed., pp.3-5, Lippincott Williams & Wilkins, Philadelphia.
5. Jorgensen, E.C. (1978) Thyroid Hormones and Analogs. I. Synthesis, Physical Properties, and Theoretical Calculation. In *Hormonal Proteins and Peptides* (Li, C.H., Ed.), pp. 57-58, Academic Press, New York.
6. Bianco, A., Salvatore, D., Gereben, B., et al. (2002) Biochemistry, cellular and molecular biology, and physiological roles of the iodothyronine selenodeiodinases. *Endocr. Rev.* 23, 38-89.

7. Scanlan, T.S., Suchland, K.L., Hart, M.E., et al. (2004) 3-Iodothyronamine is an endogenous and rapid-acting derivative of thyroid hormone. *Nature Medicine* 10, 638-642.
8. Hart, M.E., Suchland, K.L., Miyakawa, M., et al. (2006) Trace amine-associated receptor agonists: Synthesis and evaluation of thyronamines and related analogues. *J. Med. Chem.* 49, 1101-1112.
9. Snead, A.N., Santos, M.S., Seal, R.P., et al. (2007) Thyronamines inhibit plasma membrane and vesicular monoamine transport. *ACS Chem. Biol.* 2, Article ASAP.
10. Berry, M.J., Banu, L., and Larsen, P.R. (1991) Type I iodothyronine deiodinase is a selenocysteine-containing enzyme. *Nature* 349, pp. 438-440.
11. Behne, D., Kyriakopoulos, A., Meinhold, H., and Kohrle, J. (1990) Identification of type I iodothyronine 5'-deiodinase as a selenoenzyme. *Biochem. Biophys. Res. Commun.* 173, pp. 1143-1149.
12. Davey, J.C., Becker, K.B., Schneider, M.J., et al. (1995) Cloning of a cDNA for the type II iodothyronine deiodinase. *J. Biol. Chem.* 270, pp. 26786-26789.
13. Croteau, W., Davey, J.C., Galton, V.A., and St. Germain, D.L. (1996) Cloning of the mammalian type II iodothyronine deiodinase. A selenoprotein differentially expressed and regulated in human and rat brain and other tissues. *J. Clin. Invest.* 98, pp. 405-417.

14. St. Germain, D.L., Schwartzman, R.A., Croteau, W., et al. (1994) A thyroid hormone-regulated gene in *Xenopus laevis* encodes a type III iodothyronine 5-deiodinase. *PNAS USA* 91, pp. 7767-7771.
15. Leonard, J.L., Visser, T.J., and Leonard, D.M. (2000) Characterization of the subunit structure of the catalytically active type I iodothyronine deiodinase. *J. Biol. Chem.* 276, pp. 2600-2607.
16. Fekkes, D., Hennemann, G., and Visser, T.J. (1982) Evidence for a single enzyme in rat liver catalyzing the deiodination of the tyrosyl and the phenolic ring of iodothyronines. *Biochem. J.* 201, pp. 673-676.
17. Koenig, R.J. (2003) Ubiquitinated deiodinase: Not dead yet. *J. Clin. Invest.* 112, 145-147.
18. Gill, G.N. (2001) Biosynthesis, Secretion, and Metabolism of Hormones. In *Endocrinology and Metabolism* (Felig, P. and Frohman, L.A., Eds.) 4th ed., pp. 29-48, McGraw-Hill, Inc., New York.
19. Morkin, E., Ladenson, P., Goldman, S., et al. (2004) Thyroid hormone analogs for treatment of hypercholesterolemia and heart failure: Past, present, and future prospects. *J. Mol. Cell. Cardiol.* 37, pp. 1137-1146.
20. Kahaly, G. and Dillman, W. (2005) Thyroid hormone action in the heart. *Endocr. Rev.* 0, er.2003-0033v2.
21. Yen, P. (2001) Physiological and molecular basis of thyroid hormone action. *Physiol. Rev.* 81, pp. 1097-1142.

22. Gullberg, H., Rudling, M., Saltó, C., et al. (2002) Requirement for thyroid hormone receptor β in T3 regulation of cholesterol metabolism in mice. *Mol. Endo.* 16, pp. 1767-1777.
23. Mai, W., Janier, M., Allioli, N., et al. (2004) Thyroid hormone receptor α is a molecular switch of cardiac function between fetal and postnatal life. *PNAS*, 101, pp. 10332-10337.
24. Baxter, J., Dillmann, W., West, B., et al. (2001) Selective modulation of thyroid hormone receptor action. *J. Steroid. Biochem. Mol. Biol.* 76, pp. 31-42.
25. Gullberg, H., Rudling, M., Saltó, C., et al. (2002) Requirement for thyroid hormone receptor β in T3 regulation of cholesterol metabolism in mice. *Mol. Endo.* 16, pp. 1767-1777.
26. Ness, G., Lopez, D., Chambers, C., et al. (1998) Effects of L-triiodothyronine and the thyromimetic L-94901 on serum lipoprotein levels and hepatic low-density lipoprotein receptor, 3-hydroxy-3-methylglutaryl coenzyme A reductase, and apo A-I gene expression. *Biochem. Pharmacol.* 56, pp. 121-129.
27. Grover, G., Mellstrom, K., Ye, L., et al. (2003) Selective thyroid hormone receptor- β activation: a strategy for reduction of weight, cholesterol, and lipoprotein (a) with reduced cardiovascular liability. *PNAS* 100, pp. 10067-10072.
28. Grover, G., Egan, D., Sleph, P., et al. (2004) Effects of the thyroid hormone receptor agonist GC-1 on metabolic rate and cholesterol in rats

and primates: selective actions relative to 3,5,3'-triido-L-thyronine.

Endocrinology 145, pp. 1656-1661.

29. Brent, G. (2000) Tissue-specific actions of thyroid hormone: insights from animal models. *Rev. Endocr. Metab. Disord.* 1, pp. 27-33.
30. Manzano, J., Morte, B., Scanlan, T.S., and Bernal, J. (2003) Differential effects of triiodothyronine and the thyroid hormone receptor β -specific agonist GC-1 on thyroid hormone target genes in the brain. *Endocrinology* 144, pp. 5480-5487.
31. Jones, I., Srinivas, M., Ng, L., and Forest, D. (2003) The thyroid hormone receptor β gene: Structure and functions in the brain and sensory systems. *Thyroid* 13, pp. 1057-1067.
32. Freitas, F., Capelo, L., O'Shea, P., et al. (2005) The thyroid hormone receptor β -specific agonist GC-1 selectively affects the bone development of hypothyroid rats. *J. Bone. Miner. Res.* 20, pp. 294-304.
33. Utiger, R. (2001) The thyroid: physiology, thyrotoxicosis, hypothyroidism, and the painful thyroid. In *Endocrinology and Metabolism* (Felig, P. and Frohman, L.A., Eds.) 4th ed., pp. 261-347, McGraw-Hill, Inc., New York.
34. Franklin, J. (2000) Metabolic changes in thyrotoxicosis. In *Werner & Ingbar's The Thyroid: A Fundamental and Clinical Text* (Braverman, L. and Utiger, R. Eds.) 8th ed., pp. 667-672, Lippincott Williams & Wilkins, Philadelphia.

35. Malloy, M. and Kane, J. (2001) Agents used in hyperlipidemia. In *Basic and Clinical Pharmacology* (Katzung, B. Ed.) 8th ed., pp. 581-595, McGraw-Hill, Inc., New York.
36. Woeber, K. (1992) Thyrotoxicosis and the heart. *New. Engl. J. Med.* 327, pp. 94-98.
37. Danzi, S. and Klein, I. (2002) Thyroid hormone-regulated cardiac gene expression and cardiovascular disease. *Thyroid* 12, pp. 467-472.
38. De, K., Gosh, G., Datta, M., et al. (2004) Analysis of differentially expressed genes in hyperthyroid-induced hypertrophied heart by cDNA microarray. *J. Endocrinol.* 182, pp. 303-314.
39. Fadel, B., Ellahham, S., Ringel, M., et al. (2000) Hyperthyroid heart disease. *Clin. Cardiol.* 23, pp. 402-408.
40. Scanlan, T., Yoshihara, H., Nguyen, N.H., and Chiellini, G. (2001) Selective thyromimetics: tissue-selective thyroid hormone analogs. *Curr. Opin. Drug. Discov. Devel.* 1, pp. 614-622.
41. Greenspan, F.S. and Dong, B.J. (2001) Thyroid and Antithyroid Drugs. In *Basic and Clinical Pharmacology* (Katzung, B.G., Eds.) 8th ed., pp. 644-659, Lange Medical Books/McGraw-Hill, New York.
42. Ichikawa, K., Miyamoto, T., Kakizawa, T., et al. (2000) Mechanism of liver-selective thyromimetic activity of SK&F L-94901: evidence for the presence of a cell-type-specific nuclear iodothyronine transport process. *J. Endocrinol.* 165, pp. 391-397.

43. Friesema, E.C.H., Ganguly, S., Abdalla, A., et al. (2003) Identification of monocarboxylate transporter 8 as a specific thyroid hormone transporter. *J. Biol. Chem.* 278, pp. 40128-40135.
44. Weinberger, C., Thompson, C., Ong, E., et al. (1986) The c-erb-A gene encodes a thyroid hormone receptor. *Nature* 324, pp. 641-646.
45. Sap, J., Muñoz, A., Damm, K., et al. (1986) The c-erb-A protein is a high-affinity receptor for thyroid hormone. *Nature* 324, pp. 635-639.
46. Robinson-Rechavi, M., Carpentier, A.S., Duffraisse, M., and Laudet, V. (2001) How many nuclear receptors are there in the human genome? *Trends Genet.* 17, pp. 554-556.
47. Weatherman, R., Fletterick, R., and Scanlan, T.S. (1999) Nuclear-receptor ligands and ligand-binding domains. *Annu. Rev. Biochem.* 68, pp. 559-581.
48. Evans, R. (1988) The steroid and thyroid hormone receptor superfamily. *Science* 240, pp. 889-895.
49. Harvey, C. and Williams, G. (2002) Mechanism of thyroid hormone action. *Thyroid* 12, pp. 441-446.
50. Lazar, M. (1993) Thyroid hormone receptors: Multiple forms, multiple possibilities. *Endocr. Rev.* 14, pp. 184-193.
51. Aranda, A. and Pascual, A. (2001) Nuclear hormone receptors and gene expression. *Physiological Reviews* 81, pp. 1269-1304.
52. Rastinejad, F. (1998) Structure and function of the steroid and nuclear receptor DNA binding domain. In *Molecular Biology of Steroid and Nuclear*

Hormone Receptors (Freedman, L., Ed.), pp. 105-131, Birkhauser, Boston.

53. Glass, C.K. (1996) Some new twists in the regulation of gene expression by thyroid hormone and retinoic acid receptors. *J. Endocrinol.* 150, pp. 349-357.
54. Miyamoto, T., Kakizawa, T., Ichikawa, K., et al. (2001) The role of hinge domain in heterodimerization and specific DNA recognition by nuclear receptors. *Molecular and Cellular Endocrinology* 181, pp. 229-238.
55. Ribeiro, R.C.J., Apriletti, J.W., Wagner, R.L., Feng, W., et al. (1998) X-ray crystallographic and functional studies of thyroid hormone receptor. *J. Steroid Biochem. Molec. Biol.* 65, pp. 133-141.
56. Wagner, R., Hubber, B., Shiau, A., et al. (2001) Hormone selectivity in thyroid hormone receptors. *Mol. Endo.* 15, pp. 398-410.
57. Nuclear Receptor Signaling Atlas. 2003-2007. Available at: <http://www.nursa.org/index.cfm>. Accessed April 14, 2007.
58. Rosenfeld, M. and Glass, C. (2001) Coregulator codes of transcriptional regulation by nuclear receptors. *J. Biol. Chem.* 276, pp. 36865-36868.
59. Robyr, D., Wolffe, A., and Wahli, W. (2000) Nuclear hormone receptor coregulators in action: diversity for shared tasks. *Mol. Endo.* 14, pp. 329-347.
60. Shibusawa, N., Hollenberg, A., and Wondisford, F. (2003) Thyroid hormone receptor DNA binding is required for both positive and negative gene regulation. *J. Biol. Chem.* 278, pp. 732-738.

61. Ribeiro, R., Feng, W., Wagner, R., et al. (2001) Definition of the surface in the thyroid hormone receptor ligand binding domain for association as homodimers and heterodimers with retinoid X receptor. *J. Biol. Chem.* 276, pp. 14987-14995.
62. Mangelsdorf, D.J. and Evans, R.M. (1995) The RXR heterodimers and orphan receptors. *Cell* 83, pp. 841-850.
63. Holmbeck, S.M.A, Dyson, H.J., and Wright, P.E. (1998) DNA-induced conformational changes are the basis for cooperative dimerization by the DNA binding domain of the retinoid X receptor. *J. Mol. Biol.* 284, pp. 533-530.
64. DeGroot, L.J. (1993) TRAPS—thyroid receptor auxiliary proteins. *Endocrinology* 133, pp. 963-964.
65. Tagami, T., Madison, L.D., Nagaya, T., et al. (1997) Nuclear receptor corepressors activate rather than suppress basal transcription of genes that are negatively regulated by thyroid hormone. *Mol. Cell Biol.* 17, pp. 2642-2648.
66. Tagami, T., Park, Y., and Jameson, J.L. (1999) Mechanisms that mediate negative regulation of the thyroid-stimulating hormone alpha gene by the thyroid hormone receptor. *J. Biol. Chem.* 274, pp. 22345-22353.
67. Davis, P.J., Shih, A., Lin, H.-Y., et al. (2000) Thyroxine promotes association of mitogen-activated protein kinase and nuclear thyroid hormone receptor (TR) and causes serine phosphorylation of TR. *J. Biol. Chem.* 275, pp. 38032-38039.

68. Chen, S.L., Chang, Y.J., Wu, Y.H., and Lin, K.H. (2003) Mitogen-activated protein kinases potentiate thyroid receptor transcriptional activity by stabilizing its protein. *Endocrinology* 144, pp. 1407-1419.

CHAPTER TWO

Rationale and Bioisosteric Replacement Strategy for the Development of Thyroid Hormone Analogues with Novel Pharmacology

2.1 Overview

Thyroid hormone has a vast role in mammalian physiology, and thus the thyroid hormone receptor is a major target for drug therapy. Scientists have been studying liver-selective thyroid hormone analogs developed between the late 1980s through the late 1990s in order to validate their utility in treating hypercholesterolemia, diabetes, atherosclerosis, and obesity. Recently, a number of thyromimetics with agonistic or antagonist properties have been developed and their clinical utility is just now being explored. For example, GC-1 exhibits cholesterol lowering effects in hypothyroid mice, cholesterol-fed rats, and cynomolgus monkeys. DITPA is currently being investigated for use in treatment of congestive heart failure. $TR\beta$ -selective agonist, GC-24, KB-141, and KAT-681, as well as $TR\alpha$ - and $TR\beta$ -selective antagonists, dronedarone and NH-3, show promise in treating hypercholesterolemia, hyperlipidemia, hepatocarcinogenesis, heart failure, and hyperthyroidism. This panel of thyromimetics and the involvement of the thyroid hormone receptor in a diverse array of physiological activities gives credence to the idea that thyroid hormone analogues that selectively modulate thyroid hormone receptor isoforms could serve as potential therapeutics in treating a number of metabolic and cardiac related diseases as well as serve as probes of TR biology. This chapter focuses on the design and characterization of novel thyroid hormone analogues.

2.2 Tissue-Specific TR Isoform Action

Clinical manifestations of thyroid hormone excess (hyperthyroidism) and deficiency (hypothyroidism) and resistance to thyroid hormone (RTH) underscore the importance of balanced thyroid hormone action. The hyperthyroid state leads to an increase in heart rate and a decrease in bodyweight and serum cholesterol, whereas hypothyroidism produces the opposite effects (1-4). Studies on RTH shed light on how thyroid hormone orchestrates its tissue-specific actions. The etiology of RTH is attributed to mutations in the TR β LBD, causing a decrease in T₃ binding and transcription. Patients with RTH exhibit pituitary and peripheral resistance to T₃, resulting in increased levels of T₄, T₃, TSH, and tachycardia (5-7). This suggests TR β is responsible for the negative regulation of TSH secretion in the pituitary and the remaining normal TR α ₁ regulates heart function.

The undesirable and unsafe effects of thyroid hormone action on the heart have been long considered a major obstacle to thyromimetic development, but other tissue selective effects must be considered as well. T₃ action on skeletal remodeling leads to an increase in bone formation and resorption which may ultimately lead to a decrease in bone mineral density and osteoporosis, especially among hyperthyroid post-menopausal women. Many thyrotoxic patients also have muscle weakness and experience nervousness, anxiety, hyperactivity, and heat sensitivity (1-4,8-10).

2.2.1 Murine “Knockout/Knock-In” Studies of TR

Murine “knockout/knock-in” strategies confirm that different TR isoforms have different roles in different tissues and that this division of labor is a result of both isoform expression pattern and isoform specific regulation of target genes. In mice, the phenotypes of TR β $-/-$ and the “knock-in” TR β^{PV} (a C-terminal frameshift mutant that attenuates TR β induced transactivation) are similar to those in RTH patients, minus the tachycardia, with TR β $-/-$ mice showing an additional phenotype of hearing loss which results from the predominant expression of TR β in the developing cochlea (Table 2.1) (5,6,11). In addition to the above phenotypes, the TR β^{PV} mutant mice show a decrease in contractile function and a slight decrease in heart-rate relative to wild-type mice (12). Deletion of TR α_1 leads to bradycardia and a decrease in body temperature, and in the combined TR α_1 and TR α_2 (TR α $-/-$) knockout, a low survival rate, impaired growth, and impaired bone and small intestine development (7,13-15).

Although TR β_2 is mainly expressed in the pituitary, studies show that TR α_1 has a compensatory role in RTH (6). Mice heterozygous for TR β^{PV} exhibit mild signs of resistance to thyroid hormone, possibly due to compensation by TR α . In TR β^{PV} and TR α $-/-$ mice, dysregulation of the hypothalamic-pituitary-thyroid axis (HPTA) is exacerbated, postnatal development is severely impaired, and expression of TSH α and TSH β mRNAs are significantly up-regulated compared with TR β^{PV} and TR α $+/+$ mice. This suggests that although expression pattern significantly

Table 2.1 TR knockout/knock-in mice phenotypes

Genotype	Phenotype	Reference
TR β -/-	Goiter, elevated T ₃ , T ₄ , and TSH, hearing impairment	11
TR β -/-, TR β ^{PV} +/+	Decreased contractile function and heart rate relative to wild type, and a phenotype similar to TR β -/-	6,12
TR β +/-, TR β ^{PV} +/-	Like TR β -/-, but symptoms are less severe	6
TR α -/-	Progressive hypothyroidism and growth arrest, low survival rate, impaired bone and small intestine development, impaired T ₄ synthesis, low TSH levels	13
TR α ₁ -/-	Lower heart rate and body temperature(both unresponsive to T ₃), a prolonged QT interval on EKG, low TSH levels, normal survival and fertility	14
TR α -/-, TR β ^{PV} +/+	Like TR α -/-, but with more severe impairment of postnatal growth and dysregulation of HPT axis	6
TR α ₁ -/-, TR β -/-	Like TR α ₁ -/- mice, but with goiter, elevated T ₃ , T ₄ , and TSH, impaired growth and bone development, females showed impaired fertility, decrease in survival	16
TR α -/-, TR β -/-	Similar to the TR α -/- mice, but with goiter and elevated T ₃ , T ₄ , and TSH	17

contributes to tissue-specificity in the pituitary, compensation by other receptor isoforms is important in maintaining receptor function (Table 2.1) (6,13).

Mice with deletions in both TR α and TR β have been reported and share some common features, but there are some distinctions. For example, TR α ₁ -/- and TR β -/- mice show a decrease in heart rate and body temperature and signs of RTH, but these mice also have a lower survival rate, impaired growth and bone development, and females showed impaired fertility. This phenotype is like the TR α knockout mice in many ways, except that these mice have RTH symptoms (16). Knocking out all receptors led to mice very similar to the TR α -/- mice, but with RTH symptoms; increased levels of T₃, T₄, TSH, and goiter (Table 2.1) (17).

TR isoforms may confer tissue-specific activities by regulating a different set of target genes. Studies aimed at defining the role of TR β in the heart of mutant mice where TR α predominates over TR β (~3:1), reveal that TR α specifically regulates hyperpolarization-activated cyclic nucleotide-gated channel 4 (HCN4), the pacemaker of the heart, and is the sole mediator of heart rate (12,18-19). In rodent livers, where TR β_1 is the most abundant isoform, 6 fold over-expression of TR α_1 cannot compensate for TR β regulation of cholesterol 7 α -hydroxylase in TR β ^{-/-} animals (20). These data indicate a special role for TR α in the heart and the requirement for TR β in cholesterol metabolism in the liver (20,21).

2.2.2 Selective Thyromimetics as Probes of TR Biology

Due to the extensive role of T₃ in physiology, it is conceivable that pharmacologically different thyromimetics would have therapeutic benefits. In years past, TR β -selective agonists have received a great deal of attention due to their cholesterol and weight lowering potential; however, the full scope of thyromimetic utility is largely unexplored as basic studies on new thyroid hormone analogs with varying pharmacological profiles are still in their infancy. The differences in these thyromimetics are mostly attributed to their ability to preferentially bind to and activate (agonistic) or inactivate (antagonistic) one of the three TR isoforms, TR α_1 , TR β_1 , and TR β_2 . In addition, other modes of tissue-selective modulation are possible, including tissue-selective accumulation; however, this mechanism for selective action is far less predictable (22-24). In

this case, selective action may be achieved by the active transport of thyromimetics into the cytoplasm of target cells of a particular tissue (*i.e.* hepatic or cardiac tissue) by thyroid hormone transporters (25,26). In some cases, the mode of selectivity is unclear.

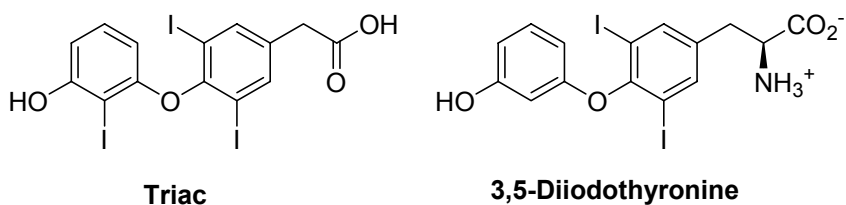
2.2.2.1 TR β - and Liver-Selective Thyromimetics

TR β -selective thyromimetics are among the largest group of thyroid hormone analogues. They include analogues that selectively bind and activate or inactivate TR β . TR β is implicated in regulating cholesterol and lipid levels, and hence TR β -selective agonists may be useful in treating hypercholesterolemia, hyperlipidemia, obesity, and other metabolic disorders. An antagonist of TR β may be useful in treating hyperthyroidism. Also, these ligands may be useful probes of TR biology. The role of TR isoforms in regulating adaptive thermogenesis in hypothyroid mice best illustrates this. Mice treated for 10 days with varying doses of T₃ and GC-1 restored uncoupling protein 1 levels (UCP1), the key thermogenic protein in brown adipose tissue (BAT). However, when treated with norepinephrine, interscapular BAT in T₃ treated mice experienced a 3.0° C elevation in temperature, but this was not the case in GC-1 treated mice. Also, GC-1 treated mice upon cold exposure were unable to restore core body temperature. Overall, this suggests that two distinct TR-dependent pathways, stimulation of UCP1 and stimulation of adrenergic responsiveness, are mediated by different TR isoforms in the same tissue (27).

2.2.2.1.1 Prototypical Thyromimetics: Triac and 3,5-Diiodothyronine

Thyroid hormone analogues with tissue-specific effects have been reported for years, and the prototypical thyromimetics tiratricol (Triac) and 3,5-diiodothyronine are among the first few to show liver selectivity (Fig. 2.1) (8,28,29). These analogues are naturally occurring metabolites with 3,5-diiodothyronine displaying slight liver selectivity. The most promising analogue, Triac, exhibited 2-3-fold greater affinity for TR β ₁ but lower biological activity compared to that of T₃ and was proposed as a possible treatment for RTH. This discrepancy between binding and biological activity was shown to be due to the rapid metabolism and clearance of Triac *in vivo* (28,29).

Figure 2.1 Structures of Triac and 3,5-diiodothyronine



2.2.2.1.2 SFK-94901

The first synthetic, selective thyromimetic was developed by Smith, Kline, and French and was intended to treat hypercholesterolemia. The medicinal chemistry focused on exploring the tolerance of the 3' position of the 3,5-

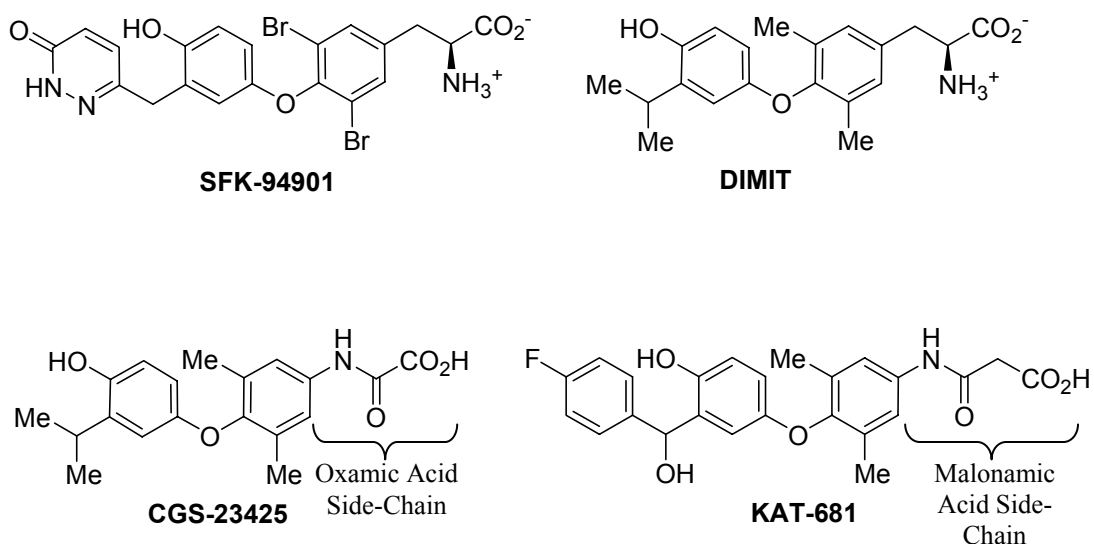
dibromo-L-thyronine scaffold. Ultimately, the lead compound SFK-94901 was developed and had the most desirable properties. SFK-94901 (Fig. 2.1) is a cardiac-sparing, liver-selective thyromimetic that is as active as T₃ on the liver but has 0.1% of the activity of T₃ on the heart. In direct receptor binding assays, SFK-94901 has equal affinity for both receptor subtypes and is 500-fold weaker in binding to TRs than T₃. The liver-selective activity of SFK-94901 is explained by cell uptake experiments showing that SFK-94901 is taken up more effectively by hepatic cells versus pituitary cells (8,30-32).

2.2.2.1.3 Oxamic and Malonamic Acid Derivatives

The non-selective thyromimetic analogue DIMIT (Fig. 2.2) displays 100-fold weaker activity than T₃; however, replacement of the alanine side-chain with oxamic acid compensates for the loss of activity that is likely due to the replacement of the inner- and outer-ring iodides with alkyl substituents (8). CGS-23425 (Fig. 2.2) is a cardiac-sparing oxamic acid thyroid hormone analogue that lowers plasma cholesterol (60%) and LDL-cholesterol (44%) in fat-fed rats (33). These effects are mostly attributed to an increase in hepatic LDL receptor activity and plasma apolipoprotein-AI, a major constituent of antiatherogenic HDL particles (28,33). In addition to oxamic acid, malonamic acid is also tolerated by the one position of the thyronine scaffold. KAT-681 (Fig. 2.2), a novel TR β -selective thyromimetic from the Kissei Pharmaceutical Company bearing a malonamic acid side-chain, inhibits the development of preneoplastic lesions in

rat livers and may be a candidate chemopreventive agent for hepatocarcinogenesis (34,35).

Figure 2.2 Structures of SFK-94901, DIMIT, and oxamic and malonamic acid derivatives

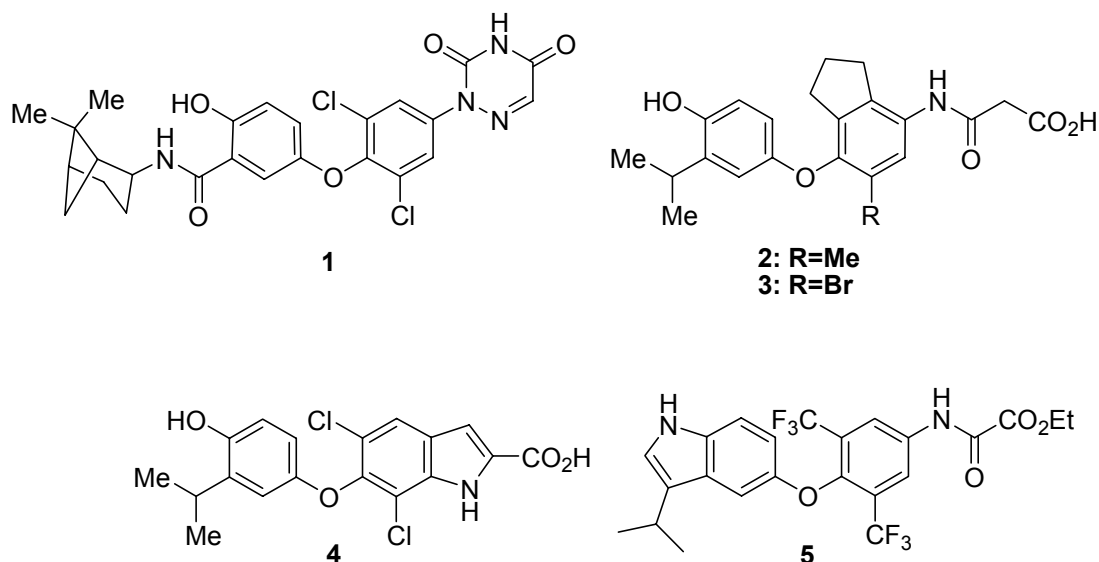


2.2.2.1.4 Azauracil and Bicyclic Inner- and Outer-Ring Derivatives

Noting an increase in selectivity with increasing 3' lipophilicity, Pfizer improved on an older 6-azauracil based scaffold by substituting the 3' position with bicyclic-based secondary carboxamides. Compound 1 (Fig. 2.3) is a highly selective (77-fold) and potent (EC₅₀=12nM) TR β -selective agonist (36). Lately, potent compounds that preferentially bind to TR β are receiving much attention due to their efficacy in lowering cholesterol and lipid levels and due to their unique scaffolds which include bicyclic inner- and outer-rings. Kissei has recently

expanded their series of thyromimetics by developing analogs with an inner indan-ring. Compounds 2 and 3 (Fig. 2.3) display ~20 and 60 fold TR β -selectivity

Figure 2.3 Structures of azauracel and bicyclic inner- and outer-ring analogues



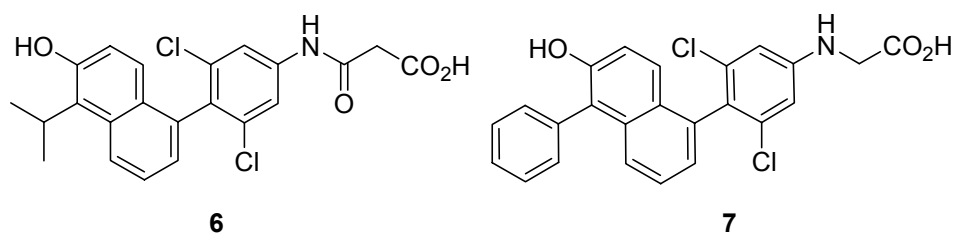
and both reduce plasma cholesterol in hypercholesterolemic rats with ED₅₀ values (nmol/kg) of 37 and 300 (37). Karo Bio has also developed thyromimetics with a bicyclic inner-ring. Compound 4 (Fig. 4) has an inner indole-ring and binds with high affinity to TR β (38,39). In addition to thyromimetics with bicyclic inner-rings, bicyclic outer-ring thyromimetics also exist. The medicinal chemistry of compound 5 focused on outer-ring as the TR β binding pocket seems to accommodate ligands with larger groups by movement of amino acid residues, Met442 in particular. This flexibility may in part be responsible for increased

selectivity. This observation along with the existence of thyroid hormone analogues with indoles in place of the phenolic outer-ring, lacking substituents and biological activity, prompted the development of analogues with indole outer-rings bearing substituents in the indole 3 position. Compound 5 shows great promise in that it displays about 10-fold weaker potency than T_3 and a 10-fold preference in $TR\beta$ activation in transient transfection transactivation assays (40).

2.2.2.1.5 Thyromimetics with a Novel Phenyl-Naphthylene Core

Most thyromimetics retain two structural features including a diphenyl ether and 3,5-disubstituted inner-ring. These two features are important in orienting the phenyl rings in a skewed position. This skewed position is considered ideal, and ligands bound to $TR\alpha$ or $TR\beta$ deviate from this “ideal” orientation. Forcing ligands into the skewed position by generation of thyromimetics with a phenyl-naphthylene core provides one way to determine if orthogonal phenyl rings lead to high affinity and/or selective thyromimetics. Compounds 6 and 7 are two examples from this panel of ligands and represent the best and worst binding affinities and selectivity respectively. Compound 6 is equivalent to T_3 in binding $TR\beta$ and displays 25-fold selectivity. Compound 7, displaying 100-fold weaker binding affinity to $TR\beta$ than T_3 , was 3-fold $TR\beta$ selective and a partial agonist; 19% induction of $TR\alpha$ and 50% induction for $TR\beta$. This suggests that the phenyl-naphthylene core provides yet another avenue to engender cardiac sparing agonists and possibly antagonists (41).

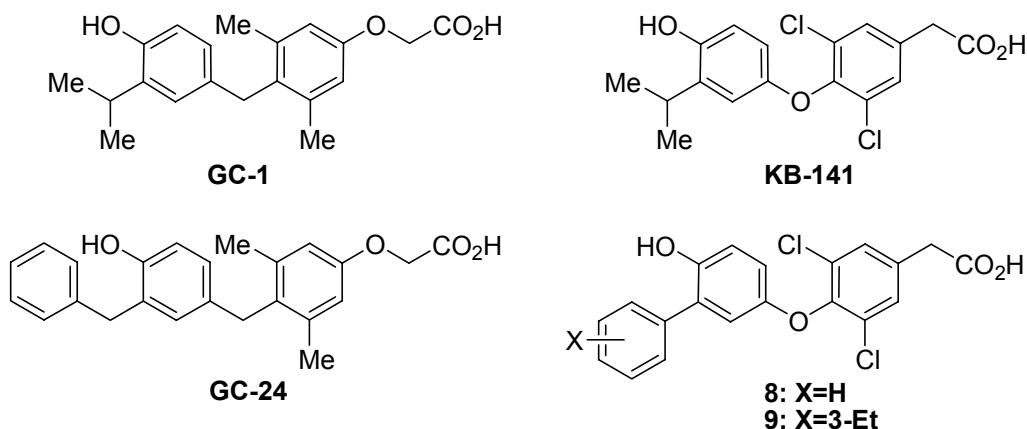
Figure 2.4 Structure of thyromimetics with a phenyl-naphthylene core



2.2.2.1.6 GC-1 and KB-141

GC-1 (Fig. 2.5) is a cardiac-sparing, halogen-free thyromimetic that differs from T_3 by replacement of the inner-ring iodides with methyl groups, the outer ring iodide is substituted with an isopropyl moiety, an oxoacetic acid replaces the aminopropionate, and the two aryl rings are joined by a methylene bridge rather than a biaryl ether linkage (42-45). GC-1 is equivalent to T_3 in binding to $TR\beta$ and displays approximately 4-10-fold $TR\beta$ -selectivity (8,42). In transfection assays with a DR4-driven luciferase reporter construct, GC-1 displays even greater selectivity for $TR\beta$ activation and only a 5-fold drop in potency compared with T_3 activation of $TR\beta$ (8). *In vivo*, GC-1 exploits another mode of selectivity through selective-accumulation in the liver versus the heart (8,46,47).

Figure 2.5 GC-1, KB-141, and a second generation of TR β -selective thyromimetics



Encouraged by its potency and β -isoform selectivity, GC-1 was tested in cholesterol fed rats, hypothyroid mice, and primates in order to elucidate its effects on cholesterol and triglyceride levels, obesity, and cardiac activity. In three model systems, GC-1 suppressed circulating cholesterol levels (90% in rats and 35-40% in cynomolgus monkeys at the highest dose) at concentrations that did not significantly affect heart rate (48). The efficacy of GC-1 in monkeys is substantial since their lipid profile is closer to man than any other species. In fact, this cholesterol lowering effect is similar to that of pravastatin, an HMG-CoA inhibitor, in primates (42). In addition to cholesterol lowering, lipoprotein (a) levels were reduced by ~50% and monkeys treated for 7 days experienced a ~4% reduction in body weight, likely due to a modest increase in basal metabolic rate (48). KB-141 (Fig. 2.5), a recently reported TR β -selective agonist, displays 14-fold binding affinity for TR β , and like GC-1, lowers cholesterol and increases

metabolic rate selectively compared to heart rate (42,49,50). In terms of weight loss, KB-141 reduced body weight up to 7% after one week of treatment in monkeys (50).

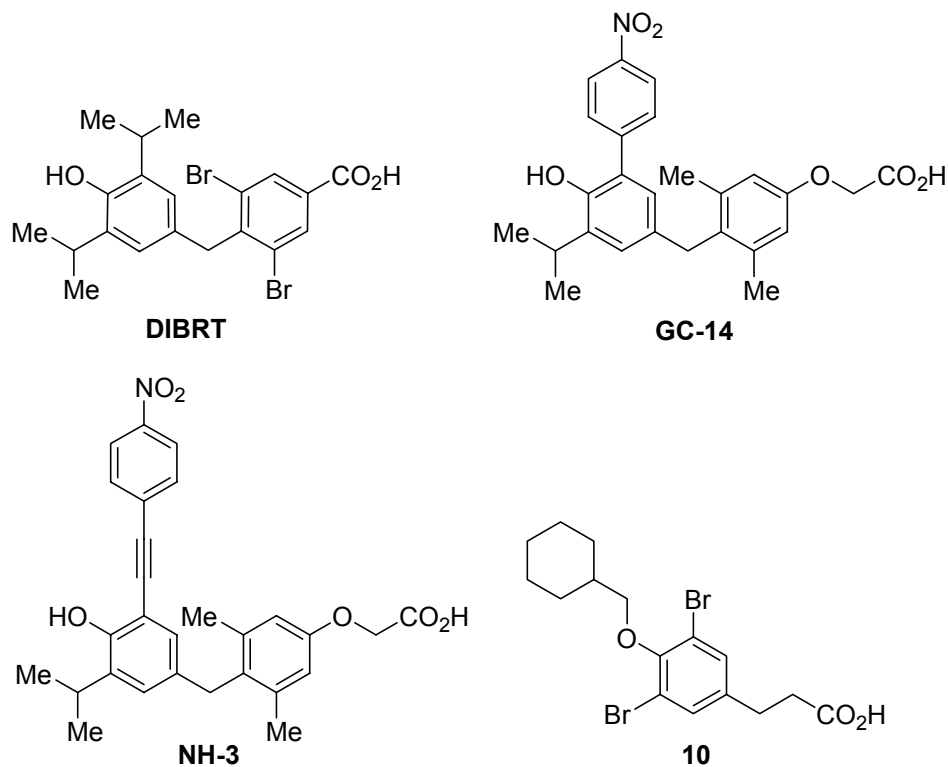
2.2.2.1.7 Second Generation TR β -Selective Thyromimetics

GC-24 (Fig. 2.5) is a second generation thyromimetic that differs from GC-1 in the 3' position; a benzyl group is substituted for the isopropyl group (51). This replacement improves TR β -selectivity by a factor of 10 with respect to binding (relative to GC-1) (51). It turns out that replacement of the 3' substituent with hydrophobic groups provides an excellent strategy for enhancing the TR β -selectivity of known thyromimetics. For example, compounds 8 and 9 (Fig. 2.5) are second generation thyromimetics similar to KB-141 modified at the 3' position with hydrophobic phenyl groups that exhibit improved TR β -selectivity (~2 fold) (52). Although GC-24 and compounds 8 and 9 have not yet been explored *in vivo*, it will be exciting to see if these second generation TR β -selective thyromimetics offer any advantages compared to their efficacious and less selective counterparts, GC-1 and KB-141 (51,52).

2.2.2.1.8 TR β -Selective Antagonists and Indirect Antagonists

According to the "extension hypothesis," coactivator recruitment is impeded by perturbing helix 12 packing in the TR LBD with thyroid hormone analogs that

Figure 2.6 NH-3, prototypical TR β -selective antagonists DIBRT and GC-14, and an indirect antagonist



have a bulky 5' extension (53-55). The prototypical thymomimetics DIBRT and GC-14 (Fig. 2.6) confirmed this theory as the 5' isopropyl group of DIBRT was required for conferring antagonism and the 5' nitrophenyl group of GC-14 led to partial antagonism (54,56). Unfortunately, *in vivo* studies on their antagonistic properties were not possible due to their modest affinity and potency for TR, but this situation was resolved with the development of NH-3. NH-3 (Fig. 2.6) is a TR β -selective antagonist with improved binding affinity and potency (53,54). Compared to GC-14, NH-3 has a larger and more rigid phenylethynyl moiety in

position 5' that protrudes closer to the coactivator interface (53-56). A high-throughput *in vitro* binding assay showed that the binding affinity of all coregulators tested with TR was ablated by NH-3, and *in vivo*, NH-3 inhibits *Xenopus laevis* tadpole metamorphosis, a T₃-dependent developmental process (57,58). Future prospects for NH-3 include testing its clinical in treating hyperthyroidism and continuing its use as a molecular probe of TR biology.

In addition to perturbing helix 12 with large 5' extensions on the outer-ring, a novel theory for antagonist design termed "indirect antagonism" was successfully applied to engender TR antagonists. The objective behind this concept is to stabilize a nonproductive conformation of key residues in the ligand binding pocket, and thus disfavor equilibrium to an active agonist conformation of helix 12. ERβ antagonists were designed based on this concept, and interestingly, these ligands were smaller than the endogenous hormone. In terms of TR antagonists, it was assumed that replacing the outer-ring, the ring closest to helix 12, with smaller moieties might also achieve indirect antagonism. To this end, a small panel of compounds were developed and ligand 10 displayed full antagonism with modest binding affinity similar to that seen with other reported antagonists, while not as good as high affinity TR antagonists such as NH-3 (59).

2.2.2.2 Cardiac- and TR α -Selective Thyromimetics

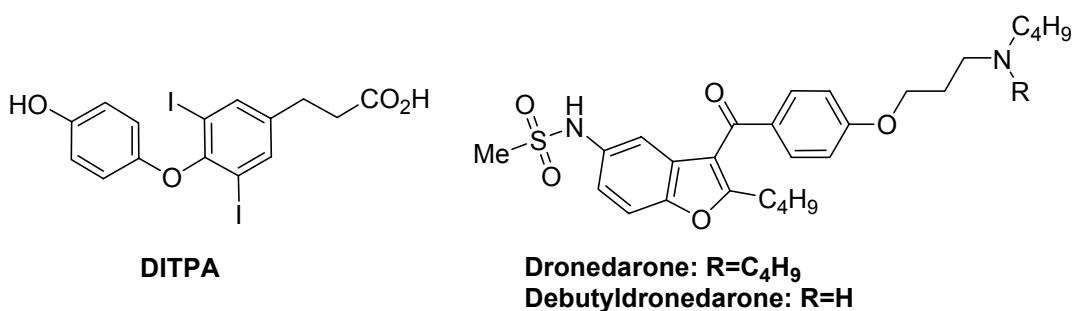
The development of cardiac- or TR α -selective thyromimetics has not experienced the same level of success as liver- and TR β -selective thyroid hormone analogues. However, there are a few notable exceptions such as 3,5-diiodothyropropionic acid (DITPA) and dronedarone. DITPA is being investigated for use in the treatment of congenital heart failure and dronedarone, via its active metabolite, is a *bona fide* TR α -selective antagonist and has benefits over amiodarone drugs which are used to treat cardiac arrhythmia and angina.

2.2.2.2.1 DITPA: A Thyromimetic with Cardiac-Selective Effects

The thyroid hormone analogue DITPA (Fig. 2.7) binds with approximately equal affinity to both TR α_1 and TR β_1 , but with 100 times lower affinity than T₃ (60). DITPA was identified by screening compounds structurally similar to T₃ for potential use in treatment of congestive heart failure (28,60-62). In cultured cardiomyocytes, DITPA induces α -myosin heavy chain gene expression, an indicator of inotropic activity (61). Administration of DITPA to hypothyroid rats improved cardiac performance with about half of the chronotropic effect (increase in heart rate) and less metabolic stimulation than T₄ (60-62). DITPA treatment also improved left ventricular performance in rabbit and rat postinfarction models of heart failure when administered alone or in combination with captopril, an angiotensin-converting enzyme inhibitor (61). With the backing of these data, a

pilot clinical study was undertaken and showed that DITPA was well tolerated by patients with congestive heart failure. Patients also experienced an increase in cardiac index, decreased systemic vascular resistance, and a lowering in serum cholesterol and triglycerides (28,60-62).

Figure 2.7 Structures of DITPA, Dronedarone, and Debutyldronedarone



Post-infarct remodeling is characterized by infarct-expansion, chamber dilation, and hypertrophy of the surviving myocardium without a sufficient angiogenic response, and hence, perfusion and coronary reserve in postinfarction models are severely compromised (62,63). DITPA treatment of male rats after induction of myocardial infarction (MI) facilitated arteriolar growth and modified ventricular remodeling (63,64). Another benefit of DITPA administration after MI includes improvement of endothelial function. It is known that endothelial nitric oxide synthase (eNOS) and β -adrenergic receptor (β -AR) mediated vasorelaxation goes awry in heart failure and *in vivo* and *in vitro* data suggest that DITPA may ameliorate this phenomenon by stimulating eNOS protein levels and enhancing β -adrenergic mediated vasorelaxation by an NO-dependent mechanism (65).

These new insights along with DITPA's past successes have prompted its use in a phase 2 clinical trial that is currently underway (65).

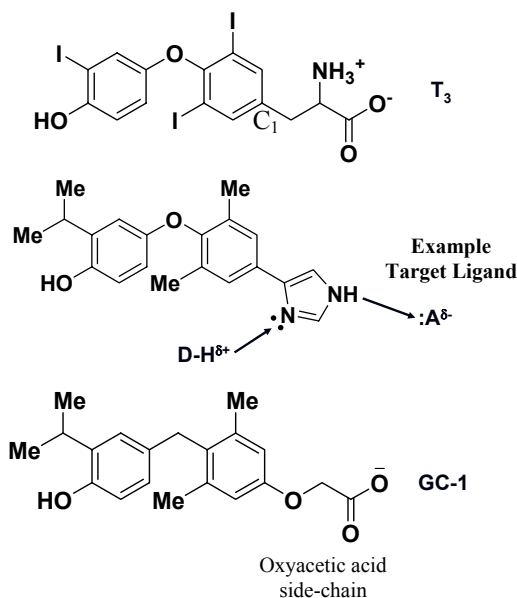
2.2.2.2.2 Dronedarone

Dronedarone, via its active metabolite debutyldronedarone (Fig. 2.7), is an antiarrhythmic drug devoid of iodine developed to eliminate the undesirable side-effects caused by iodine release of its predecessor, amiodarone (66). Unlike amiodarone, which is a competitive inhibitor of T_3 binding to TR_{α_1} and a noncompetitive inhibitor with respect to TR_{β_1} , debutyldronedarone is a true TR_{α_1} -selective antagonist in that it inhibits T_3 binding to TR_{α_1} by 77% versus 25% for TR_{β_1} (66,67). More importantly, dronedarone treatment recapitulates the effects of amiodarone on the heart (decrease in heart rate and lengthening of the QTc interval) without inhibiting the cholesterol lowering activity of thyroid hormone in the liver (66). More recently, dronedarone treatment of rats was shown to mimic the cardioprotective properties associated with hypothyroidism. Hypothyroidism confers protection against ischemia-reperfusion by reducing heart rate and contractility while increasing myocardial glycogen content, an energy providing substrate under anaerobic conditions (68). Lastly, dronedarone treatment resulted in appetite suppression and subsequent weight loss. The mechanism by which dronedarone causes weight loss is unclear, but it has been postulated that this may be through antagonism of thyroid hormone action in the hypothalamus (68).

2.3 Rationale Behind Modifying the C₁ Moiety: Bioisosteric Replacement

After the discovery of T₄ by Harington and Barger in 1927, medicinal chemists synthesized a plethora of thyroid hormone analogues in order to delineate the

Figure 2.8 Bioisosteric replacement of the alanine side chain with heterocycles or carbocycles

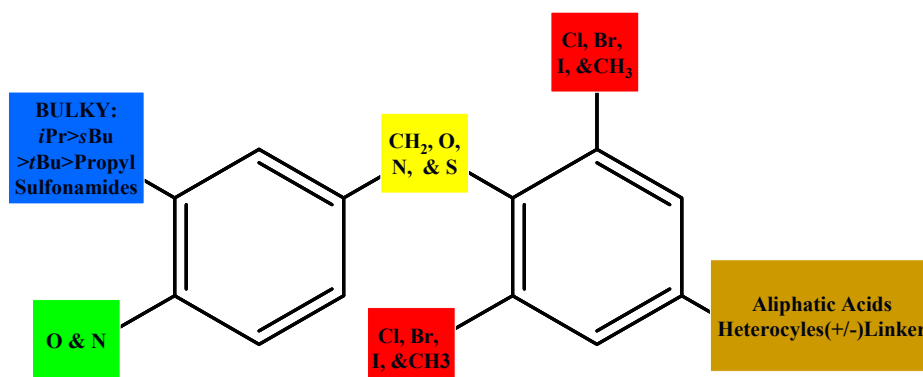


minimal structural requirements for hormonal activity (69). Several TR_β-selective agonists and antagonists arose from this body of work that spans about 80 years.

In order to generate thyromimetics with novel pharmacology, preferentially TR_α-selective agonism or antagonism, a bioisosteric replacement strategy was

devised and includes replacement of the C₁ position alanine side-chain with heterocycles and in some cases, carbocycles (Fig. 2.8). This strategy has several advantages: 1) Like the oxyacetic acid side-chain of GC-1, heterocycles have hydrogen bond acceptors, but they also have hydrogen bond donors; 2) heterocycles are structurally diverse and they provide the opportunity to expand the structure-activity relationship data for TR; 3) the halogen-free, 3,5-dimethyl-3'-isopropyl substitutions on the inner- and outer-rings as seen with the highly potent analogue GC-1 simplifies synthesis of target compounds; 4) in one study, the biphenyl ether linkage conferred less TR β -selectivity than the methylene linkage; and 5) modern synthetic methods makes the formation of a biphenyl ether linkage rather than a methylene linker quite facile (70). Furthermore, structure-activity relationship (SAR) data (Fig. 2.9) support thyromimetics of this design as all of the proposed structural elements and substitutions on the inner- and outer-rings are well tolerated.

Figure 2.9 Structure-activity data for the TR ligand binding pocket



Generating structural diversity at the C₁ position is also important because the ligand binding pocket of TR is well conserved across subtypes and something

Figure 2.10 Sequence alignment of TR α and TR β

```

hTR $\alpha$  201 IVSMPDGDVK DLEAFSEFTK IITPAITRVV DFAKKLPMFS ELPCEDQIIL 250
hTR $\beta$  255 IVNAPEGGKV DLEAFSHFTK IITPAITRVV DFAKKLPMFC ELPCEDQIIL 304

hTR $\alpha$  251 LKGCCMEIMS LRAAVRYDPE SDTLTLSGEM AVKREQLKNG GLGVVSDAIF 300
hTR $\beta$  305 LKGCCMEIMS LRAAVRYDPE SETLTLNGEM AVIRGQLKNG GLGVVSDAIF 354

hTR $\alpha$  301 ELGKSLSAFN LDDTEVALLQ AVLLMSTDRS GLLCVDKIEK SQEAYLLAFE 350
hTR $\beta$  355 DLGMSLSSFN LDDTEVALLQ AVLLMSSDRP GLACVERIEK YQDSFLLAFE 404

hTR $\alpha$  351 HYVNRKHNI PHFWPKLLMK VTDLRMIGAC HASRFLHMKV ECPTLFPPL 400
hTR $\beta$  405 HYINRKHVV THFWPKLLMK VTDLRMIGAC HASRFLHMKV ECPTLFPPL 454

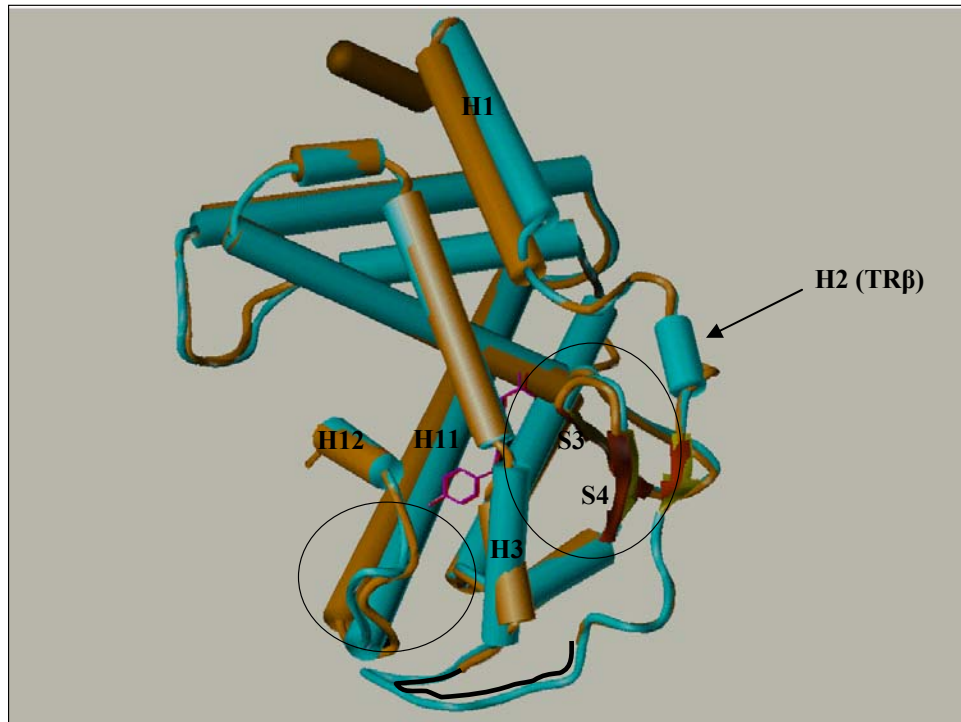
hTR $\alpha$  401 FLEVFEDQEV 410
hTR $\beta$  455 FLEVFED 461

```

Sequences were aligned with a blastp local alignment algorithm provided by NCBI (<http://www.ncbi.nlm.nih.gov/blast/Blast.cgi>). Residues highlighted in blue make contact with DIMIT in the human TR α and TR β crystal structures. The residue highlighted in red indicates the single amino acid difference between the TR α and TR β ligand binding pocket.

besides a carboxylate linked to the 1 position, as seen in many thymomimetics, may be required for conferring selectivity while maintaining potency. In fact, in the ligand binding pocket, the only difference among amino acid residues that contact ligand is a serine (TR α S277) in place of an asparagine (TR β N331) (Fig. 2.10) (45). Also, the LBDs of TR α ₁ and TR β ₁ share 88% sequence identity and overlaying their tertiary structures highlights several major differences (Fig. 2.11) (45). The first obvious difference is an additional helix in hTR β , helix 2.

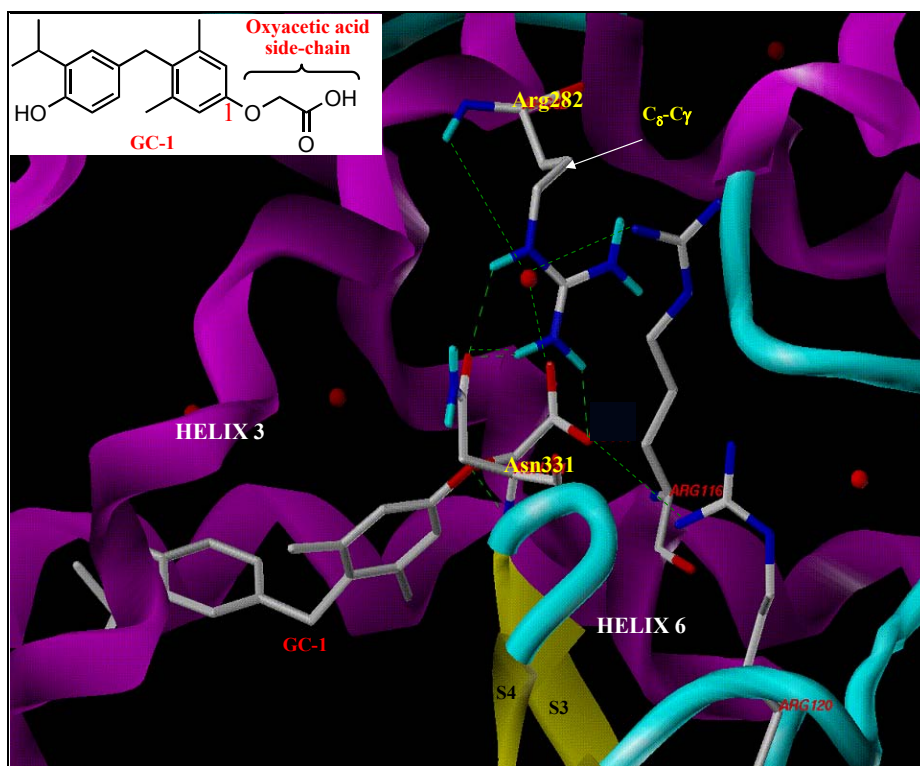
Figure 2.11 Structural alignment of TR α (LBD):Triac and TR β (LBD):Triac



The tertiary structures of the rat(r)TR α and hTR β LBDs bound to Triac were generated and overlaid using Sybil (Tripos Associates). The Magenta backbone represents rTR α and brown backbone represents hTR β . Red sheets are from rTR α and yellow sheets are from hTR β . Coordinates used are from Wagner, R.L. et al. (2001) Mol. Endocrinol. 15, 398-410.

There is also a difference in the loop between helices 1 and 3. rTR α shows more disorder in this loop, evidenced by the lack of electron density in the X-ray crystal structure. A bend in the final two turns of helix 11 in hTR β shifts the loop between helices 11 and 12. Furthermore, in terms of the β -hairpin between sheets 3 and 4, the β -hairpin in hTR β is shifted 0.9 Å closer to the carboxylate of Triac (45). Other than these differences, there are not any other features to exploit that could potentially lead to ligand selectivity in the binding pocket.

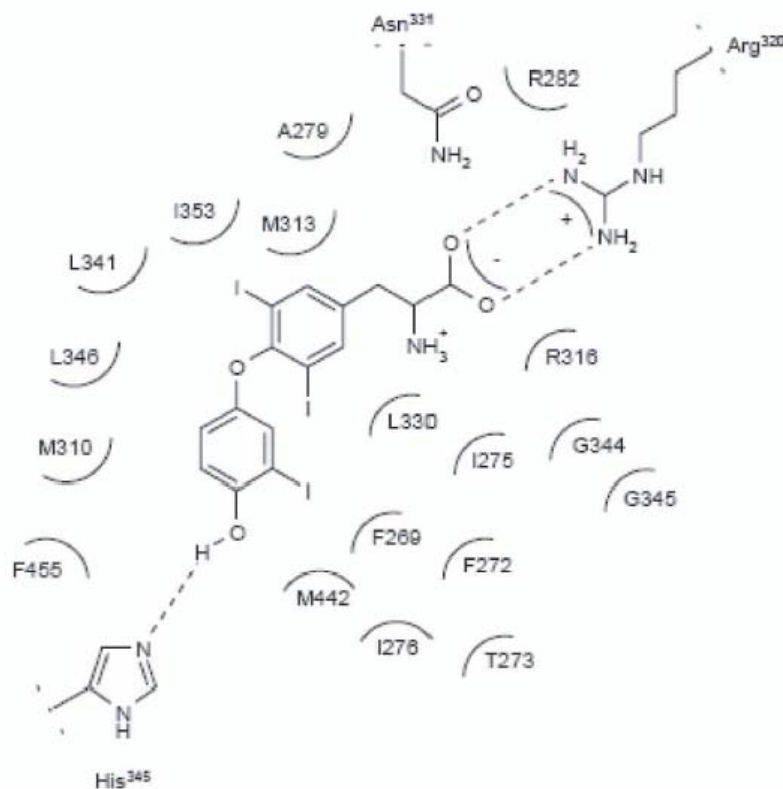
Figure 2.12 Crystal structure of the hTR β (LBD) complexed with GC-1



The ligand binding pocket of hTR β complexed with GC-1 was generated using Sybil (Tripos Associates). Coordinates used are from Wagner, R.L. et al. (2001) Mol. Endocrinol. 15, 398-410.

Despite having very similar LBDs and ligand binding cavities, the hTR β crystal structure complexed with GC-1 sheds light on how TR β -selectivity is achieved (Fig. 2.12). Zooming in on the hTR β ligand binding pocket reveals several features of the pocket. Firstly, Arg282, Arg316, and Arg320 form a hydrophilic, cationic pocket deep in the core of the LBD, and this polar region also includes Asn331. The highly cationic environment deep in the pocket explains why acidic groups such as carboxylic acids are favored in this region. The polar clamp is completed by His435 which forms a hydrogen bond with the 4'-phenolic hydroxyl group at the other of the pocket (Fig. 2.13). In the cationic pocket, a water

Figure 2.13 Diagram showing T₃-hormone interactions in the TR ligand binding pocket



Reproduced, with permission from The Thomson Corporation and Scanlan TS, Yoshihara HA, Nguyen NH, Chiellini G: Selective thyromimetics: Tissue-selective thyroid hormone analogs. Current Opinion in Drug Discovery & Development (2001) 4(5):614-622. Copyright 2001, The Thomson Corporation.

molecule partakes in an extensive hydrogen bonding network between the oxyacetic acid side-chain of GC-1, the cationic Arg residues, and the Asn residue. The role of Asn is critical as it interacts with Arg282 and orients this residue such that it interacts with the oxyacetic acid side-chain of GC-1. The remainder of the pocket forms the hydrophobic portion which stabilizes the core

of the thyronine scaffold, particularly the iodides for T₃ (Fig. 2.13) or in the case of GC-1, the inner- and outer-ring substituents (45).

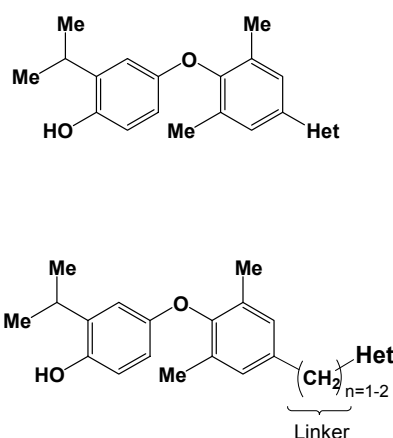
TR β -selectivity is likely achieved by this hydrogen bonding network in the ligand binding pocket, and Asn is a critical component of this network. The presence of Ser may not recapitulate the role Asn, and hence binding energy is lost due to a loss in hydrogen bonds. In fact, in hTR β and rTR α LBD crystal structures with Triac, Asn precludes the inward rotation of Arg282 about the C $_{\gamma-\delta}$ bond, placing it away from the ligand (Fig. 2.12). In rTR α , Ser277 forms a hydrogen bond with the analogous residue (Arg228), not the ligand. The importance of Asn331 is further highlighted in mutagenesis experiments whereby variant receptors hTR β (Asn331 \rightarrow Ser) and rTR α (Ser277 \rightarrow Asn) show that a Ser can not fulfill the role of Asn in TR β for binding GC-1. Reciprocally, Asn in place of a Ser in rTR α rescues binding affinity and GC-1 preferentially binds to this variant over the other (45). Collectively, these data corroborate a special role for C₁ position substituents of the ligand in conferring subtype-selectivity.

2.4 Synthesis of Thyromimetics with Heterocycles or Carbocycles in the C₁ Region (CO1-CO22)

The synthesis of thyromimetics with heterocycles attached directly to the C₁ position or attached via a linker (Fig. 2.14) is important as heterocycles or substituents on heterocycles may not plunge as deep into the ligand binding

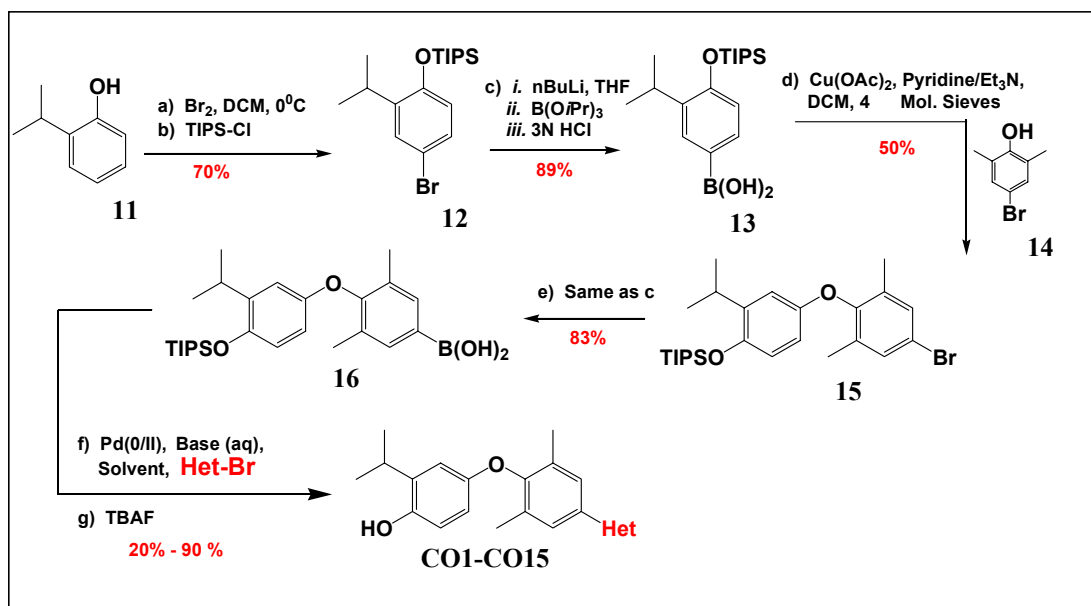
pocket as carboxylates with linkers of two or more methylene units. It is serendipitous that synthesis of such ligands with or without linkers is efficient by means of Suzuki and Stille organometallic assisted couplings and a Knoevenagel condensation (71-73).

Figure 2.14 Target thyroid hormone analogues with and without a linker



A common feature shared amongst all proposed ligands is a biaryl ring system connected by an ether bridge as seen in T₃. The generation of this common intermediate commences by bromination and TIPS protection of 2-isopropylphenol (**11**), which is then converted to a boronic acid (**13**) through a lithium-halogen exchange reaction followed by addition of triisopropyl borate and acid hydrolysis (Scheme 2.1) (74). This sets up a copper-mediated Evan's coupling between the boronic acid and 4-bromo-2,6-dimethylphenol, giving rise to biaryl ether **15** (75). This compound is then converted to a boronic acid then subjected to Suzuki cross-couplings to give final compounds after deprotection

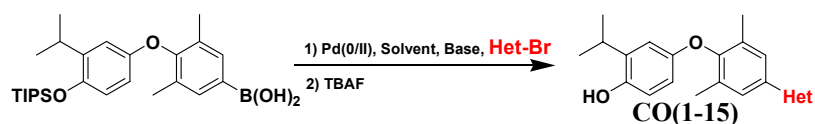
Scheme 2.1 Synthesis of ligands without a linker



with tetrabutylammonium fluoride (TBAF) (71,74). Table 2.2 shows Suzuki conditions and yields for compounds with heterocycles directly linked to the C_1 position.

Heterocycles with an ethylene or ethyl linker are prepared by performing Stille couplings in tandem. In this case, compound **15** (Scheme 2.1) undergoes cross-coupling with (E)-1,2-bis(tributylstannyl)ethylene, a bifunctional organotin reagent, to generate biaryl ether intermediate **18** (Scheme 2.2) (76,77). An additional Stille coupling with 2-bromothiazole and 3-bromothiophene gives rise to CO16 and CO18 (77). In order to expand the SAR data and see if an ethyl linker offers any advantages as a result of it having more rotational degrees

Table 2.2 Reaction conditions for Suzuki couplings



Compound	Het-Br	Pd(0/II) ^a	Solvent ^b	Base	Yield (%)
CO1		Pd(PPh ₃) ₄	Benzene/EtOH	K ₂ CO ₃	70
CO2		Pd(PPh ₃) ₄	Benzene/EtOH	K ₂ CO ₃	78
CO3		Pd(PPh ₃) ₄	Benzene/EtOH	K ₂ CO ₃	22
CO4		Pd(PPh ₃) ₄	Benzene/EtOH	K ₂ CO ₃	90
CO5		Pd(PPh ₃) ₄	Benzene/EtOH	K ₂ CO ₃	20
CO6		Pd(PPh ₃) ₄	Benzene/EtOH	K ₂ CO ₃	24
CO7		Pd(PPh ₃) ₄	Benzene/EtOH	K ₂ CO ₃	95
CO8		Pd(PPh ₃) ₄	Benzene/EtOH	K ₂ CO ₃	18
CO9		PdCl ₂ (dppf)	DME	K ₃ PO ₄	46
CO10		Pd(PPh ₃) ₄	Dioxane/H ₂ O	K ₂ CO ₃	31
CO11		Pd(PPh ₃) ₄	Dioxane/H ₂ O	K ₂ CO ₃	<10
CO12		Pd(PPh ₃) ₄	Benzene/EtOH	Na ₂ CO ₃	76
CO13		Pd(PPh ₃) ₄	Benzene/EtOH	Na ₂ CO ₃	24
CO14		PdCl ₂ (dppf)	DME	K ₃ PO ₄	25
CO15 ^{*c}		Pd(PPh ₃) ₄	Toluene/EtOH	K ₂ CO ₃	<10

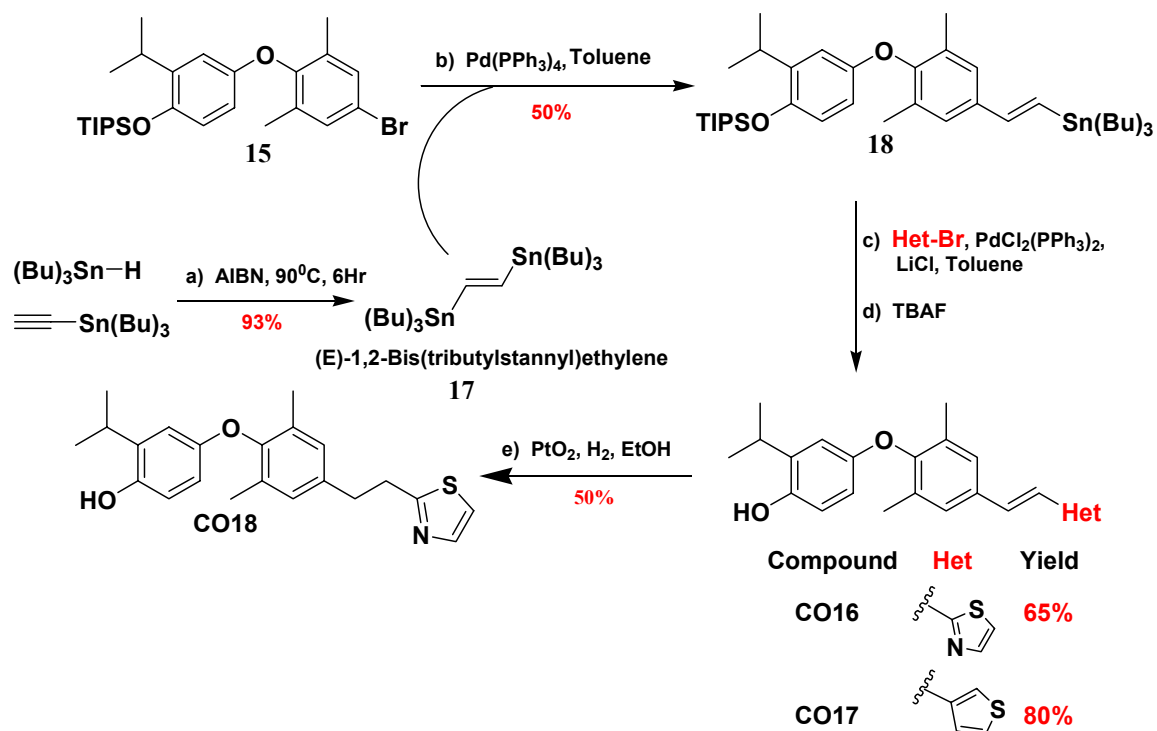
a) The following solvents systems were prepared in the following proportions: Benzene/EtOH, 2:1 and Dioxane/H₂O, 6:1.

b) Reactions contained 5-10 mole% Palladium catalyst and 3-5 equivalents of base

c) CO15^{*} is a precursor to CO15; the aldehyde generated after the Suzuki reaction is first oxidized to the carboxylic acid with NaClO₂, H₂O₂, and NaH₂PO₄ in acetonitrile before deprotection with TBAF to give CO15.

of freedom in comparison to an ethylene linker, CO16 was subjected to catalytic hydrogenation with a platinum oxide catalyst yielding CO18. The last class of

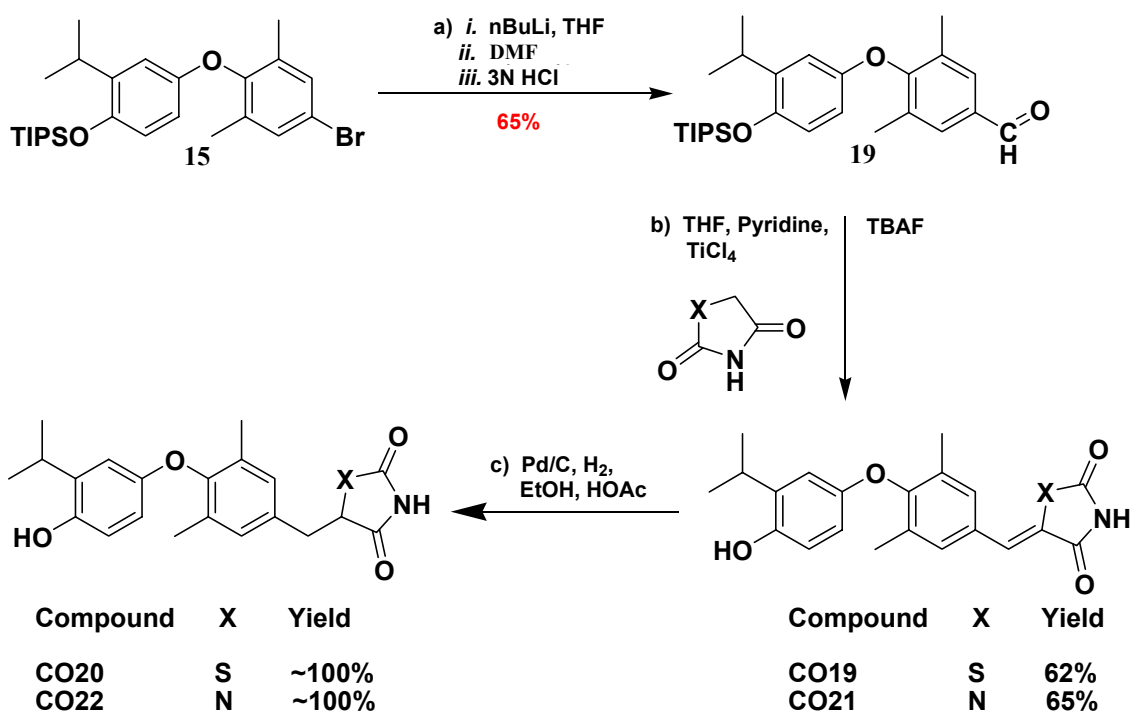
Scheme 2.2 Synthesis of ligands with an ethylene or ethyl linker



ligand which has a single carbon unit connecting the heterocycle to the C₁ position is generated by means of condensing two molecules, an aldehyde with a carbanion equivalent, to yield α,β conjugated enones after the elimination of a water molecule (78). Intermediate **15** containing the biaryl ether ring system (Scheme 2.1) is subjected to lithium-halogen followed by treatment with dimethylformamide (DMF) in order to generate intermediate **19** with an aldehyde in the C₁ position (Scheme 2.3). **19** is condensed with hydantoin or

thiazolidinedione in the presence of titanium tetrachloride (TiCl₄) and pyridine to give CO19 and CO21 in moderate yield (78). Both of these olefins are readily hydrogenated under a hydrogen atmosphere in the presence of activated 10% palladium on carbon, yielding CO20 and CO22 quantitatively (73).

Scheme 2.3 Synthesis of ligands with a single carbon linker



2.5 *In vitro* Analysis of Selected C₁ Derivatized Thyromimetics

After generation of a collection of ligands, CO1-CO22, compounds were subjected to two types of analysis: Competitive binding and transactivation assays. The principle behind competitive binding is that radiolabeled natural

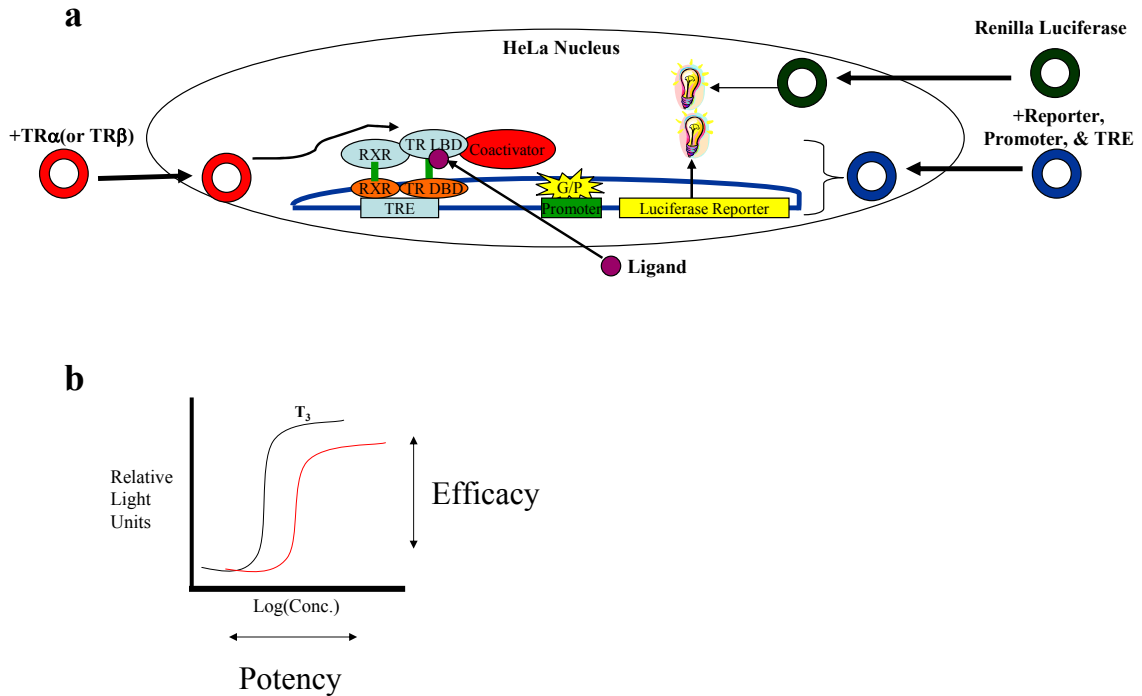
hormone, and in this case and ^{125}I tag, binds with high affinity to both TRs and upon addition of increasing amounts of cold ligand, T_3 will be displaced. This competition is detected by analyzing the amount of radioactivity left after allowing TR α or TR β to reach a thermodynamic equilibrium in the presence of both radiolabeled hormone and test ligand. The binding affinity (K_d), relative to the T_3 , is determined through obtaining the IC_{50} or the concentration of test ligand required to compete for half the specific binding according to the equation (GraphPad Prism 4.0):

$$K_d = \text{IC}_{50} / (1 + [\text{T}_3, \text{nM}]/K_D),$$

where K_D is the concentration of T_3 required for half maximal binding (79).

The transactivation assay measures the efficacy and potency of a test ligand. This type of experiment works by introduction of a reporter plasmid containing a TRE (DR4) and reporter gene, firefly luciferase, into mammalian cells (i.e. HeLa or U2OS cells). In addition, the wild-type protein of interest (TR α or TR β) and an internal control, which contains a *Renilla* luciferase gene that is constitutively transcribed, are introduced into the same cells. Ligands that enter cells, bind to the receptor, and transactivate via the normal mode of action of thyroid hormone will cause generation of luciferase (Fig. 2.15a). Firefly and *Renilla* luciferases are evolutionary divergent homologues that produce light upon treatment with different substrates, and thus they make for a suitable dual reporter system.

Figure 2.15 Dual-luciferase transactivation assay and dose-response curves



a) G/P represents the general transcriptional apparatus and
 b) the red line is a theoretical dose-response curve generated by a test ligand

Treating cells with different concentration of test ligands generates dose-response curves (Fig. 2.15b) which reveal two important pharmacologic parameters: the potency and efficacy. The EC_{50} indicates the concentration of ligand required for half-maximal activation and is a measure of potency, whereas efficacy which is measured with the ordinate axis provides an assessment of how well the ligand elicits the desired effect at saturation.

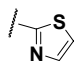
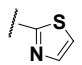
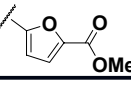
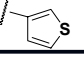
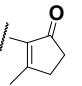
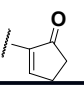
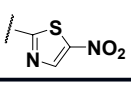
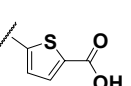
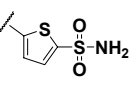
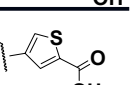
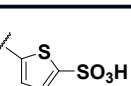
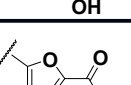
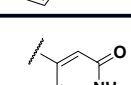
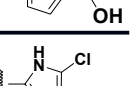
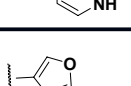
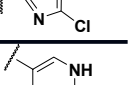
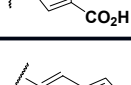
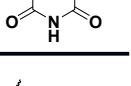
2.5.1 ¹²⁵I-T₃ Competitive Binding Analysis

Select compounds from the small panel of synthetic ligands compete with T₃ for binding to TRs both selectively and with varying affinities (Table 2.3). Also, by varying the substituents on heterocycles in the C₁ position, several trends become apparent. Firstly, without electron withdrawing substituents, heterocycles engender unselective thyromimetics that bind with 100-fold weaker affinity than T₃, as is the case with CO1 and CO2. Heterocycles bearing electron withdrawing groups on the heterocyclic moiety engendered TR β -selectivity; however, at the expense of binding affinity. CO6, CO7, and CO8 are 7-, 15-, and 5-fold TR β -selective respectively and up to 30-fold weaker in binding TR β than CO1 and CO2.

Carbocycles cyclopenten-2-one and 3-methylcyclopenten-2-one offered very little in terms of binding and selectivity. Similarly, thiophenes (CO9 and CO11) bearing sulfonamide and sulfonic acid groups in position 2 of the heterocyclic moiety are unselective and very weak binders. Although not shown in Table 2.3, the thiazolidinedione CO20 showed very weak binding for TR α and TR β , 124 nM and 314 nM K_ds respectively, and the SAR data indicates that the unsaturated precursor CO19 would only decrease binding.

Furanoic acids conjugated to the thyronine scaffold via positions 5 and 4, CO10 and CO15, both showed impressive TR β -selectivity, approximately 16-fold TR β -

Table 2.3 ¹²⁵I-T₃ competitive binding data: Screen of CO1 – CO17

Het	Compound	K _d , nM (beta)	K _d , nM (alpha)	Kd(alpha)/Kd(beta)	Compound	Het
	T ₃	0.081	0.06	~1	T ₃	
	CO1	2.5	2.31	1.3	CO1	
	CO2	3.45	2.93	1.16	CO2	
	CO3	63.7	93.2	1.7	CO3	
	CO4	90	118	1.3	CO4	
	CO5	82	120	1.46	CO5	
	CO6	81	580	7.16	CO6	
	CO7	56	859	15.28	CO7	
	CO8	17	91.5	5.39	CO8	
	CO9	692	510	0.74	CO9	
	CO10	3.5	50.5	16	CO10	
	CO11	486	---	---	CO11	
	CO12	16.6	199.2	12	CO12	
	CO13	117	137	1.17	CO13	
	CO14	0.2	17	85.8	CO14	
	CO15	268	2672	15.35	CO15	
	CO16	786	-	n/a	CO16	
	CO17	1.5X10 ⁵	-	n/a	CO17	

selective, but the position of the linkage decreased binding of CO15 significantly; by about 100-fold. Interestingly, conversion of CO10 to the methyl ester CO3 reduced both selectivity and binding, suggesting that both electron delocalization and acidity are instrumental for avidity and selectivity. This observation is recapitulated in the case of CO13 and CO14 where presentation of an imide to the ligand binding pocket engenders both binding affinity and TR β -selectivity. CO13 displayed meager binding affinity and was unselective, yet CO14 bound with the greatest affinity, demonstrating only a 10-fold decrease in binding

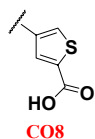
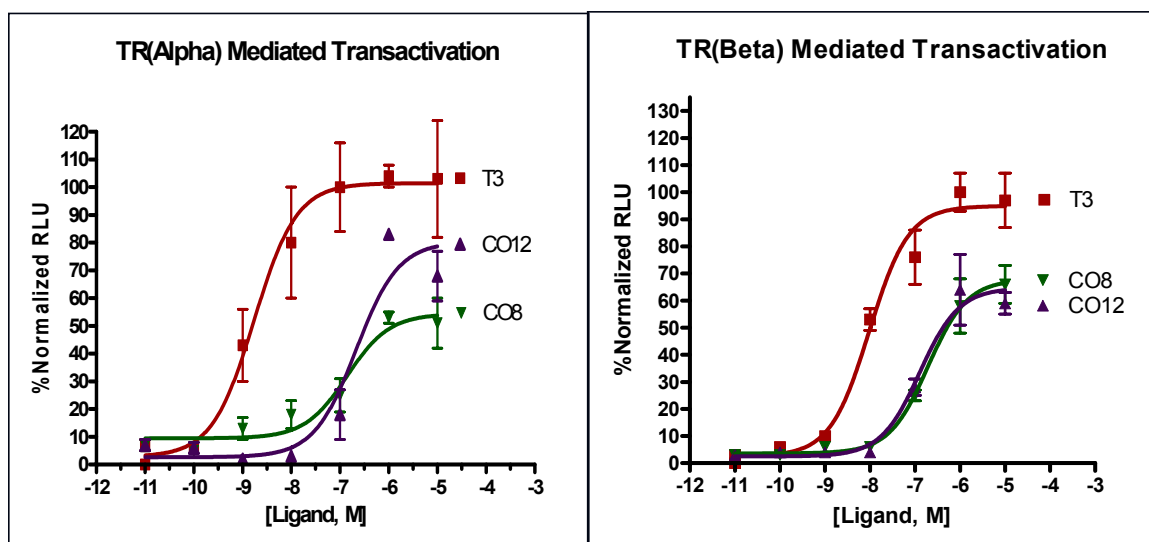
compared to T_3 , and was about 80-fold $TR\beta$ -selective. CO12, bearing a dichloroimidazole, was also reasonably $TR\beta$ -selective and was among one of the most avid compounds for $TR\beta$. The ethylene linker of CO16 and CO17 nearly ablated binding all together. Overall, the best compounds generally bound with 10-100-fold weaker affinity than T_3 and only $TR\beta$ -selectivity was observed, suggesting that a different approach must be employed in order to generate $TR\alpha$ -selective thyromimetics.

2.5.2 Transactivation Analysis

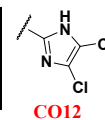
After screening compounds CO1-CO17 and CO20 in the competitive binding assay, several compounds were selected based on their binding affinity and $TR\beta$ -selectivity to undergo testing for their transcriptional activity in cells. Ligands CO8, CO10, CO12, and CO14 exhibited the best combinations of affinity and $TR\beta$ -selectivity; therefore, they were tested for transactivation to see if their desirable binding properties would translate into desirable functional properties.

After transactivation analysis, it was apparent that the best of the $TR\beta$ -selective compounds could be split into two groups: 1) Unselective partial agonists and 2) $TR\beta$ -selective agonists showing selectivity in fold induction by inducing luciferase to a greater extent when tested with $TR\beta$. Compounds CO8 and CO12 both showed partial agonism with $TR\alpha$ and $TR\beta$ (Fig. 2.16), with potencies of 140 – 170 nM in $TR\alpha$ to 380 – 280 nM respectively for $TR\beta$. Considering that T_3

Figure 2.16 Transactivation data for CO8 and CO12



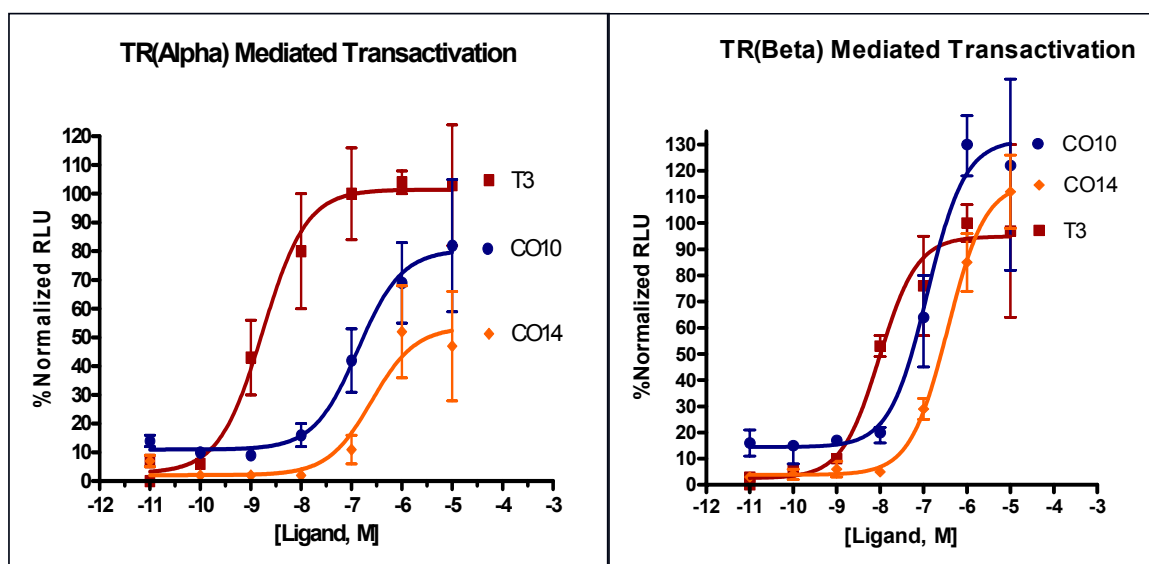
Compound	EC50, nM (alpha)	EC50, nM (beta)	%E(alpha)	%E(beta)
T ₃	2	7.5	100	100
CO8	139	378	54	67
CO12	173	273	80	64



activates from this TRE to a different extent with TR α and TR β , this slight difference in TR α vs. TR β activation for CO8 and CO12 does not represent selective activation. Also, these compounds are partial agonists for both TRs; however, they agonize to 54% the efficacy of maximal T₃ activation at best, indicating that these compounds are not likely to achieve antagonism through partial agonism.

The best compounds from the series are CO10 and CO14 (Fig. 2.17), as they demonstrated TR β -selectivity in terms of efficacy. After testing with TR α and TR β , CO10 transactivated unselectively with EC₅₀ values of 130 – 120 nM

Figure 2.17 Transactivation data for CO10 and CO14



Compound	EC50, nM (alpha)	EC50, nM (beta)	%E(alpha)	%E(beta)
T ₃	2	7.5	100	100
CO10	134.0	122	80	130
CO14	232	407	53	115

respectively; however, in TR β , CO10 demonstrated 130% E compared to only 80% when tested with TR α . Similarly, CO14 recapitulated this trend, with potencies of 230 – 400 nM and %E values of 50 – 115 when tested with TR α and TR β respectively.

Unfortunately, although compound CO14 had the highest binding affinity, this did not translate into potency, although CO14 was a full agonist, demonstrating enhanced activity compared to T₃. It is surprising that CO10 was the most potent agonist against TR β , and with an EC₅₀ value greater than 100 nM, it is unlikely

that this compound will have utility as a pharmacologic probe of TR biology nor as a therapeutic agent particularly as it is unselective.

2.6 Conclusion

Applying a bioisosteric replacement strategy whereby the C₁ position of the thyronine scaffold is substituted with heterocycles or carbocycles with or without a linker revealed several trends after binding analysis. Firstly, ligands bearing unsubstituted heterocyclic rings did not demonstrate selectivity; however, electron withdrawing groups such as nitro and carboxyl conferred TR β -selectivity, but with a decrease in binding affinity. Presenting heterocycles into the ligand binding pocket by attaching them to the C₁ position with an ethyl or ethylene linker ablated binding. Several TR β -selective ligands (CO8, CO10, CO12, and CO14) with the greatest binding affinity were subjected to transactivation analysis and the data showed that ligands CO8 and CO12 acted as unspecific partial agonists, agonizing to 54% the efficacy of maximal T₃ activation at best. Compounds CO10 and CO14, the most promising TR β -selective ligands from this panel, demonstrated EC₅₀ values greater than 100 nM and showed greater efficacy when tested with TR β rather than TR α .

2.7 References

1. Greenspan, F.S. (2001) The thyroid gland. In *Basic and Clinical Endocrinology* (Greenspan, F.S. and Gardner, D.G., Eds.) 6th ed., pp. 201-271, Lange Medical Books/McGraw-Hill, New York.
2. Utiger, R. (2001) The thyroid: physiology, thyrotoxicosis, hypothyroidism, and the painful thyroid. In *Endocrinology and Metabolism* (Felig, P. and Frohman, L., Eds.) 4th ed., pp. 261-347, McGraw-Hill, New York.
3. Franklin, J. (2000) Metabolic changes in thyrotoxicosis. In *Werner & Ingbar's The Thyroid: A Fundamental and Clinical Text* (Braverman, L.E. and Utiger, R.D., Eds.) 8th ed., pp. 667-672, Lippincott Williams & Wilkins, Philadelphia.
4. Malloy, M. and Kane, J. (2001) Agents used in hyperlipidemia. In *Basic and Clinical Pharmacology* (Katzung, B., Ed.) 8th ed., pp. 581-595, McGraw-Hill, New York.
5. Yen, P. (2003) Molecular basis of resistance to thyroid hormone. *Trends Endocrinol. Metab.* 14, pp. 327-333.
6. Suzuki, H. and Cheng, S.-Y. (2003) Compensatory role of thyroid hormone receptor TR α 1 in resistance to thyroid hormone: study in mice with a targeted mutation in the TR β gene and deficient in TR α 1. *Mol. Endo.* 17, pp. 1647-1655.

7. Flamant, F. and Samarut, J. (2003) Thyroid hormone receptors: lessons from knockout and knock-in mutant mice. *Trends Endocrinol. Metab.* 14, pp. 85-90.
8. Scanlan, T.S., Yoshihara, H., Nguyen, N.-H., and Chiellini, G. (2001) Selective thyromimetics: tissue-selective thyroid hormone analogs. *Curr. Opin. Drug Discov. Devel.* 4, pp. 614-622.
9. Yen, P. (2001) Physiological and molecular basis of thyroid hormone action. *Physiol. Rev.* 81, pp. 1097-1142.
10. Brent, G. (2000) Tissue-specific actions of thyroid hormone: insights from animal models. *Rev. Endocr. Metab. Disord.* 1, pp. 27-33.
11. Forrest, A., Hanebuth, E., Smeyne, R.J., et al. (1996) Recessive resistance to thyroid hormone in mice lacking thyroid hormone receptor beta: Evidence for tissue-specific modulation of receptor function. *EMBO J* 15, pp. 3006-3015.
12. Swanson, E., Gloss, B., Belke, D., et al. (2003) Cardiac expression and function of thyroid hormone receptor β and its PV mutant. *Endocrinology* 144, pp. 4820-4825.
13. Mai, W., Janier, M., Allioli, N., et al. (2004) Thyroid hormone receptor α is a molecular switch of cardiac function between fetal and postnatal life. *PNAS* 101, pp. 10332-10337.
14. Fraichard, A., Chassande, O., Plateroti, M., et al. (1997) The *T3R α* gene encoding a thyroid hormone receptor is essential for post-natal

- development and thyroid hormone production. *EMBO J* 16, pp. 4412-4420.
15. Wikstrom, L., Johansson, C., Salto, C., et al. (1998) Abnormal heart rate and body temperature in mice lacking thyroid hormone receptor α -1. *EMBO J* 17, pp. 455-461.
 16. Gothe, S., Wang, Z., Ng, L., et al. (1999) Mice devoid of all known thyroid receptors are viable but exhibit disorders of the pituitary-thyroid axis, growth, and bone maturation. *Genes Dev.* 13, pp. 1329-1341.
 17. Gauthier, K., Chassande, O., Plateroti, M., et al. (1999) Different functions of the thyroid hormone receptors TR α and TR β in the control of thyroid hormone production and post-natal development. *EMBO J* 18, pp. 623-631.
 18. Ortiga-Carvalho, T., Hashimoto, K., Pazos-Moura, C., et al. (2004) Thyroid hormone resistance in the heart: role of the thyroid hormone receptor β isoform. *Endocrinology* 145, pp. 1625-1633.
 19. Weiss, R., Korcarz, C., Chassande, O., et al. (2002) Thyroid hormone and cardiac function in mice deficient in thyroid hormone receptor- α or - β : an echocardiograph study. *Am. J. Physiol. Endocrinol. Metab.* 283, pp. E428-E435.
 20. Gullberg, H., Rudling, M., Saltó, C., et al. (2002) Requirement for thyroid hormone receptor β in T3 regulation of cholesterol metabolism in mice. *Mol. Endo.* 16, pp. 1767-1777.

21. Yen, P., Feng, X., Flamant, F., et al. (2003) Effects of ligand and thyroid hormone receptor isoforms on hepatic gene expression profiles of thyroid hormone receptor knockout mice. *EMBO reports* 4, pp. 581-587.
22. Schwartz, H., Trence, D., Oppenheimer, J., et al. (1983) Distribution and metabolism of L- and D-triiodothyronine (T3) in the rat: preferential accumulation of L-T3 by hepatic and cardiac nuclei as a probable explanation of the differential biological potency of T3 enantiomers. *Endocrinology* 113, pp. 1236-1243.
23. Ichikawa, K., Miyamoto, T., Kakizawa, T., et al. (2000) Mechanism of liver-selective thyromimetic activity of SK&F L-94901: evidence for the presence of a cell-type-specific nuclear iodothyronine transport process. *J. Endocrinol.* 165, pp. 391-397.
24. Baxter, J., Webb, P., Grover, G., and Scanlan, T. (2004) Selective activation of thyroid hormone signaling pathways by GC-1: a new approach to controlling cholesterol and body weight. *Trends Endocrinol. Metab.* 15, pp. 154-157.
25. Hennemann, G., Docter, R., Friesma, E., et al. (2001) Plasma membrane transport of thyroid hormones and its role in thyroid hormone metabolism and bioavailability. *Endocr. Rev.* 22, pp. 451-476.
26. Fujiwara, K., Adachi, H., Nishio, T., et al. (2001) Identification of thyroid hormone transporters in humans: different molecules are involved in a tissue-specific manner. *Endocrinology* 142, pp. 2005-2012.

27. Ribeiro, M.O., Carvalho, S.D., Schultz, J.J., et al. (2001) Thyroid hormone-sympathetic interaction and adaptive thermogenesis are thyroid hormone receptor isoform-specific. *J. Clin. Invest.* 108, 97-105.
28. Morkin, E., Ladenson, P., Goldman, S., et al. (2004) Thyroid hormone analogs for treatment of hypercholesterolemia and heart failure: Past, present, and future prospects. *J. Mol. Cell. Cardiol.* 37, pp. 1137-1146.
29. Jorgensen, E.C. (1978) Thyroid Hormones and Analogs. II. Structure activity relationships. In *Hormonal Proteins and Peptides* (Li, C.H., Ed.), p. 124, Academic Press, New York.
30. Underwood, A.H., Emmett, J.C., Ellis, D., et al. (1986) A thyromimetic that decreases plasma cholesterol levels without increasing cardiac activity. *Nature* 324, pp. 425-429.
31. Yokoyama, N., Walker, G.N., Main, A.J., et al. (1995) Synthesis and structure-activity relationships of oxamic acid and acetic acid derivatives related to L-thyronine. *J. Med. Chem.* 38, 695-707.
32. Ichikawa, K., Miyamoto, T., Kakizawa, T., et al. (2000) Mechanism of liver-selective thyromimetic activity of SK&F L-94901: evidence for the presence of a cell-type-specific nuclear iodothyronine transport process. *J. Endocrinol.* 165, pp. 391-397.
33. Taylor, A., Stephan, Z., Steele, R., and Wong, N. (1997) Beneficial effects of a novel thyromimetic on lipoprotein metabolism. *Mol. Pharmacol.* 52, pp. 542-547.

34. Hayashi, M., Ohnota, H., Tamura, T., et al. (2004) Inhibitory effects of KAT-681, a liver-selective thyromimetic, on development of hepatocellular proliferative lesions in rats induced by 2-acetylaminofluorene and partial hepatectomy after diethylnitrosamine initiation. *Arch. Toxicol.* 78, pp. 460-466.
35. Hayashi, M., Tamura, T., Kuroda, J., et al. (2005) Different inhibitory effects in the early and late phase of treatment with KAT-681, a liver-selective thyromimetic, on rat hepatocarcinogenesis induced by 2-acetylaminofluorene and partial hepatectomy after diethylnitrosamine initiation. *Toxicol. Sci.* 84:22-28.
36. Dow, R., Schneider, S., Paight, E., et al. (2003) Discovery of a novel series of 6-azauracil-based thyroid hormone receptor ligands: potent, TR β subtype-selective thyromimetics. *Bioorg. Med. Chem. Lett.* 13, pp. 379-382.
37. Kissei Pharmaceutical Co. (Shiohara H, Nakamura T, Kikuchi N, et al.): Novel thyroid hormone receptor ligand, medicinal compositions containing the same and use thereof. EP-1471049A1 (2004).
38. Karo Bio (Malm J, Koehler K, Collard G, et al.): Preparation of indole derivatives as new thyroid receptor agonist ligands and methods of use. WO-2004018421 (2004).
39. Collazo, A.-M.G., Koehler, K.F., Garg, N., et al. (2006) Thyroid receptor ligands. Part 5: Novel bicyclic agonist ligands selective for the thyroid hormone receptor β . *Bioorg. Med. Chem. Lett.* 16, pp. 1240-1244.

40. Haning, H., Woltering, M., Mueller, U., et al. (2005) Novel heterocyclic thyromimetic. *Bioorg. Med. Chem. Lett.* 15, pp. 1835-1840.
41. Hangeland, J.J., Friends, T.J., Doweiko, A.M., et al. (2005) A new class of high affinity thyromimetics containing a phenyl-naphthylene core. *Bioorg. Med. Chem. Lett.* 15, pp. 4579-4584.
42. Baxter, J., Webb, P., Grover, G., and Scanlan, T. (2004) Selective activation of thyroid hormone signaling pathways by GC-1: a new approach to controlling cholesterol and body weight. *Trends Endocrinol. Metab.* 15, pp. 154-157.
43. Chiellini, G., Apriletti, J., Yoshihara, H., et al. (1998) A high-affinity subtype-selective agonist ligand for the thyroid hormone receptor. *Chem. Biol.* 5, pp. 299-306.
44. Trost, S., Swanson, E., Gloss, B., et al. (2000) The thyroid hormone receptor- β -selective agonist GC-1 differentially affects plasma lipids and cardiac activity. *Endocrinology* 141, pp. 3057-3064.
45. Wagner, R., Hubber, B., Shiao, A., et al. (2001) Hormone selectivity in thyroid hormone receptors. *Mol. Endo.* 15, pp. 398-410.
46. Baxter, J., Dillmann, W., West, B., et al. (2001) Selective modulation of thyroid hormone receptor action. *J. Steroid. Biochem. Mol. Biol.* 76, pp. 31-42.
47. Hennemann, G., Docter, R., Friesma, E., et al. (2001) Plasma membrane transport of thyroid hormones and its role in thyroid hormone metabolism and bioavailability. *Endocr. Rev.* 22, pp. 451-476.

48. Grover, G., Egan, D., Sleph, P., et al. (2004) Effects of the thyroid hormone receptor agonist GC-1 on metabolic rate and cholesterol in rats and primates: selective actions relative to 3,5,3'-triido-L-thyronine. *Endocrinology* 145, pp. 1656-1661.
49. Ye, L., Li, Y.-L., Mellstrom, K., et al. (2003) Thyroid Receptor Ligands. 1. agonist ligands selective for the thyroid receptor β 1. *J. Med. Chem.* 46, pp. 1580-1588.
50. Grover, G., Mellstrom, K., Ye, L., et al. (2003) Selective thyroid hormone receptor- β activation: a strategy for reduction of weight, cholesterol, and lipoprotein (a) with reduced cardiovascular liability. *PNAS* 100, pp. 10067-10072.
51. Borngraeber, S., Budny, M.-J., Chiellini, G., et al. (2003) Ligand selectivity by seeking hydrophobicity in thyroid hormone receptor. *PNAS* 100, pp. 15358-15363.
52. Hangeland, J., Doweiko, A., Dejneka, T., et al. (2004) Thyroid receptor ligands. part 2. thyromimetics with improved selectivity for the thyroid hormone receptor beta. *Bioorg. Med. Chem. Lett.* 14, pp. 3549-3553.
53. Webb, P., Nguyen, N.-H., Chiellini, G., et al. (2003) Design of thyroid hormone receptor antagonists from first principles. *J. Steroid. Biochem. Mol. Biol.* 83, pp. 59-73.
54. Nguyen, N.-H., Apriletti, J., Cunha-Lima, S., et al. (2002) Rational design and synthesis of a novel thyroid hormone antagonist that blocks coactivator recruitment. *J. Med. Chem.* 45, pp. 3310-3320.

55. Yoshihara, H., Apriletti, J., Baxter, J., Scanlan, T. (2001) A designed antagonist of the thyroid hormone receptor. *Bioorg. Med. Chem. Lett.* 11, pp. 2821-2825.
56. Chiellini, G., Nguyen, N.-H., Apriletti, J., et al. (2002) Synthesis and biological activity of novel thyroid hormone analogues: 5'-aryl substituted GC-1 derivatives. *Bioorg. Med. Chem. Lett.* 10, pp. 333-346.
57. Moore, J., Galicia, S., McReynolds, A., et al. (2004) Quantitative proteomics of the thyroid hormone receptor-coregulator interactions. *J. Biol. Chem.* 279, pp. 27584-27590.
58. Lim, W., Nguyen, N.-H., Yang, H.Y., et al. (2002) A thyroid hormone antagonist that inhibits thyroid hormone action *in vivo*. *J. Biol. Chem.* 277, pp. 35664-35670.
59. Hedfors, Å., Appelqvist, T., Carlsson, B., et al. (2005) Thyroid receptor ligands. 3. Design and Synthesis of 3,5-dihalo-4-alkoxyphenylalkanoic acids as indirect antagonists of the thyroid hormone receptor. *J. Med. Chem.* 48, 3114-3117.
60. Adamson, C., Maitra, N., Bahl, J., et al. (2004) Regulation of gene expression in cardiomyocytes by thyroid hormone and thyroid hormone analogs 3,5-diiodothyropropionic acid and CGS 23425 [N-[3,5-dimethyl-4-(4'-hydroxy-3'-isopropylphenoxy)-phenyl]-oxamic acid]. *J. Pharmacol. Exp. Ther.* 311, pp. 164-171.

61. Morkin, E., Pennock, G., Spooner, P., et al. (2002) Clinical and experimental studies on the use of 3,5-diiodothyropropionic acid, a thyroid hormone analog, in heart failure. *Thyroid* 6, pp. 527-533.
62. Tomanek, R., Zimmerman, M., Suvarna, P., et al. (1998) A thyroid hormone analog stimulates angiogenesis in the post-infarcted rat heart. *J. Mol. Cell. Cardiol.* 30, pp. 923-932.
63. Zheng, W., Weiss, R., Wang, X., et al. (2004) DITPA stimulates arteriolar growth and modifies myocardial postinfarction remodeling. *AJP-Heart* 286, pp. 1994-2000.
64. Wang, X., Zheng, W., Christensen, L., and Tomanek, R. (2003) DITPA stimulates bFGF, VEGF, angiopoietin, and Tie-2 and facilitates coronary arteriolar growth. *AJP-Heart* 284, pp. 613-618.
65. Spooner, P., Thai, H., Goldman, S., and Gaballa, M. (2004) Thyroid hormone analog, DITPA, improves endothelial nitric oxide and beta-adrenergic mediated vasorelaxation after myocardial infarction. *J. Cardiovasc. Pharmacol.* 44, pp. 453-459.
66. van Beeren, H., Jong, W., Kaptein, E., et al. (2003) Dronedarone acts as a selective inhibitor of 3,5,3'-triiodothyronine binding to thyroid hormone receptor- α 1: *in vitro* and *in vivo* evidence. *Endocrinology* 144, pp. 552-558.
67. van Beeren, H., Bakker, O., and Wiersinga, W. (1996) Structure-function relationship of the inhibition of the 3,5,3'-triiodothyronine binding to the α 1- and β 1-thyroid hormone receptor by amiodarone analogs. *Endocrinology* 137, pp. 2807-2814.

68. Pantos, C., Mourouzis, I., Malliopoulou, V., et al. (2005) Dronedarone administration prevents body weight gain and increases tolerance of the heart to ischemic stress: a possible involvement of thyroid hormone receptor $\alpha 1$. *Thyroid* 15, pp. 16-22.
69. Jorgensen, E.C. (1978) Thyroid Hormones and Analogs. I. Synthesis, Physical Properties, and Theoretical Calculation. In *Hormonal Proteins and Peptides* (Li, C.H., Ed.), pp. 57-58, Academic Press, New York.
70. Yoshihara, H.A.I., Apriletti, J.W., Baxter, J.D., and Scanlan, T.S. (2003) Structural Determinants of Selective Thyromimetics. *J. Med. Chem.* 46, pp. 3152-3161.
71. Ishiyama, T., Murata, M., and Miyaura, N. (1995) Palladium (0)-catalyzed cross-coupling reaction of alkoxydiboron with haloarenes: A direct procedure for arylboronic esters. *J. Org. Chem.* 60, pp. 7508-7510.
72. Mitchell, T.N. (1992) Palladium-catalysed reactions of organotin compounds. *Synthesis* 1992, pp. 803-815.
73. Ebisawa, M., Inoue, N., Fukasawa, H., et al. (1999) Thiazolidinediones with thyroid hormone receptor agonistic activity. *Chem. Pharm. Bull.* 47, 1348-1350.
74. Hart, M., Suchland, K., Miyakawa, M., et al. (2006) Trace amine receptor-associated agonists: synthesis and evaluation of thyronamines and related analogues. *J. Med. Chem.* 49, 1101-1112.

75. Evans, D., Katz, J., and West, T. (1998) Synthesis of diaryl ethers through the copper-promoted arylation of phenols with arylboronic acids - an expedient synthesis of thyroxine. *Tet. Lett.* 39, 2937-2940.
76. Renaldo, A.F., Labadie, J.W., and Stille, J.K. (1998) Palladium-catalyzed coupling of acid chlorides with organotin reagents: ethyl (e)-4-(4-nitrophenyl)-4-oxo-2-butenolate [2-butenic acid, 4-(4-nitrophenyl)-4-oxo-, ethyl ester, (e)-]. In *Organic Syntheses* (Aslanian, R., Smith, C.A., and Kende, A.S., Eds.) 67, p. 87.
77. Brucker, S., Abraham, E., Klotz, P., and Suffert, J. (2002) Cascade cyclization: An easy access to highly unsaturated polycyclic ring systems through a tandem Stille/[4+2] reaction under mild conditions. *Org. Lett.* 4, pp. 3391-3393.
78. Ocasio, C.A. and Scanlan, T.S. (2006) Design and characterization of a thyroid hormone receptor α (TR α)-specific agonist. *ACS Chem. Biol.* 1, 585-593.
79. Bourne, H.R. and von Zastrow, M. (2001) Drug receptors and pharmacodynamics. In *Basic and Clinical Pharmacology* (Katzung, B.G., Ed.) 8th ed., pp. 9-34, McGraw-Hill, New York.

CHAPTER THREE

Design and Characterization of CO23 – The First Thyromimetic with TR α -Specific Effects *In vitro* and *In vivo*

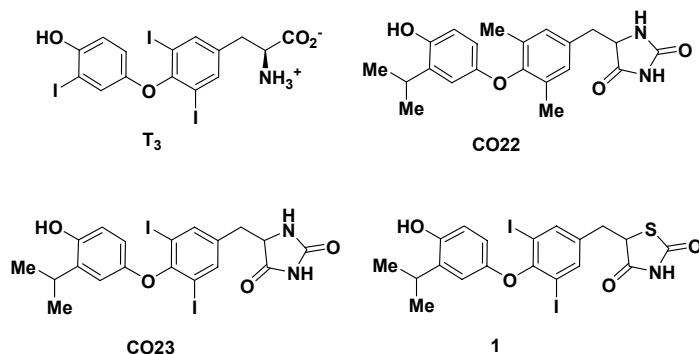
3.1 Overview

*Although the in vitro analysis of a small panel of ligands, CO1-CO17 and CO20, did not elucidate any ligands with significant effects, there was one ligand, CO22, that showed TR α -specificity when tested against TR α and TR β for transcriptional activity. CO22 itself was not a potent agonist; however, the SAR data shed light on how to improve the effectiveness of the CO22 core structure. It was surmised that the hydantoin moiety, an imidazolidinedione, conferred TR α -specificity, and hence the inner-ring methyl groups of CO22 were replaced with iodides, similar to a thyromimetic with a thiazolidinedione linked to the C₁ position with a methylene linker. This change in the inner-ring of CO22 led to an increase in potency and retained some TR α -specificity. As a result of its superior in vitro activity, the resulting thyroid hormone analogue, CO23, was tested on *Xenopus laevis* tadpoles in order to access its in vivo effects. Tadpoles precociously induced to undergo metamorphosis by CO23 show morphogenic effects and effects on the rate of hind leg growth that correlate with the selective activation of TR α while lacking effects such as larval tissue and tail resorption that correlates with TR β activity.*

3.2 Design and Synthesis of CO23

The genesis of CO23 (Fig. 3.1) came about by first looking at a class of structurally related compounds, the TR β -selective agonists (1-6). All of these compounds were derivatized from the thyronine backbone of T₃ by modifying either the moiety in the C₁ region of the scaffold, consisting of a linker capped by an acid group (i.e. carboxylic, oxamic, and malonamic acids), or both the C₁ region and the 3' position of the outer-ring. It has been shown that placing large, hydrophobic groups in the 3' position improves the β -selectivity for this class of thyromimetic (3). It has also been reported that compounds with a phenyl-naphthylene core bind to TR β in the sub-nanomolar range and display low to modest selectivity for TR β . Interestingly, these thyromimetics are the first to display an SAR that diverges from other thyromimetics which are based on the biaryl ether core found in the thyronine backbone of T₃ (7).

Figure 3.1 Structures of CO22 and CO23



After surveying a list of β -selective agonists, it was observed that heterocycles were underutilized in generating chemical diversity at the C₁ region, with few exceptions (5,6,8). Recent examples of thyromimetics with heterocycles in the C₁ region and outer-ring include thyromimetics that incorporate inner-ring fused quinoline-2-carboxylates and indole-2-carboxylates in the C₁ region and indoles and indazoles forming heterocycle-fused outer-rings (9,10). Despite these examples, thyromimetics with use in the clinic and as pharmacologic probes of TR biology containing heterocycles are rare, and hence the infrequent use of heterocycles in thyromimetic design coupled with their relatively low cost and availability, chemical diversity (particularly with respect to pK_a), and ease of synthetic incorporation into the C₁ region prompted the synthesis of a small panel of thyroid hormone analogues bearing heterocycles at the 1 position with or without a linker. The halogen-free 3,5-dimethyl, 3'-isopropyl inner- and outer-ring substitution pattern was selected for this collection of thyroid hormone analogues due to ease of synthesis. An *in vitro* evaluation of a small panel of thyroid hormone analogues identified one lead compound, CO22 (Fig. 3.1).

3.2.1 Replacement of Inner-Ring Methyl Groups with Iodides

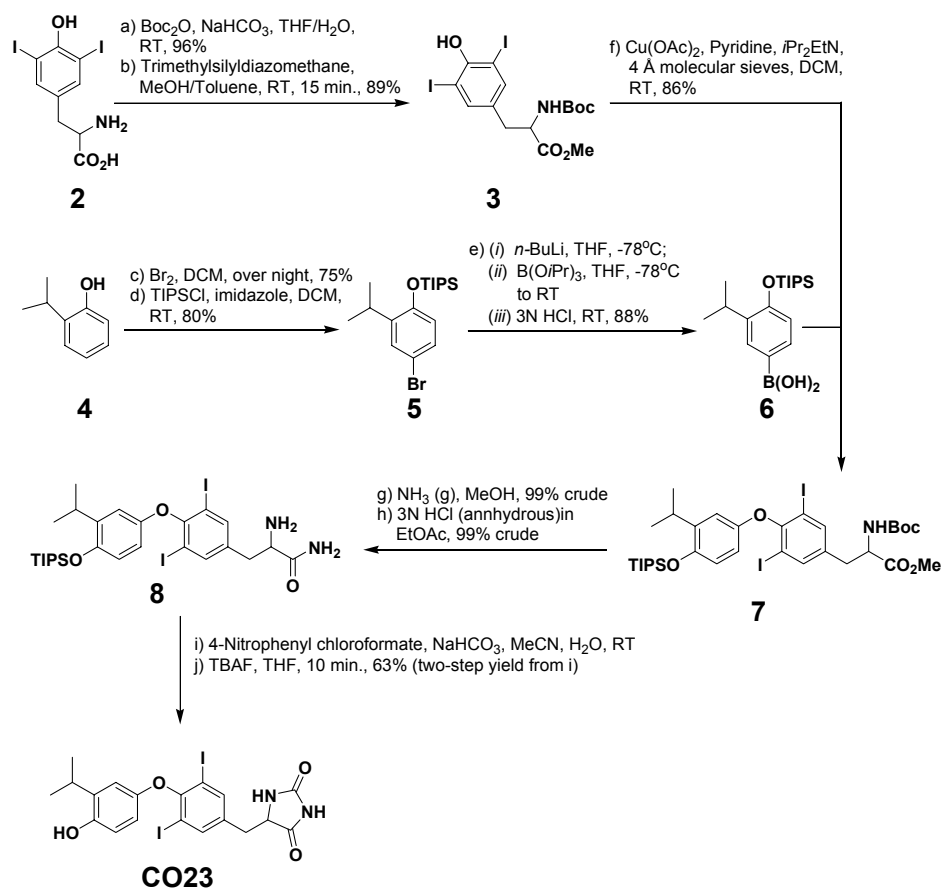
Although CO22 showed significantly lower potency and efficacy when assayed for TR β -induced transactivation, the structure-activity data revealed a way to circumvent the problem in potency of CO22. A similar thyroid hormone analogue, **1** (Fig. 3.1) displaying an EC₅₀ value of ~6 nM when tested for TR α -

induced transactivation in COS-1 cells, is different from CO22 in two ways: 1) There is a thiazolidinedione in the C₁ region instead of an imidazolidinedione; and 2) the inner-ring consists of iodides rather than methyl groups (6). Although this compound is structurally similar to CO23, it is unknown whether this compound displays TR α -specificity *in vitro* as it was not tested for TR β -induced transactivation in COS-1 cells. In terms of CO23, the imidazolidinedione was deemed necessary for conferring TR α -specificity, and thus we modified the inner-ring of CO22 by replacing the methyl groups with iodides (Scheme 3.1).

3.2.2 Synthesis of CO23

Replacement of the inner-ring methyl groups with iodides was accomplished by coupling of a Boc-protected diiodotyrosine methyl ester (**3**) with a TIPS-protected 4-hydroxy, 3-isopropylphenyl boronic acid (**6**) resulting in the biaryl ether intermediate **7** (11-14). Subsequent amidation of the methyl ester and deprotection of the Boc group set up the amino acid amide side chain (**8**) for cyclization into the imidazolidinedione by 4-nitrophenyl chloroformate and water (11,15,16). The synthesis of CO23 was finalized by deprotection of the TIPS group with TBAF (Scheme 3.1).

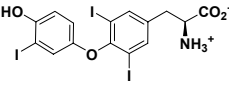
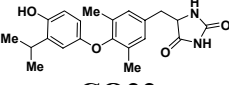
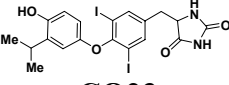
Scheme 3.1 Synthesis of CO23



3.3 *In vitro* Analysis of CO22 and CO23: Binding and Transactivation Against Human and *Xenopus* TRs

CO22 displays modest binding affinity and potency, but at the highest concentration is as efficacious as T₃ when tested for TR α -induced transactivation in U2OS cells (Table 3.1, Fig. 3.2a). In fact, at the highest concentration tested (10 μ M), transcriptional activity did not plateau and it displayed about half the efficacy of T₃, indicating that CO22 is a poor agonist against TR β (Fig. 3.2b).

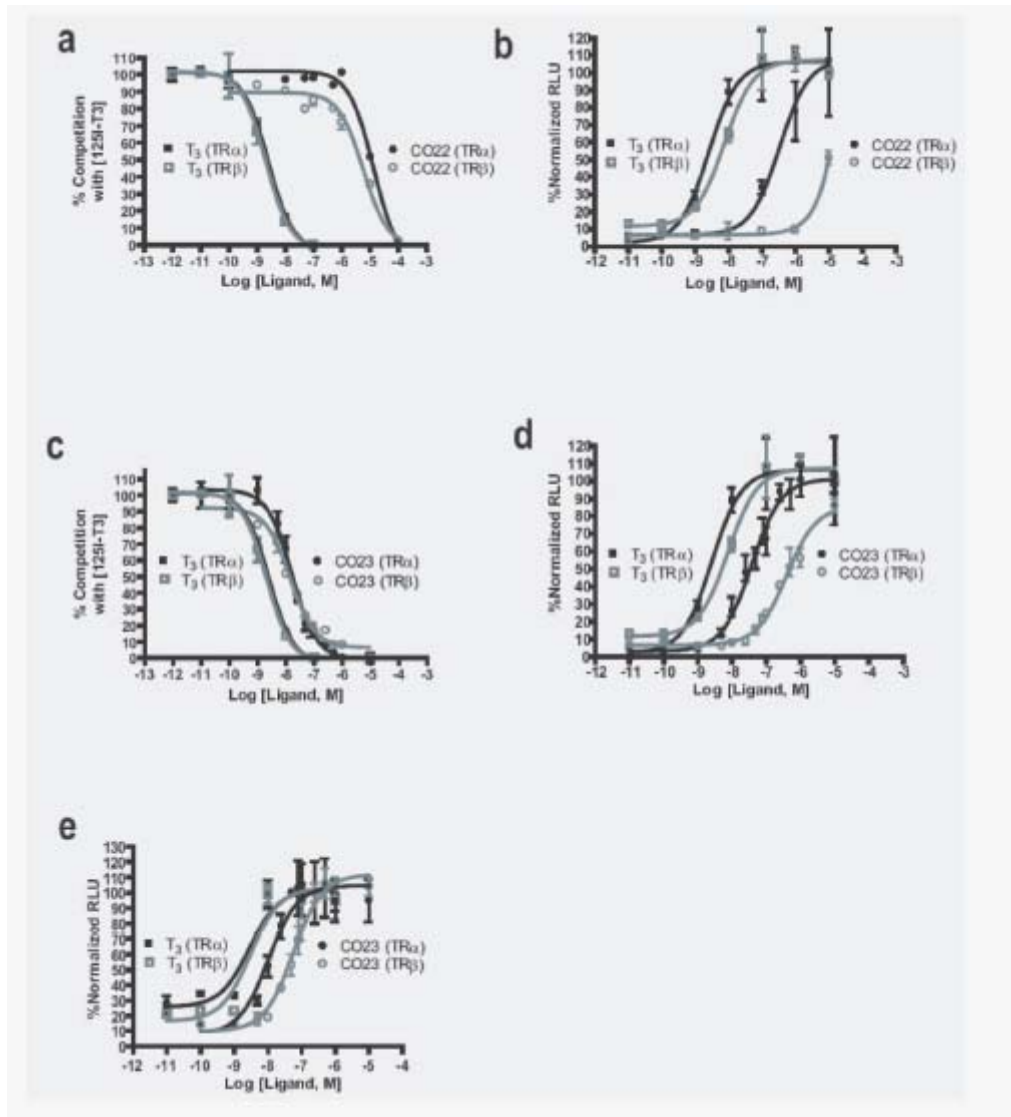
Table 3.1 Binding affinity and potency of CO22 and CO23

Compound	<u>K_d and EC_{50} values (nM)</u>					
	<u>Binding affinity (K_d)^a</u>		<u>Transactivation in U2OS cells (EC_{50})^b</u>		<u>Transactivation in HeLa cells (EC_{50})^b</u>	
	TR α	TR β	TR α	TR β	TR α	TR β
 T₃	0.058	0.081	2.4 ± 0.4	11 ± 2	2.4 ± 0.5	2.4 ± 0.5
 CO22	286 ± 27	280 ± 102	3870 ± 1	NA ^c	NA ^c	NA ^c
 CO23	1.2 ± 0.2	1.7 ± 0.3	34 ± 4	390 ± 3	11 ± 1	58 ± 1

^aDetermined by means of an ¹²⁵I-T₃ competitive binding assay and data is reported as the mean K_d ± standard error of the mean, $n=3$. ^bDetermined through use of a TRE-driven dual-luciferase reporter assay in U2OS or HeLa cells and the data is reported as the mean EC_{50} value ± standard error of the mean, $n=3$ (T₃, CO22, and CO23 in HeLa cells) and $n=6$ (CO23 in U2OS cells). ^cNA, not applicable.

CO23 proved superior to CO22 with respect to binding and transactivation as it exhibits a >200-fold improvement in binding affinity as well as a >100-fold improvement in potency (as determined by transactivation in U2OS cells) compared to CO22 (Table 3.1, Fig. 3.2, panels c and d). Although CO23, like CO22, shows no preference in binding to TR α_1 in a ¹²⁵I-T₃ competitive binding assay, it shows selective activation of TR α_1 in a DR4-driven dual-luciferase reporter assay using U2OS cells (Fig. 3.2, panels c and d). Note that the replacement of the inner-ring methyl groups with iodides results in diminished TR α -selectivity (Fig. 3.2d). It is likely that the polarizability and increased

Figure 3.2 *In vitro* evaluation of CO22 and CO23



(a & c) ^{125}I -T₃ competitive binding curves for T₃, CO22, and CO23 against hTR α_1 and hTR β_1 . (b & d) A TRE-driven dual-luciferase reporter assay showing transactivation curves for T₃, CO22, and CO23 against hTR α_1 and hTR β_1 in U2OS cells. (e) A TRE-driven dual-luciferase reporter assay showing transactivation curves for T₃ and CO23 against hTR α_1 and hTR β_1 in HeLa cells. Plots show mean of triplicates with s.d.

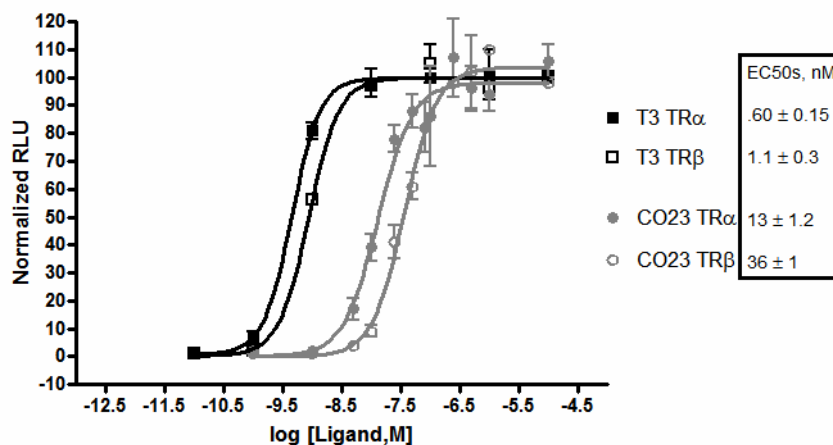
electronegativity of iodides favor binding to the TR binding pocket in a steric and electronic sense, making it more potent to both receptors. However, the methyl groups, which are smaller and less polarizable and electronegative than iodides,

may cause negative interactions that decrease both binding affinity and transactivation through TR, but affect TR α activation to a lesser extent than TR β activation. With this in mind, modification of the inner-ring substituents may serve to optimize the selectivity of an already selective thyromimetic, whereas the C₁ moiety may be responsible for setting the selectivity of a thyromimetic for TR α or TR β .

When determining selective activation of TRs using this cell line, it is necessary to compare the potency of the test ligand to the control ligand T₃ as T₃ shows a difference in activation of TR α ₁ and TR β ₁ using a synthetic TRE-driven luciferase reporter construct; CO23 selectively activated TR α ₁ by ~3-fold in U2OS cells relative to T₃ (Table 3.1, Fig. 3.2d). Due to this difference in T₃ activation of TR α ₁ and TR β ₁ in U2OS cells, it was necessary to directly determine the TR α ₁-selectivity of CO23. In HeLa cells, a cell line where T₃ is equipotent with respect to TR α ₁ and TR β ₁ activation, CO23 showed a ~5-fold preference in TR α ₁ activation (Table 3.1, Fig. 3.2e).

Compound CO23 shows impressive TR α -specificity *in vitro* using *Homo sapien* TRs; however, testing them against *Xenopus* TRs may be informative and provide further support for testing this compound on an *in vivo* system. Against xTR α in U2OS cells, CO23 displayed a reasonable EC₅₀ value of 13 ± 1 nM and appears selective as its potency diminished by about 3-fold when tested against TR β (Fig. 3.3).

Figure 3.3 CO23 transactivation against *Xenopus* TRs in U2OS cells



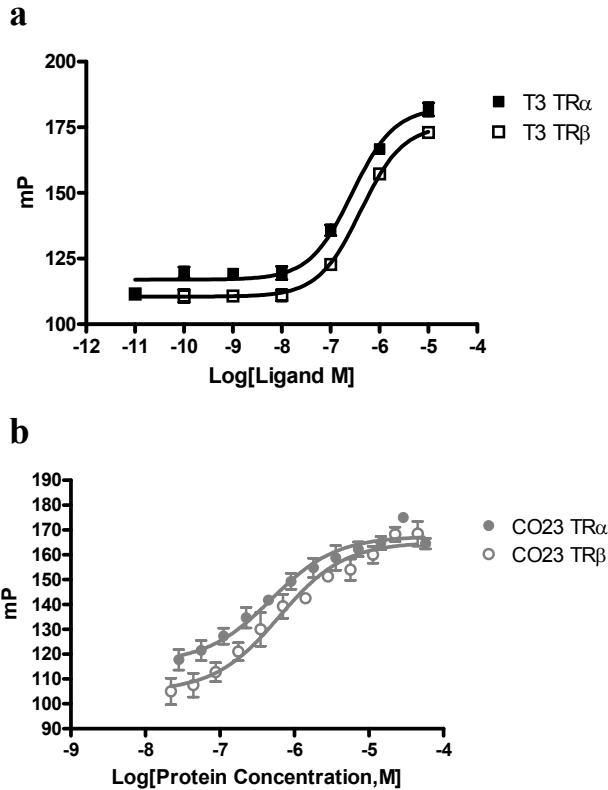
Three sets of EC₅₀ values were determined independently and the error is reported as \pm std. error of the mean.

3.4 A High-Throughput *In vitro* Binding Assay for Recruitment of Coactivator Peptides

It is not surprising due to the similarities between the TR α and TR β binding pockets that CO23 does not preferentially bind to one subtype over another.

This phenomenon, however, raises the question: How does the same compound elicit disparate transcriptional responses while binding to the same pocket of a receptor with equal affinity? Perhaps there are two energetically equivalent but different binding modes, and one of the binding orientations places helix 12 in the active agonist conformation such that the coactivator interface can form. In order to address this issue, CO23 was tested against TR α and TR β for its ability to recruit various coactivator peptides (17).

Figure 3.4 A high-throughput *in vitro* binding assay for recruitment of coactivator peptide SRC2-2



a) Recruitment of the peptide SRC2-2 by T_3 -liganded TR α and TR β .
b) Recruitment of the peptide SRC2-2 by CO23-liganded TR α and TR β .

Interestingly, CO23 was not capable of preferentially recruiting the coactivator peptide SRC2-2 containing the thiol reactive fluorophore 5-iodoacetamidofluorescein conjugated to an N-terminal cystein (Fig. 3.4a) (17). The peptide SRC2-2 was recruited to both TR α and TR β with K_d values of $0.44 \pm 0.06 \mu\text{M}$ and $0.59 \pm 0.04 \mu\text{M}$ respectively. Compared to peptide recruitment with T_3 saturated receptors, K_d values of $0.54 \pm 0.29 \mu\text{M}$ and $1.2 \pm 0.8 \mu\text{M}$ against TR α and TR β respectively, CO23 induced recruitment of peptide is only slightly

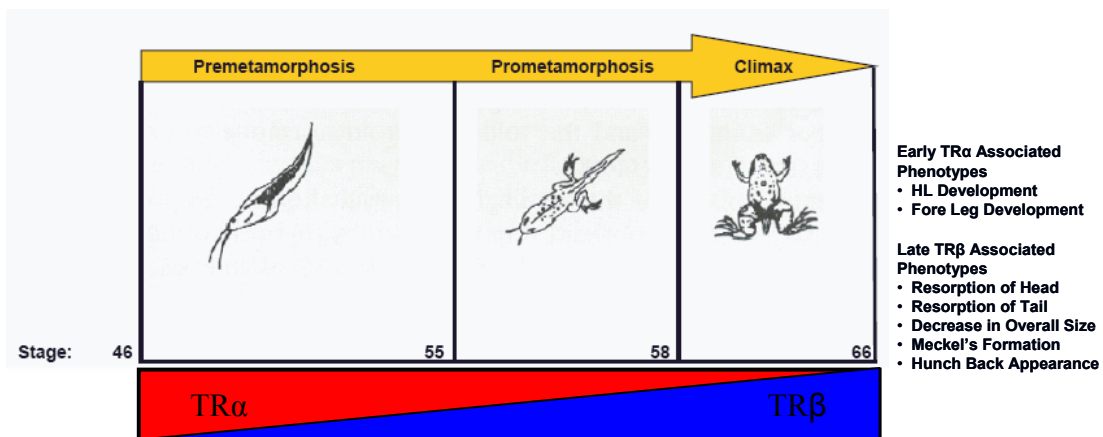
preferred by liganded TRs (Fig. 3.4, panels a and b); hence, this lack of difference in peptide recruitment does not substantiate a mechanism for the selective activation of TR α by CO23 by the preferential recruitment of coactivators.

3.5 *In vivo* Analysis of CO23

3.5.1 *Xenopus laevis* Tadpole Metamorphosis

After establishing the TR α -selectivity of CO23 *in vitro*, CO23 was further investigated in precociously induced amphibian metamorphosis. Amphibian metamorphosis occurs in three distinct stages: premetamorphosis, prometamorphosis, and climax (Fig. 3.5, 18). The premetamorphic tadpole

Figure 3.5 *Xenopus laevis* tadpole metamorphosis



primarily undergoes larval growth; however, the onset of prometamorphosis is marked by secretion of thyroid hormone from the developing thyroid gland giving rise to a number of morphological and biochemical changes such as hind limb (HL) proliferation, differentiation, and induction of genes including TR β (18,19). Fore leg emergence and the rapid and complete resorption of gills and tail mark metamorphic climax, and thus, completes the developmental program (Fig. 3.5, 18,19).

3.5.1.1 Amphibian Metamorphosis as a Model System for a TR α -Specific Thyromimetic

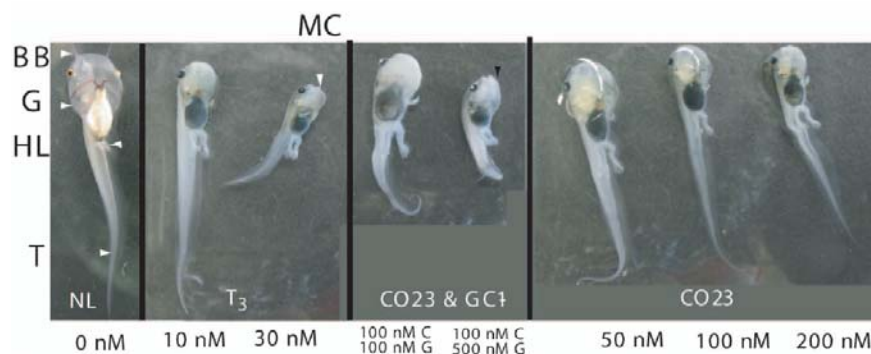
Using *Xenopus laevis* metamorphosis as a model system for studying biologically active and selective thyroid hormone agonists offers several advantages. Firstly, *Xenopus* and mammalian TRs, their heterodimer partners, and the receptor-associated coregulators are structurally and functionally well conserved (19). Furthermore, *Xenopus* metamorphosis has been extensively studied, and detailed molecular events throughout the process are well known (19). *Xenopus* TR α (xTR α) is expressed early on in the developing embryo and before the larval tadpole has a functional thyroid gland (19,20). Just prior to metamorphosis xTR α expression becomes widespread with locally high levels occurring in tissues that are destined to undergo proliferation and differentiation such as the limb buds, brain, and skin (19,20). The gene for TR β is itself an early-response gene of thyroid hormone and its mRNA levels increase as thyroid hormone levels

increase during the progression of metamorphosis, reaching a peak at metamorphic climax where death and resorption of larval tissue predominate (Fig. 3.5, 18,21). This correlation between metamorphic stage, TR-isoform expression, and morphogenic response is ideal for the study of a TR α -selective thyromimetic.

3.5.1.2 Effects of CO23 on Amphibian Metamorphosis

Stage-53/54 tadpoles treated with CO23 (50, 100, and 200 nM) experienced hind-limb growth as extensive as, or greater than, that of tadpoles treated with 30 nM T₃ after one-week (Fig. 3.6). In addition, CO23 treated tadpoles exhibited less tail, gill, and head resorption at concentrations (50 and 100 nM) that yielded greater or equal HL growth as compared to 30 nM T₃ treated tadpoles (Fig. 3.6).

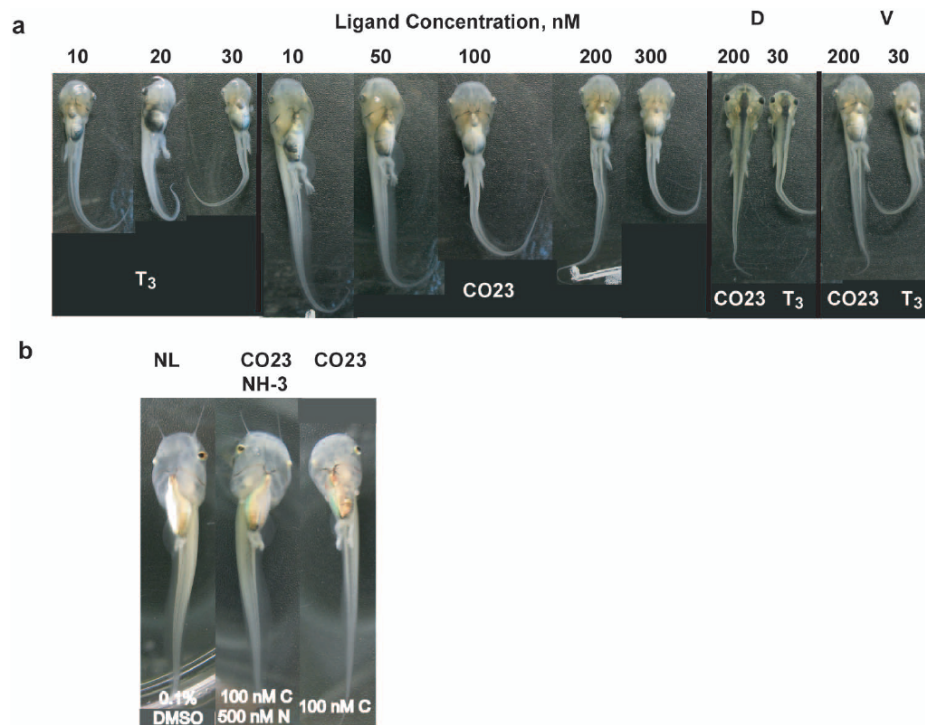
Figure 3.6 Effects of CO23 on amphibian metamorphosis



Induced metamorphosis of stage-53/54 tadpoles, n=3, treated for 7-days with vehicle, T₃ (10 and 30 nM), CO23 (50, 100, and 200 nM) and a combination of CO23 (100 nM) and GC-1 (100 and 500 nM).

A combination experiment whereby stage-53/54 tadpoles subjected to 100 nM CO23 and the TR β -selective agonist GC-1 (100 or 500 nM) showed that tadpoles treated with CO23 and a low dose of GC-1 resembled 10 nM T₃ treated tadpoles and tadpoles treated with CO23 and a high dose of GC-1 resembled 30 nM T₃ treated tadpoles (2,19) (Fig. 3.6). Therefore, this combination treatment rescues the β -isoform effects (resorption of gills, head, and bar bells, reorganization of the

Figure 3.7 Induction of metamorphosis by CO23 in a dose-dependent manner and inhibition of CO23 induced metamorphosis with NH-3



(a) Tadpoles, $n=3$, were treated for 4-days with T₃ and CO23 (C) in a dose-dependent manner. (b) Tadpoles, $n=3$, were treated for 5-days with 100 nM CO23 (C), 500 nM NH-3 (N), and a combination of 100 and 500 nM CO23 and NH-3 respectively; NH-3 blocks CO23 induced metamorphosis; experiment performed once. All images are to scale for ease of comparison.

brain, and development of Meckel's cartilage in the jaw area) at the CO₂ concentration tested.

3.5.1.3 Dose Response and Inhibition of CO₂ Induced Metamorphosis

Treating tadpoles in a dose-dependent manner with T₃ (10, 20, and 30 nM) and CO₂ (10, 50, 100, 200, and 300 nM) showed that after 4-days, concentrations of up to 200 nM CO₂ were more or just as effective as 30 nM T₃ in promoting HL development (Fig. 3.7a). The same CO₂ treated tadpoles displayed less head and tail resorption as did 30 nM T₃ treated tadpoles (Fig. 3.7a).

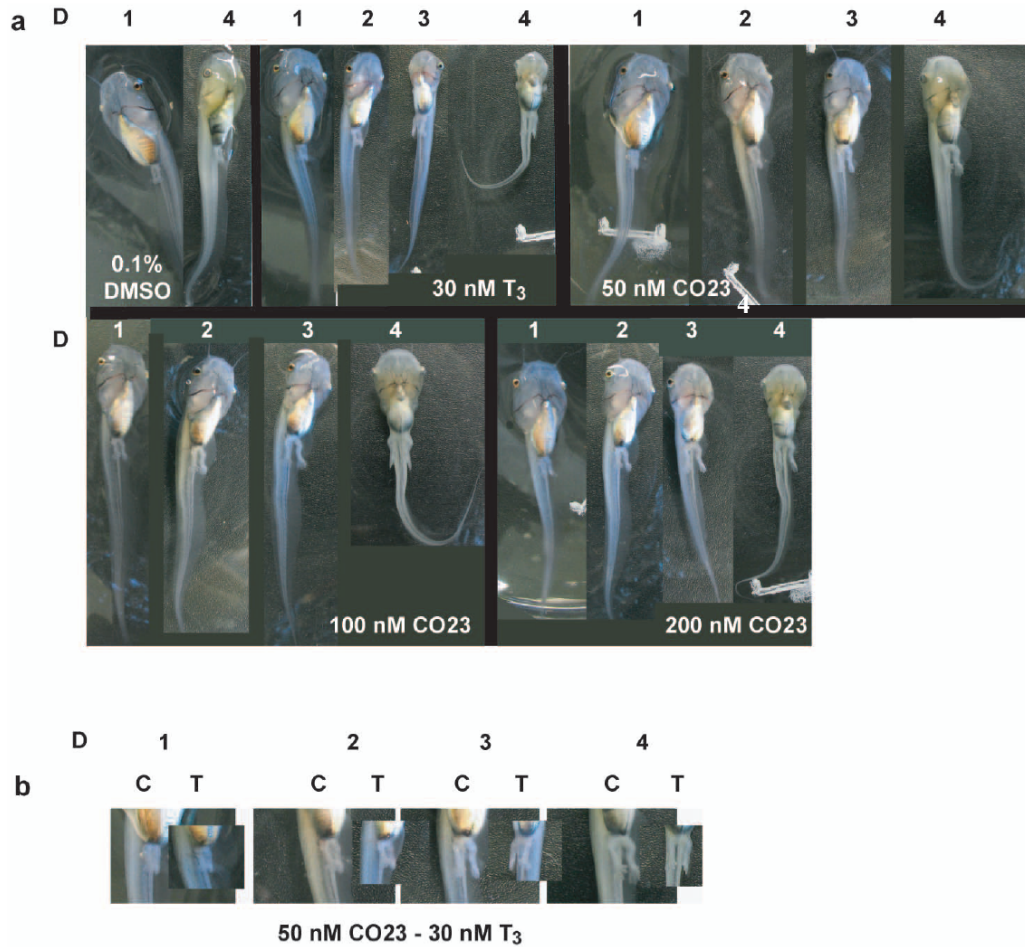
Furthermore, to show that CO₂ works through TR, tadpoles were treated with CO₂ and NH-3, a TR antagonist (19). Tadpoles treated with 100 nM CO₂ and 500 nM NH-3 displayed less HL and fore leg development and resorption compared to the CO₂ treated control and only slightly more HL development compared to the no ligand control after 5 days (Fig. 3.7b).

3.5.2 Hind Leg Growth

Perhaps one of the most dramatic effects on tadpoles upon CO₂ treatment is the rapid and extensive hind leg development. These changes also correlate with the presence of the TR α early gene. Albeit TR β is induced rapidly, in the early going, hind leg development is likely mediated by TR α with TR β having effects later on in the metamorphic process (16). Hence, tadpole metamorphosis

was monitored over 4 and 5 days for hind leg development to minimize the effects of TR β .

Figure 3.8 Progression of induced metamorphosis over four days



(a) Tadpoles, $n=3$, were treated with vehicle, T_3 , and CO₂₃ and their progression through metamorphosis was monitored every 24-h. (b) Closer comparison between 50 nM CO₂₃ (C) and 30 nM T_3 (T) induced HL development over 4-days. All images are to scale for ease of comparison

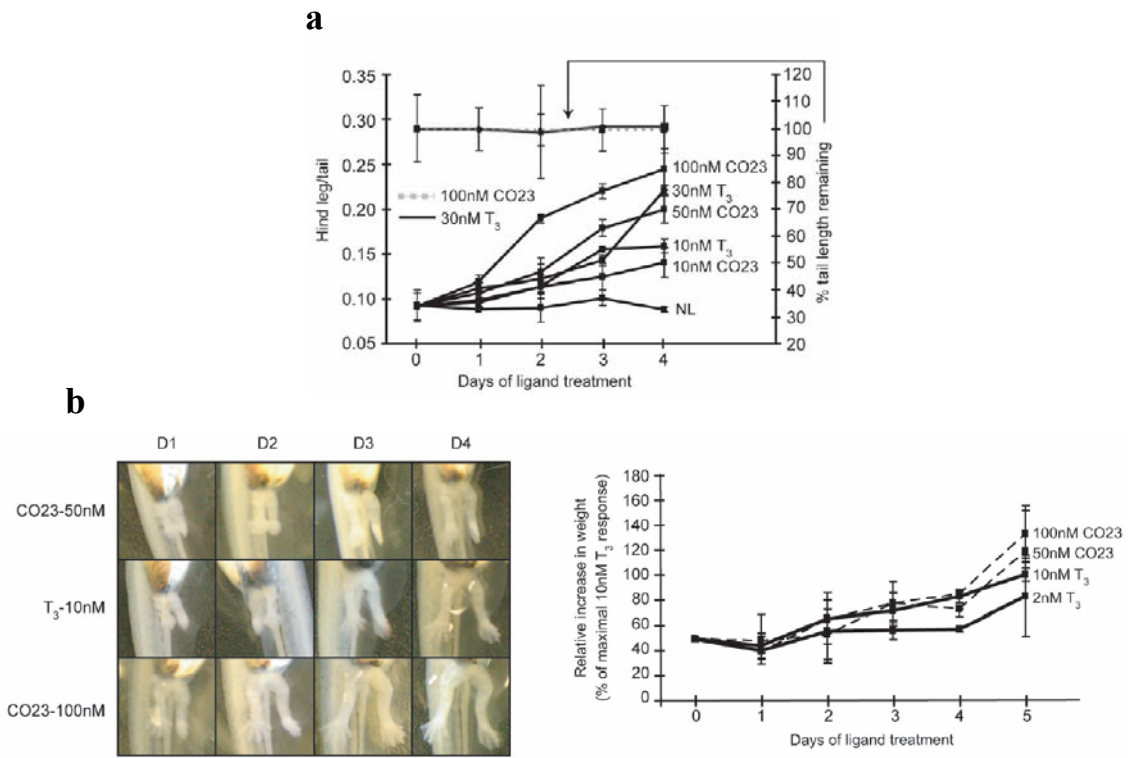
3.5.2.1 Four-Day Time Course and Hind Leg Growth

In a four-day time-course, tadpoles treated with CO₂ (50, 100, and 200 nM) showed more extensive hind-limb development after each successive day compared to tadpoles treated with 30 nM T₃ (Fig. 3.8a). Furthermore, it is apparent that on the fourth day, all CO₂ treated tadpoles showed less larval tissue resorption, particularly in the head. Zooming in on the hind legs of 50 nM CO₂ treatment tadpoles showed that their legs developed more rapidly after each consecutive day compared to 30 nM T₃ treated tadpoles (Fig. 3.8b).

3.5.2.2 Quantification of Hind Leg Growth

The effects of CO₂ on HL development were further explored by measuring the length and mass of growing HLs in response to CO₂ and T₃ treatment. In the first experiment, tadpoles treated with 100 nM CO₂ yielded the longest limbs after each successive day up to 4-days; whereas the progression in length of 50 nM CO₂ treated tadpole limbs were similar to those of 30 nM T₃ treated tadpole limbs (Fig. 3.9a). At low concentrations of T₃ and CO₂ (10 nM), HL lengthening was less rapid and extensive compared to the no ligand control (Fig. 3.9a). In the presence of a thyroid hormone biosynthesis inhibitor (methimazole), the HLs of CO₂ (50 and 100 nM) treated tadpoles grew more rapidly (100 nM CO₂) or in similar fashion (50 nM CO₂) than those of 10 nM T₃ treated tadpoles (Fig. 3.9b). It should be noted that 1 mM methimazole renders tadpoles much more sensitive to T₃.

Figure 3.9 Quantification of hind leg development



(a,b) HL development of tadpoles, $n=3$, treated with (b) and without (a) 1 mM methimazole, and vehicle, T₃ (2, 10, and 30 nM) and CO23 (10, 50, and 100 nM) up to 4- and 5-days as measured by HL/tail ratio (a) or relative increase in weight (b, represented as a percentage of the maximal T₃ response).

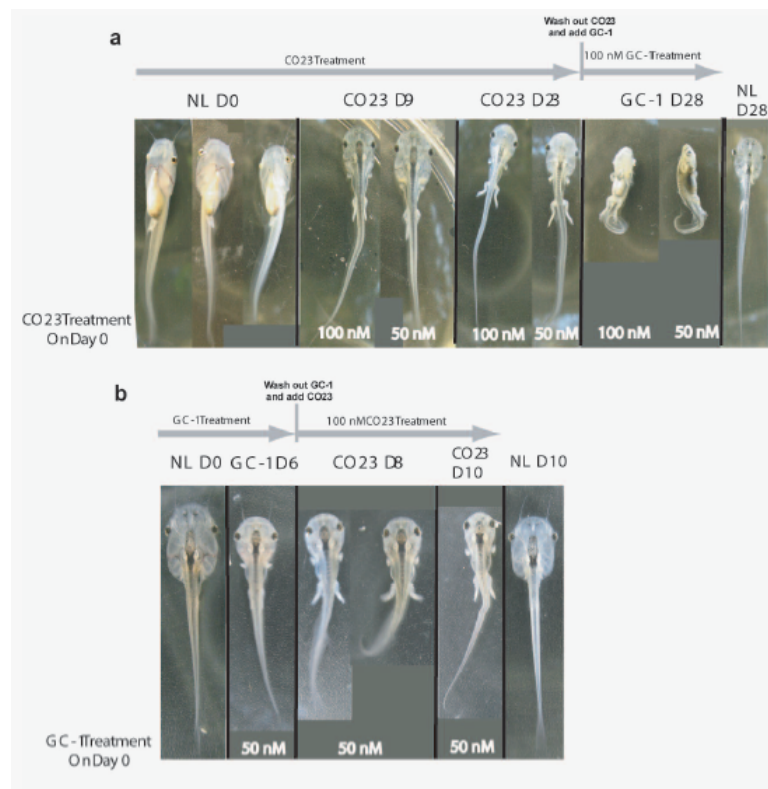
3.5.3 Temporal Separation of TR Subtype Mediated Effects on Morphogenesis

Further studies with CO23 and GC-1 indicated that sequential treatment with isoform-selective agonists can temporally control tadpole morphogenesis.

Treating tadpoles with CO23 (50 and 100 nM) for up to 23 days led to massive HL growth with slight resorption of head and gills, and replacing it with 100 nM GC-1 on the 23rd day led to the rapid resorption of head and tail, shrinking of

body size, and a hunch-back appearance after five days of treatment (Fig. 3.10a). Conversely, treating with 50 nM GC-1 and replacing it with 100 nM CO23

Figure 3.10 Temporal separation of TR subtype-mediated metamorphic effects



(a) Tadpoles were treated with vehicle for 28 days and 50 and 100 nM CO23 for 23-days, then placed in 100 nM GC-1 for 5-days more. (b) Tadpoles were treated with vehicle for 10 days and 50 nM GC-1 for 6-days, then placed in 100 nM CO23 for 4-days more. All images are to scale for ease of comparison.

yielded opposite results, although some limb growth did occur with GC-1 (Fig. 3.10b). In fact, limb growth resulting from GC-1 may be attributed to GC-1 activation of TR α . This is likely because in the early stages of tadpole metamorphosis TR α is the most abundant isoform present and its activation

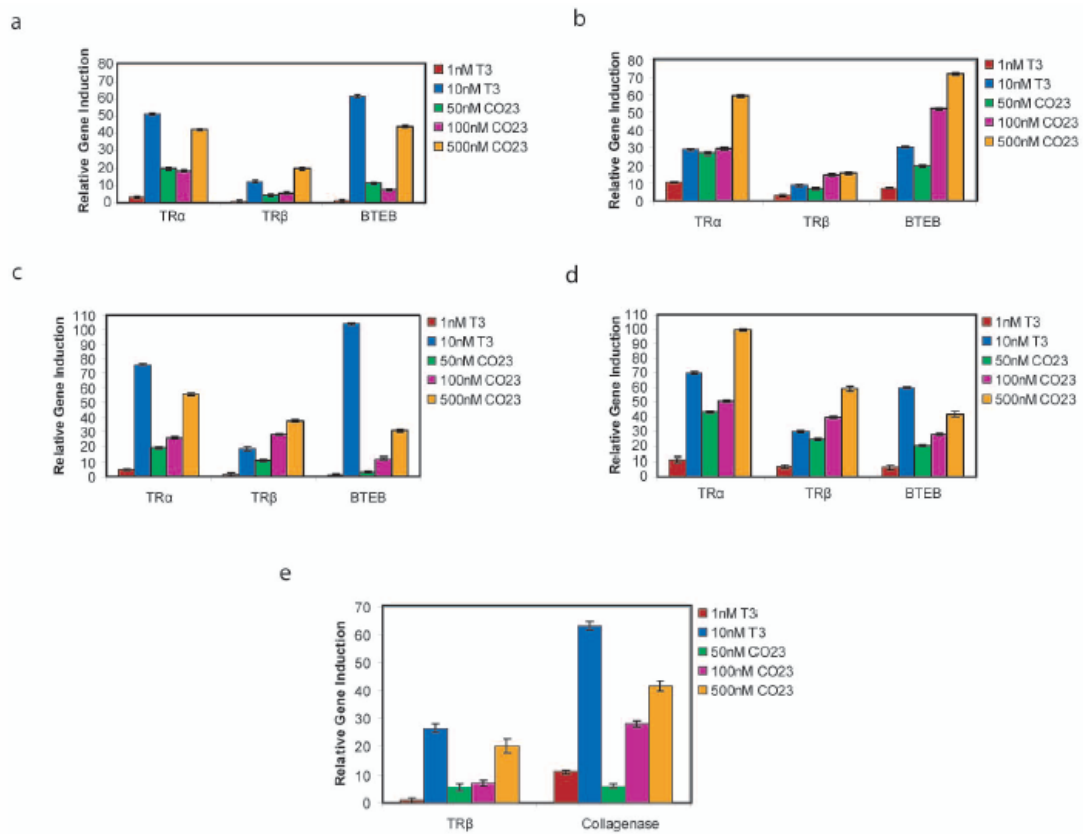
leads to induction of TR β , which then carries out the β -isoform effects upon activation by GC-1.

3.5.4 Quantitative Real-Time PCR Analysis

Next, we sought evidence for the TR α -specificity of CO23 by monitoring induction of early and late thyroid hormone responsive genes. This was done by performing quantitative rt-PCR on cDNAs derived from various *Xenopus* tissues. TR β and xBTEB, a zinc-finger transcription factor, are early response genes that are both rapidly induced by T₃, and in the case of xBTEB, by GC-1 as well (19,20). As such, xBTEB can be viewed as a TR β -induced early gene, and hence, its induction by CO23 should be less intense compared to T₃. The next gene of interest, collagenase-3, is a late responsive gene that is up-regulated in tail tissue and should not respond to CO23 as effectively as with T₃, particularly on day 6 (21). In this experiment CO23 acted as hypothesized; in HL and head tissue after 2 and 6 days of treatment, CO23 (100 and 500 nM) induced TR β levels were higher than those induced by T₃ (10 nM), except in HL tissue treated with 100 nM CO23 for 2 days (Fig. 3.11, panels a-d). In terms of xBTEB induction, CO23 (50, 100, and 500 nM) is less effective than T₃ (10 nM) (Fig. 3.11, panels a, c, and d). It is only in HL tissue after 6 days of treatment (late prometamorphosis) that CO23 (100 and 500 nM) induced xBTEB more effectively than T₃ (Fig. 3.11b). Up-regulation of the late response gene collagenase-3 by CO23 is also less effective at all concentrations compared to T₃

(10 nM) (Fig. 3.11e). As for xTR α , only the highest dose of CO₂3 (500 nM) was as effective as T₃ (10 nM) at its up-regulation (Fig. 3.11, panels a-d).

Figure 3.11 Quantitative real-time PCR of late and early TR-responsive genes in developing *X. laevis* tadpoles



(a-b) Relative gene induction by T₃ and CO₂3 in HL tissue after 2 (a) and 6 (b) days of treatment. (c-d) Relative gene induction by T₃ and CO₂3 in head tissue after 2 (c) and 6 (d) days of treatment. (e) Relative gene induction by T₃ and CO₂3 in tail tissue after 6 days of treatment.

3.6 Conclusion

CO23, the first potent thyromimetic with TR α -specific effects *in vitro* and *in vivo*, demonstrates 3 to 5-fold TR α -specificity in transactivation assays using U2OS and HeLa cells respectively. Despite not having an overwhelming preference for TR α activation, CO23 has profound effects on precocious *X. laevis* tadpole metamorphosis that correlates with the selective activation of TR α . For example, after 1 week of CO23 treatment tadpoles experienced equal and even greater hind leg growth, depending on the dose, compared to the T₃ treated control group. In terms of the rate of hind length growth, CO23 induced hind leg growth more so than T₃ after 4 and 5 day time-courses in the presence of or without methimazole, a T₃ biosynthesis inhibitor, and when treated in combination with GC-1 tadpoles resembled T₃ treated tadpoles.

In order to separate the contribution of each TR subtype to metamorphosis, tadpoles were sequentially treated with CO23 and GC-1. After 23 days of CO23 treatment followed by GC-1 treatment for five days, tadpoles experienced primarily hind length growth with some resorption of larval tissue in the head and tail then massive resorption of the head and tail and an overall decrease in body size and shape; after GC-1 treatment, tadpoles also developed a hunch back appearance. Reversing the order of thyromimetic treatment (GC-1 for 6 days and CO23 for 4 days) had the opposite effects; mostly resorption of larval tissue followed by hind leg growth.

Further evidence for the TR α -specificity of CO23 comes from quantitative rt-PCR studies. CO23 induced TR β gene expression, a gene expressed in the early stages of precocious metamorphosis, to an equal or greater extent than T₃ in hind leg and head tissue after 2 and 6 days of treatment. xBTEB, a zinc finger transcription factor and TR β -induced early gene, is induced to a lesser extent by CO23 compared to T₃ in hind leg and head tissue. Lastly, collagenase-3, a TR β -induced late gene, was also induced to a lesser extent by CO23 compared to T₃ in tail tissue after 6 days of treatment. Overall, these data corroborate the selective activation of TR α by CO23.

3.7 References

1. Morkin, E., Ladenson, P., Goldman, S., and Adamson, C. (2004) Thyroid hormone analogs for treatment of hypercholesterolemia and heart failure: past, present, and future prospects. *J. Mol. Cell. Cardiol.* **37**, 1137-1146.
2. Chiellini, G., Apriletti, J., Yoshihara, H., et al. (1998) A high-affinity subtype-selective agonist ligand for thyroid hormone receptor. *Chem. Biol.* **5**, 299-306.
3. Borngraeber, S., Budny, M.-J., Chiellini, G., et al. (2003) Ligand selectivity by seeking hydrophobicity in the thyroid hormone receptor. *Proc. Natl. Acad. Sci. USA* **100**, 15358-15363.
4. Hayashi, M., Ohnota, H., Tamura, T., et al. (2004) Inhibitory effects of KAT-681, a liver-selective thyromimetic, on development of hepatocellular proliferative lesions in rats induced by 2-acetylaminofluorene and partial hepatectomy after diethylnitrosamine initiation. *Arch. Toxicol.* **78**, 460-466.
5. Dow, R., Schneider, S., Paight, E., et al. (2003) Discovery of a novel series of 6-azauracil-based thyroid hormone receptor ligands: potent, TR β subtype-selective thyromimetics. *Bioorg. Med. Chem. Lett.* **13**, 379-382.
6. Ebisawa, M., Inoue, N., Fukasawa, H., et al. (1999) Thiazolidinediones with thyroid hormone receptor agonistic activity. *Chem. Pharm. Bull.* **47**, 1348-1350.

7. Hangeland, J., Friends, T., Doweiko, A., (2005) A new class of high affinity thyromimetics containing a phenyl-naphthylene core. *Bioorg. Med. Chem. Lett.* **15**, 4579-4584.
8. Chiang, Y.-C., for Pfizer Products Inc., USA. Preparation of [(hydroxyphenoxy)benzyl]thiazolidinediones and analogs as thyroid receptor ligands. Eur. Pat. Appl. EP-1148054, 17 Apr 2004.
9. Collazo, A.-M., Koehler, K., Garg, N., et al. (2006) Thyroid receptor ligands. Part 5: Novel bicyclic agonist ligands selective for the thyroid hormone receptor β . *Bioorg. Med. Chem. Lett.* **16**, 1240-1244.
10. Hanig, H., Woltering, M., Mueller, U., et al. (2005) Novel heterocyclic thyromimetics. *Bioorg. Med. Chem. Lett.* **15**, 1835-1840.
11. Hart, M., Suchland, K., Miyakawa, M., et al. (2006) Trace amine receptor-associated agonists: synthesis and evaluation of thyronamines and related analogues. *J. Med. Chem.* **49**, 1101-1112.
12. Hodnett, N. (2003) Trimethylsilyldiazomethane. *Synlett.* **13**, 2095-2096.
13. Yoshihara, H., Apriletti, J., Baxter, J., and Scanlan, T. (2001) A designed antagonist of the thyroid hormone receptor. *Bioorg. Med. Chem. Lett.* **11**, 2821-2825.
14. Evans, D., Katz, J., and West, T. (1998) Synthesis of diaryl ethers through the copper-promoted arylation of phenols with arylboronic acids - an expedient synthesis of thyroxine. *Tet. Lett.* **39**, 2937-2940.
15. Mishra, A., Panwar, P., Chopra, M., et al. (2003) Synthesis of novel bifunctional Schiff-base ligands derived from condensation of 1-(*p*-

- nitrobenzyl)ethylenediamine and 2-(*p*-nitrobenzyl)-3-monooxo-1,4,7-triazaheptane with salicylaldehyde. *New. J. Chem.* 27, 1054-1058.
16. Yamaguchi, J., Harada, M., Kondo, T., et al. (2003) A facile method for preparation of optically active hydantoin. *Chem. Lett.* 32, 372-373.
 17. Moore, J., Galicia, S., McReynolds, A., et al. (2004) Quantitative proteomics of the thyroid hormone receptor-coregulator interactions. *J. Biol. Chem.* 279, pp. 27584-27590.
 18. Kalttenbach, J. C. (1996) Endocrinology of Amphibian Metamorphosis. In *Metamorphosis postembryonic reprogramming of gene expression in amphibian and insect cells* (Gilbert, L., Tata, J., and Atkinson, B., Eds.), pp 403-431, Academic Press, San Diego.
 19. Furlow, J., Yung-Yang, H., Hsu, M., et al. (2004) Induction of larval tissue resorption in *Xenopus laevis* tadpoles by the thyroid hormone receptor agonist GC-1. *J. Biol. Chem.* 279, 26555-26562.
 20. Lim, W., Nguyen, N.-H., Yang, H., et al. (2002) A thyroid hormone antagonist that inhibits thyroid hormone action *in vivo*. *J. Biol. Chem.* 277, 35664-35670.
 21. Wang, Z., and Brown, D. (1993) Thyroid hormone-induced gene expression program for amphibian tail resorption. *J. Biol. Chem.* 268, 16270-16278.

CHAPTER FOUR

Novel CO23 Analogues with Enhanced TR α -Specificity

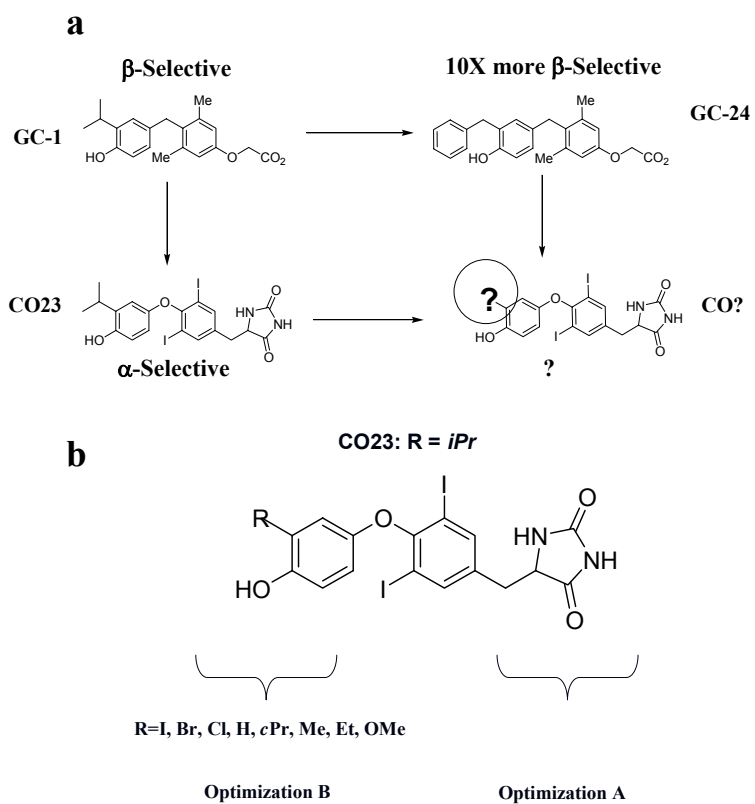
4.1 Overview

Analogues of the TR α -specific thyromimetic CO23 were synthesized and analyzed in vitro using competitive binding and transactivation assays. Like CO23, all analogues bind to both thyroid hormone receptor subtypes with about the same affinity; however, modification of CO23 by derivatization of the 3' position of the outer ring or replacement of the inner-ring iodides with bromides attenuates binding. Despite lacking a preference in binding to TR α , all analogues display TR α -specificity in transactivation assays using U2OS and HeLa cells. At best, several agonists exhibit an approximately 6-12 fold preference in transactivation when tested with TR α in HeLa cells. Improving specificity for TR α would not only make the resulting compounds more valuable as pharmacologic probes of TR biology, but it would also make them more desirable for drug therapy as they could likely have fewer side-effects.

4.2 Rationale Behind Expanding the SAR Data for Inner- and Outer-Ring CO23 Derivatives

CO23 (Fig. 4.1a), the first potent thyromimetic with TR α -specific effects *in vitro* and *in vivo*, demonstrates 3 to 5-fold TR α -specificity in transactivation assays

Figure 4.1 Optimization of the CO23 scaffold by derivatization of the 3' position



(a) Applying the GC-1/GC-24 paradigm for improvement of subtype specificity. (b) Optimization of the outer-ring position with varying substituent; smaller and hydrophobic or electron withdrawing; not large and bulky as is the case with GC-24

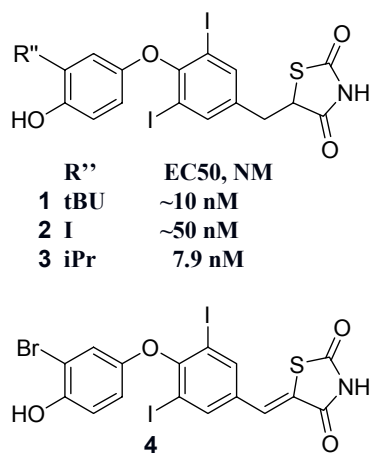
using U2OS and HeLa cells respectively (1). Despite not having an overwhelming preference for TR α activation, CO23 has profound effects on precocious *X. laevis* tadpole metamorphosis that correlates with the selective activation of TR α .

Although CO23 has not been tested on mammals as yet, seminal studies suggest that CO23 may have cardiac specific effects. TR α plays a major role in maintaining the health of the human heart; therefore, ascertaining the effects of CO23 on the mammalian heart is critical as it may have the potential to treat cardiac diseases. One caveat, however, is that it is hard to predict the outcome of CO23 based compounds on the mammalian heart from preliminary studies of CO23 on amphibian metamorphosis. Regardless, such compounds are of particular interest as compounds like DITPA, a cardiac specific agonist, and dronedarone, a TR α -selective antagonist, are proving to have therapeutic potential (2,3).

The hydantoin moiety attached to position one of the inner-ring by a methylene linker was deemed necessary for conferring TR α -specificity (1), and hence to improve TR α -specificity CO23 was derivatized by modification of inner- and outer-ring substituents (Fig. 4.1b). This strategy was designed due to the ability of the thyronine scaffold to tolerate a diversity of substituents in this position. For example, replacement of the 3' *i*Pr group of GC-1 to a benzyl group renders GC-24 about 10-fold more selective for TR β (Fig. 4.1a) (4). It is uncertain if the

same strategy will apply to CO23, as many TR β -selective agonists contain a bulky, hydrophobic group in the 3' position. According to the literature, there are thyromimetics with a thiazolidinedione in the C₁ position that contain varying substituents such as Br, I, *i*Pr, and *t*Bu (Fig. 4.2) (5). Compounds 1 – 3 all transactivate with reasonable potencies against TR α in COS-1 cells containing a DR4-luciferase reporter. Furthermore, bromides are well tolerated on the inner-ring and their synthesis is rapid and efficient; therefore, the synthesis of a CO23 analogue with bromides on the inner-ring was attempted in hopes of improving TR α -specificity.

Figure 4.2 Evidence that the 3' position tolerates derivatization



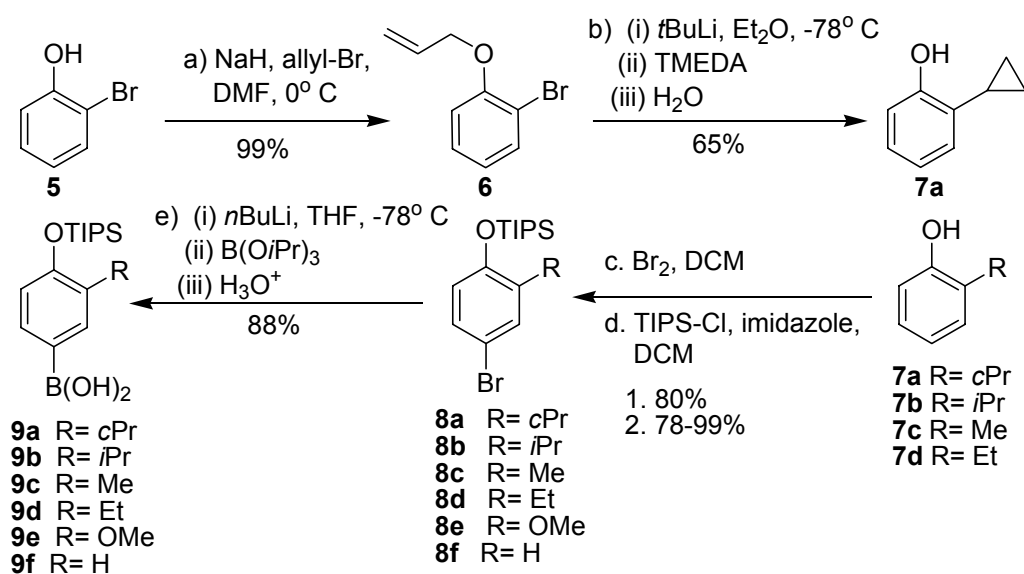
4.3 Synthesis of CO23 Analogues

CO23 was derivatized by modification of inner- and outer-ring substituents.

Substitution of the outer ring was achieved by preparation or purchase of *para*-

brominated phenols with varying groups in the *ortho*-position followed by TIPS protection (Scheme 4.1). One of the rare *para*-brominated phenols was generated by protection of 2-bromophenol (**5**) using allyl bromide which gives rise to allyl 2-bromophenyl ether (**6**). Lithiation of **6** causes it to undergo an intramolecular carbolithiation/1,3-elimination reaction that gives rise to 2-cyclopropylphenol (**7a**) (**6**). After generation of TIPS protected bromophenols

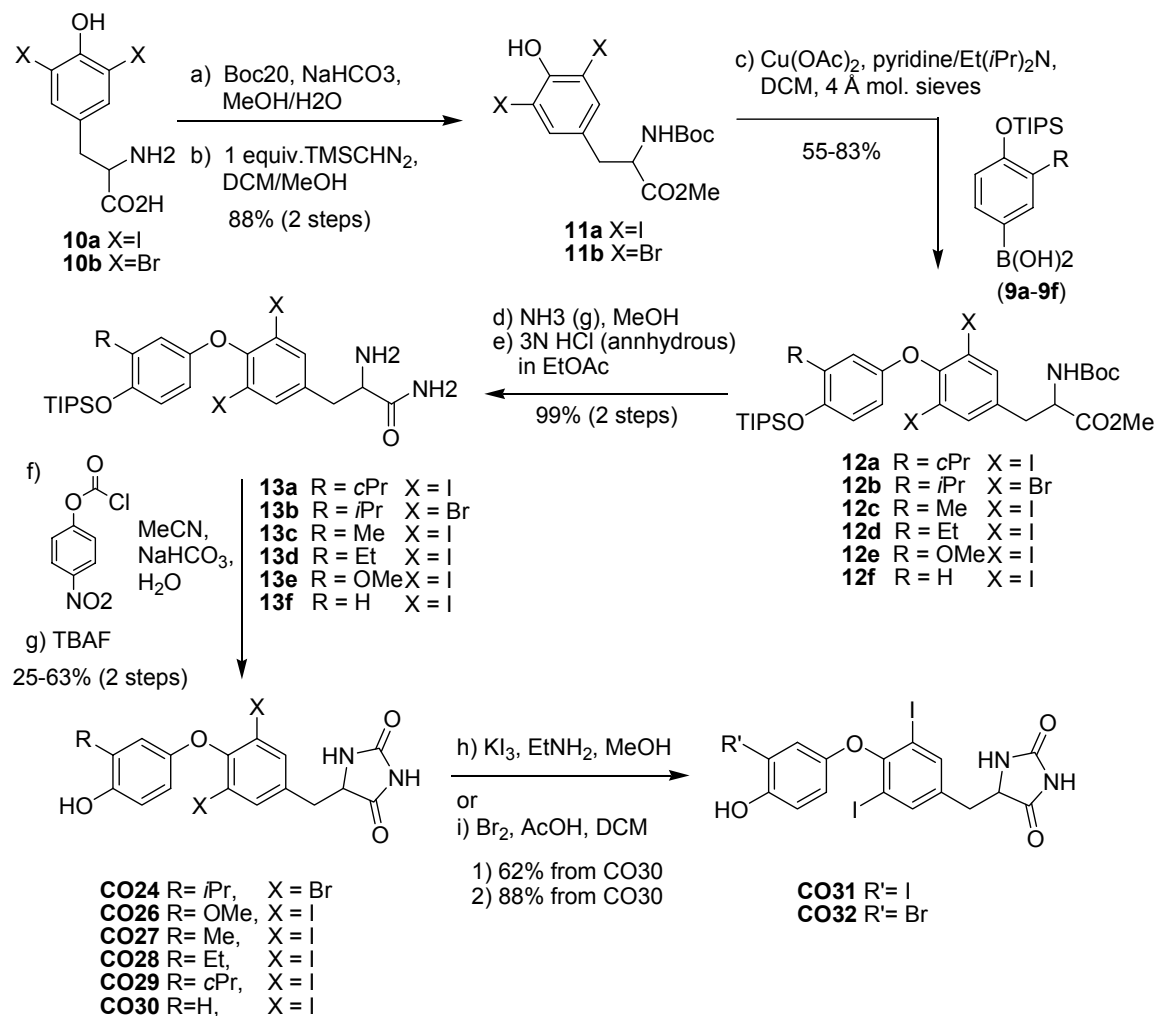
Scheme 4.1 Synthesis of boronic acids



(**8a-8f**), they were all converted to boronic acids (**9a-9f**) by treatment with *n*-butyllithium followed by addition of triisopropylborate and 3N hydrochloric acid and used at a later stage for the generation of biaryl ethers (Scheme 4.1) (1). At this stage, another level of thyromimetic diversity is achieved by starting with either diiodo-L-tyrosine or dibromo-L-tyrosine (**10a-10b**) and converting them to

Boc-protected dihalotyrosine methyl esters (**11a-11b**) (Scheme 4.2) (1). **11a-11b** and boronic acids **9a-9f** were coupled under Evan's conditions using Cupric

Scheme 4.2 Synthesis of ligands CO24 and CO26-CO32



acetate as a catalyst leading to biaryl ethers (**12a-12f**) (1). It should be noted that in order to prepare biaryl ethers in high yield, the boronic acid should be mixed with the following extremely dry reagents under argon: Diisopropyl

ethylamine and pyridine, cupric acetate thoroughly dried to a *verdigris* green color, 4 Å molecular sieves, and DCM followed by addition of phenol after about 5 minutes.

Adding the phenol last and slowly in portions slightly improves the yield for this reaction. After combining all reagents, the reaction should mix under ambient atmosphere with a drying tube attached to the round-bottom flask in order to minimize exposure to moisture (1). Amidation of **12a-12f** in methanol saturated with ammonia gas and Boc-deprotection yields biaryl ethers with amino acid amide side chains (**13a-13f**) (Scheme 4.2) (1). This side chain undergoes cyclization to form the imidazolidinedione after treatment with *para*-nitrophenylchloroformate, sodium bicarbonate, and water (1). Deprotection of the TIPS groups with tetrabutylammonium fluoride leads to several CO23 analogues (CO24 and CO26-CO30). The iodination (7) or bromination (1) of the 3' position of CO30 leads to two further analogues, CO31 and CO32 (Scheme 4.2).

4.4 *In vitro* Characterization of CO23 Analogues

The biological activity of the aforementioned CO23 analogues was measured *in vitro* using ¹²⁵I-T₃ competitive binding and transactivation assays. In terms of binding, replacement of inner-ring iodides with bromides causes a ~10-fold decrease in binding compared to CO23 and in U2OS cells (Table 4.1, Fig. 4.3a),

CO24 was not TR α -specific compared to the T₃ control. In U2OS cells, it is important to compare the potencies of test ligands to that of T₃ as thyroid hormone shows a difference in activation of TR α ₁ and TR β ₁ using a synthetic thyroid hormone response element driven luciferase reporter construct. However, in HeLa cells, a cell line where thyroid hormone consistently shows

Table 4.1 Binding affinity and potency of CO23 analogues

Compound	K _d and EC ₅₀ values (nM)					
	Binding affinity (K _d) ^a		Transactivation in U2OS cells (EC ₅₀) ^b		Transactivation in HeLa cells (EC ₅₀) ^b	
	TR α	TR β	TR α	TR β	TR α	TR β
T ₃ ^c	0.058	0.081	2.4 ± 0.4	11 ± 2	2.4 ± 0.5	2.4 ± 0.5
CO23 ^c	1.2 ± 0.2	1.7 ± 0.3	34 ± 4	390 ± 3	11 ± 1	58 ± 1
CO24	17 ± 1	18.4 ± 1	128 ± 5	421 ± 3	8.4 ± 3	32 ± 3
CO26	82 ± 21	119 ± 30	870 ± 160	8000 ± 1800	42 ± 6	265 ± 10
CO27	42 ± 13	53 ± 17	146 ± 28	4000 ± 1000	27 ± 6	180 ± 30
CO28	15 ± 6	18 ± 2	87 ± 14	1400 ± 170	10 ± 1	27 ± 6
CO29	25 ± 7	49 ± 5	145 ± 10	2000 ± 290	39 ± 4	100 ± 14
CO30	1700 ± 10	2000 ± 360	>20000 ^d	>20000 ^d	>10000 ^d	>10000 ^d
CO31	24 ± 3	36 ± 1	105 ± 8	2000 ± 170	21 ± 3	216 ± 80
CO32	43 ± 6	68 ± 10	206 ± 41	5200 ± 670	44 ± 1	530 ± 170

(a) Determined by means of an ¹²⁵I-T₃ competitive binding assay and data is reported as the mean K_d ± standard error of the mean, n=3. (b) Determined through use of a TRE-driven dual-luciferase reporter assay in U2OS or HeLa cells and the data is reported as the mean EC₅₀ value ± standard error of the mean, n=3. (c) See reference 1. (d) Dose-response curves generated using CO30 in transactivation assays did not plateau, and hence the EC₅₀ value is an approximated value based on extrapolation.

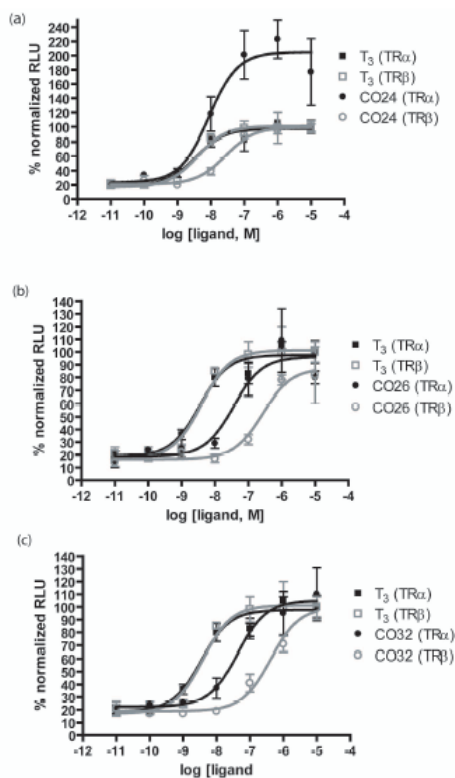
equal activation of both TR subtypes, not only does CO24 show fourfold TR α -specificity in terms of EC₅₀ values, it is TR α -specific in terms of efficacy in that it

causes transcriptional activity to plateau at a level that is twice as efficacious as T_3 (Table 4.1 and Fig. 4.3a).

CO23 analogues with outer-ring substitutions all displayed a decrease in binding affinity and potency when tested in U2OS cells compared to CO23 (Table 4.1).

In U2OS cells, the extent of transactivation of the following substituents against

Figure 4.3 Transactivation analysis of CO24, CO26, and CO32 in HeLa cells



TRE-driven dual-luciferase reporter assays showing transactivation curves for T_3 , (a) CO24, (b) CO26, and (c) CO32 against $hTR\alpha_1$ and $hTR\beta_1$, in HeLa cells. Plots show mean of triplicates with s.d.

TR α decreases from left to right: Ethyl > iodo > cyclopropyl > methyl > bromo > methoxy > hydrogen (Table 4.1). Unlike CO23, displaying only modest

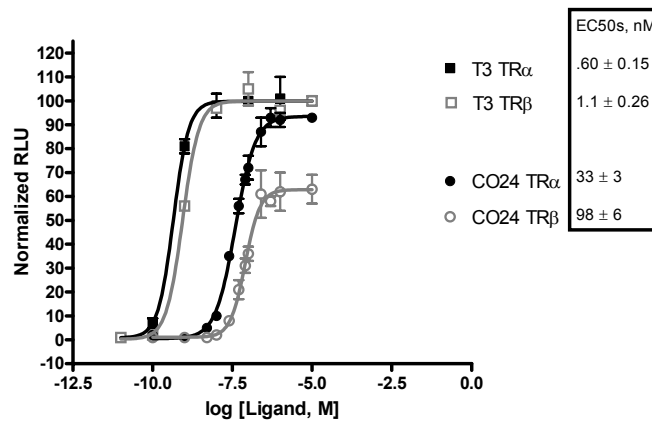
transcriptional activity in U2OS cells, outer-ring analogues transactivated in the presence of TR β very poorly. The best outer-ring analogue had an EC₅₀ value of 1.4 μ M compared to 390 nM for CO23 when tested in U2OS cells in the presence of TR β (Table 4.1).

Like CO24, in order to get a more direct measure of TR α -specificity, all analogues were assayed in HeLa cells. With the exception of CO30, which lacked activity in both U2OS and HeLa cells, all analogues demonstrated TR α -specificity with a few proving superior to CO23. CO26, CO27, CO31, and CO32 demonstrated 6-, 6-, 10-, and 12-fold TR α -specificity respectively, all of which are an improvement over the 5-fold TR α -specificity of CO23. Dose-response curves for CO26 and CO32 showing transactivation in the presence of TR α and TR β clearly demonstrate TR α -specificity despite the inferior potencies of the compounds compared to CO23 (Fig. 4.3, panels b and c). The rank order potency from left to right in HeLa cells is also impressive as some compounds are about equipotent to CO23-mediated TR α transactivation: Ethyl > iodo > methyl > cyclopropyl > methoxy > bromo > hydrogen.

In order to determine if the observation that CO24 acts as an enhanced agonist and a partial agonist with hTR α and hTR β , respectively, is reproducible against TRs from another species, the transcriptional activity of CO24 was assessed in the presence of *X. laevis* TR α and TR β . Interestingly, CO24 repeats the same behavior as seen in HeLa cells with hTRs; it shows about 3-fold xTR α -specificity,

full agonism, although not enhanced compared to T_3 , against $xTR\alpha$, and partial agonism against $xTR\beta$ (Fig 4.4). Furthermore CO24 transactivated more strongly when tested with $xTR\alpha$ as opposed to $hTR\alpha$ in U2OS cells, 33 ± 3 nM vs. 128 ± 5 nM respectively (Fig. 4.4, Table 4.1).

Figure 4.4 Transactivation analysis of CO24 in U2OS cells against xTRs



TRE-driven dual-luciferase reporter assay showing transactivation curves for T_3 and CO24 against $xTR\alpha_1$ and $xTR\beta_1$ in U2OS cells. Plots show mean of triplicates with s.d.

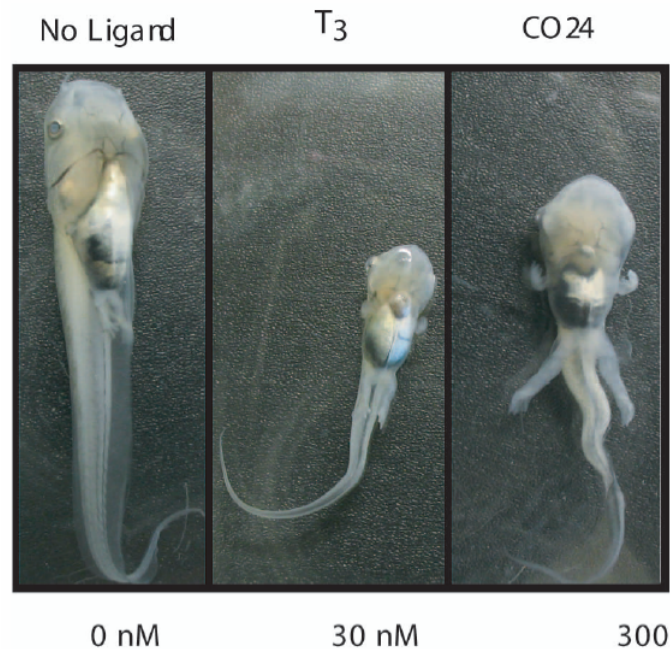
4.5 *In vivo* Analysis of CO24

4.5.1 Effects of CO24 on Amphibian Metamorphosis

CO24 *in vivo* led to changes that are consistent with enhanced $TR\alpha$ -activity compared to T_3 treated controls, particularly as demonstrated by the massive hind and fore leg emergence in precociously induced *X. laevis* tadpoles (Fig. 4.5) (8,9). After 4-days of treatment with 300 nM CO24, tadpoles exhibited massive hind legs and fore legs compared to the 30 nM T_3 treated control. Furthermore,

CO24 treated tadpoles were generally larger and exhibited less resorption of tissue in the head.

Figure 4.5 *In vivo* analysis of CO24



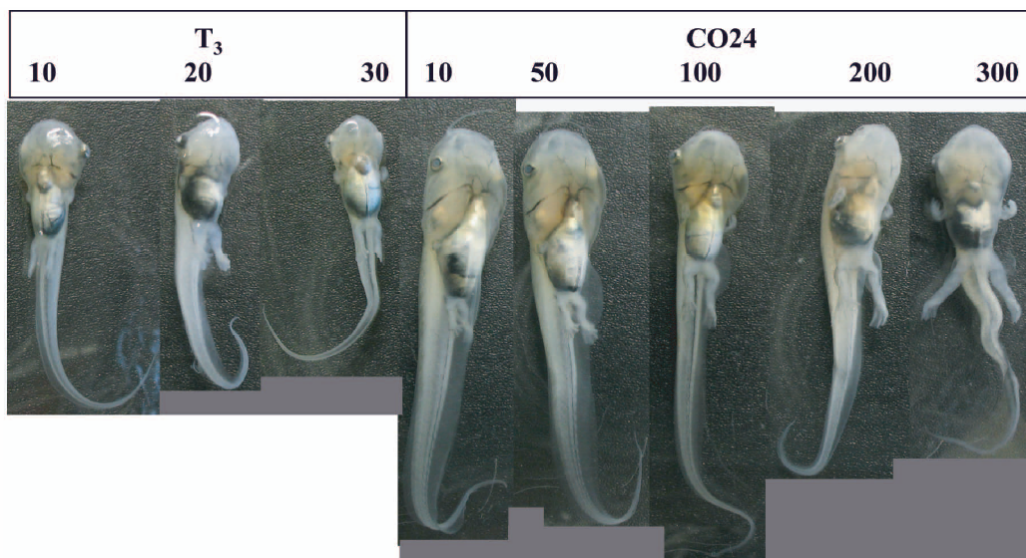
Induced metamorphosis of stage-53/54 tadpoles, n=3, treated for 4-days with DMSO, 30 nM T₃, and 300 nM CO₂₄.

4.5.2 Dose-Response of CO₂₄ Induced Metamorphosis

After four days of T₃ and CO₂₄ treatment, tadpoles treated with 10, 20, and 30 nM T₃ showed increasing tissue resorption; however, the difference between 10 and 30 nM T₃ treated tadpoles is very subtle, as 30 nM treated tadpoles are slightly smaller. Also, the 30 nM T₃ treated group demonstrated a thinning tail and slightly smaller head compared to 10 nM T₃ treated tadpoles. The dose-

response of CO24 induced tadpoles is starkly different compared to that of T₃, particularly at concentrations of 200 and 300 nM (Fig. 4.6). At these concentrations, CO24 causes gross morphogenic changes in all limbs and of particular notice is how massive the limbs become after only four days.

Figure 4.6 Induction of metamorphosis by CO24 in a dose-dependent manner



Induced metamorphosis of stage-53/54 tadpoles, n=3, treated for 4-days with 10, 20, and 30 nM T₃ and 10, 50, 100 200, 300 nM CO24.

4.6 Conclusion and Future Directions

CO23, the first potent thyromimetic to demonstrate TR α -specificity *in vitro* and *in vivo* (1), was derivatized at the 3, 5, and 3' positions in order to generate thyromimetics with enhanced TR α -specificity. In HeLa cells, four of eight ligands showed greater TR α -specificity with CO32 achieving greater than a two-fold gain

in specificity. Although all analogues bound poorly to both TR α_1 and TR β_1 and with about equal binding affinity to both receptor subtypes, analogues CO24 and CO28 were about equipotent to CO23 in their ability to cause TR α -mediated transcription. This phenomenon brings attention to a mode of subtype specificity which has gone unnoticed for some time. Analogues reported herein are not the first to demonstrate functional specificity. Considering that there is only one amino acid side chain difference in the TR LBD, Ser277 (TR α) to Asn331 (TR β), the similarity in affinity is not surprising (10). However, previous studies of related estrogen receptors demonstrate that subtle differences in the induced conformations of amino acid side chains may result in this selectivity (11). In this case, the same ligand may cause minor differences in one receptor LBD that causes amino acid side chains to perturb the conformationally mobile helix-12, an important mediator of coactivator recruitment, gene regulation, and potentiation of interactions with the transcriptional machinery (10). Future goals on CO23 and its derivatives should focus on how such specificity is achieved as understanding this would open a door to an underutilized mechanism of achieving isoform/subtype specificity, and not only amongst nuclear hormone receptor but for any receptor.

The *in vitro* binding and transactivation data of CO24 suggested that CO24 may elicit TR α -specificity *in vivo*; however, the effect of CO24 on precociously induced *X. laevis* tadpoles led to changes that far exceeded expectations based on its *in vitro* analysis. The hind leg development of 300 nM CO24 treated tadpoles after

four days of treatment yielded tadpoles with some of the most massive pairs of legs ever to be seen on tadpoles treated with thyroid hormone analogues or the natural hormone T₃. The inner-ring bromides probably confer resistance to dehalogenation by deiodinases, and therefore provide one explanation for the potency and efficacy of CO24 *in vivo* and *in vitro* (12). Although it is a leap to suggest from studies on amphibian metamorphosis that these analogues would have beneficial effects in mammals and possibly humans, other studies with TR α and cardiac-selective ligands suggest that TR α -specific thyromimetics may have therapeutic utility in the area of heart disease (2,3).

Just as placing a bulky, hydrophobic group on the outer-ring of GC-1 in the 5' position yields NH-3, a potent, TR β -selective antagonist, it is a wonder if applying the same methodology towards CO23 or CO24 could engender a potent and TR α -specific antagonist (5). To date, dronedarone is the most potent and selective TR α -selective antagonist; However, its binding is meager with IC₅₀ values of $59 \pm 4 \mu\text{M}$ and $280 \pm 30 \mu\text{M}$ for TR α_1 and TR β_1 respectively (3). Suffice it to say that the development of more potent and selective TR α -selective antagonists is highly desirable and CO23 and CO24 lay the foundation toward achieving this goal.

4.7 References

1. Ocasio, C.A. and Scanlan, T.S. (2006) Design and characterization of a thyroid hormone receptor α (TR α)-specific agonist. *ACS Chem. Biol.* 1, 585-593.
2. Morkin, E., Pennock, G., Spooner, P., et al. (2002) Clinical and experimental studies on the use of 3,5-diiodothyropropionic acid, a thyroid hormone analog, in heart failure. *Thyroid* 6, pp. 527-533.
3. van Beeren, H., Jong, W., Kaptein, E., et al. (2003) Dronedarone acts as a selective inhibitor of 3,5,3'-triiodothyronine binding to thyroid hormone receptor- α 1: *in vitro* and *in vivo* evidence. *Endocrinology* 144, pp. 552-558.
4. Borngraeber, S., Budny, M.-J., Chiellini, G., et al. (2003) Ligand selectivity by seeking hydrophobicity in thyroid hormone receptor. *PNAS* 100, pp. 15358-15363.
5. Ebisawa, M., Inoue, N., Fukasawa, H., et al. (1999) Thiazolidinediones with thyroid hormone receptor agonistic activity. *Chem. Pharm. Bull.* 47, 1348-1350.
6. Barluenga, J., Fañanás, F.J., Sanz, R., and Marcos, C. (2005) Intramolecular carbolithiation of Allyl o-Lithioaryl Ethers: A new enantioselective synthesis of functionalized 2,3-dihydrobenzofurans. *Chemistry - A European Journal* 11, 5397-5407.
7. Hart, M.E., Suchland, K.L., Miyakawa, M., et al. (2006) Trace amine-associated receptor agonists: Synthesis and evaluation of thyronamines and related analogues. *J. Med. Chem.* 49, 1101-1112.

8. Kalténbach, J. C. (1996) Endocrinology of Amphibian Metamorphosis. In *Metamorphosis postembryonic reprogramming of gene expression in amphibian and insect cells* (Gilbert, L., Tata, J., and Atkinson, B., Eds.), pp 403-431, Academic Press, San Diego.
9. Furlow, J., Yung-Yang, H., Hsu, M., et al. (2004) Induction of larval tissue resorption in *Xenopus laevis* tadpoles by the thyroid hormone receptor agonist GC-1. *J. Biol. Chem.* 279, 26555-26562.
10. Peterson, B. R. (2006) Small-molecule triggers of tadpole metamorphosis. *ACS Chem. Biol.* 1, 559.
11. Shiau, A.K., Barstad, D., Radek, J.T., et al. (2002) Structural characterization of a subtype-selective ligand reveals a novel mode of estrogen receptor antagonism. *Nat. Struct. Biol.* 9, pp. 359-364.
12. Bianco, A., Salvatore, D., Gereben, B., et al. (2002) Biochemistry, cellular and molecular biology, and physiological roles of the iodothyronine selenodeiodinases. *Endocr. Rev.* 23, 38-89.

Appendix A
Experimental Procedures

A.1 Synthetic Organic Chemistry Procedures

General Synthesis. All chemicals used for organic synthesis were purchased from Aldrich, Sigma-Aldrich, Fluka, or Acros and were used without further purification. Anhydrous conditions were maintained under argon using standard schlenk line techniques and oven-dried glassware. Anhydrous THF, DCM, pyridine, and diisopropyl ethylamine were available in house and dispensable from a solvent purification system. Compounds were purified by either flash chromatography using silica gel (VWR Scientific) or through preparatory thin layer chromatography (prep TLC) using Analtech prep TLC plates (20 X 20 cm, 1000 μm). ^1H NMR spectra were taken on the Varian Utility 400 MHz spectrometer in CDCl_3 or DMSO-d_6 solvents and chemical shifts were reported as δ (part per million) downfield of the internal control trimethylsilane (TMS) for all solvents. High resolution mass spectrometry (HRMS) using electrospray ionization was performed by the National Bio-Organic, Biomedical Mass Spectrometry Resource at UCSF and specific rotation was determined using a Perkin Elmer 241 Polarimeter. Purity of final compounds was assessed using Rainin HPXL Pumps, an Altech Nucleosil 100 (C_{18}) 10 μ 4.6 x 250-mm column with a 7.5-mm guard column, and a Varian ProStar 330 Photo Diode Array Detector controlled by a Varian Star Chromatography Workstation. All final compound are >95% pure. HPLC grade Acetonitrile and H_2O were purchased from Fisher.

A.1.1 General Chemical Procedures, Chapter 2

Preparation of TIPS-protected, 4-hydroxy, 3-isopropylphenyl boronic acid. 2-isopropylphenol (**11**) (10.0 g, 73.4 mmol) was added to a dry three-neck round-bottom flask fitted with an addition funnel and an exhaust line that runs into a base trap (6 M KOH). This solution was allowed to stir at 0°C after which Br₂ (14 g, 4.5 ml, 88.1 mmol) was added drop-wise over a period of 15 min. Stirring commenced for an additional 3-h before addition of sat. NaHCO₃, water, and EtOAc. The aqueous phase was extracted with EtOAc and the combined organic layers were washed with brine and then dried over MgSO₄. After concentration of the organic phase *in vacuo*, the crude product was purified by flash chromatography (10% EtOAc in hexanes) to give a slightly yellow clear oil (11.8 g, 75%). ¹H NMR (CDCl₃) δ 7.29 (d, *J* = 2.5 Hz, 1H), 7.14 (dd, *J* = 2.5 Hz, *J* = 8.0 Hz, 1H), 6.61 (d, *J* = 8.0 Hz, 1H), 4.84 (s, 1H), 3.17 (hep, 1H), 1.22 (d, 6H). This material (5 g, 23.3 mmol) was combined with TIPSCI (5.9 ml, 27.8 mmol) in a dry round-bottom flask containing 50 ml of anhydrous DCM and stirred at 0°C. To this solution was added imidazole (3.9 g, 58 mmol) and stirring commenced for an additional 18-h. The next day, the reaction was quenched with water and the aqueous phase extracted with ethyl acetate. The combined organic layers were washed with brine, dried over MgSO₄, concentrated *in vacuo*, and then purified with a short-path distillation column under high vacuum (0.5 mtorr). Pure fractions were collected at 130°C to give **4** as a clear white solid (**12**) (6.9 g, 80%). ¹H NMR (CDCl₃) δ 7.26 (d, *J* = 4 Hz, 1H), 7.11 (dd, *J* =

4.0 Hz, $J = 8.0$ Hz, 1H), 6.63 (d, $J = 8.0$ Hz, 1H), 3.30 (hep, 1H), 1.26 (m, 3H), 1.18 (d, 6H), 1.10 (d, 18H). This material was carried on to make (**13**). A dry round-bottom flask was charged with (**12**) (6.9 g, 18.6 mmol) and 100 ml of anhydrous THF and stirred at -78°C . To this solution was added drop-wise 2.5 M *n*-BuLi in hexanes (9.7 ml, 24.2 mmol) after which stirring commenced for 30 min. To this solution was added triisopropyl borate (8.7 ml, 37.2 mmol) and stirring commenced for 45 min. before warming to room temperature. After 1-h, the reaction was quenched with 0.5 N HCl and the aqueous phase extracted with EtOAc. The combined organic layers were washed with water and brine, dried over MgSO_4 , concentrated *in vacuo*, and purified by flash chromatography (10-40% EtOAc in hexanes) to give (**13**) (5.5 g, 88%) as a white solid. ^1H NMR (CDCl_3) δ 8.10 (s, 1H), 7.92 (d, $J = 8.0$ Hz, 1H), 6.89 (d, $J = 8.0$ Hz, 1H), 3.42 (hep, 1H), 1.40 (m, 3H), 1.33 (d, 6H), 1.13 (d, 18H).

General procedure for the Evans biary ether coupling. 4 Å molecular sieves were flame dried under high vacuum in a dry round-bottom flask. To this flask was added boronic acid (3 mmol) and copper acetate (dried to a *verdigris* color). These components were dissolved in 10 ml anhydrous DCM after which anhydrous pyridine (5 mmol) and diisopropyl ethylamine (5 mmol) were added. This mixture was then allowed to stir at room temperature for 5 min. before addition of phenol (1 mmol) in three portions separated by 5 min. each. At this point, the flask was fitted with a drying tube containing drierite and allowed to stir under ambient air over night, ~16-24-h. After this time, the reaction mixture was

concentrated *in vacuo* and purified by flash chromatography to give product (yield generally from 75-90%).

Biaryl ether (**15**) was prepared according to the general procedure for the Evans biaryl ether coupling. Intermediate (**13**) (1 g, 3.0 mmol) and 4-bromo-2,6-dimethylphenol (**14**) (3 g, 15.0 mmol) were coupled in the general way except that the limiting reagent was switched to the boronic acid. This gave (**15**) in 81% yield (1.3 g, 2.4 mmol). ¹H NMR (CDCl₃) δ 7.21 (s, 2H), 6.70 (d, *J* = 3.0 Hz, 1H), 6.58 (d, *J* = 9.0 Hz, 1H), 6.23 (dd, *J* = 3.0 Hz, *J* = 8.0 Hz, 1H), 3.32 (hep, 1H), 1.26 (m, 3H), 1.18 (d, 6H), 1.13 (d, 18H).

Intermediate (**15**) was carried on to make 4-(4-triisopropylsiloxy-3-isopropylphenoxy)-3,5-dimethylphenylboronic acid (**16**). A dry round-bottom flask was charged with (**15**) (6.9 g, 18.6 mmol) and 100 ml of anhydrous THF and stirred at -78°C. To this solution was added drop-wise 2.5 M *n*-BuLi in hexanes (9.7 ml, 24.2 mmol) after which stirring commenced for 30 min. To this solution was added triisopropyl borate (8.7 ml, 37.2 mmol) and stirring commenced for 45 min. before warming to room temperature. After 1-h, the reaction was quenched with 0.5 N HCl and the aqueous phase extracted with EtOAc. The combined organic layers were washed with water and brine, dried over MgSO₄, concentrated *in vacuo*, and purified by flash chromatography (10-40% EtOAc in hexanes) to give (**16**) (5.5 g, 88%) as a white solid. ¹H NMR (CDCl₃) δ 7.42 (s, 2H), 6.71 (d, *J* = 3.0 Hz, 1H), 6.58 (d, *J* = 8.0 Hz, 1H), 6.27 (dd, *J* = 3.0 Hz, *J* =

8.0 Hz, 1H), 3.19 (heptet, 1H), 2.06 (s, 6H), 1.25 (m, 3H), 1.21 (d, 6H), 1.02 (d, 18H).

(A) *General procedure for the Suzuki coupling*. A dry 2-neck round bottom flask fitted with a reflux condenser was charged with a heterocyclic bromide or iodide (1 mmol), 4-(4-triisopropylsiloxy-3-isopropylphenoxy)-3,5-dimethylphenylboronic acid (**16**) (1.5 mmol), and Pd(PPh₃)₄ (5 – 10 mol%). After addition of 3 ml of benzene, 1.5 ml of EtOH, and 1.5 ml of an aqueous solution of 2 M K₂CO₃, the solution was brought to reflux under argon and allowed to stir overnight. After completion, the reaction was quenched with water, diluted with EtOAc, and filtered through a pad of celite to remove palladium residue. The organic layer was extracted three times with EtOAc, washed with brine, dried over MgSO₄, concentrated *in vacuo*, and purified by flash chromatography (10% EtOAc in hexanes).

(B) *General procedure for the Suzuki coupling*. A dry 2-neck round bottom flask fitted with a reflux condenser was charged with a heterocyclic bromide or iodide (1 mmol), 4-(4-triisopropylsiloxy-3-isopropylphenoxy)-3,5-dimethylphenylboronic acid (**16**) (1.5 mmol), and PdCl₂(dppf) (20 mol%). After addition of 12 ml of dimethoxyethane (DME), and K₃PO₄ (5 mmol), the solution was brought to reflux under argon and allowed to stir overnight. After completion, the reaction was quenched with water, diluted with EtOAc, and filtered through a pad of celite to remove palladium residue. The organic layer was extracted three times with

EtOAc, washed with brine, dried over MgSO₄, concentrated *in vacuo*, and purified by flash chromatography (10% EtOAc in hexanes).

General procedure for the deprotection of the TIPS protecting group. To a stirred solution of protected phenol (1 mmol) in 10 ml of THF was added tetrabutylammonium fluoride (1.5 ml, 1.5 mmol, 1 M solution in THF). The reaction mixture was allowed to stir until completion of deprotection as determined by TLC analysis and then diluted with EtOAc. The reaction mixture was washed with 0.5 M HCl and the aqueous phase extracted with EtOAc. The organic layers were washed with water and brine and then dried over MgSO₄. The crude product was purified by flash chromatography to give product in quantitative yield.

4-(2,6-Dimethyl-4-(thiazol-2-yl)phenoxy)-2-isopropylphenol (CO1) was prepared according to general procedure (A) for the Suzuki coupling with 2-bromothiazole (27 μ l, 0.30 mmol) to give 71.1 mg (0.21 mmol, 70%) of the desired final compound after TIPS deprotection. ¹H NMR (CDCl₃) δ 1.21 (d, 6H, J=7.2Hz), 2.16 (s, 6H), 3.17 (heptet, 1H, J=7.2Hz), 5.4 (s, 1H broad), 6.28 (dd, 1H, J=2.8Hz, J=8Hz), 6.57 (d, 1H, J=8Hz), 6.76 (d, 1H, J=2.8Hz), 7.31 (d, 1H, J=3.2Hz), 7.69 (s, 2H), 7.85 (d, 1H, J=3.2Hz). ¹³C NMR (CDCl₃) δ 16.6, 22.9, 28.2, 112.5, 113.4, 113.6, 116.4, 120.4, 128.0, 128.3, 131.0, 133.8, 137.7, 144.2, 150.2, 152.2, 152.6, 155.0, 167.6. HRMS (*m/z*): [M]⁺ calcd for C₂₀H₂₁NO₂S,

339.1293; found, 339.1308. CO1 HPLC (MeCN/water, 65-100%, 12 min.), retention time 4.1 min.

4-(2,6-Dimethyl-4-(thiophen-3-yl)phenoxy)-2-isopropylphenol (CO2) was prepared according to general procedure (A) for the Suzuki coupling with 3-bromothiophene (27 μ l, 0.30 mmol) to give 115.5 mg (0.34 mmol, 78%) of the desired final compound after TIPS deprotection. ^1H NMR (CDCl_3) δ 1.21 (d, 6H, $J=7.2\text{Hz}$), 2.17 (s, 6H), 3.17 (heptet, 1H, $J=7.2\text{Hz}$), 4.5 (s, 1H), 6.33 (dd, 1H, $J=2.8\text{Hz}$, $J=8.4\text{Hz}$), 6.59 (d, 1H, $J=8.4\text{Hz}$), 6.77 (d, 1H, $J=2.8\text{Hz}$), 7.32 (s, 2H), 7.38 (d, 2H, $J=2.4\text{Hz}$), 7.42 (s, 1H). ^{13}C NMR (CDCl_3) δ 16.6, 22.5, 27.3, 111.5, 113.2, 115.7, 119.7, 126.1, 126.3, 127.0, 131.9, 132.4, 136.0, 141.9, 147.1, 150.8, 152.1. HRMS (m/z): $[\text{M}]^+$ calcd for $\text{C}_{21}\text{H}_{22}\text{O}_2\text{S}$, 338.1340; found, 338.1334. CO2 HPLC (MeCN/water, 65-100%, 12 min.), retention time 6.4 min.

Methyl 5-(4-(4-hydroxy-3-isopropylphenoxy)-3,5-dimethylphenyl)furan-2-carboxylate (CO3) was prepared according to general procedure (A) for the Suzuki coupling with a few modifications. 5-bromofuran-2-carboxylic acid (44.9 mg, 0.22 mmol) and a mixture of MeOH and toluene (3:9) were added to a dry round bottom flask and treated drop-wise with a 2 M solution of trimethylsilyldiazomethane (TMSD) until esterification was complete as determined by TLC to give methyl 5-bromofuran-2-carboxylate. This bromide was then subjected to Suzuki coupling with **16** to give 26.9 mg (0.07 mmol, 22%) of the desired final compound after TIPS deprotection. ^1H NMR (CDCl_3) δ 1.21

(d, 6H, J=7.2Hz), 2.15 (s, 6H), 3.18 (heptet, 1H, J=7.2Hz), 3.93 (s, 3H), 5.05 (s, 1H), 6.30 (dd, 1H, J=2.8Hz, J=8.8Hz), 6.62 (d, 1H, J=8.8Hz), 6.68 (d, 1H, J=3.6Hz), 6.73 (d, 1H, J=2.8Hz), 7.24 (d, 1H, J=3.6Hz), 7.51 (s, 2H). ¹³C NMR (CDCl₃) δ 16.6, 22.9, 28.1, 48.7, 52.4, 107.8, 112.5, 113.5, 116.7, 121.3, 126.4, 126.6, 127.4, 133.6, 137.7, 144.4, 150.1, 152.3, 153.9, 159.1, 160.9. HRMS (*m/z*): [M]⁺ calcd for C₂₃H₂₄O₅, 380.1623; found, 380.1621. CO3 HPLC (MeCN/water, 65-100%, 12 min.), retention time 7.1 min.

2-(4-(4-Hydroxy-3-isopropylphenoxy)-3,5-dimethylphenyl)cyclopent-2-enone (CO4) was prepared according to general procedure (A) for the Suzuki coupling with 2-bromocyclopent-2-enone (47 mg, 0.30 mmol) to give 89.0 mg (0.26 mmol, 90%) of the desired final compound after TIPS deprotection. ¹H NMR (CDCl₃) δ 1.21 (d, 6H, J=7.2Hz), 2.14 (s, 6H), 2.61 (m, 2H), 2.71 (m, 2H), 3.17 (heptet, 1H, J=7.2Hz), 4.49 (s, 1H), 6.30 (dd, 1H, J=2.8Hz, J=8.4Hz), 6.57 (d, 1H, J=8.4Hz), 6.75 (d, 1H, J=2.8Hz), 7.42 (s, 2H), 7.80 (t, 1H). ¹³C NMR (CDCl₃) δ 16.5, 16.8, 18.3, 22.9, 23.1, 28.0, 28.2, 30.7, 35.3, 112.3, 113.1, 113.3, 116.0, 116.1, 116.5, 116.6, 124.9, 133.3, 137.4, 145.7, 149.5, 153.0, 154.9, 215.2. HRMS (*m/z*): [M]⁺ calcd for C₂₂H₂₄O₃, 335.1725; found, 336.1725. CO4 HPLC (MeCN/water, 65-100%, 12 min.), retention time 4.9 min.

2-(4-(4-Hydroxy-3-isopropylphenoxy)-3,5-dimethylphenyl)-3-methylcyclopent-2-enone (CO5) was prepared according to general procedure (A) for the Suzuki coupling with 2-bromo-3-methylcyclopent-2-enone (50.8 mg, 0.30 mmol) to give

20.5 mg (0.06 mmol, 20%) of the desired final compound after TIPS deprotection. ^1H NMR (CDCl_3) δ 1.21 (d, 6H, $J=7.2\text{Hz}$), 2.14 (s, 6H), 2.2 (s, 3H), 3.16 (heptet, 1H, $J=7.2\text{Hz}$), 4.34 (s, 1H), 6.30 (dd, 1H, $J=2.8\text{Hz}$, $J=8.4\text{Hz}$), 6.57 (d, 1H, $J=8.4\text{Hz}$), 6.80 (d, 1H, $J=2.8\text{Hz}$), 7.00 (s, 2H). ^{13}C NMR (CDCl_3) δ 16.4, 16.7, 23.0, 28.1, 32.7, 35.8, 112.4, 113.6, 116.1, 116.6, 129.6, 130.9, 132.5, 137.6, 140.9, 149.9, 152.5, 175.6, 210.9. HRMS (m/z): $[\text{M}]^+$ calcd for $\text{C}_{23}\text{H}_{26}\text{O}_3$, 350.1882; found, 350.1882. CO5 HPLC (MeCN/water, 65-100%, 12 min.), retention time 4.0 min.

5-(4-(4-Hydroxy-3-isopropylphenoxy)-3,5-dimethylphenyl)thiophene-2-carboxylic acid (CO6) was prepared according to general procedure (A) for the Suzuki coupling with 5-bromothiophene-2-carboxylic acid (90.7 mg, 0.44 mmol) to give 40.0 mg (0.10 mmol, 24%) of the desired final compound after TIPS deprotection. ^1H NMR (CDCl_3) δ 1.16 (d, 6H, $J=6.8\text{Hz}$), 2.17 (s, 6H), 3.33 (heptet, 1H, $J=6.8\text{Hz}$), 5.30 (s, 1H), 6.30 (dd, 1H, $J=2.8\text{Hz}$, $J=8.4\text{Hz}$), 6.60 (d, 1H, $J=8.4\text{Hz}$), 6.76 (d, 1H, $J=2.8\text{Hz}$), 7.24 (d, 1H, $J=4.0\text{Hz}$), 7.37 (s, 2H), 7.82 (d, 1H, $J=4.0\text{Hz}$). ^{13}C NMR (CDCl_3) δ 14.3, 16.4, 18.6, 23.2, 28.1, 112.4, 113.7, 119.7, 121.8, 124.8, 127.8, 133.6, 134.1, 135.6, 141.2, 145.5, 148.8, 153.6, 170.2, 199.9. HRMS (m/z): $[\text{M}]^+$ calcd for $\text{C}_{22}\text{H}_{22}\text{O}_4\text{S}$, 382.1239; found, 382.1246. CO6 HPLC (MeCN/water, 65-100%, 12 min.), retention time 3.9 min.

4-(2,6-Dimethyl-4-(5-nitrothiazol-2-yl)phenoxy)-2-isopropylphenol (CO7) was prepared according to general procedure (A) for the Suzuki coupling with 2-

bromo-5-nitrothiazole (92.0 mg, 0.44 mmol) to give 161.5 mg (0.42 mmol, 95%) of the desired final compound after TIPS deprotection. ^1H NMR (CDCl_3) δ 1.21 (d, 6H, $J=7.2\text{Hz}$), 2.15 (s, 6H), 3.18 (heptet, 1H, $J=7.2\text{Hz}$), 6.30 (dd, 1H, $J=2.8\text{Hz}$, $J=8.8\text{Hz}$), 6.60 (d, 1H, $J=8.8\text{Hz}$), 6.76 (d, 1H, $J=2.8\text{Hz}$), 7.32 (s, 2H), 7.57 (s, 1H). ^{13}C NMR (CDCl_3) δ 16.7, 22.9, 28.2, 112.5, 113.4, 113.5, 116.5, 116.6, 131.8, 135.5, 135.58, 137.59, 149.8, 152.5, 154.4, 177.8. HRMS (m/z): $[\text{M}]^+$ calcd for $\text{C}_{20}\text{H}_{20}\text{N}_2\text{O}_4\text{S}$, 384.1000; found, 384.1000. CO7 HPLC (MeCN/water, 65-100%, 12 min.), retention time 5.7 min.

4-(4-(4-Hydroxy-3-isopropylphenoxy)-3,5-dimethylphenyl)thiophene-2-carboxylic acid (CO8) was prepared according to general procedure (A) for the Suzuki coupling with 4-bromothiophene-2-carboxylic acid (92.0 mg, 0.44 mmol) to give 29.0 mg (0.08 mmol, 18%) of the desired final compound after TIPS deprotection. ^1H NMR (CDCl_3) δ 1.21 (d, 6H, $J=7.2\text{Hz}$), 2.14 (s, 6H), 3.17 (heptet, 1H, $J=7.2\text{Hz}$), 5.39 (s, 1H), 6.32 (dd, 1H, $J=2.4\text{Hz}$, $J=8.0\text{Hz}$), 6.59 (d, 1H, $J=8.0\text{Hz}$), 6.76 (d, 1H, $J=2.4\text{Hz}$), 7.30 (s, 2H), 7.62 (s, 1H), 8.13 (s, 1H). ^{13}C NMR (CDCl_3) δ 16.7, 23.0, 28.2, 112.5, 113.6, 116.5, 116.7, 127.8, 128.5, 132.9, 133.2, 137.6, 143.7, 149.9, 152.4, 152.7. HRMS (m/z): $[\text{M}]^+$ calcd for $\text{C}_{22}\text{H}_{22}\text{O}_4\text{S}$, 382.1241; found, 382.1258. CO8 HPLC (MeCN/water, 65-100%, 12 min.), retention time 4.5 min.

4-(4-(4-Hydroxy-3-isopropylphenoxy)-3,5-dimethylphenyl)thiophene-2-sulfonamide (CO9) was prepared according to general procedure (B) for the

Suzuki coupling with 5-bromothiophene-2-sulfonamide (142 mg, 0.59 mmol) to give 101 mg (0.24 mmol, 46%) of the desired final compound after TIPS deprotection. ^1H NMR (CDCl_3) δ 1.21 (d, 6H, $J=7.2\text{Hz}$), 2.16 (s, 6H), 3.17 (heptet, 1H, $J=7.2\text{Hz}$), 4.68 (s, 1H), 5.11 (s, 2H), 6.30 (dd, 1H, $J=2.8\text{Hz}$, $J=8.4\text{Hz}$), 6.60 (d, 1H, $J=8.4\text{Hz}$), 6.75 (d, 1H, $J=2.8\text{Hz}$), 7.17 (d, 1H, $J=4.0\text{Hz}$), 7.30 (s, 2H), 7.61 (d, 1H, $J=4.0\text{Hz}$). ^{13}C NMR (CDCl_3) δ 19.6, 25.9, 31.0, 106.8, 113.6, 115.5, 119.5, 126.0, 129.3, 130.1, 130.6, 133.5, 135.4, 136.7, 140.5, 143.8, 150.3, 153.1, 166.4. HRMS (m/z): $[\text{M}]^+$ calcd for $\text{C}_{21}\text{H}_{23}\text{NO}_4\text{S}_2$, 417.1069; found, 417.1080. CO9 HPLC (MeCN/water, 65-100%, 12 min.), retention time 3.9 min.

5-(4-(4-Hydroxy-3-isopropylphenoxy)-3,5-dimethylphenyl)furan-2-carboxylic acid (CO10) was prepared according to general procedure (A) for the Suzuki coupling with minor changes. 5-Bromofuranoic acid (97.4 mg, 0.51 mmol), 277.5 mg of (**16**) (0.61 mmol), and Pd catalyst (0.025 mmol) were charged to a two-neck round bottom flask. After the addition 36.5 ml of dioxane:water (5:1), the procedure was carried out as usual to give 81.9 mg (0.22 mmol, 31%) of the desired final compound after TIPS deprotection. ^1H NMR (DMSO-d_6) δ 1.13 (d, 6H, $J=7.2\text{Hz}$), 2.10 (s, 6H), 3.33 (heptet, 1H, $J=7.2\text{Hz}$), 4.89 (s, 1H), 6.22 (dd, 1H, $J=2.8\text{Hz}$, $J=8.4\text{Hz}$), 6.58 (d, 1H, $J=2.4\text{Hz}$), 6.73 (d, 1H, $J=8.4\text{Hz}$), 6.77 (d, 1H, $J=2.8\text{Hz}$), 6.81 (d, 1H, $J=2.4\text{Hz}$), 7.48 (s, 2H), 9.33 (s, 1H). ^{13}C NMR (Acetone- d_6) δ 16.7, 23.0, 28.2, 107.2, 112.6, 113.5, 116.7, 117.5, 126.2, 128.6, 133.3, 137.7, 143.0, 150.0, 152.5, 153.2, 156.4, 167.1, 168.7. HRMS (m/z): $[\text{M}]^+$

calcd for C₂₂H₂₂O₅, 366.1467; found, 366.1466. CO10 HPLC (MeCN/water, 65-100%, 12 min.), retention time 3.6 min.

5-(4-(4-Hydroxy-3-isopropylphenoxy)-3,5-dimethylphenyl)thiophene-2-sulfonic acid (CO11) was prepared according to general procedure (A) for the Suzuki coupling with minor changes. 5-Bromothiophene-2-sulfonic acid (165.6 mg, 0.68 mmol), 370 mg of (**16**) (0.81 mmol), and Pd catalyst (0.034 mmol) were charged to a two-neck round bottom flask. After the addition 34 ml of dioxane:water (5:1), the procedure was carried out as usual to give 20 mg (0.05 mmol, <10%) of the desired final compound after TIPS deprotection. ¹H NMR (DMSO-d₆) δ 1.21 (d, 6H, J=7.2Hz), 2.18 (s, 6H), 3.15 (heptet, 1H, J=7.2Hz), 6.25 (dd, 1H, J=3.2Hz, J=8.8Hz), 6.62 (d, 1H, J=8.8Hz), 6.65 (d, 1H, J=3.2Hz), 6.81 (s, 2H), 7.10 (d, 1H, J=4.0), 7.38 (d, 1H, J=4.0Hz). HRMS (*m/z*): [M]⁺ calcd for C₂₁H₂₂O₅S₂, 418.1000; found, 418.1000. CO11 HPLC (MeCN/water, 65-100%, 12 min.), retention time 8.4 min.

4-(4-(4,5-Dichloro-1H-imidazol-2-yl)-2,6-dimethylphenoxy)-2-isopropylphenol (CO12) was prepared according to general procedure (A) for the Suzuki coupling (Na₂CO₃ was used in place K₂CO₃) with 2-bromo-4,5-dichloro-1H-imidazole (65.0 mg, 0.30 mmol) to give 88.5 mg (0.23 mmol, 76%) of the desired final compound after TIPS deprotection. ¹H NMR (CDCl₃) δ 1.15 (d, 6H, J=7.2Hz), 2.12 (s, 6H), 3.24 (heptet, 1H, J=7.2Hz), 6.22 (dd, 1H, J=2.8Hz, J=8.4Hz), 6.63 (d, 1H, J=8.8Hz), 6.79 (d, 1H, J=2.8Hz), 7.57 (s, 2H), 8.05 (s, 1H). HRMS (*m/z*): [M]⁺

calcd for C₂₀H₂₀Cl₂N₂O₂, 391.9826; found, 391.9819. CO12 HPLC (MeCN/water, 65-100%, 12 min.), retention time 3.8 min.

4-(4-(4-Hydroxy-3-isopropylphenoxy)-3,5-dimethylphenyl)pyridin-2(1H)-one (CO13) was prepared according to general procedure (A) for the Suzuki coupling (Na₂CO₃ was used in place K₂CO₃) with 4-bromopyridin-2(1H)-one (58.0 mg, 0.33 mmol) to give 27.5 mg (0.08 mmol, 24%) of the desired final compound after TIPS deprotection. ¹H NMR (CDCl₃) δ 1.21 (d, 6H, J=7.2Hz), 2.19 (s, 6H), 3.18 (heptet, 1H, J=7.2Hz), 5.30 (s, 1H), 6.30 (dd, 1H, J=2.8Hz, J=8.8Hz), 6.35 (dd, 1H, J=3.2, J=8.8Hz), 6.55 (d, 1H, J=8.8Hz), 6.60 (d, 1H, J=8.8Hz), 6.71 (d, 1H, J=2.8Hz), 6.78 (d, 1H, J=3.2Hz), 7.31 (s, 2H). HRMS (*m/z*): [M]⁺ calcd for C₂₂H₂₃NO₃, 349.1678; found, 349.167. CO13 HPLC (MeCN/water, 65-100%, 12 min.), retention time 4.3 min.

5-(4-(4-Hydroxy-3-isopropylphenoxy)-3,5-dimethylphenyl)pyrimidine-2,4(1H,3H)-dione (CO14) was prepared according to general procedure (B) for the Suzuki coupling with 6-bromopyrimidine-2,4(1H,3H)-dione (63.0 mg, 0.33 mmol) to give 13.1 mg (0.04 mmol, 25%) of the desired final compound after TIPS deprotection. ¹H NMR (Acetone-d₆) δ 1.10 (d, 6H, J=4Hz), 2.03 (s, 6H), 3.21 (heptet, 1H, J=4Hz), 6.18 (dd, 1H, J=4Hz, J=8Hz), 6.61 (d, 1H, J=8Hz), 6.64 (d, 1H, J=4Hz), 7.30 (s, 2H), 7.61 (s, 1H), 7.78 (s, 1H), 9.95 (s, 1H), 10.11 (s, 1H). ¹³C NMR (Acetone-d₆) δ 16.6, 22.7, 27.9, 112.1, 113.6, 113.6, 116.3, 129.5,

131.7, 139.5, 151.9, 152.1. CO14 HPLC (MeCN/water, 65-100%, 12 min.), retention time 3.8 min.

4-(4-(4-Hydroxy-3-isopropylphenoxy)-3,5-dimethylphenyl)furan-2-carboxylic acid (CO15) was prepared according to general procedure (A) for the Suzuki coupling (Toluene used instead of benzene and 4-bromofuran-2-carbaldehyde [76.6 mg, 0.88 mmol] was used instead of the acid) to give 1.0 mg (0.02 mmol, <10%) of the desired final compound after TIPS deprotection and oxidation of the aldehyde using NaClO₂ and H₂O₂ in acetonitrile and an NaH₂PO₄ buffer. ¹H NMR (DMSO-d₆) δ 1.10 (d, 6H, J=7.2Hz), 2.06 (s, 6H), 3.33 (heptet, 1H, J=7.2Hz), 6.22 (dd, 1H, J=2.8Hz, J=8.4Hz), 6.64 (d, 1H, J=8.4Hz), 6.67 (s, 1H), 6.85 (d, 1H, J=2.4Hz), 7.34 (s, 2H), 7.86 (s, 1H). HRMS (*m/z*): [M]⁺ calcd for C₂₂H₂₂O₅, 366.1463; found, 366.1467. CO15 HPLC (MeCN/water, 65-100%, 12 min.), retention time 3.6 min.

Preparation of (E)-1,2-Bis(tributylstannyl)ethylene (17). To a dry round bottom flask was added tributyl(ethynyl)stannane (2.5 g, 8.0 mmol), tributyltinhydride (2.6ml, 9.6 mmol), and 2.5 mol% 2,2'-azo-bis(isobutyronitrile) (AIBN). The reaction was allowed to stir for 6-h at 90° C before short-path distillation *in vacuo* to give 3.4 g (71%) of the final compound as a clear oil. ¹H NMR (CDCl₃) δ 6.88 (s, 2H), 1.34 (m, 12H), 1.30 (m, 24H), 0.86 (m, 18H).

Preparation of (4-(4-((E)-2-(tributylstannyl)vinyl)-2,6-dimethylphenoxy)-2-isopropylphenoxy)triisopropylsilane (18). To a dry round bottom flask was added (E)-1,2-Bis(tributylstannyl)ethylene (0.96 g, 1.57 mmol), (**15**) (0.7 g, 1.31 mmol), and Pd(PPh₃)₄ (75.7 mg, 0.07 mmol). After addition of degassed toluene, the reaction was allowed to stir at reflux over night. After completion, the reaction was quenched with water and the organic layer extracted with EtOAc. The combined layers were washed with brine, dried with MgSO₄, concentrated *in vacuo* then purified by flash chromatography (1% EtOAc in hexanes) to give (**18**) in 50.9% yield (489 mg, 0.68 mmol). ¹H NMR (CDCl₃) δ 7.14 (s, 2H), 6.80 (s, 1H), 6.79 (s, 1H), 6.74 (d, J = 3.0 Hz, 1H), 6.56 (d, J = 8.0 Hz, 1H), 6.24 (dd, J = 3.0 Hz, J = 8.0 Hz, 1H), 3.35 (heptet, 1H), 1.55 (m, 12H), 1.52 (m, 24H), 1.34 (m, 3H), 1.30 (d, 6H), 1.10 (d, 18H), 0.83 (m, 18H).

General procedure for the Stille coupling. A dry 2-neck round bottom flask fitted with a reflux condenser was charged with either 2-bromothiazole or 3-bromothiophene (1 mmol), (4-(4-((E)-2-(tributylstannyl)vinyl)-2,6-dimethylphenoxy)-2-isopropylphenoxy)triisopropylsilane (**18**) (3 mmol), and PdCl₂(PPh₃)₄ (10 mol%), and LiCl (10 mmol). After addition of 100 ml of toluene, the solution was brought to reflux under argon and allowed to stir for 4-d. After completion, the reaction was quenched with water, diluted with EtOAc, and filtered through a pad of celite to remove palladium residue. The organic layer was extracted three times with EtOAc, washed with brine, dried over MgSO₄,

concentrated *in vacuo*, and purified by flash chromatography (10% EtOAc in hexanes).

4-(2,6-Dimethyl-4-((E)-2-(thiazol-2-yl)vinyl)phenoxy)-2-isopropylphenol (CO16) was prepared according to general procedure for the Stille coupling to give 21.3 mg (0.06 mmol, 65%) of the desired final compound after TIPS deprotection. ¹H NMR (CDCl₃) δ 1.08 (d, 6H, J=7.2Hz), 2.15 (s, 6H), 3.32 (heptet, 1H, J=7.2Hz), 4.60 (s, 1H), 6.31 (dd, 1H, J=2.8Hz, J=8.8Hz), 6.60 (d, 1H, J=8.8Hz), 6.75 (d, 1H, J=2.8Hz), 7.24 (d, J=3Hz), 7.27 (s, 2H), 7.28 (s, 1H), 7.36 (s, 1H), 7.80 (d, J=3Hz). HRMS (*m/z*): [M]⁺ calcd for C₂₂H₂₃NO₂S, 365.1450; found, 365.1436.

4-(2,6-Dimethyl-4-((E)-2-(thiazol-2-yl)vinyl)phenoxy)-2-isopropylphenol (CO16) was prepared according to general procedure for the Stille coupling to give 21.3 mg (0.06 mmol, 65%) of the desired final compound after TIPS deprotection. ¹H NMR (CDCl₃) δ 1.08 (d, 6H, J=7.2Hz), 2.15 (s, 6H), 3.32 (heptet, 1H, J=7.2Hz), 4.60 (s, 1H), 6.31 (dd, 1H, J=2.8Hz, J=8.8Hz), 6.60 (d, 1H, J=8.8Hz), 6.75 (d, 1H, J=2.8Hz), 7.24 (d, J=3Hz), 7.27 (s, 2H), 7.28 (s, 1H), 7.36 (s, 1H), 7.80 (d, J=3Hz). HRMS (*m/z*): [M]⁺ calcd for C₂₂H₂₃NO₂S, 365.1450; found, 365.1436.

4-(2,6-Dimethyl-4-((E)-2-(thiophen-3-yl)vinyl)phenoxy)-2-isopropylphenol (CO17) was prepared according to general procedure for the Stille coupling to give 38.2 mg (0.10 mmol, 80%) of the desired final compound after TIPS deprotection. ¹H NMR (CDCl₃) δ 1.24 (d, 6H, J=7.2Hz), 2.05 (s, 6H), 3.29 (heptet, 1H, J=7.2Hz),

4.60 (s, 1H), 6.32 (dd, 1H, J=2.8Hz, J=8.8Hz), 6.60 (d, 1H, J=8.8Hz), 6.75 (d, 1H, J=2.8Hz), 7.17 – 7.30 (m, 7H). HRMS (m/z): $[M]^+$ calcd for $C_{23}H_{24}O_2S$, 364.1463; found, 364.1478.

4-(2,6-Dimethyl-4-(2-(thiazol-2-yl)ethyl)phenoxy)-2-isopropylphenol (CO18) was prepared from CO17 by catalytic hydrogenation. 13 mg of CO17 was stirred under 1 atm H_2 with a small spatula tip amount of PtO_2 in MeOH at room temperature for 6Hr. After completion, the reaction diluted with EtOAc and filtered through celite, the organic component concentrated *in vacuo* then applied to a preparatory TLC plate and chromatographed with 5% EtOAc in hexanes. The final product was etched off of the TLC, this material applied to a fitted funnel, then the final compound was extracted from the silica with EtOAc and concentrated *in vacuo* to give 13 mg in quantitative yield. 1H NMR ($CDCl_3$) δ 1.08 (d, 6H, J=7.2Hz), 2.15 (s, 6H), 3.05 (m, 2H), 3.17 (heptet, 1H, J=7.2Hz), 3.32 (m, 2H), 4.80 (s, 1H broad), 6.31 (dd, 1H, J=2.8Hz, J=8.8Hz), 6.60 (d, 1H, J=8.8Hz), 6.75 (d, 1H, J=2.8Hz), 6.91 (s, 2H), 7.71 (d, 1H, J=3Hz), 7.80 (d, 1H, J=3Hz).

Preparation of 4-(4-Triisopropylsiloxy-3-isopropylphenoxy)-3,5-dimethylbenzaldehyde (19). A dry round-bottom flask was charged with (15) (1.0 g, 2.03 mmol) and 10 ml of anhydrous THF and stirred at $-78^\circ C$. To this solution was added drop-wise 2.5 M *n*-BuLi in hexanes (1.1 ml, 2.4 mmol) after which stirring commenced for 30 min. To this solution was added DMF (0.4 ml, 5

mmol) and stirring commenced for 45 min. before warming to room temperature. After 1-h, the reaction was quenched with H₂O and the aqueous phase extracted with EtOAc. The combined organic layers were washed with water and brine, dried over MgSO₄, concentrated *in vacuo*, and purified by flash chromatography (10-40% EtOAc in hexanes) to give (**19**) (0.8 g, 89%) as a white solid.

General procedure for the Knoevenagel condensation. TiCl₄ (596 mg, 1.72 mmol), in 1 ml of CCl₄ was added to 3 ml of THF dropwise over 15 min. at 0° C under argon and the mixture was stirred until the yellow precipitate appeared. A mixture of (**19**) (120 mg, 0.42 mmol), thiazolidinedione (58.3 mg, 0.5 mmol), and pyridine (1ml, 12.4 mmol) in 3 ml THF was added to the reaction mixture at 0° C and the mixture was stirred for 23-h at ambient temperature. After completion, the reaction was quenched with H₂O and the aqueous phase extracted with EtOAc. The combined organic layers were washed with water and brine, dried over MgSO₄, concentrated *in vacuo*, and purified by flash chromatography (10-40% EtOAc in hexanes).

(Z)-5-(4-(4-hydroxy-3-isopropylphenoxy)-3,5-dimethylbenzylidene)thiazolidine-2,4-dione (CO19) was prepared according to the general procedure for the Knoevenagel condensation to give 0.25 g (0.70 mmol, 62%) of a sticky, tan white solid after TIPS deprotection. ¹H NMR (DMSO-d₆) δ 1.05 (d, 6H, J=7.2Hz), 2.02 (s, 6H), 3.30 (heptet, 1H), 6.17 (dd, 1H, J=2.8Hz, J=8.8Hz), 6.58 (d, 1H, J=2.8Hz), 6.60 (d, 1H, J=8.8Hz), 7.19 (s, 2H), 7.25 (s, 2H), 8.89 (s, 1H). CO19 is

quantitatively converted to 5-(4-(4-hydroxy-3-isopropylphenoxy)-3,5-dimethylbenzyl)thiazolidine-2,4-dione (CO20) by catalytic hydrogenation. 100 mg CO19 stirred in a mixture of activated 10% palladium on carbon and EtOH/acetic acid under 1 atm H₂ yields 100 mg CO20. ¹H NMR (DMSO-d₆) δ 1.05 (d, 6H, J=7.2Hz), 2.02 (s, 6H), 2.81 (dd, 1H, J=8.0Hz, J=14.0Hz), 2.93 (dd, 1H, J=4.0Hz, J=14.0Hz), 3.15 (heptet, 1H, J=8.0Hz), 4.35 (dd, 1H, J=4.0Hz, J=8.0Hz), 5.57 (s, 1H broad), 6.17 (dd, 1H, J=2.8Hz, J=8.8Hz), 6.58 (d, 1H, J=2.8Hz), 6.60 (d, 1H, J=8.8Hz), 6.91 (s, 2H), 7.25 (s, 2H), 8.04 (s, 1H).

(Z)-5-(4-(4-hydroxy-3-isopropylphenoxy)-3,5-dimethylbenzylidene)imidazolidine-2,4-dione (CO21) was prepared according to the general procedure for the Knoevenagel condensation to give 55 mg (0.70 mmol, 65%) of a sticky, tan white solid. CO21 is quantitatively converted to 5-(4-(4-hydroxy-3-isopropylphenoxy)-3,5-dimethylbenzyl)imidazolidine-2,4-dione (CO22) by catalytic hydrogenation. 100 mg CO21 stirred in a mixture of activated 10% palladium on carbon and EtOH/acetic acid under 1 atm H₂ yields 100 mg CO22. ¹H NMR (DMSO-d₆) δ 1.21 (d, 6H, J=8.0Hz), 2.10 (s, 6H), 2.75 (dd, 1H, J=8.0Hz, J=12.0Hz), 3.14 (heptet, 1H, J=8.0Hz), 3.22 (dd, 1H, J=4.0Hz, J=12.0Hz), 4.28 (dd, 1H, J=4.0Hz, J=8.0Hz), 4.97 (s, 1H), 5.57 (s, 1H), 6.22 (dd, 1H, J=4.0Hz, J=8.0Hz), 6.58 (d, 1H, J=8.0Hz), 6.73 (d, 1H, J=4.0Hz), 6.91 (s, 2H), 7.27 (s, 1H), 8.04 (s, 1H). HRMS (*m/z*): [M]⁺ calcd for C₂₁H₂₄N₂O₄, 368.1736; found, 368.1749. CO22 HPLC (MeCN/water, 65-100%, 12 min.), retention time 3.9 min.

A.1.2 General Chemical Procedures, Chapter 3

General procedure for the Evans biary ether coupling. 4 Å molecular sieves were flame dried under high vacuum in a dry round-bottom flask. To this flask was added boronic acid (3 mmol) and copper acetate (dried to a *verdigris* color). These components were dissolved in 10 ml anhydrous DCM after which anhydrous pyridine (5 mmol) and diisopropyl ethylamine (5 mmol) were added. This mixture was then allowed to stir at room temperature for 5 min. before addition of phenol (1 mmol) in three portions separated by 5 min. each. At this point, the flask was fitted with a drying tube containing drierite and allowed to stir under ambient air over night, ~16-24-h. After this time, the reaction mixture was concentrated *in vacuo* and purified by flash chromatography to give product (yield generally from 75-90%).

General procedure for the deprotection of the TIPS protecting group. To a stirred solution of protected phenol (1 mmol) in 10 ml of THF was added tetrabutylammonium fluoride (1.5 ml, 1.5 mmol, 1 M solution in THF). The reaction mixture was allowed to stir until completion of deprotection as determined by TLC analysis and then diluted with EtOAc. The reaction mixture was washed with 0.5 M HCl and the aqueous phase extracted with EtOAc. The organic layers were washed with water and brine and then dried over MgSO₄. The crude product was purified by flash chromatography to give product in quantitative yield.

Preparation of TIPS-protected, 4-hydroxy, 3-isopropylphenyl boronic acid. 2-isopropylphenol (10.0 g, 73.4 mmol) was added to a dry three-neck round-bottom flask fitted with an addition funnel and an exhaust line that runs into a base trap (6 M KOH). This solution was allowed to stir at 0°C after which Br₂ (14 g, 4.5 ml, 88.1 mmol) was added drop-wise over a period of 15 min. Stirring commenced for an additional 3-h before addition of sat. NaHCO₃, water, and EtOAc. The aqueous phase was extracted with EtOAc and the combined organic layers were washed with brine and then dried over MgSO₄. After concentration of the organic phase *in vacuo*, the crude product was purified by flash chromatography (10% EtOAc in hexanes) to give a slightly yellow clear oil (11.8 g, 75%). This material (5 g, 23.3 mmol) was combined with TIPSCl (5.9 ml, 27.8 mmol) in a dry round-bottom flask containing 50 ml of anhydrous DCM and stirred at 0°C. To this solution was added imidazole (3.9 g, 58 mmol) and stirring commenced for an additional 18-h. The next day, the reaction was quenched with water and the aqueous phase extracted with ethyl acetate. The combined organic layers were washed with brine, dried over MgSO₄, concentrated *in vacuo*, and then purified with a short-path distillation column under high vacuum (0.5 mtorr). Pure fractions were collected at 130°C to give **4** as a clear white solid (6.9 g, 80%). This material was carried on to make **6**. A dry round-bottom flask was charged with **5** (6.9 g, 18.6 mmol) and 100 ml of anhydrous THF and stirred at -78°C. To this solution was added drop-wise 2.5 M *n*-BuLi in hexanes (9.7 ml, 24.2 mmol) after which stirring commenced for 30 min. To this solution was added

triisopropyl borate (8.7 ml, 37.2 mmol) and stirring commenced for 45 min. before warming to room temperature. After 1-h, the reaction was quenched with 0.5 N HCl and the aqueous phase extracted with EtOAc. The combined organic layers were washed with water and brine, dried over MgSO₄, concentrated *in vacuo*, and purified by flash chromatography (10-40% EtOAc in hexanes) to give **6** (5.5 g, 88%) as a white solid.

Preparation of 8. L-diiodotyrosine (**2**) (5 g, 11.5 mmol) was added to a round-bottom flask and dissolved in MeOH/H₂O (2:1). To this mixture was added NaHCO₃ (2.9 g, 34.5 mmol) followed by Boc₂O (3.97 ml, 17.3 mmol). The reaction mixture was allowed to stir until completion as determined by TLC analysis (product should turn blue when tested with *p*-anisaldehyde). Upon completion, the mixture was acidified to pH 4.5 and extracted with EtOAc. The combined organic layers were washed with water and brine and then dried over MgSO₄. The crude material (5.9 g, 96%) was then utilized in the next reaction. To this material (11.1 mmol) in toluene/MeOH (9:1) was added TMSCHN₂ (0.5 M, 22 ml, 11.6 mmol) drop-wise over 30 min. at room temperature using a syringe pump. The reaction was allowed to stir until complete as determined by TLC analysis then washed with 0.5 M HCl and water. The aqueous phase was extracted with EtOAc and the organic layers washed with brine, dried over MgSO₄, and concentrated *in vacuo*. The Boc-protected, diiodotyrosine methyl ester (**3**) (5.4 g, 89%) was coupled with **6** according to the general procedures for biaryl ether synthesis to give biaryl ether (**7**) in 86% yield.

Preparation of CO23. Biaryl ether (**7**) (1 g, 1.2 mmol) was dissolved in 20 ml MeOH and saturated with ammonia gas. After 16-18-h, the mixture was purged with argon, concentrated *in vacuo*, and dissolved in anhydrous 3 N HCl in EtOAc/Ether. After 3-h, the mixture was quenched with water, the pH was adjusted to 4.5, and the aqueous phase extracted with EtOAc. The organic layers were washed with water and brine, dried over MgSO₄, and purified by flash chromatography (40% EtOAc in hexanes) to give **7** (972 mg, 99%). In order to make CO23, **8** (972 mg, 1.2 mmol), 4-nitrophenyl chloroformate (254 mg, 1.26 mmol), and NaHCO₃ (352 mg, 4.2 mmol) were added to a dry round-bottom flask containing 20 ml anhydrous MeCN (**2**). The reaction was allowed to stir over night followed by addition of H₂O. The solution should quickly turn yellow due to generation of nitrophenol. After 6-h, the reaction mixture was rotovapped in order to remove MeCN, acidified to pH 5, and then extracted with EtOAc. The combined organic layers were washed with brine, dried over MgSO₄, and reconstituted in 10 ml THF. Deprotection of the TIPS group afforded CO23 (448 mg, 63%, 2-steps, see methods for spectral data) after purification by prep TLC (40% EtOAc in hexanes). CO23 $[\alpha]_{20}^D = -18.7$ (c = 0.05 in MeOH). CO23 ¹H NMR (400MHz, DMSO-d₆): δ 1.11 (d, 6H, J=8.0Hz), 2.81 (dd, 1H, J=8.0Hz, J=14.0Hz), 2.93 (dd, 1H, J=4.0Hz, J=14.0Hz), 3.15 (heptet, 1H, J=8.0Hz), 4.35 (dd, 1H, J=4.0Hz, J=8.0Hz), 6.16 (dd, 1H, J=4.0Hz, J=8.0Hz), 6.61 (d, 1H, J=8.0Hz), 6.63 (d, 1H, J=4.0Hz), 7.75 (s, 2H), 7.98 (s, 1H), 8.96 (s, 1H), 10.60 (s, 1H). CO23 HRMS (*m/z*): [M]⁺ calcd for C₁₉H₁₈I₂N₂O₄, 591.9356;

found, 591.9356. CO23 HPLC (MeCN/water, 65-100%, 12 min.): retention time 3.9 min.; 99% pure.

Preparation of 4-(4-triisopropylsiloxy-3-isopropylphenoxy)-3,5-dimethylbenzaldehyde. Intermediate **6** (1 g, 3.0 mmol) and 4-bromo-2,6-dimethylphenol (3 g, 15.0 mmol) were coupled in the general way except that the limiting reagent was switched to the boronic acid. This gave 4-(4-bromo-2,6-dimethylphenoxy)-2-isopropylphenoxy)triisopropylsilane in 81% yield (1.3 g, 2.4 mmol), by far the one of the best yields using a 2,6-dimethyl substituted phenol, which was then added to a dry round-bottom flask containing 25 ml anhydrous THF and stirred at -78°C. To this solution was added drop-wise *n*-BuLi (1.25ml, 3.12 mmol) after which stirring commenced for 30 min. Anhydrous DMF (0.37ml, 4.8 mmol) was added and the reaction mixture was allowed to stir for 45 min. After an hour, the reaction mixture was allowed to warm to room temperature followed by addition of water and ether. The aqueous phase was extracted with ether and the organic layers washed with brine, dried over MgSO₄, and concentrated *in vacuo*. Flash chromatography (10-20% EtOAc in hexanes) gave 4-(4-triisopropylsiloxy-3-isopropylphenoxy)-3,5-dimethylbenzaldehyde (635 mg, 1.44 mmol) in 60% yield.

Preparation of CO22. TiCl₄ (1 M, 5.76 ml, 5.76 mmol) was added to 10 ml anhydrous THF drop-wise over 15 min. at 0°C and the mixture was stirred until the yellow precipitate appeared. A mixture of 10 (635 mg, 1.44 mmol), hydantoin

(175 mg, 1.7 mmol), and pyridine (3.5 ml, 43.2 mmol) was added to the reaction mixture at 0°C and stirred at room temperature for 24-h. Afterwards, the mixture was diluted with EtOAc and the solids filtered off. The filtrate was washed with H₂O, 3 N HCl, sat. NaHCO₃, and brine, then dried over MgSO₄. The crude product was purified by flash chromatography (40% EtOAc in hexanes) to give a tan solid. This material was then deprotected in the general way to give (E)-5-(4-(4-hydroxy-3-isopropylphenoxy)-3,5-dimethylbenzylidene)imidazolidine-2,4-dione (216 mg, 49%). A solution of (E)-5-(4-(4-hydroxy-3-isopropylphenoxy)-3,5-dimethylbenzylidene)imidazolidine-2,4-dione (216 mg, 0.70 mmol) in 10 ml of EtOH/HOAc (9:1) containing 10% Pd/C (25 mg) was hydrogenated at 1 atm at room temperature. After completion of hydrogen uptake (16-h), the catalyst was filtered off and the filtrate was diluted with ether and washed with sat. NaHCO₃. Concentration of the organic layer *in vacuo* and purification by flash chromatography (40% EtOAc in hexanes) afforded CO22 (194 mg, 90%). CO22 ¹H NMR (400MHz, CDCl₃): δ 1.21 (d, 6H, J=8.0Hz), 2.10 (s, 6H), 2.75 (dd, 1H, J=4.0Hz, J=12.0Hz), 3.14 (heptet, 1H, J=8.0Hz), 3.22 (dd, 1H, J=8.0Hz, J=12.0Hz), 4.28 (dd, 1H, J=4.0Hz, J=8.0Hz), 4.97 (s, 1H), 5.57 (s, 1H), 6.22 (dd, 1H, J=4.0Hz, J=8.0Hz), 6.58 (d, 1H, J=8.0Hz), 6.73 (d, 1H, J=4.0Hz), 6.91 (s, 2H), 7.27 (s, 1H). CO22 HRMS (*m/z*): [M]⁺ calcd for C₂₁H₂₄N₂O₄, 368.1736; found, 368.1749. CO22 HPLC (MeCN/water, 65-100%, 12 min.): retention time 3.6 min.; 99% pure.

A.1.3 General Chemical Procedures, Chapter 4

2-Cyclopropylphenol (7a). To 2-bromophenol **5** (8 g, 46.2 mmol) in 100 ml of dimethylformamide at 0° C was added NaH (2.6 g of a 60% suspension, 64.7 mmol). The reaction mixture was stirred for about 10 min. after which allyl bromide was added dropwise. After 30 min., the reaction mixture was treated with water and extracted with diethyl ether. The organic portion was dried over MgSO₄, filtered, and concentrated *in vacuo* to give the crude product, which was purified by flash chromatography (silica gel, hexane:ethyl acetate, 5:95) to give allyl 2-bromophenyl ether **6** (9.7 g, 45.5 mmol, 99%) as a white solid. This material was carried on to the next reaction to make **7a**. A dry round-bottom flask was charged with **6** (11 g, 51.6 mmol) and 260 ml of anhydrous diethyl ether and stirred at -78° C. To this solution was added drop-wise 1.7 M *tert*-BuLi in hexanes (60.7 ml, 103.3 mmol) after which stirring commenced for 30 min. To this solution was added N,N,N',N'-tetramethylethylenediamine (17 ml, 113.5 mmol) and stirring commenced for 45 min. before warming to room temperature. The reaction was allowed to stir overnight before addition of water. The aqueous phase was extracted with EtOAc. The combined organic layers were washed with water, brine, and 3 N HCl, dried over MgSO₄, concentrated *in vacuo*, and purified by flash chromatography (silica gel, hexane:ethyl acetate, 20:80) to give **7a** (5.1 g, 38.0 mmol, 74%) as a white solid. ¹H NMR (CDCl₃) δ 7.36 (d, *J* = 8 Hz, 1H), 7.06 (m, 2H), 6.85 (d, *J* = 8 Hz), 5.45 (s, 1H), 1.81 (m, 1H), 0.95 (m, 2H), 0.64 (m, 2H).

General procedure for preparation of TIPS-protected, 4-hydroxyphenyl boronic acids substituted at the 3-position (9a-9f). 2-Isopropylphenol **8** (10.0 g, 73.4 mmol) was added to a dry three-neck round-bottom flask fitted with an addition funnel and an exhaust line that runs into a base trap (6 M KOH). This solution was allowed to stir at 0° C after which Br₂ (4.5 ml, 88.1 mmol) was added drop-wise over a period of 15 min. Stirring commenced for an additional 3-h before addition of sat. NaHCO₃, water, and EtOAc. The aqueous phase was extracted with EtOAc and the combined organic layers were washed with brine and then dried over MgSO₄. After concentration of the organic phase *in vacuo*, the crude product was purified by flash chromatography (silica gel, hexane:ethyl acetate, 10:90) to give a slightly yellow clear oil (11.8 g, 55.1 mmol, 75%). This material (5 g, 23.3 mmol) was combined with TIPS-Cl (5.9 ml, 27.8 mmol) in a dry round-bottom flask containing 50 ml of anhydrous DCM and stirred at 0° C. To this solution was added imidazole (3.9 g, 58 mmol) and stirring commenced for an additional 18-h. The next day, the reaction was quenched with water and the aqueous phase extracted with EtOAc. The combined organic layers were washed with brine, dried over MgSO₄, concentrated *in vacuo*, and then purified with a short-path distillation column under high vacuum (0.5 mtorr). Pure fractions were collected at 130° C to give **8b** as a clear white solid (6.9 g, 18.6 mmol, 80%). This material was carried on to make **9b**. A dry round-bottom flask was charged with **8b** (6.9 g, 18.6 mmol) and 100 ml of anhydrous THF and stirred at -78° C. To this solution was added drop-wise 2.5 M *n*-BuLi in hexanes

(9.7 ml, 24.2 mmol) after which stirring commenced for 30 min. To this solution was added triisopropyl borate (8.7 ml, 37.2 mmol) and stirring commenced for 45 min. before warming to room temperature. After 1-h, the reaction was quenched with 3 N HCl and the aqueous phase extracted with EtOAc. The combined organic layers were washed with water and brine, dried over MgSO₄, concentrated *in vacuo*, and purified by flash chromatography (silica gel, hexane:ethylacetate, 10-40%) to give **9b** (5.5 g, 16.4 mmol, 88%) as a white solid.

General procedure for preparation of Boc-protected dihalo-L-tyrosine methyl esters (11a-11b). L-diiodotyrosine (**10a**) (5 g, 11.5 mmol) was added to a round-bottom flask and dissolved in MeOH/H₂O (2:1). To this mixture was added NaHCO₃ (2.9 g, 34.5 mmol) followed by Boc₂O (3.97 ml, 17.3 mmol). The reaction mixture was allowed to stir until completion as determined by TLC analysis (product should turn blue when tested with *p*-anisaldehyde). Upon completion, the mixture was acidified to pH 4.5 and extracted with EtOAc. The combined organic layers were washed with water and brine and then dried over MgSO₄. The crude material (5.9 g, 11.1 mmol, 96%) was then utilized in the next reaction. To this material (5.9 g, 11.1 mmol) in toluene/MeOH (9:1) was added TMSCHN₂ (0.5 M, 22 ml, 11.6 mmol) drop-wise over 30 min. at room temperature using a syringe pump. The reaction was allowed to stir until completion as determined by TLC analysis then washed with 0.5 M HCl and water. The aqueous phase was extracted with EtOAc and the organic layers

washed with brine, dried over MgSO_4 , and concentrated *in vacuo* to give the Boc-protected, diiodotyrosine methyl ester (**11a**) (5.4 g, 9.9 mmol, 89%).

Boc-protected diiodo-L-tyrosine methyl ester. The preparation of **11a** was effected using the general procedure for the preparation of Boc-protected dihalo-L-tyrosine methyl esters to give 5.4 g (89%) of the titled compound as a white solid. $^1\text{H NMR}$ (CDCl_3) δ 7.44 (s, 1H), 5.01 (s, 1H), 4.49 (dd, $J = 4.0$ Hz, $J = 8.0$ Hz, 1H), 3.74 (s, 3H), 3.00 (dd, $J = 4.0$ Hz, $J = 14.0$ Hz, 1H), 2.91 (dd, $J = 8.0$ Hz, $J = 14.0$ Hz, 1H), 1.45 (s, 9H).

Boc-protected dibromo-L-tyrosine methyl ester. The preparation of **11b** was effected using the general procedure for the preparation of Boc-protected dihalo-L-tyrosine methyl esters to give 1.1 g (87%) of the titled compound as a white solid. $^1\text{H NMR}$ (CDCl_3) δ 7.22 (s, 1H), 5.02 (s, 1H), 4.50 (dd, $J = 4.0$ Hz, $J = 8.0$ Hz, 1H), 3.74 (s, 3H), 3.05 (dd, $J = 4.0$ Hz, $J = 14.0$ Hz, 1H), 2.93 (dd, $J = 8.0$ Hz, $J = 14.0$ Hz, 1H), 1.44 (s, 9H).

General procedure for the preparation of biary ethers (12a-12f). 4 Å molecular sieves were flame dried under high vacuum in a dry round-bottom flask. To this flask was added boronic acid (3 mmol) and copper acetate (dried to a *verdigris* color). These components were dissolved in 10 ml anhydrous DCM after which anhydrous pyridine (5 mmol) and diisopropyl ethylamine (5 mmol) were added. This mixture was then allowed to stir at room temperature for 5 min. before addition of phenol (1 mmol) in three portions separated by 5 min. each. At this

point, the flask was fitted with a drying tube containing drierite and allowed to stir under ambient air over night, ~16-24-h. After this time, the reaction mixture was concentrated *in vacuo* and purified by flash chromatography to give products **12a-12f** (yield generally from 55-83%).

General procedure for the preparation of 5-(4-(4-hydroxyphenoxy)-3,5-dihalobenzyl)imidazolidine-2,4-diones (CO24 and CO26-CO30). Biaryl ether **12b** (510 mg, 0.69 mmol) was dissolved in 20 ml MeOH and saturated with ammonia gas. After 16-18-h, the mixture was purged with argon, concentrated *in vacuo*, and dissolved in anhydrous 3 N HCl in EtOAc/Ether. After 3-h, the mixture was quenched with water, the pH was adjusted to 4.5, and the aqueous phase extracted with EtOAc. The organic layers were washed with water and brine, dried over MgSO₄, and the crude material 9b (410 mg, 0.67 mmol, 99%) was carried on to make CO24. **13b** (410 mg, 0.67 mmol), 4-nitrophenyl chloroformate (160 mg, 0.78 mmol), and NaHCO₃ (218 mg, 2.6 mmol) were added to a dry round-bottom flask containing 10 ml anhydrous MeCN. The reaction was allowed to stir overnight followed by addition of 6.5 ml of H₂O. The solution should quickly turn yellow due to generation of nitrophenol. After 6-h, the reaction mixture was roto-vapped in order to remove MeCN, acidified to pH 5, and then extracted with EtOAc. The combined organic layers were washed with brine, dried over MgSO₄, and reconstituted in 10 ml THF. Deprotection of the TIPS group afforded CO24 (204 mg, 0.41 mmol, 63%, 2-steps from 9b) after purification by prep TLC (silica gel, hexane:ethyl acetate, 40:60).

Preparation of CO24. The preparation of CO24 was effected using the general procedure for the preparation of 5-(4-(4-hydroxyphenoxy)-3,5-dihalobenzyl)imidazolidine-2,4-diones to give 204 mg (63%, 2-steps from **13b**) of the titled compound as a white solid. ¹H NMR (DMSO-d₆) δ 10.65 (s, 1H), 9.06 (s, 1H), 7.99 (s, 1H), 7.58 (s, 2H), 6.64 (d, *J* = 8.0 Hz, 1H), 6.63 (d, *J* = 4.0 Hz, 1H), 6.20 (dd, *J* = 4.0 Hz, *J* = 8.0 Hz, 1H), 4.39 (dd, *J* = 4.0 Hz, *J* = 8.0 Hz, 1H), 3.15 (heptet, *J* = 8.0 Hz, 1H), 2.99 (dd, *J* = 4.0 Hz, *J* = 14.0 Hz, 1H), 2.87 (dd, *J* = 8.0 Hz, *J* = 14.0 Hz, 1H), 1.10 (d, *J* = 8.0 Hz, 6H). HPLC (MeCN/water, 50-100%, 15 min.): retention time 3.1 min. HR-MS calcd for C₁₉H₁₈Br₂N₂O₄: 497.9613. Found: 497.9607.

Preparation of CO26. The preparation of CO26 was effected using the general procedure for the preparation of 5-(4-(4-hydroxyphenoxy)-3,5-dihalobenzyl)imidazolidine-2,4-diones to give 80 mg (41%, 2-steps from **13e**) of the titled compound as a white solid. ¹H NMR (DMSO-d₆) δ 10.61 (s, 1H), 8.65 (s, 1H), 7.99 (s, 1H), 7.75 (s, 2H), 6.64 (d, *J* = 8.0 Hz, 1H), 6.50 (d, *J* = 4.0 Hz, 1H), 5.90 (dd, *J* = 4.0 Hz, *J* = 8.0 Hz, 1H), 4.37 (dd, *J* = 4.0 Hz, *J* = 8.0 Hz, 1H), 3.72 (s, 3H), 2.94 (dd, *J* = 4.0 Hz, *J* = 14.0 Hz, 1H), 2.81 (dd, *J* = 8.0 Hz, *J* = 14.0 Hz, 1H). HPLC (MeCN/water, 50-100%, 15 min.): retention time 1.8 min. HR-MS calcd for C₁₇H₁₄I₂N₂O₅: 579.8992. Found: 579.9004.

Preparation of CO27. The preparation of CO27 was effected using the general procedure for the preparation of 5-(4-(4-hydroxyphenoxy)-3,5-

dihalobenzyl)imidazolidine-2,4-diones to give 50 mg (25%, 2-steps from **13c**) of the titled compound as a white solid. $^1\text{H NMR}$ (DMSO- d_6) δ 10.65 (s, 1H), 9.09 (s, 1H), 7.97 (s, 1H), 7.77 (s, 2H), 6.66 (d, $J = 8.0$ Hz, 1H), 6.48 (d, $J = 4.0$ Hz, 1H), 6.26 (dd, $J = 4.0$ Hz, $J = 8.0$ Hz, 1H), 4.40 (dd, $J = 4.0$ Hz, $J = 8.0$ Hz, 1H), 2.94 (dd, $J = 4.0$ Hz, $J = 14.0$ Hz, 1H), 2.81 (dd, $J = 8.0$ Hz, $J = 14.0$ Hz, 1H), 2.07 (s, 3H). HPLC (MeCN/water, 50-100%, 15 min.): retention time 1.9 min. HR-MS calcd for $\text{C}_{17}\text{H}_{14}\text{I}_2\text{N}_2\text{O}_4$: 563.9043. Found: 563.9045.

Preparation of CO28. The preparation of CO28 was effected using the general procedure for the preparation of 5-(4-(4-hydroxyphenoxy)-3,5-dihalobenzyl)imidazolidine-2,4-diones to give 91 mg (35%, 2-steps from **13d**) of the titled compound as a white solid. $^1\text{H NMR}$ (DMSO- d_6) δ 10.60 (s, 1H), 8.94 (s, 1H), 7.98 (s, 1H), 7.75 (s, 2H), 6.64 (d, $J = 8.0$ Hz, 1H), 6.53 (d, $J = 4.0$ Hz, 1H), 6.24 (dd, $J = 4.0$ Hz, $J = 8.0$ Hz, 1H), 4.36 (dd, $J = 4.0$ Hz, $J = 8.0$ Hz, 1H), 3.16 (q, 2H), 2.95 (dd, $J = 4.0$ Hz, $J = 14.0$ Hz, 1H), 2.85 (dd, $J = 8.0$ Hz, $J = 14.0$ Hz, 1H), 1.11 (t, 3H). HPLC (MeCN/water, 50-100%, 15 min.): retention time 2.1 min. HR-MS calcd for $\text{C}_{18}\text{H}_{16}\text{I}_2\text{N}_2\text{O}_4$: 577.9199. Found: 577.9198.

Preparation of CO29. The preparation of CO29 was effected using the general procedure for the preparation of 5-(4-(4-hydroxyphenoxy)-3,5-dihalobenzyl)imidazolidine-2,4-diones to give 1.0 g (67%, 2-steps from **13a**) of the titled compound as a white solid. $^1\text{H NMR}$ (DMSO- d_6) δ 10.60 (s, 1H), 9.00 (s, 1H), 7.98 (s, 1H), 7.74 (s, 2H), 6.62 (d, $J = 8.0$ Hz, 1H), 6.24 (d, $J = 4.0$ Hz,

1H), 6.13 (dd, $J = 4.0$ Hz, $J = 8.0$ Hz, 1H), 4.37 (dd, $J = 4.0$ Hz, $J = 8.0$ Hz, 1H), 3.17 (m, 1H), 2.94 (dd, $J = 4.0$ Hz, $J = 14.0$ Hz, 1H), 2.85 (dd, $J = 8.0$ Hz, $J = 14.0$ Hz, 1H), 0.84 (m, 2H), 0.53 (m, 2H). HPLC (MeCN/water, 50-100%, 15 min.): retention time 2.0 min. HR-MS calcd for C₁₉H₁₆I₂N₂O₄: 589.9199. Found: 589.9209.

Preparation of CO30. The preparation of CO30 was effected using the general procedure for the preparation of 5-(4-(4-hydroxyphenoxy)-3,5-dihalobenzyl)imidazolidine-2,4-diones to give 1.3 g (65%, 2-steps from **13f**) of the titled compound as a white solid. ¹H NMR (DMSO-d₆) δ 10.61 (s, 1H), 9.09 (s, 1H), 7.98 (s, 1H), 7.76 (s, 2H), 6.67 (d, $J = 8.0$ Hz, 2H), 6.51 (d, $J = 8.0$ Hz, 2H), 4.36 (dd, $J = 4.0$ Hz, $J = 8.0$ Hz, 1H), 2.95 (dd, $J = 4.0$ Hz, $J = 14.0$ Hz, 1H), 2.84 (dd, $J = 8.0$ Hz, $J = 14.0$ Hz, 1H). HPLC (MeCN/water, 50-100%, 15 min.): retention time 1.7 min. HR-MS calcd for C₁₆H₁₂I₂N₂O₄: 549.8886. Found: 549.8900.

Preparation of 5-(4-(4-hydroxy-3-iodophenoxy)-3,5-diiodobenzyl)imidazolidine-2,4-dione (CO31). 5-(4-(4-hydroxyphenoxy)-3,5-diiodobenzyl)imidazolidine-2,4-dione (CO30, 100 mg, 0.2 mmol) in 0.2 ml of MeOH was added to a round-bottom flask at -5° C and dissolved in 5 ml of a 70% solution of aqueous ethylamine. To this mixture was added drop-wise Iodine (I₂) as a 1N aqueous solution saturated with KI (0.24 ml, 0.24 mmol). After 6-h, the reaction was acidified to pH 4.5, extracted with EtOAc, concentrated *in vacuo*, and purified by

flash chromatography (silica gel, hexane:ethyl acetate, 40:60) to give CO31 (85 mg, 0.13 mmol, 62%). $^1\text{H NMR}$ (DMSO- d_6) δ 10.62 (s, 1H), 9.97 (s, 1H), 8.00 (s, 1H), 7.77 (s, 2H), 7.02 (d, $J = 4.0$ Hz, 1H), 6.81 (d, $J = 8.0$ Hz, 1H), 6.58 (dd, $J = 4.0$ Hz, $J = 8.0$ Hz, 1H), 4.37 (dd, $J = 4.0$ Hz, $J = 8.0$ Hz, 1H), 2.95 (dd, $J = 4.0$ Hz, $J = 14.0$ Hz, 1H), 2.84 (dd, $J = 8.0$ Hz, $J = 14.0$ Hz, 1H). HPLC (MeCN/water, 50-100%, 15 min.): retention time 2.1 min. HR-MS calcd for $\text{C}_{16}\text{H}_{11}\text{I}_3\text{N}_2\text{O}_4$: 675.7853. Found: 675.7877.

Preparation of 5-(4-(4-hydroxy-3-iodophenoxy)-3,5-diiodobenzyl)imidazolidine-2,4-dione (CO32). 5-(4-(4-hydroxyphenoxy)-3,5-diiodobenzyl)imidazolidine-2,4-dione (CO30, 100 mg, 0.2 mmol) was added to a round-bottom flask and dissolved in 2 ml of DCM and 0.25 ml of glacial acetic acid at 0°C . To this mixture was added drop-wise bromine (12.3 μl , 0.24 mmol) in 1 ml of DCM. After 1-h, the reaction was extracted with EtOAc, concentrated *in vacuo*, and purified by flash chromatography (silica gel, hexane:ethyl acetate, 40:60) to give CO32 (109 mg, 0.18 mmol, 88%). $^1\text{H NMR}$ (DMSO- d_6) δ 10.61 (s, 1H), 9.90 (s, 1H), 7.98 (s, 1H), 7.76 (s, 2H), 6.87 (d, $J = 8.0$ Hz, 1H), 6.82 (d, $J = 4.0$ Hz, 1H), 6.55 (dd, $J = 4.0$ Hz, $J = 8.0$ Hz, 1H), 4.36 (dd, $J = 4.0$ Hz, $J = 8.0$ Hz, 1H), 2.96 (dd, $J = 4.0$ Hz, $J = 14.0$ Hz, 1H), 2.79 (dd, $J = 8.0$ Hz, $J = 14.0$ Hz, 1H). HPLC (MeCN/water, 50-100%, 15 min.): retention time 2.0 min. HR-MS calcd for $\text{C}_{16}\text{H}_{11}\text{BrI}_2\text{N}_2\text{O}_4$: 627.7992. Found: 627.7981.

A.2 Preparation of Chemicals for Use *In vitro* or *In vivo*

Preparation of chemicals. Stocks of T₃, CO23, GC-1, and NH-3 were prepared with DMSO at a concentration of 10 mM and stored at -20°C until use; GC-1 and NH-3 were prepared as described previously (3,4). All other chemicals were purchased from Sigma unless otherwise indicated. Methimazole (Aldrich) was dissolved in sterile water to a final concentration of 1 M and stored at -20°C. 0.1% aminobenzoic acid ethyl ester (Tricaine or MS222) was made fresh in sterile ddH₂O and kept at 4°C for no longer than 1 week.

A.3 ¹²⁵I-T₃ Competitive Binding Assay

Thyroid Hormone Competition Binding Assay. Full-length hTRα₁ and hTRβ₁ were expressed using a TNT T7 quick-coupled transcription translation system (Promega). Competition assays for binding of unlabeled T₃ and CO23 were performed using 1 nM ¹²⁵I-T₃ in a gel filtration binding assay as described (5).

A.4 TR Transactivation Assay

Transient Transfection Assays. Human bone osteosarcoma epithelial (U2OS) cells or human uterine cervix cancer (HeLa) cells (Cell Culture Facility, UCSF) were grown to ~80% confluency in Dulbecco's modified Eagles (DME) /H-21, 4.5 g/liter glucose medium containing 10% newborn calf serum (NCS) or fetal bovine

serum (FBS) respectively (both heat-inactivated), 2 mM glutamine, 50 units ml⁻¹ penicillin, and 50 µg ml⁻¹ streptomycin. Cells (~1.5-2 X 10⁶) were collected and resuspended in 0.5 ml of electroporation buffer (Dulbecco's phosphate-buffered saline containing 0.1% glucose and 10 mg/ml bioprene) with 1.5 µg of a TR expression vector (full-length hTRα₁-CMV or hTRβ₁-CMV), 0.5 µg of pRL-TK constitutive *Renilla* luciferase reporter plasmid (Promega), 5 µg of a reporter plasmid containing a synthetic TR response element (DR-4) containing two copies of a direct repeat spaced by four nucleotides (AGGTCAcaggAGGTCA) cloned immediately upstream of a minimal thymidine kinase promoter linked to a luciferase coding sequence (6). Cells were electroporated using a Bio-Rad gene pulser at 350 V and 960 microfarads in 0.4-cm cuvettes, pooled in DME/F-12 Ham's 1:1 without phenol red (U2OS) or DME/H-21 (HeLa) supplemented as above except that NCS and FBS were hormone stripped using dextrose-coated charcoal, and plated in 96-well (U2OS) or 12-well (HeLa) plates to a final density of 20,000 cells/well and 100,000 cells per well respectively. After a 2-h incubation period, compounds in 1% dimethyl sulfoxide (DMSO) were added to the cell culture medium in triplicate. After an additional 16-h incubation period, cells were harvested and assayed for luciferase activity using the Promega dual-luciferase kit (Promega) and an Analyst AD (Molecular Devices). Data normalized to the *Renilla* internal control were analyzed with GraphPad Prism, v4, using the sigmoid-dose response model to generate EC₅₀ values; EC₅₀ values were obtained by fitting data to the following equation: $Y = \text{Bottom} + (\text{Top} - \text{Bottom}) / (1 + 10^{((\text{LogEC}_{50} - X) * \text{HillSlope}))}$.

A.5 High-Throughput *In vitro* Binding Assay for TR-Coregulator Interactions

Protein Expression and Purification. hTR β LBD (His6; residues T209-D461) was expressed in BL21(DE3) (Invitrogen) (10X 1L culture) at 20 °C, 0.5 mM isopropyl-1-thio- β -D-galactopyranoside added at OD₆₀₀ = 0.6 (7). When the OD₆₀₀ reached 4, cells were harvested, resuspended in 20 ml of buffer/1 liter of culture (20 mM Tris, 300 mM NaCl, 0.025% Tween 20, 0.10 mM phenylmethylsulfonyl fluoride, 10 mg of lysozyme, pH 7.5), incubated for 30 min on ice, and then sonicated for 3 X 3 min on ice. The lysed cells were centrifuged at 100,000 X g for 1 h, and the supernatant was loaded onto Talon resin (20 ml, Clontech). Protein was eluted with 500 mM imidazole (3 X 5 ml) plus ligand (3,5,3'-triiodo-L-thyronine (Sigma)). Protein purity (>90%) was assessed by SDS-PAGE and high pressure size exclusion chromatography, and protein concentration was measured by the Bradford protein assay. The protein was dialyzed overnight against assay buffer (3 X 4 liters, 50 mM sodium phosphate, 150 mM NaCl, pH 7.2, 1 mM dithiothreitol, 1 mM EDTA, 0.01% Nonidet P-40, 10% glycerol). hTR α LBD (His6; residues Glu148-Val410) was expressed using the same procedure as hTR β with the exception that 0.5mMisopropyl-1-thio- β -D-galactopyranoside was added at OD₆₀₀ = 1.2. Unliganded protein was eluted with 100 mM imidazole.

Direct Binding Assay. The protein was serially diluted from 70 to 0.002 μM in binding buffer (50 mM sodium phosphate, 150 mM NaCl, pH 7.2, 1 mM dithiothreitol, 1 mM EDTA, 0.01% Nonidet P-40, 10% glycerol) containing 1 μM ligand T3 in 96-well plates (7). Then 10 μl of diluted protein was added to 10 μl of labeled SRC2-2 (20 nM) in 384-well plates yielding final protein concentrations of 35–0.001 μM and 10 nM fluorescent peptide concentration. The samples were allowed to equilibrate for 30 min. Binding was then measured using fluorescence polarization (excitation λ 485 nm, emission λ 530 nm) on an AnalystAD plate-reader (Molecular Devices). Two independent experiments, each in quadruplicate, were carried out for each state. Data were analyzed using GraphPad Prism, v4, and the K_d values were obtained by fitting data to the following equation ($y = \text{min} + (\text{max} - \text{min}) / (1 + (x/K_d)^{\text{Hill slope}})$).

A.6 *Xenopus laevis* Induced Metamorphosis Procedures

A.6.1 General *X. laevis* Tadpole Procedures, Aquaculture, and Euthanasia

General Xenopus laevis tadpole procedures. *Xenopus laevis* stage-53/54 tadpoles were purchased from NASCO, Inc. and staged according to Nieuwkoop and Faber (8). Upon receipt, tadpoles were allowed to set over night at room temperature (18-25°C) in order to recover from shipping shock, after which half of the initial rearing water was replaced with 0.1X Marc's Modified Ringer's (MMR) buffer (10X solution consists of 100 mM NaCl (Fisher), 2 mM KCl (Fisher), 1 mM

MgCl₂, 2 mM CaCl₂, 0.1 mM EDTA, and 5 mM Hepes, pH 7.8) and in some cases, the tadpoles were maintained at a concentration of 1 mM methimazole. Tadpoles were ultimately maintained in fresh 0.1X MMR buffer, changed every 2-days, with or without methimazole. After completion of experiments, live tadpoles were euthanized by treatment with 0.01% Tricaine, exposure to an ice-bath, and either fixed in phosphate-buffered saline containing 3.5% formalin or decapitated in order to ensure death. Animals were photographed with a Canon PowerShot A510 and images were processed with Adobe Photoshop CS, v8, and Adobe Illustrator CS, v11. All tadpole experiments were conducted in accordance with Institutional Animal Care and Use Committee approval (animal protocol #: A7228-23070-01).

A.6.2 Induced Metamorphosis Experiments

Induced metamorphosis experiments. Stage-53/54 tadpoles were added to Extra-Deep petri dishes (Fisher) in triplicate containing 50 mL of 0.1X MMR buffer and vehicle or the appropriate concentration(s) and combination of ligand(s) (T₃, CO23, GC-1, and NH-3) with or without methimazole. The final DMSO concentration was 0.1%. Induced metamorphosis experiments were repeated at least threefold.

A.6.3 Quantification of Hind Leg Development

Quantification of Hind Leg development. Groups of tadpoles were treated with the appropriate concentration of ligand and photographed live daily, every 24-h, for 4-days or sacrificed before excision of HLs. One method of quantifying HL development was through measuring the HL length (pixels) to tail length (pixels) (H/T) ratio, as this ratio correlates reasonably well with metamorphic stage and serves to normalize for differences in initial tadpole size (9). The percentage of tail length remaining was also determined for the highest ligand concentrations tested (30 nM T₃ and 100 nM CO₂) in order to show that tail length remains constant, and thus, leaves the H/T ratio unaffected. These experiments were repeated twice and each experimental point consisted of the mean H/T ratio and percent tail length remaining for three tadpoles. HL development was also monitored by recording the increase in mass as compared to day zero of HLs over a 5-day time period. Tadpole HLs from different groups of tadpoles in 1 mM methimazole were excised every 24-h, placed on pre-tared weighing paper, dried in ambient air for 3-h, and then weighed on a Sartorius balance accurate to the 0.01 mg. These experiments were repeated twice and each experimental point consisted of the mean increase in weight normalized to maximal T₃ response for 3-5 tadpoles.

A.6.4 Temporal Separation of TR Subtype Mediated Effects on Morphogenesis

Temporal control over morphogenesis. These experiments were carried out in the presence of 1 mM methimazole as in induced metamorphosis experiments except that at the indicated time point, 0.1X MMR buffer containing either CO23(50 and 100nM) or GC-1 (50nM) was replaced with 0.1X MMR containing GC-1 (50nM) or CO23 (100nM) respectively. Each experimental point consisted of three tadpoles and each experiment was repeated twice .

A.6.5 Quantitative Real-Time PCR

Quantitative real-time PCR assay. Total RNA was extracted from head, HL, and tail tissue from groups of 6-10 tadpoles using TRIzol reagent (Invitrogen) according to the manufacturer's specifications. The total RNA was processed as described previously (10) and the C_T method (Applied Biosystems User Bulletin #2) was employed to quantify gene induction normalized to the *Xenopus* 18S rRNA subunit (RL8) and relative to a physiological calibrator. Relative gene induction was quantified with the equation $2^{-\Delta\Delta C_T}$ in sextuplicate and the standard deviation was calculated using the comparative method described in User Bulletin #2. rt-PCR reactions were carried out on a DNA Engine Opticon2 and the data were analyzed using Opticon software. Primers used to detect RL8 and collagenase-3 were the same as reported previously (10). Primers used to

detect all other target genes were designed using the Primer3 website (http://frodo.wi.mit.edu/cgi-bin/primer3/primer3_www.cgi) and the sequences are as follows:

xTR α f: 5'-CTA CGA TCC AGA CAG CGA GAC-3',

xTR α r: 5'- GTT CAA AGG CGA GAA GGT AGG-3',

xTR β f: 5'- ATG GCA ACA GAC TTG GTT TTG-3',

xTR β r: 5'- CGC ATT AAC TAT GGG AGC TTG-3',

xBTEB f: 5'-CCA TCT CAA AGC CCA CTA CAG-3',

xBTEB r: 5'- GAA TTG GAC CTT TTG GAC CTT-3'.

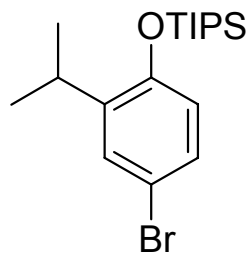
A.7 References

1. Renaldo, A.F., Labadie, J.W., and Stille, J.K. (1998) Palladium-catalyzed coupling of acid chlorides with organotin reagents: ethyl (e)-4-(4-nitrophenyl)-4-oxo-2-butenoate [2-butenoic acid, 4-(4-nitrophenyl)-4-oxo-, ethyl ester, (e)-]. In *Organic Syntheses* (Aslanian, R., Smith, C.A., and Kende, A.S., Eds.) 67, p. 87.
2. Yamaguchi, J., Harada, M., Kondo, T., et al. (2003) A facile method for preparation of optically active hydantoin. *Chem. Lett.* 32, 372-373.
3. Chiellini, G., Nguyen, N.-H., Yoshihara, H., and Scanlan, T. (2000) Improved synthesis of the iodine-free thyromimetic GC-1. *Bioorg. Med. Chem Lett.* 10, 2607-2611.
4. Nguyen, N.-H., Apriletti, J., Cunha-Lima, S., Webb, P., Baxter, J., and Scanlan, T. (2002) Rational design and synthesis of a novel thyroid hormone antagonist that blocks coactivator recruitment. *J. Med. Chem.* 45, 3310-3320.
5. Apriletti, J., Baxter, J., Lau, K., and West, B. (1995) *Protein Express. Purif.* 6, 363-370.
6. Chiellini, G., Apriletti, J., Yoshihara, H., Baxter, J., Ribeiro, R., and Scanlan, T. (1998) A high-affinity subtype-selective agonist ligand for thyroid hormone receptor. *Chem. Biol.* 5, 299-306.

7. Moore, J., Galicia, S., McReynolds, A., et al. (2004) Quantitative proteomics of the thyroid hormone receptor-coregulator interactions. *J. Biol. Chem.* 279, pp. 27584-27590.
8. Nieuwkoop, P. D., and Faber, J. (1994) *Normal Table of Xenopus Laevis (Daudin): A Systematical and Chronological Survey of the Development From the Fertilized Egg Till the End of Metamorphosis* 2nd ed., Garland Publishing, New York and London.
9. Li, H. C. (1978) *Hormonal Proteins and Peptides* 6th ed., Academic Press, New York.
10. Lim, W., Nguyen, N.-H., Yang, H., Scanlan, T., and Furlow, J. (2002) A thyroid hormone antagonist that inhibits thyroid hormone action *in vivo*. *J. Biol. Chem.* 277, 35664-35670.

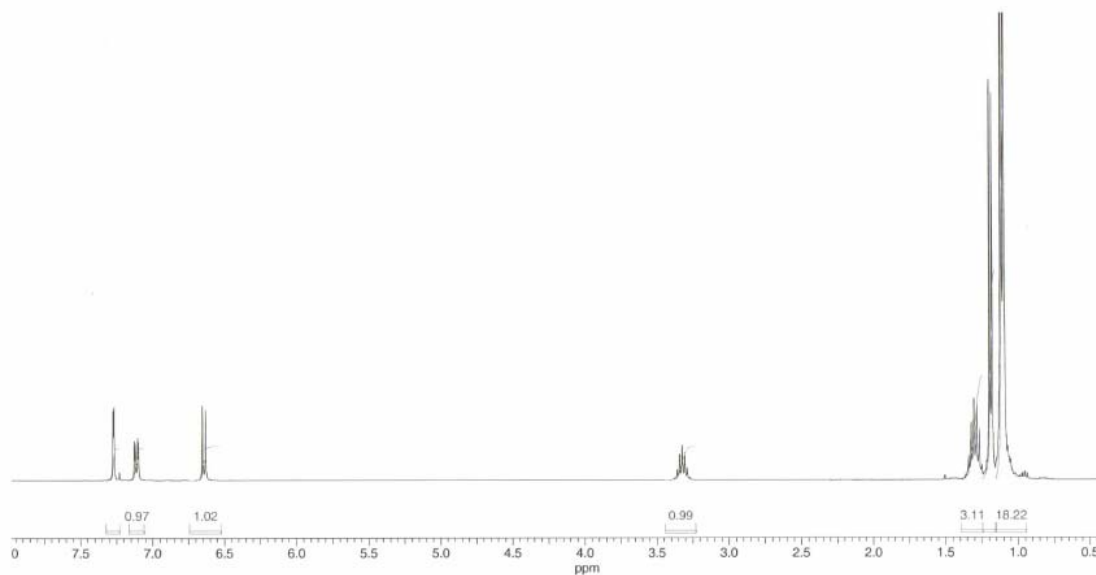
Appendix B
 ^1H and ^{13}C Nuclear Magnetic Resonance (NMR)
Characterization of Compounds

B.1 NMR Spectra of Compounds from Chapter 2

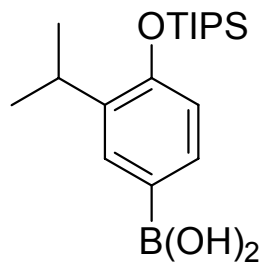


(4-Bromo-2-isopropylphenoxy)triisopropylsilane (12)

^1H NMR (CDCl_3)

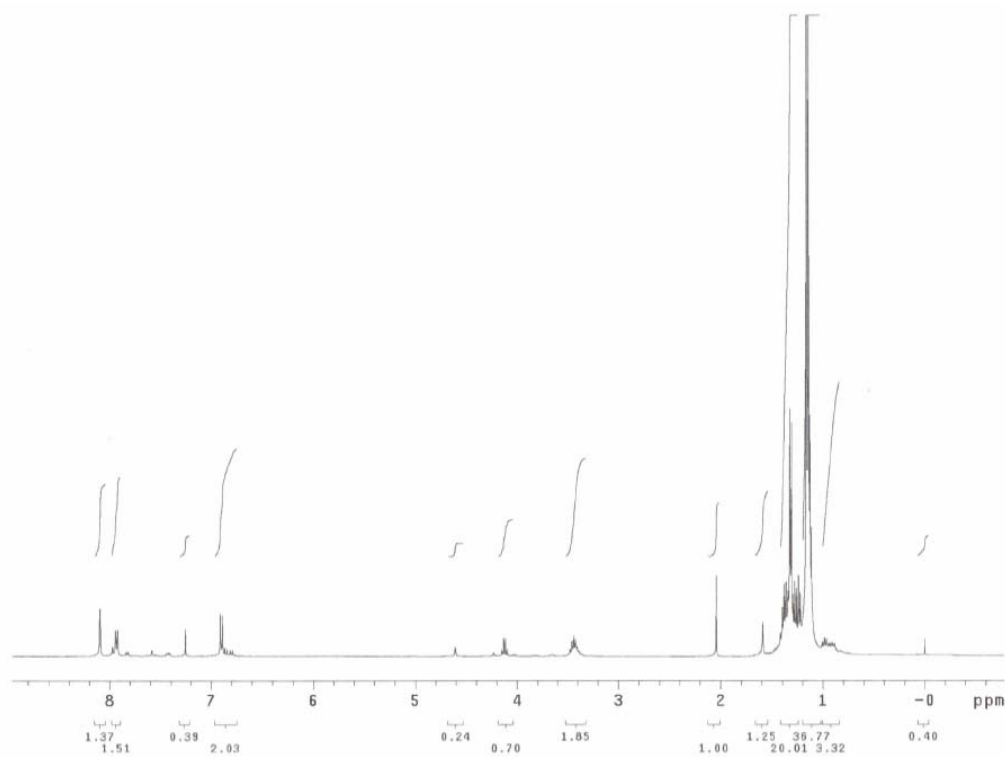


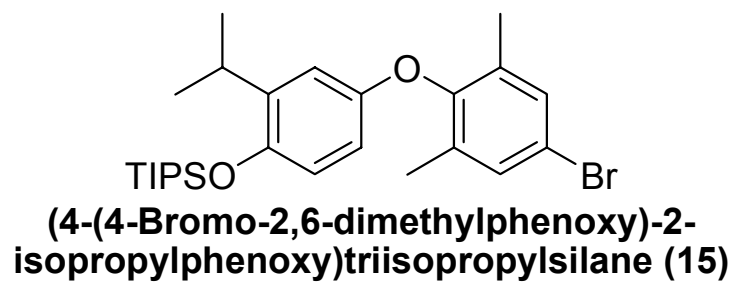
No.	(ppm)	(Hz)	Height	No.	(ppm)	(Hz)	Height	No.	(ppm)	Value	Absolute Value
1	1.07	426.9	0.0305	12	3.32	1327.7	0.0318	1	[0.95 .. 1.15]	18.220	4.28391e+8
2	1.07	428.8	0.0312	13	3.34	1334.7	0.0238	2	[1.16 .. 1.25]	6.184	1.45398e+8
3	1.10	438.3	0.7816	14	6.63	2649.9	0.0650	3	[1.25 .. 1.39]	3.110	7.31141e+7
4	1.12	445.6	1.0000	15	6.65	2658.3	0.0686	4	[3.23 .. 3.44]	0.992	2.33356e+7
5	1.18	470.9	0.3544	16	7.10	2836.3	0.0355	5	[6.52 .. 6.75]	1.022	2.40332e+7
6	1.19	477.5	0.3667	17	7.10	2838.8	0.0392	6	[7.06 .. 7.17]	0.965	2.26926e+7
7	1.27	506.0	0.0465	18	7.12	2845.1	0.0336	7	[7.23 .. 7.32]	0.958	2.25307e+7
8	1.28	513.4	0.0710	19	7.13	2847.6	0.0360				
9	1.30	521.0	0.0749	20	7.27	2904.0	0.0671				
10	1.32	528.4	0.0529	21	7.27	2906.6	0.0639				
11	3.31	1321.1	0.0247								



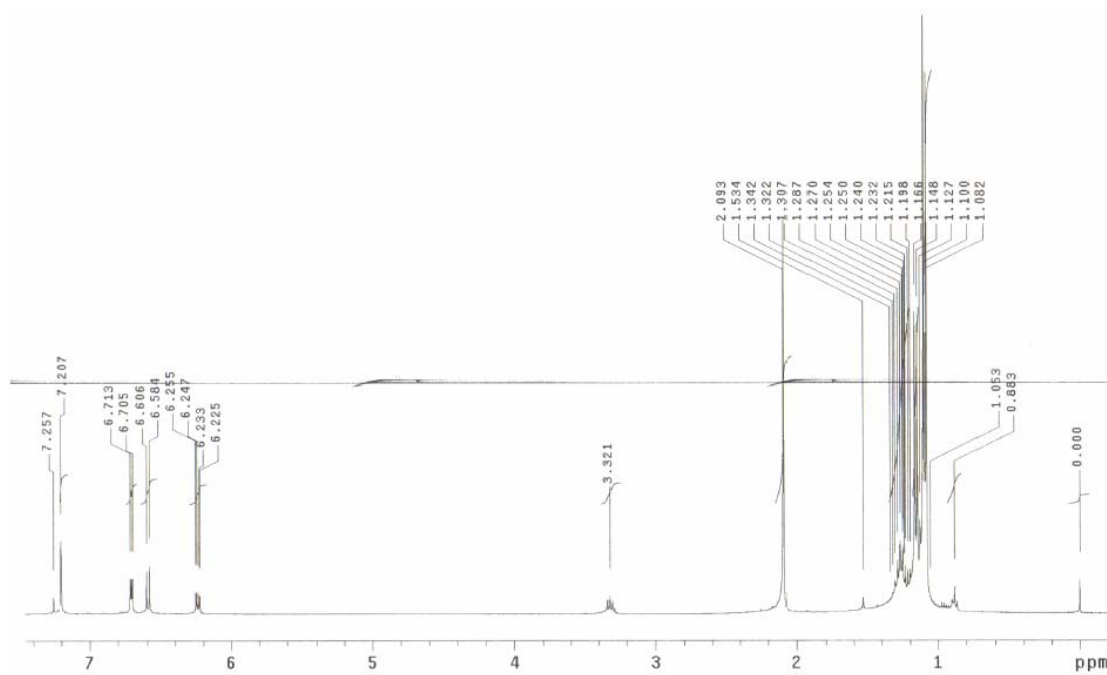
4-Triisopropylsiloxy-3-isopropylphenylboronic acid (13)

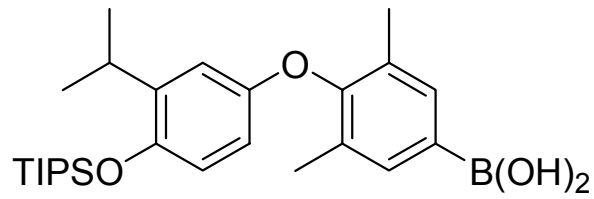
¹H NMR (CDCl₃)





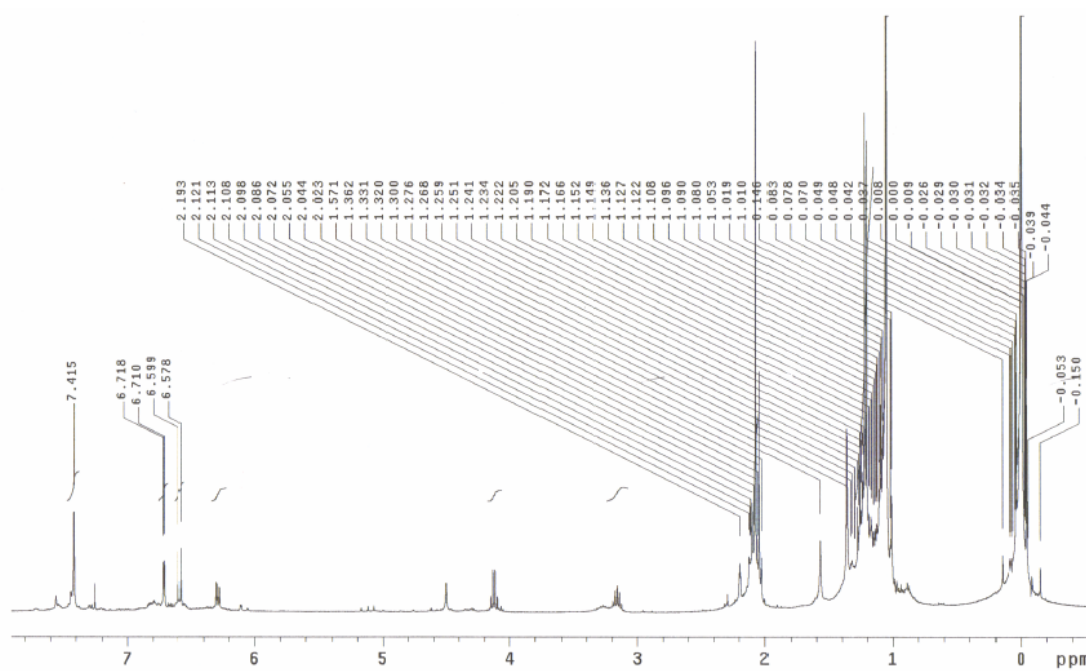
¹H NMR (CDCl₃)

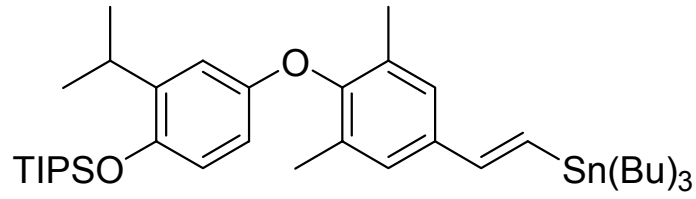




**4-(4-Triisopropylsiloxy-3-isopropylphenoxy)-
3,5-dimethylphenylboronic acid (16)**

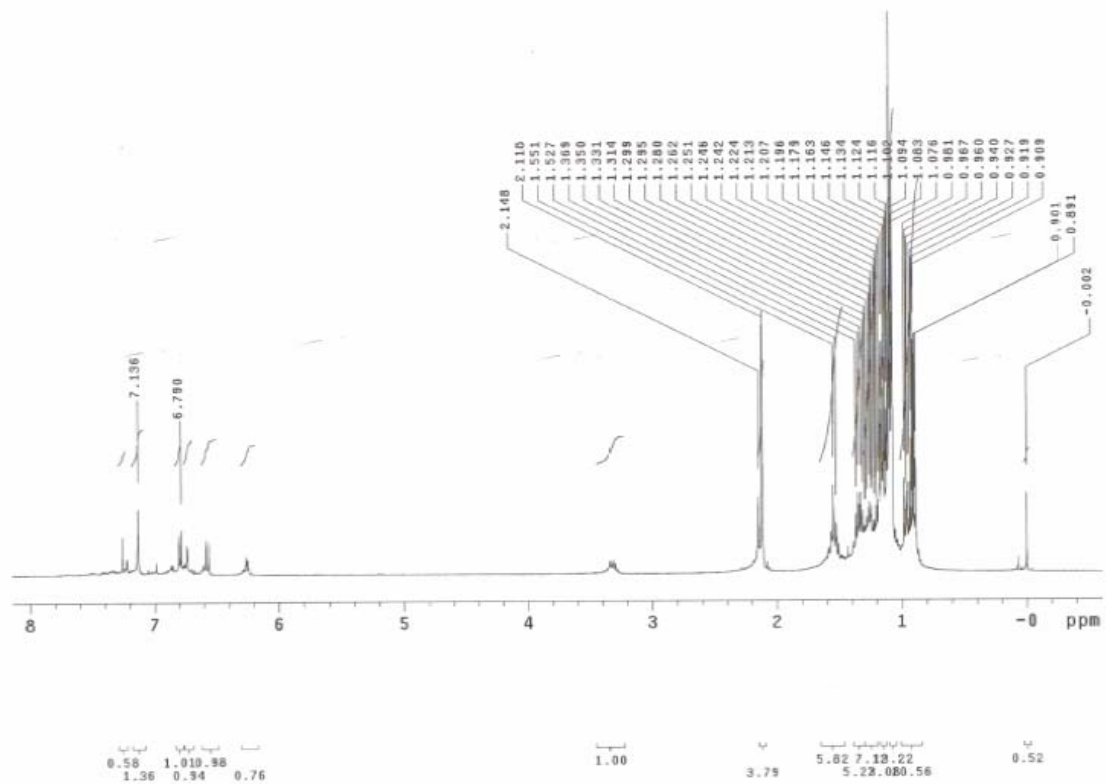
¹H NMR (CDCl₃)

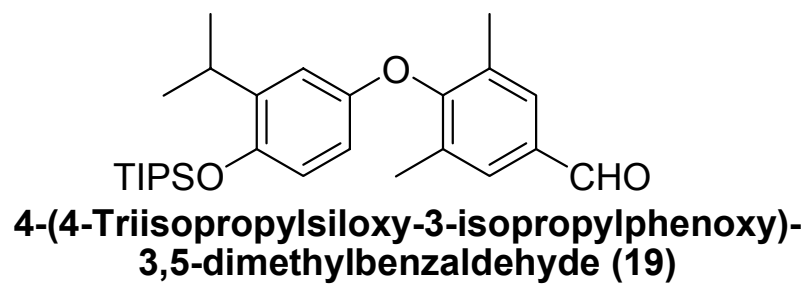




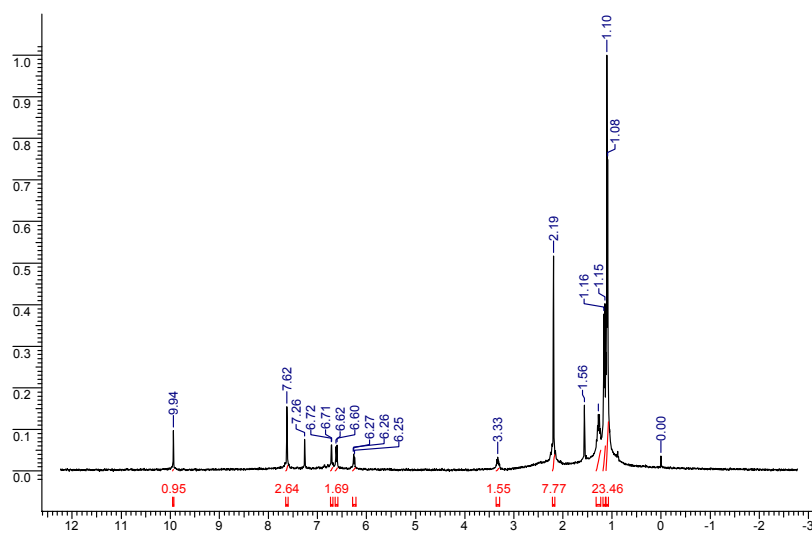
4-(4-((*E*)-2-(tributylstannyl)vinyl)-2,6-dimethylphenoxy)-2-isopropylphenoxytriisopropylsilane (18)

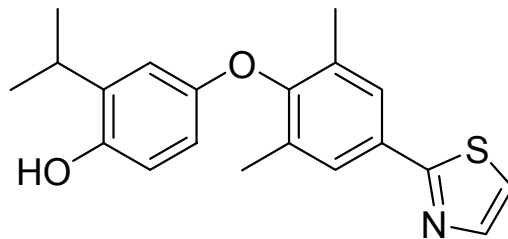
$^1\text{H NMR}$ (CDCl_3)





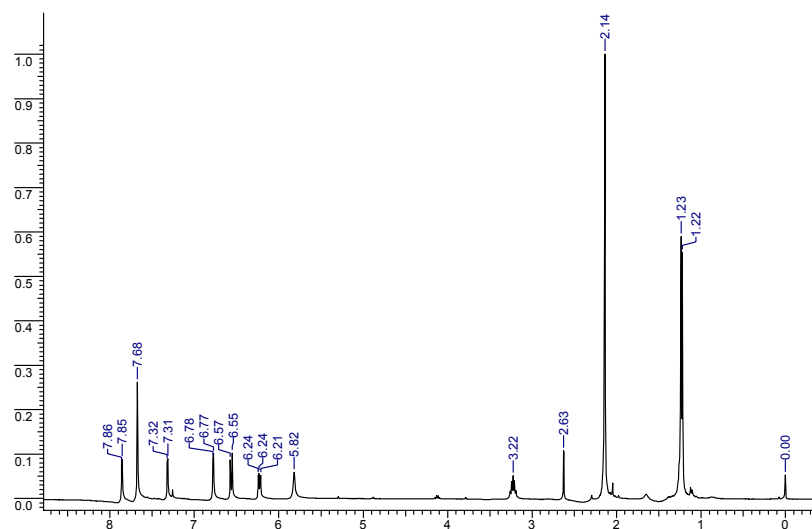
¹H NMR (CDCl₃)



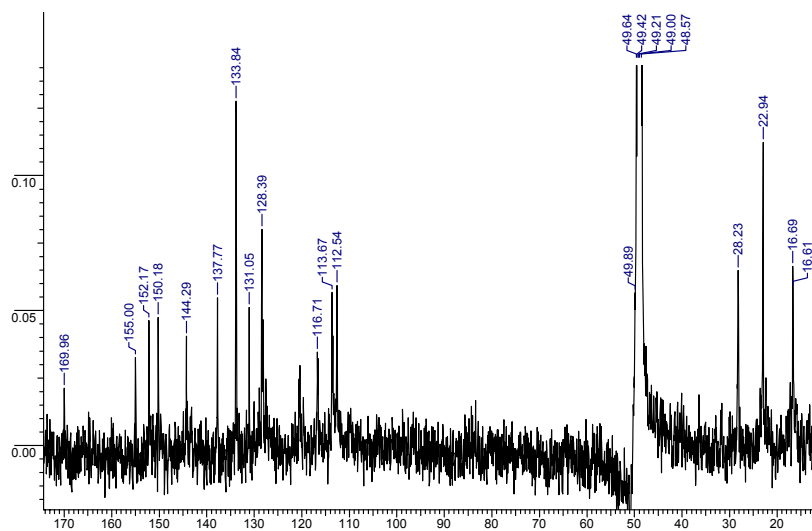


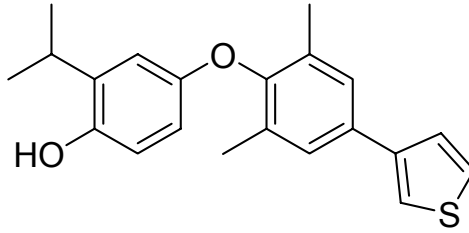
4-(2,6-Dimethyl-4-(thiazol-2-yl)phenoxy)-2-isopropylphenol (CO1)

$^1\text{H NMR (CDCl}_3\text{)}$



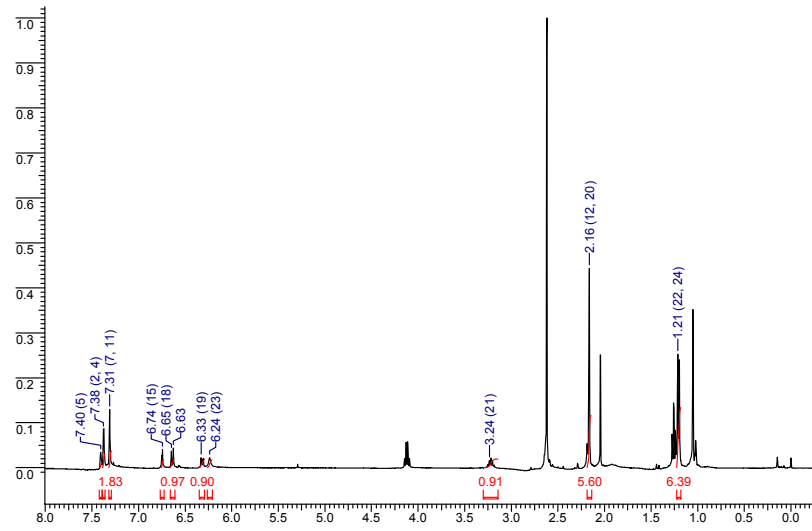
$^{13}\text{C NMR (CDCl}_3\text{)}$



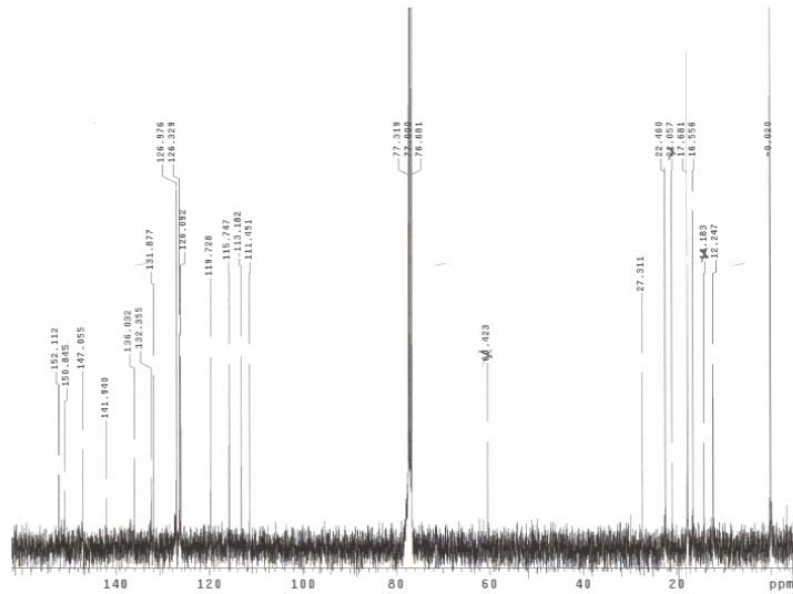


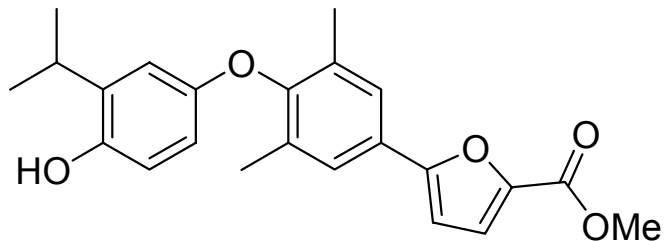
4-(2,6-Dimethyl-4-(thiophen-3-yl)phenoxy)-2-isopropylphenol (CO2)

$^1\text{H NMR (CDCl}_3\text{)}$



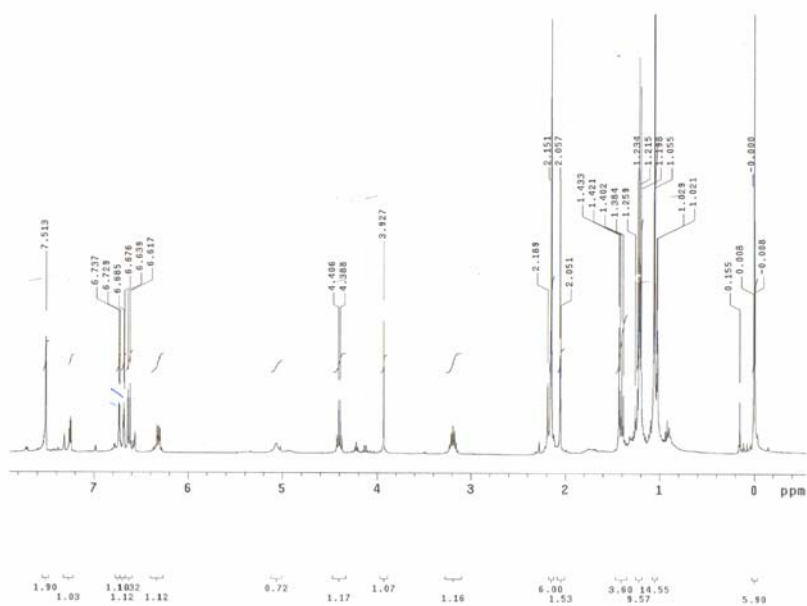
$^{13}\text{C NMR (CDCl}_3\text{)}$



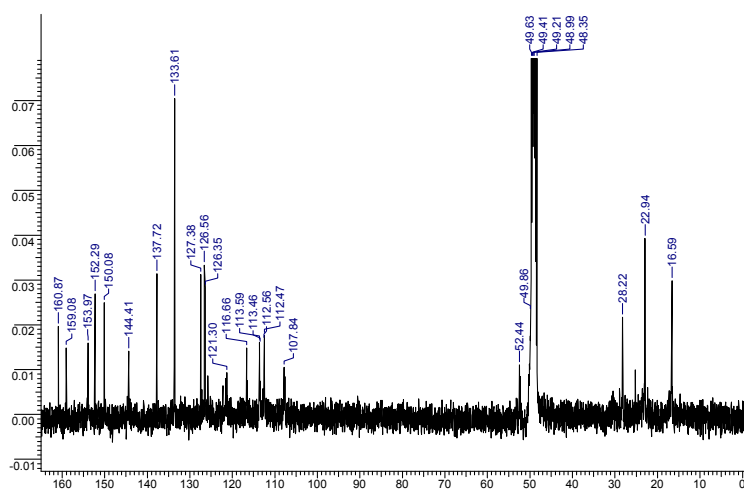


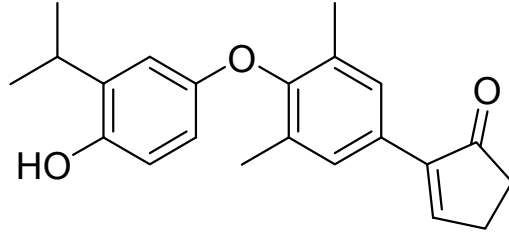
Methyl 5-(4-(4-hydroxy-3-isopropylphenoxy)-3,5-dimethylphenyl)furan-2-carboxylate (CO3)

¹H NMR (CDCl₃)



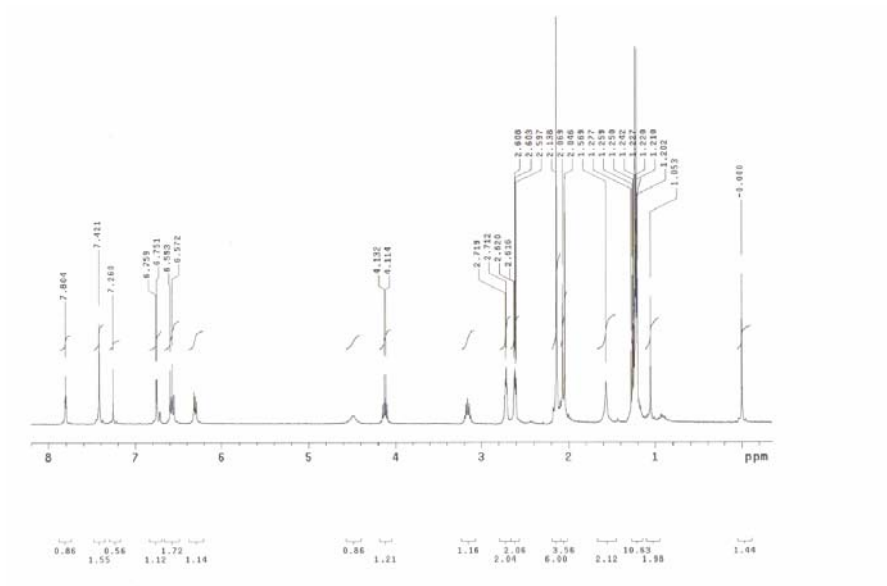
¹³C NMR (CD₃OD)



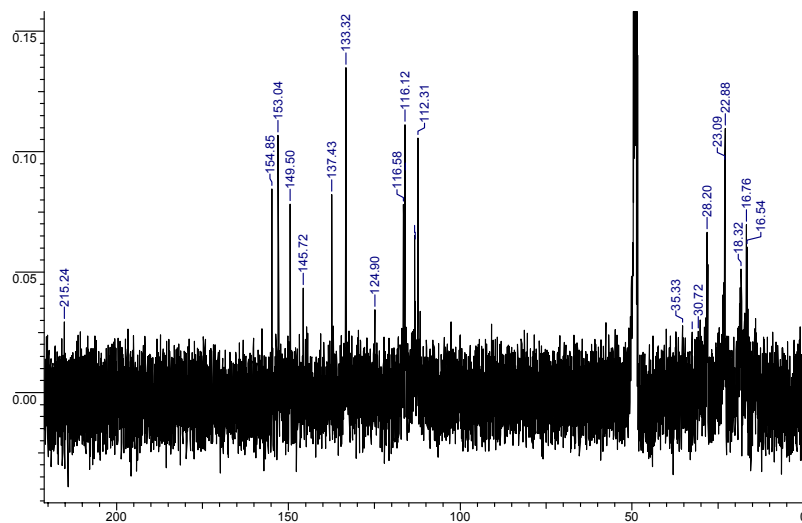


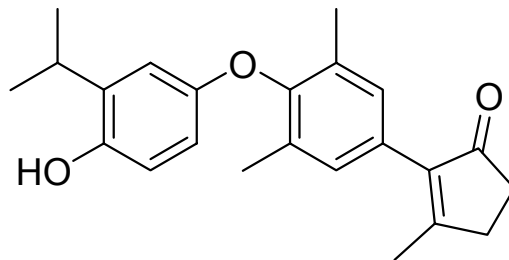
2-(4-(4-Hydroxy-3-isopropylphenoxy)-3,5-dimethylphenyl)cyclopent-2-enone (CO4)

$^1\text{H NMR}$ (CDCl_3)



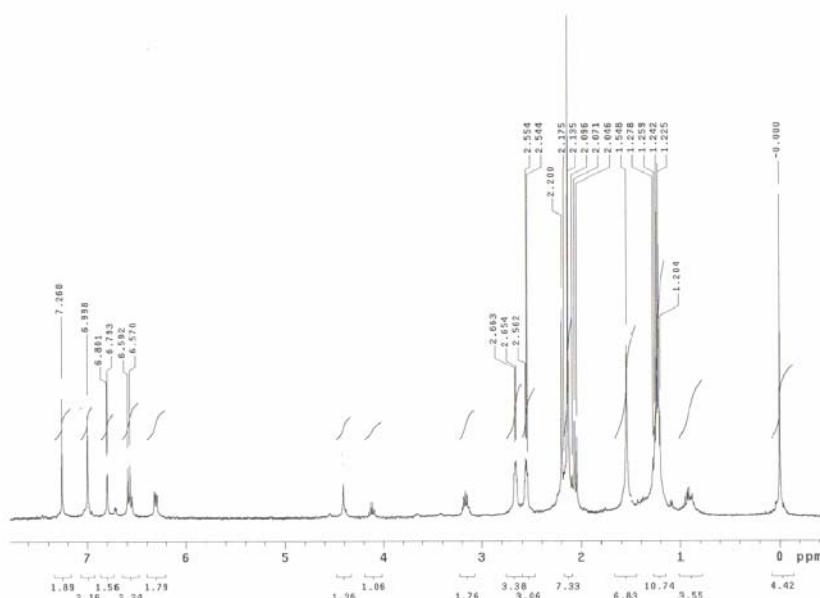
$^{13}\text{C NMR}$ (CD_3OD)



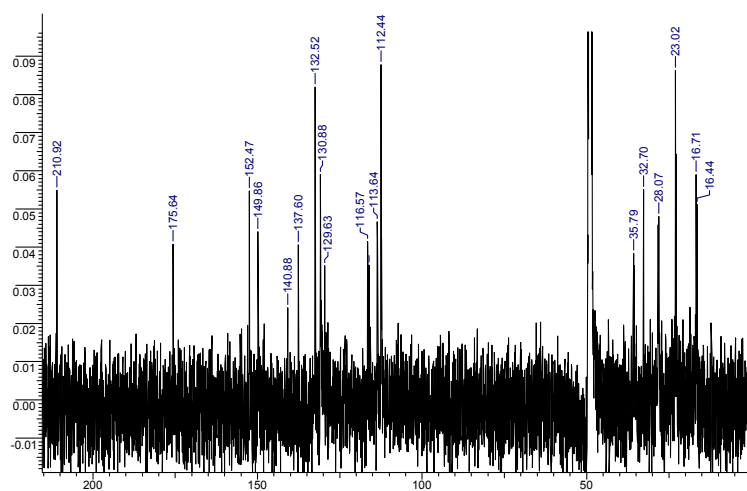


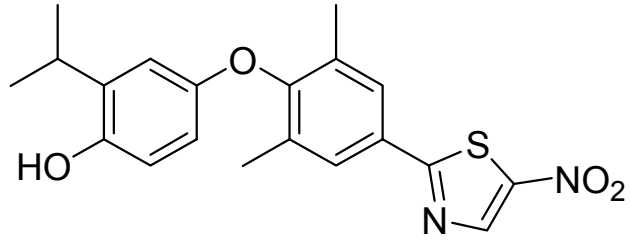
2-(4-(4-Hydroxy-3-isopropylphenoxy)-3,5-dimethylphenyl)-3-methylcyclopent-2-enone (CO5)

$^1\text{H NMR}$ (CDCl_3)



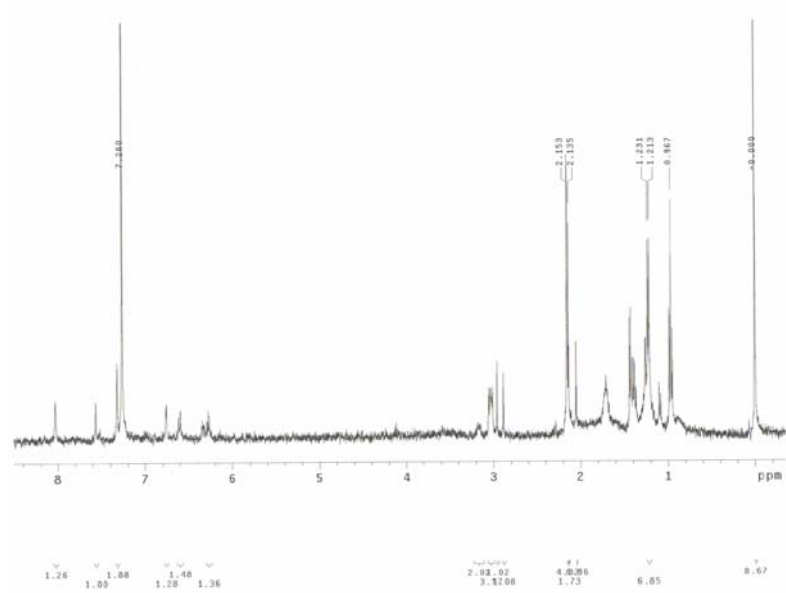
$^{13}\text{C NMR}$ (CD_3OD)



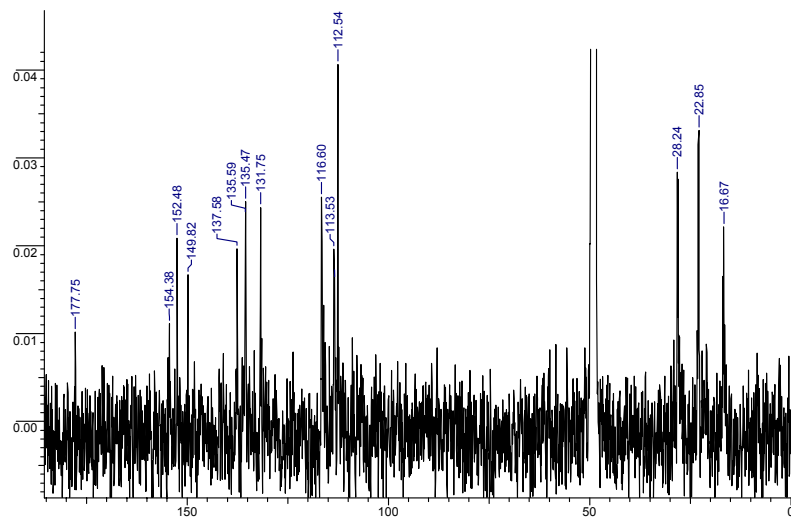


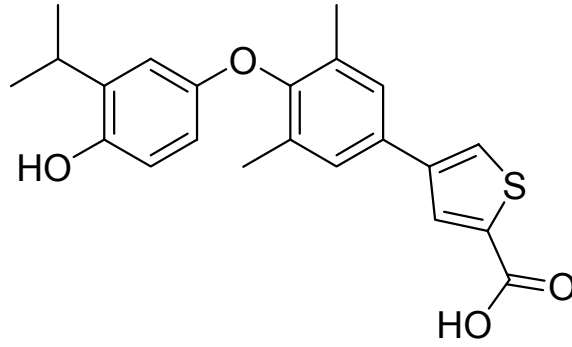
4-(2,6-Dimethyl-4-(5-nitrothiazol-2-yl)phenoxy)-2-isopropylphenol (CO7)

¹H NMR (CDCl₃)



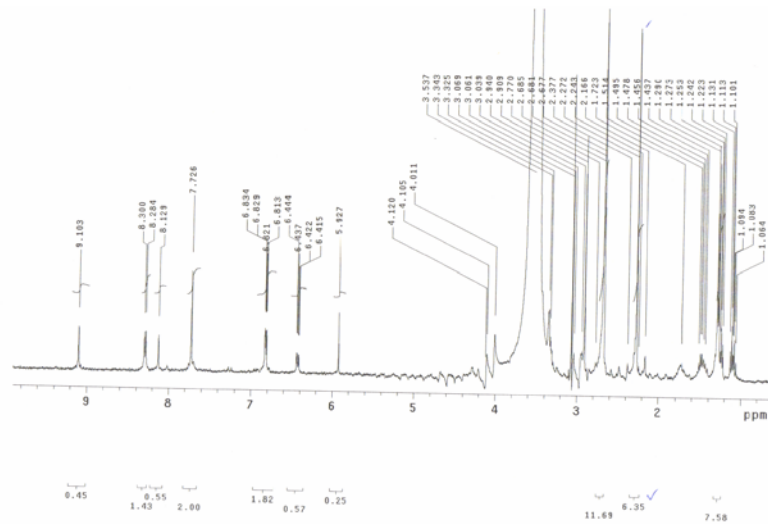
¹³C NMR (CD₃OD)



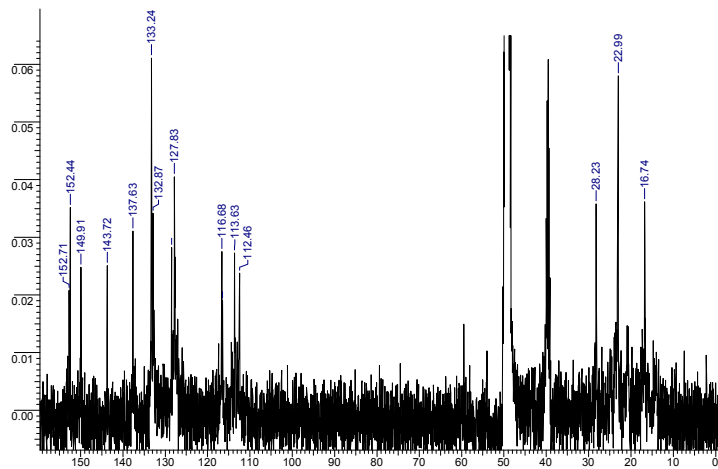


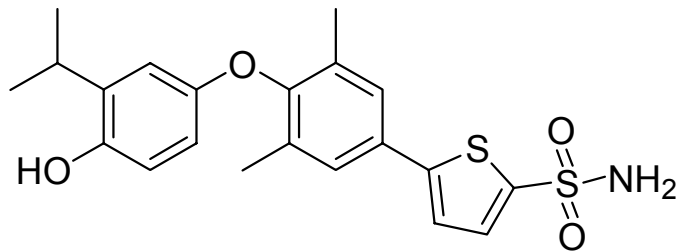
4-(4-(4-Hydroxy-3-isopropylphenoxy)-3,5-dimethylphenyl)thiophene-2-carboxylic acid (CO8)

¹H NMR (DMSO-d₆)



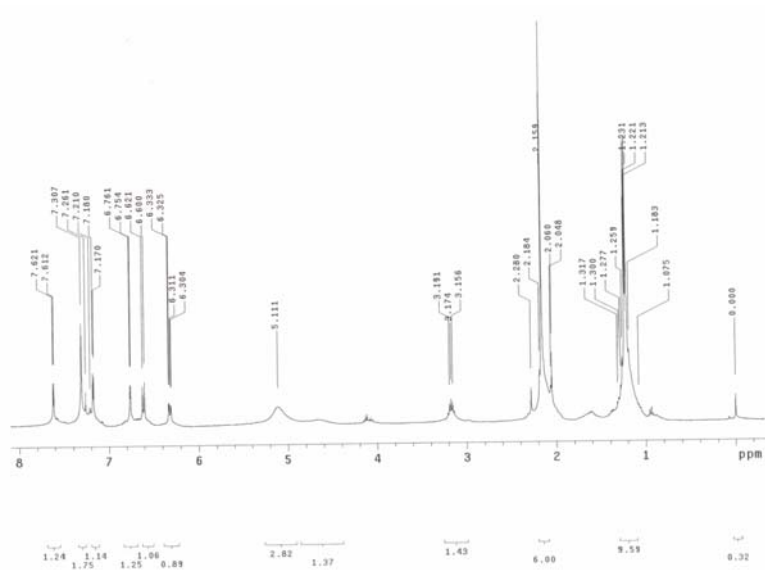
¹³C NMR (CD₃OD)



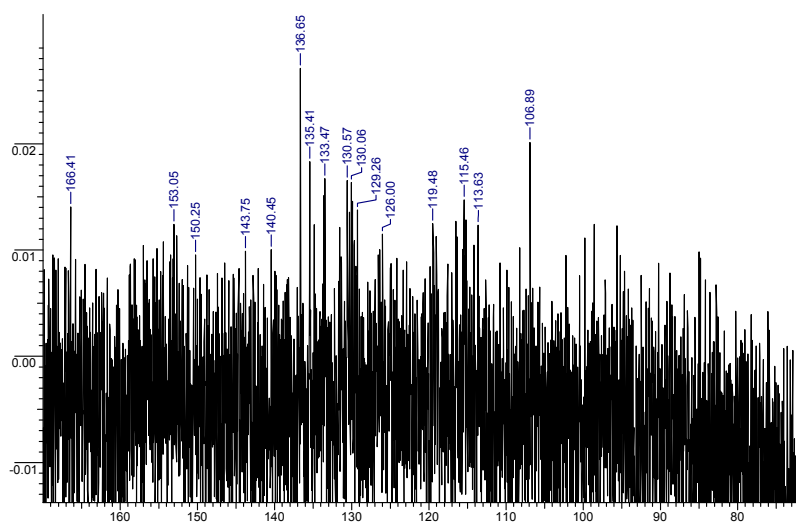


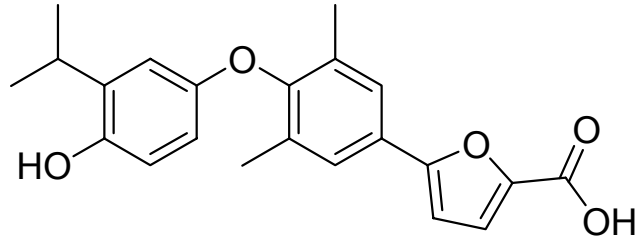
5-(4-(4-Hydroxy-3-isopropylphenoxy)-3,5-dimethylphenyl)thiophene-2-sulfonamide (CO9)

¹H NMR (CDCl₃)



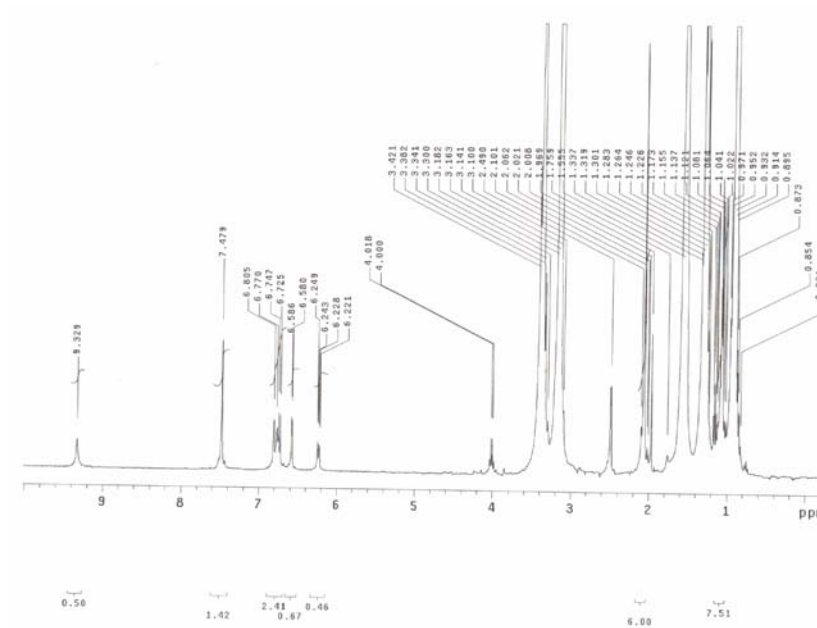
¹³C NMR (CD₃OD)



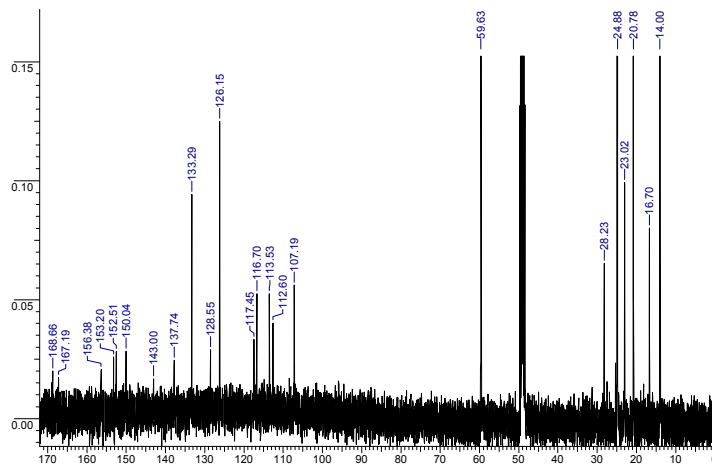


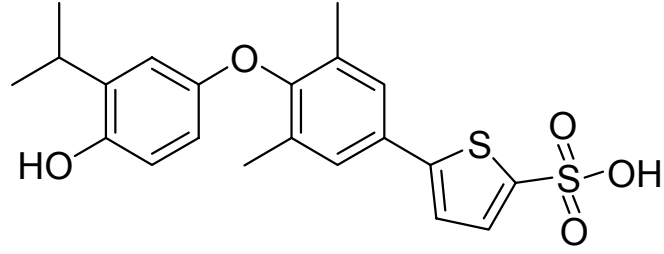
5-(4-(4-Hydroxy-3-isopropylphenoxy)-3,5-dimethylphenyl)furan-2-carboxylic acid (CO10)

¹H NMR (DMSO-d₆)



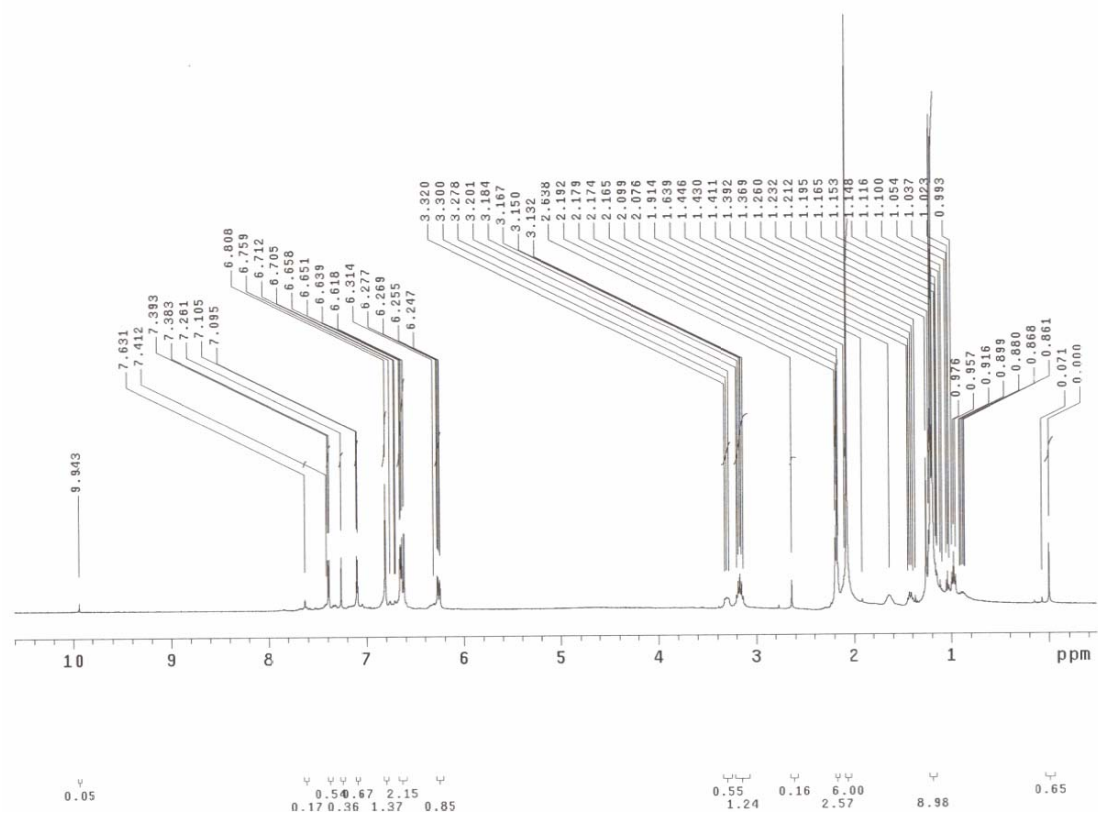
¹³C NMR (Acetone)

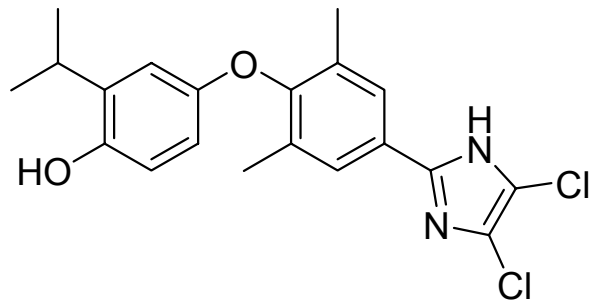




5-(4-(4-Hydroxy-3-isopropylphenoxy)-3,5-dimethylphenyl)thiophene-2-sulfonic acid (CO11)

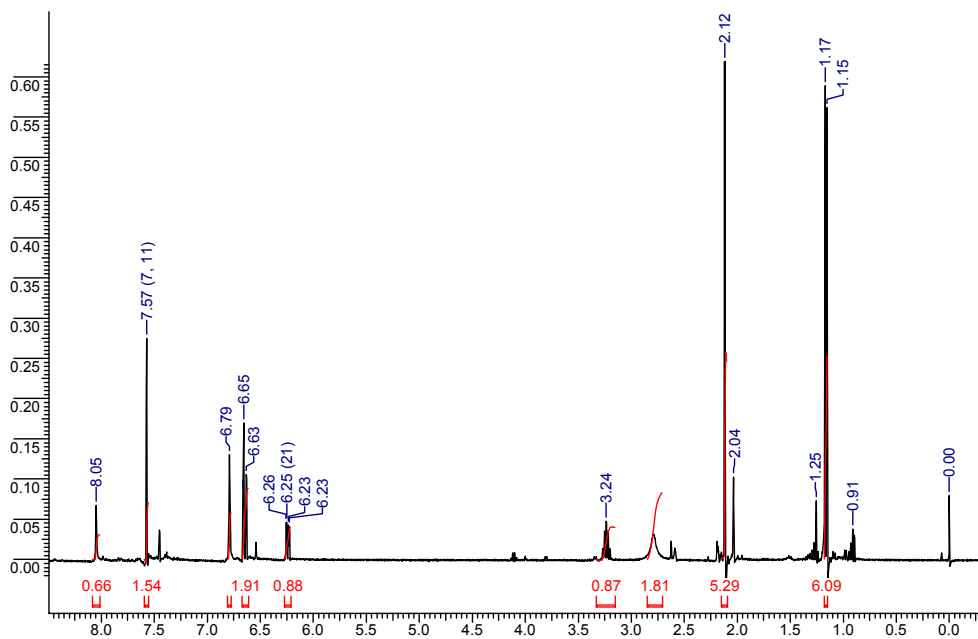
¹H NMR (CDCl₃)

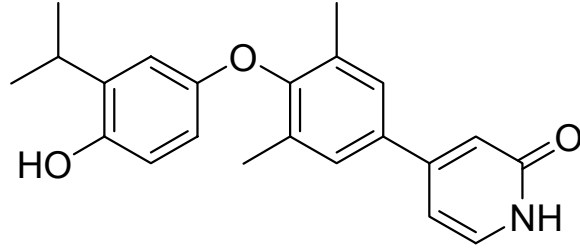




4-(4-(4,5-Dichloro-1*H*-imidazol-2-yl)-2,6-dimethylphenoxy)-2-isopropylphenol (CO12)

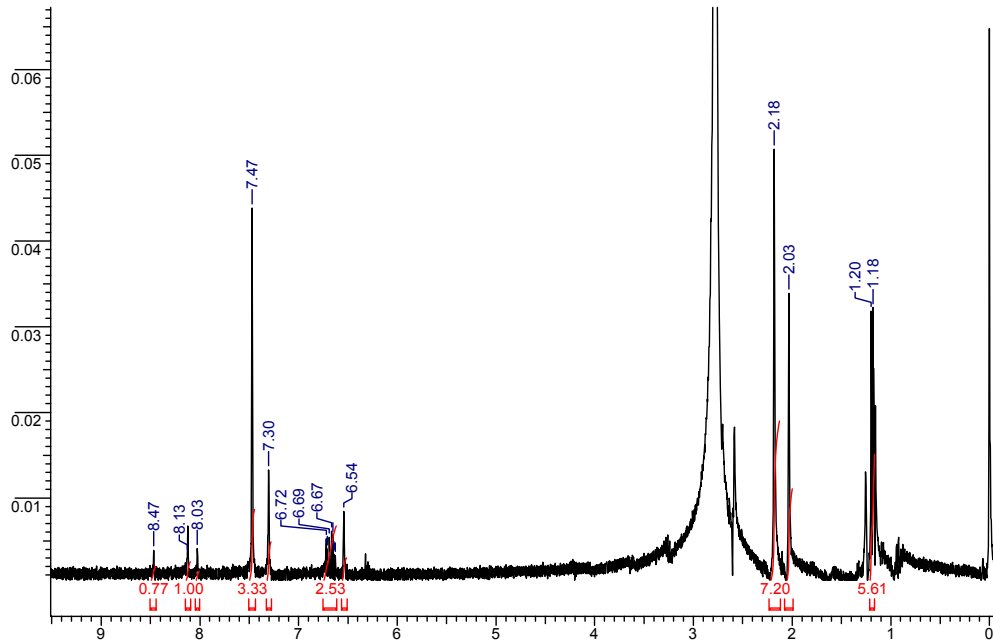
^1H NMR (DMSO- d_6)

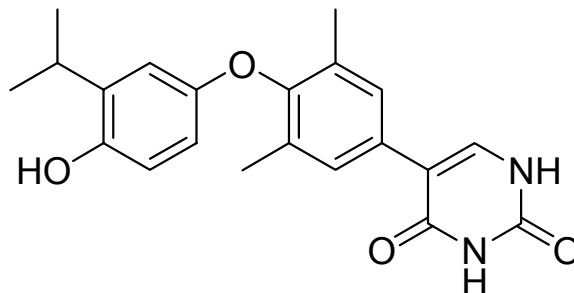




4-(4-(4-Hydroxy-3-isopropylphenoxy)-3,5-dimethylphenyl)pyridin-2(1H)-one (CO13)

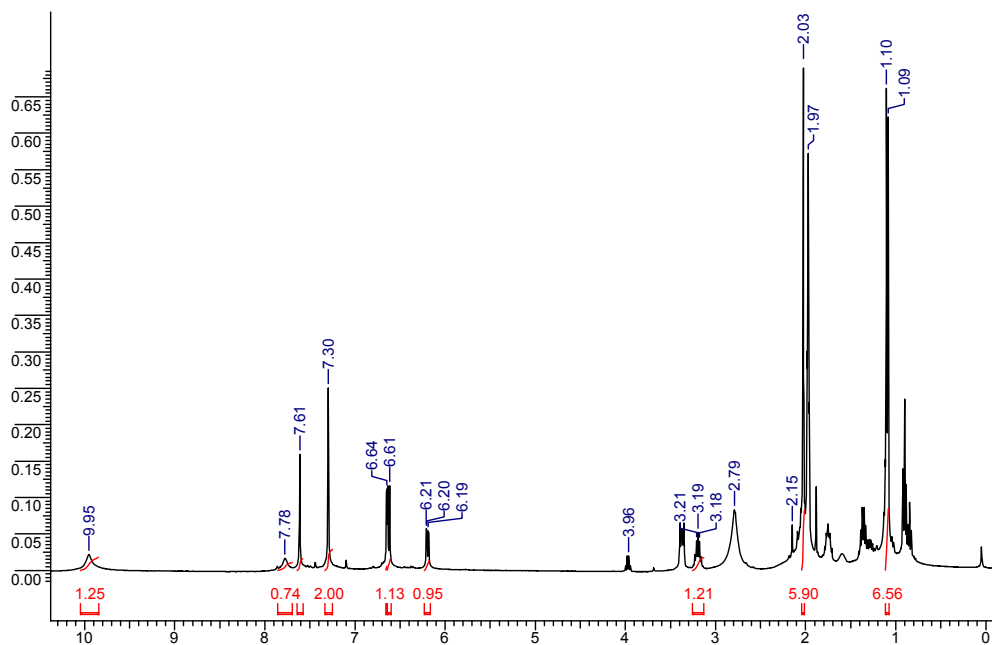
¹H NMR (DMSO-d₆)

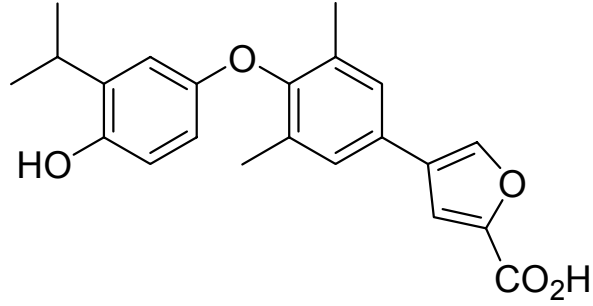




5-(4-(4-Hydroxy-3-isopropylphenoxy)-3,5-dimethylphenyl)pyrimidine-2,4(1H,3H)-dione (CO14)

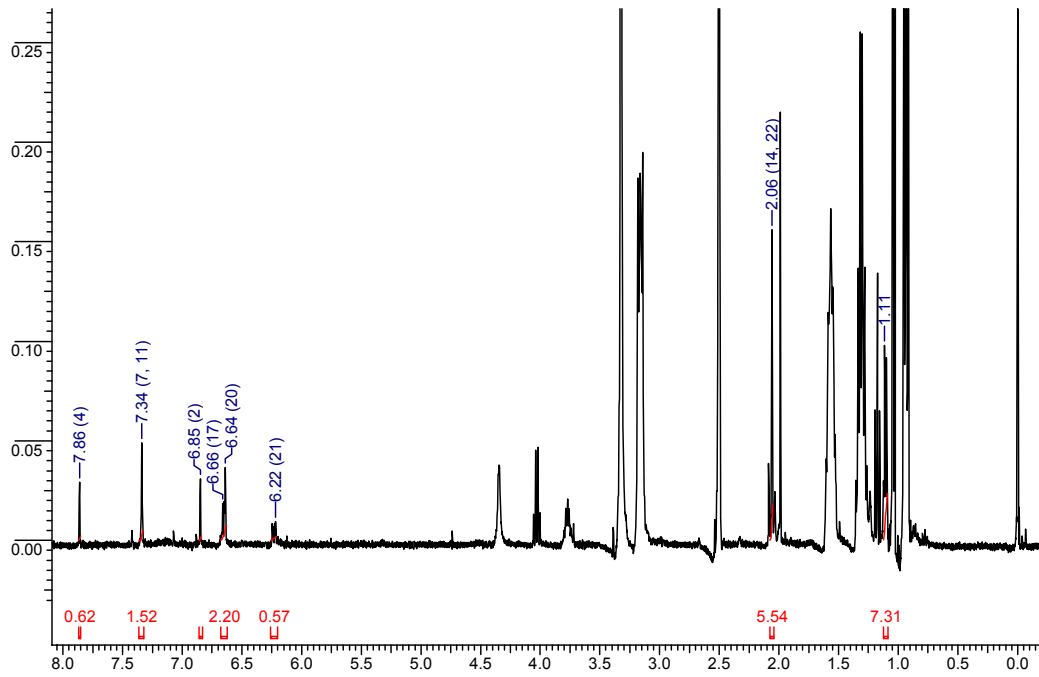
¹H NMR (Acetone)

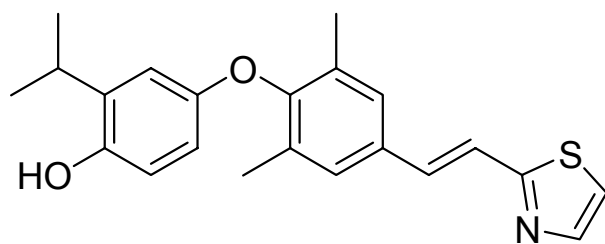




4-(4-(4-Hydroxy-3-isopropylphenoxy)-3,5-dimethylphenyl)furan-2-carboxylic acid (CO15)

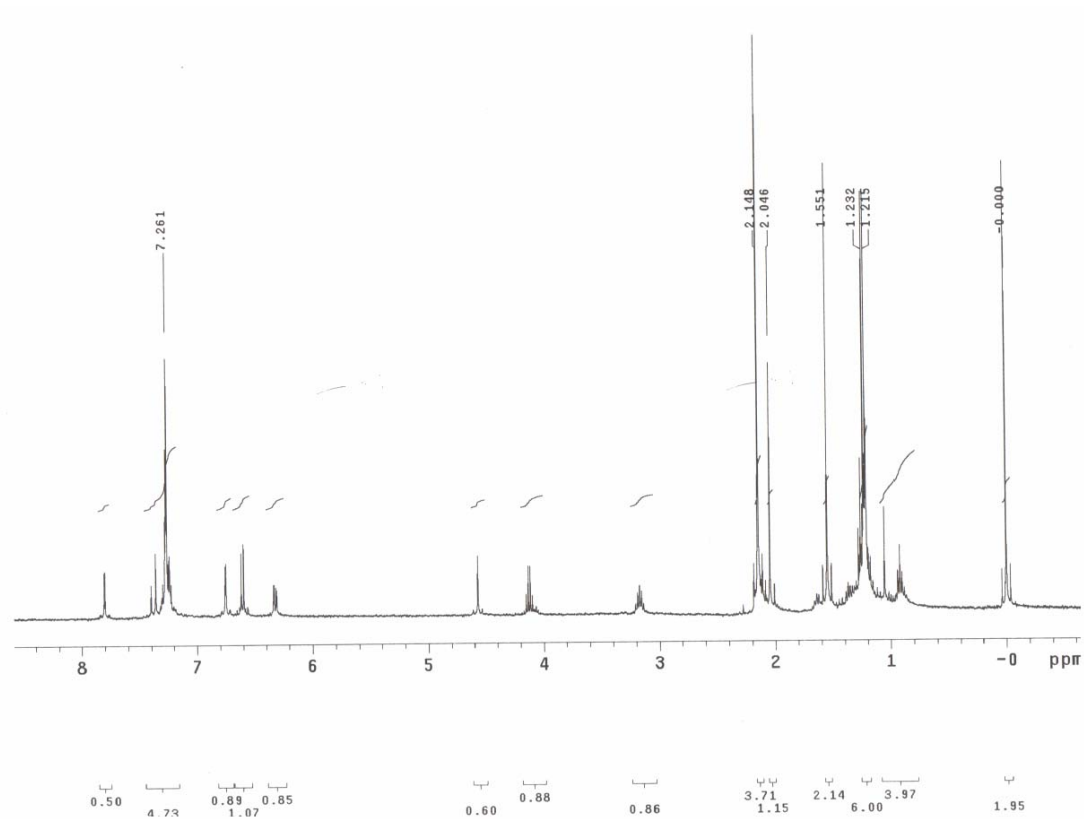
¹H NMR (DMSO-d₆)

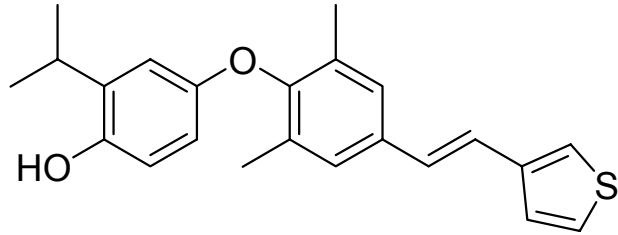




4-(2,6-Dimethyl-4-((*E*)-2-(thiazol-2-yl)vinyl)phenoxy)-2-isopropylphenol (CO16)

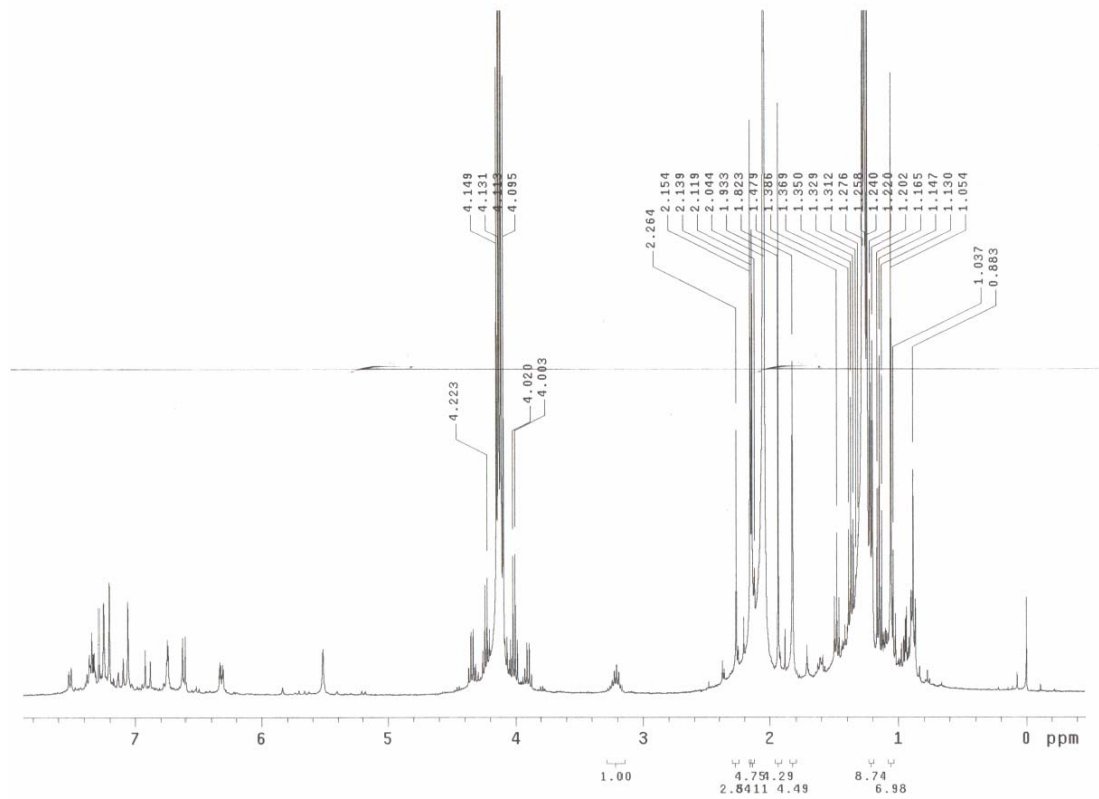
¹H NMR (CDCl₃)

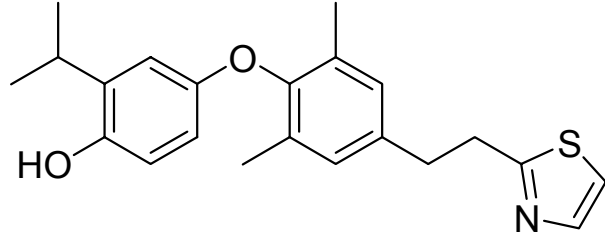




4-(2,6-dimethyl-4-((*E*)-2-(thiophen-3-yl)vinyl)phenoxy)-2-isopropylphenol (CO17)

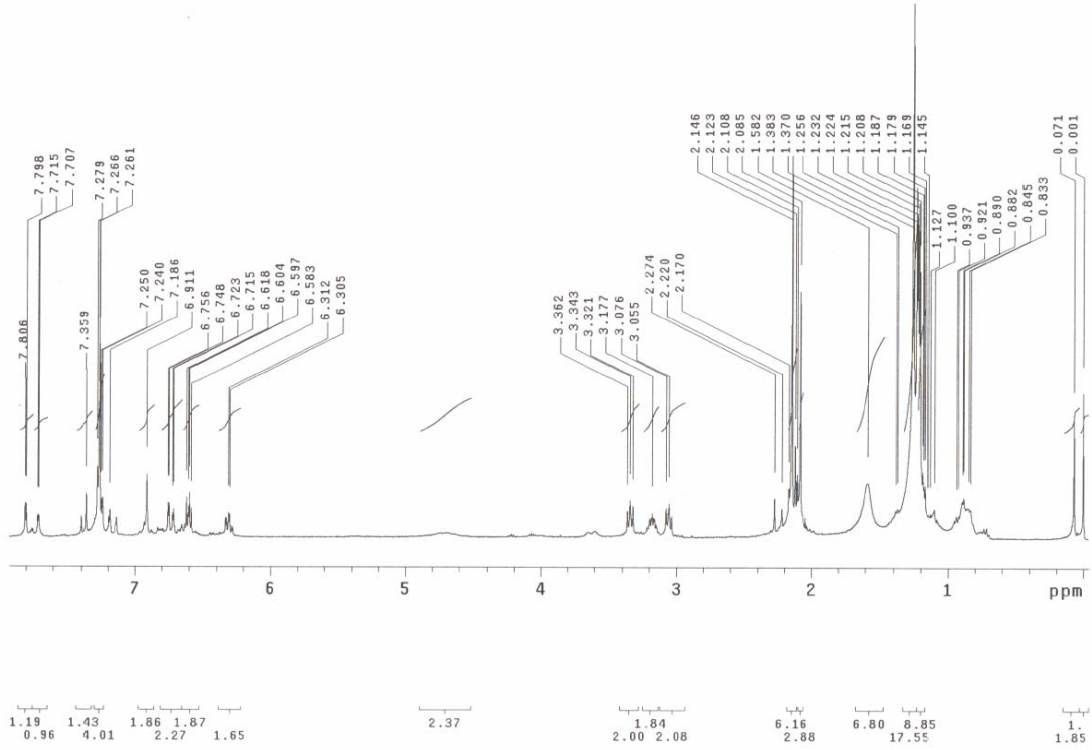
^1H NMR (CDCl_3)

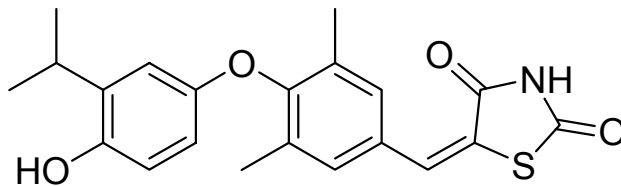




4-(2,6-Dimethyl-4-(2-(thiazol-2-yl)ethyl)phenoxy)-2-isopropylphenol (CO18)

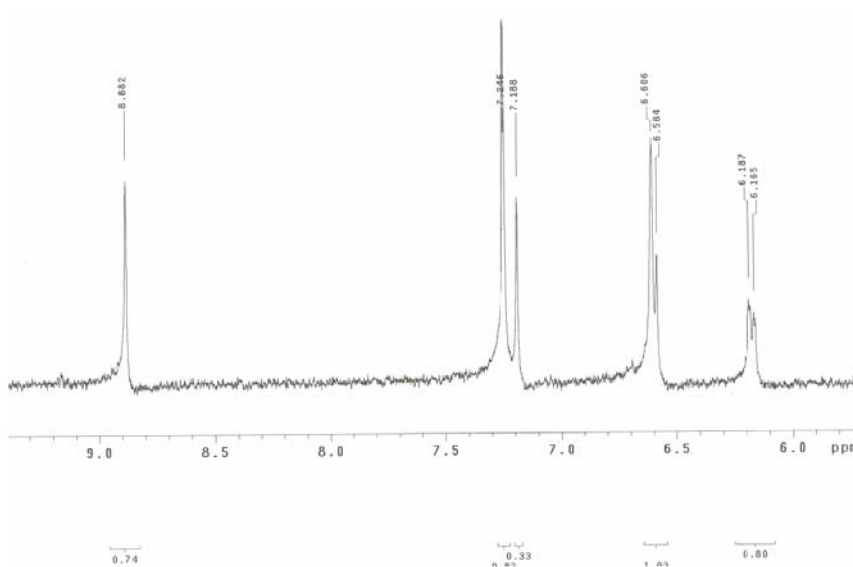
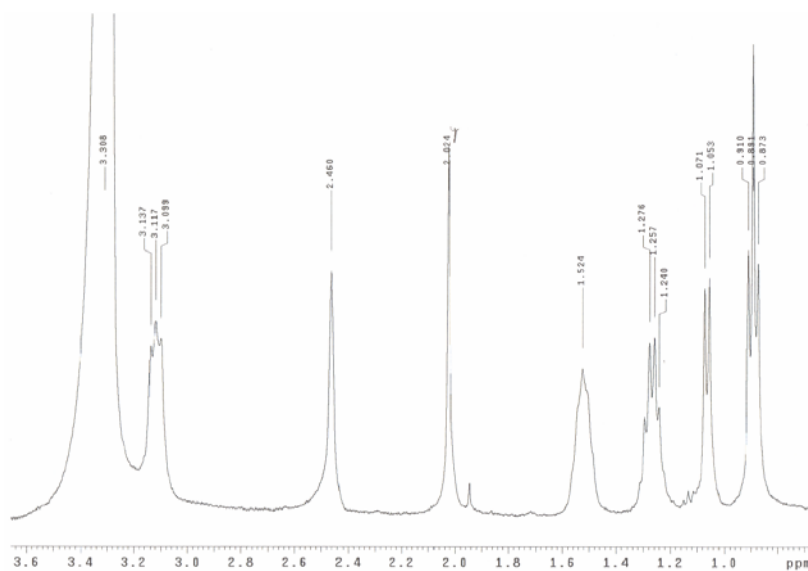
¹H NMR (CDCl₃)

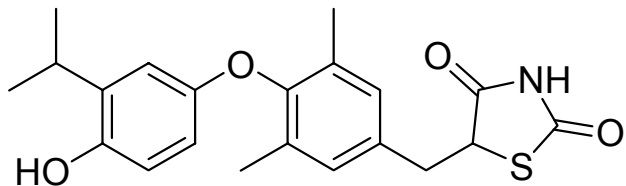




(Z)-5-(4-(4-hydroxy-3-isopropylphenoxy)-3,5-dimethylbenzylidene)thiazolidine-2,4-dione (CO19)

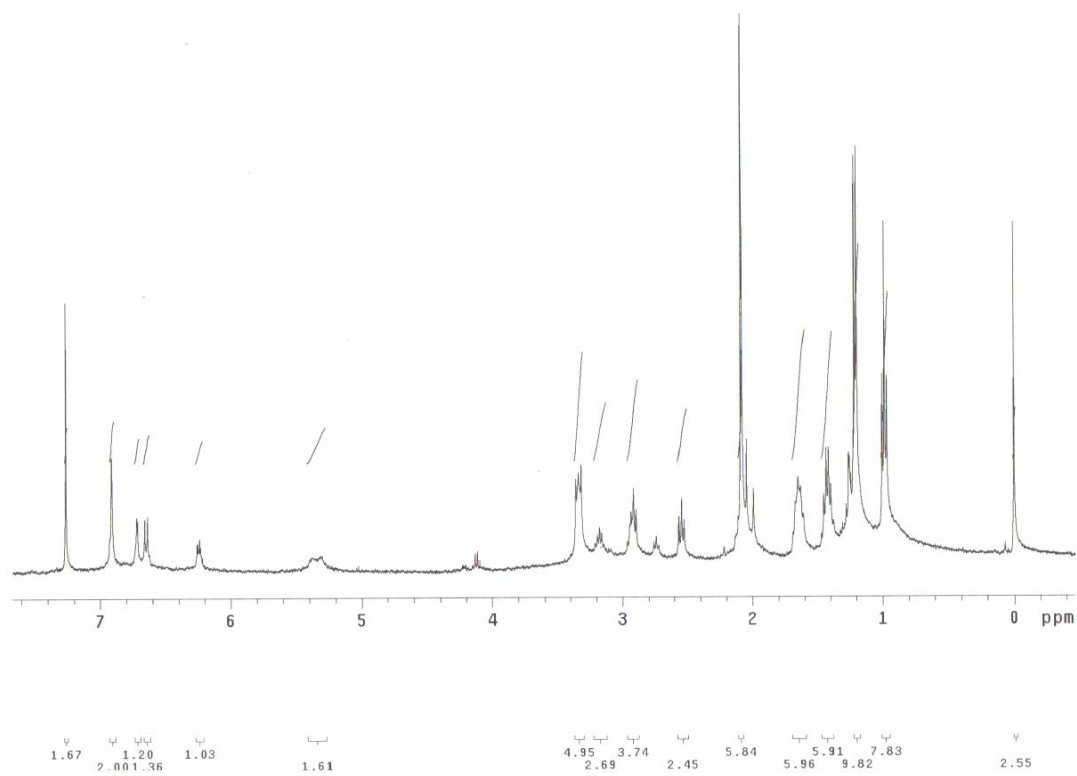
^1H NMR (DMSO- d_6)



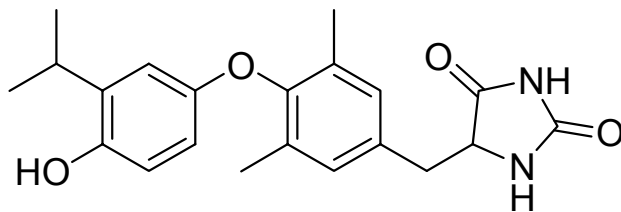


5-(4-(4-Hydroxy-3-isopropylphenoxy)-3,5-dimethylbenzyl)thiazolidine-2,4-dione (CO20)

¹H NMR (DMSO-d₆)

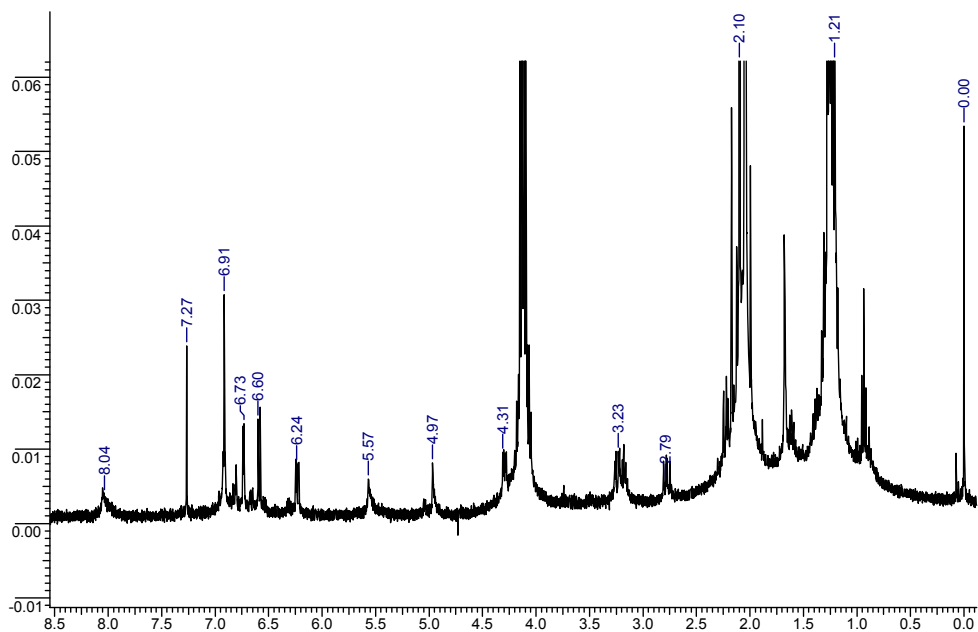


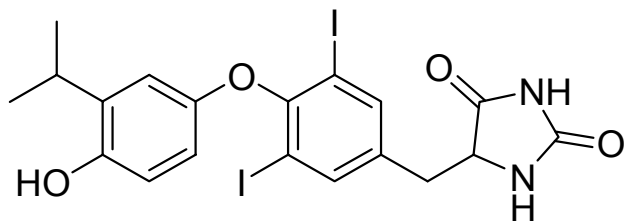
B.2 NMR Spectra of Compounds from Chapter 3



5-(4-(4-Hydroxy-3-isopropylphenoxy)-3,5-dimethylbenzyl)imidazolidine-2,4-dione (CO22)

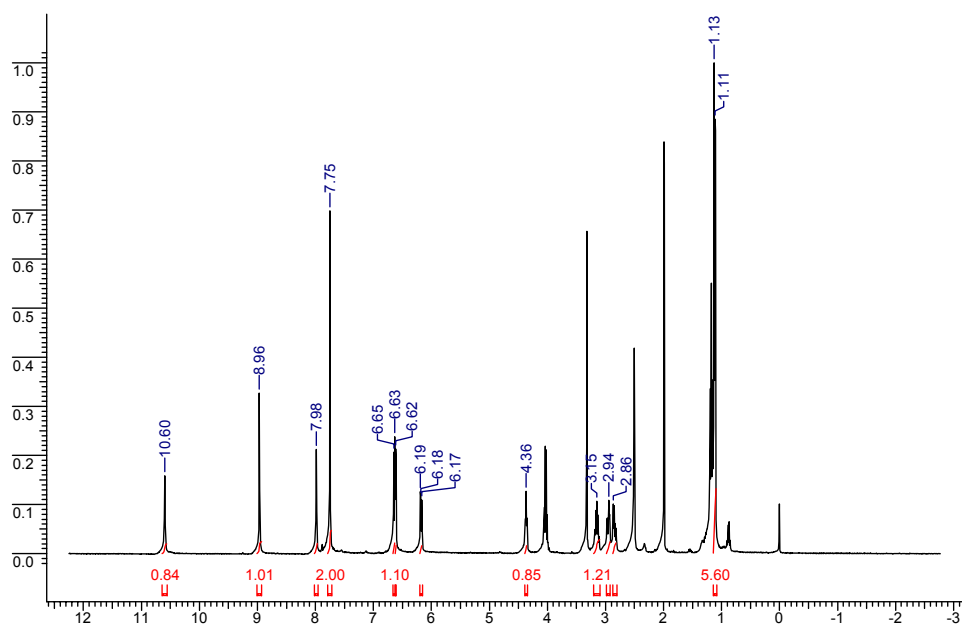
¹H NMR



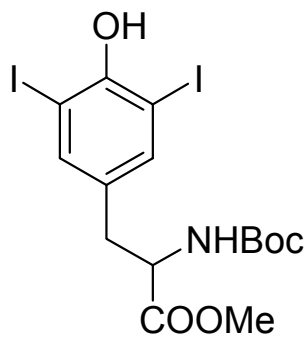


5-(4-(4-Hydroxy-3-isopropylphenoxy)-3,5-diiodobenzyl)imidazolidine-2,4-dione (CO23)

^1H NMR

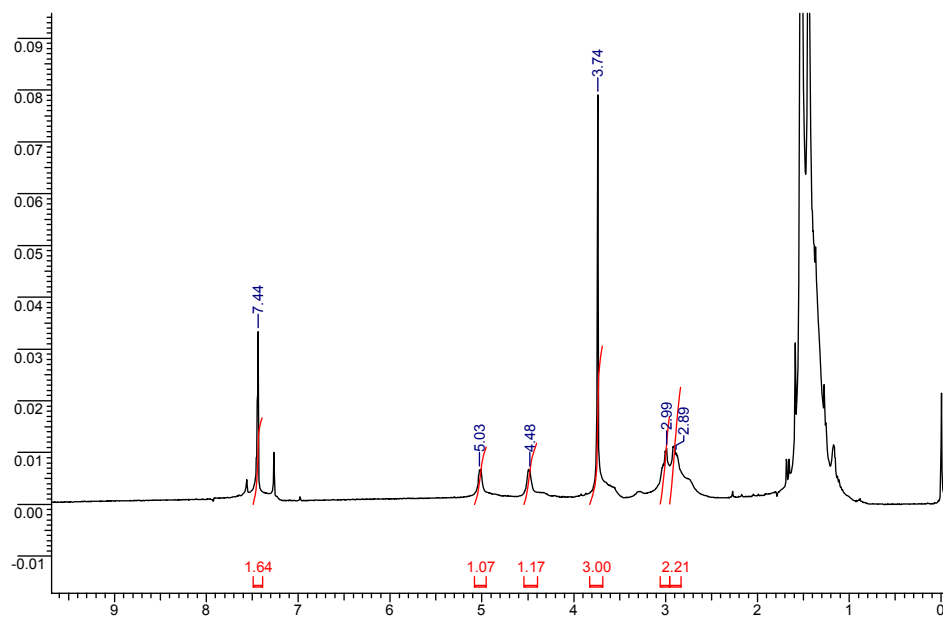


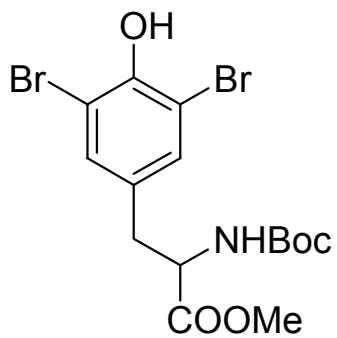
B.3 NMR Spectra of Compounds from Chapter 4



***tert*-Butyl 1-(methoxycarbonyl)-2-(4-hydroxy-3,5-diiodophenyl)ethylcarbamate (11a)**

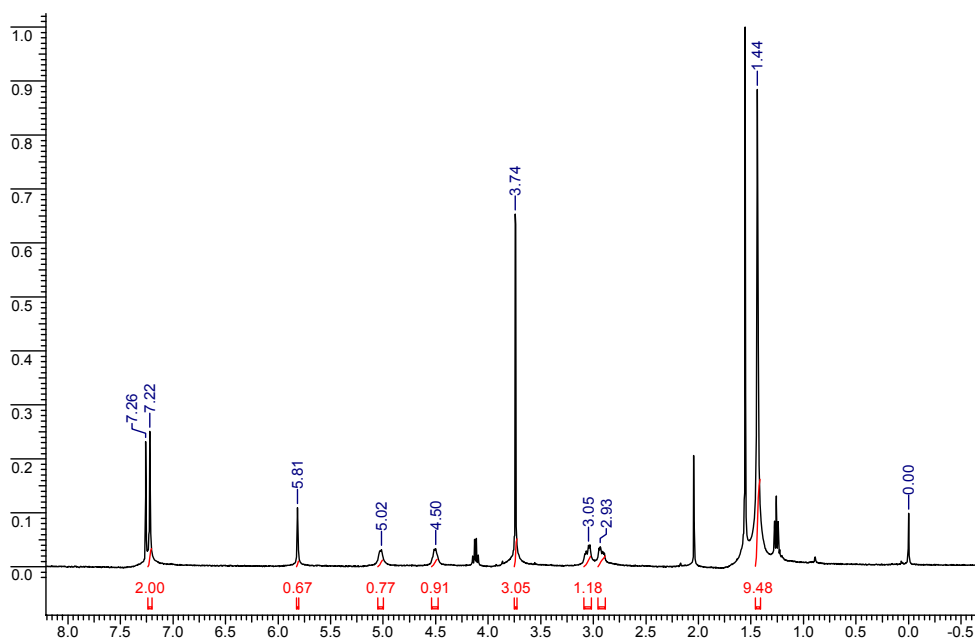
¹H NMR

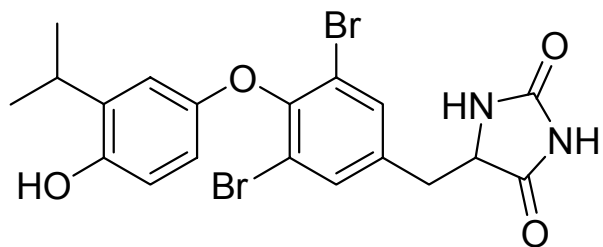




***tert*-Butyl 1-(methoxycarbonyl)-2-(3,5-dibromo-4-hydroxyphenyl)ethylcarbamate (11b)**

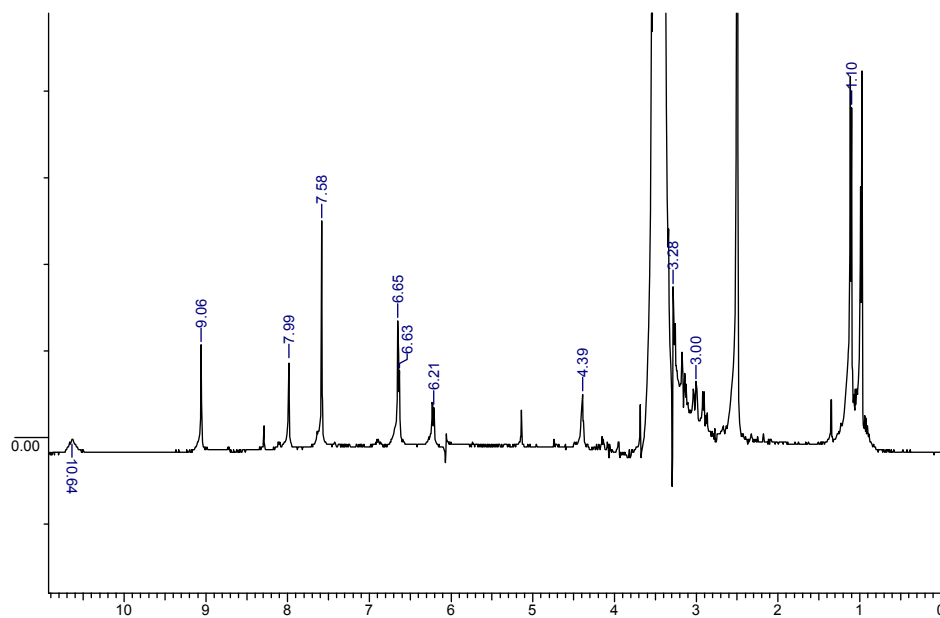
¹H NMR

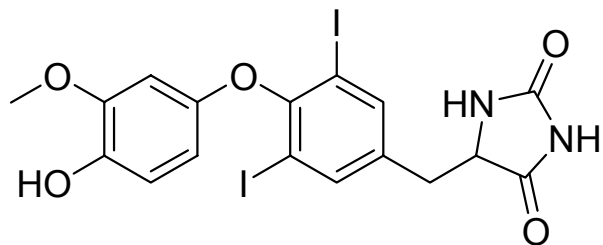




5-(4-(4-Hydroxy-3-isopropylphenoxy)-3,5-dibromobenzyl)imidazolidine-2,4-dione (CO24)

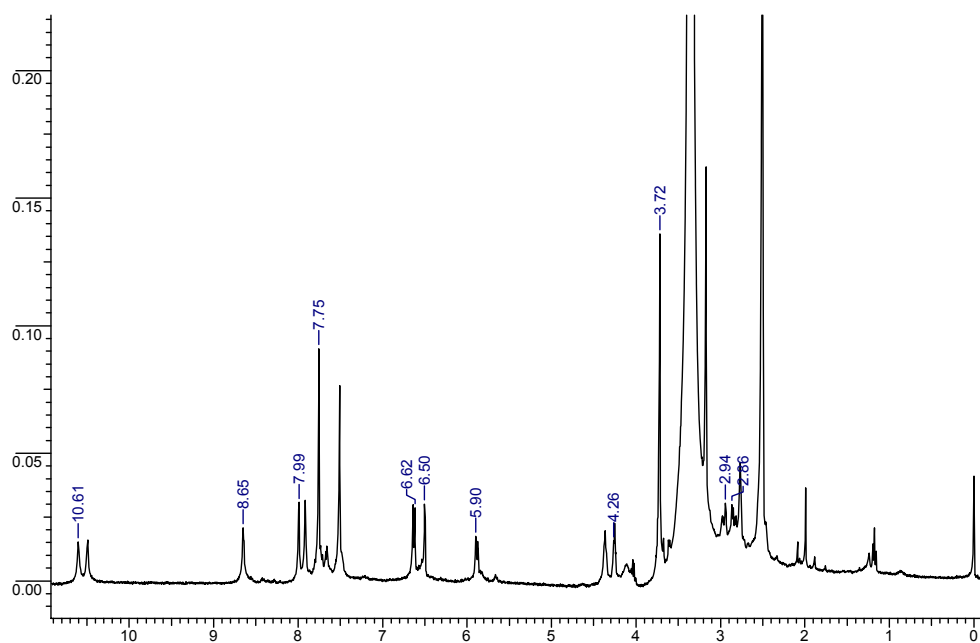
^1H NMR

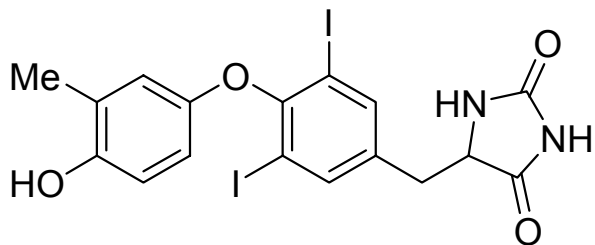




5-(4-(4-Hydroxy-3-methoxyphenoxy)-3,5-diiodobenzyl)imidazolidine-2,4-dione (CO26)

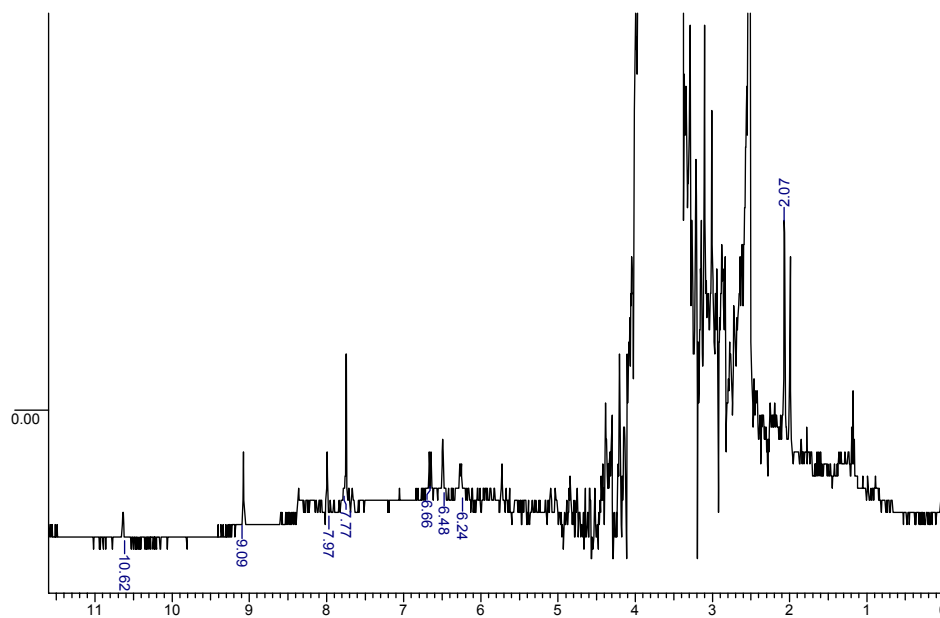
¹H NMR

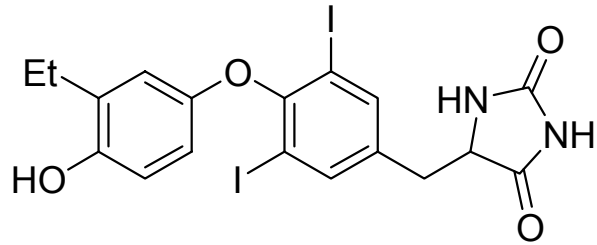




5-(4-(4-Hydroxy-3-methylphenoxy)-3,5-diiodobenzyl)imidazolidine-2,4-dione (CO27)

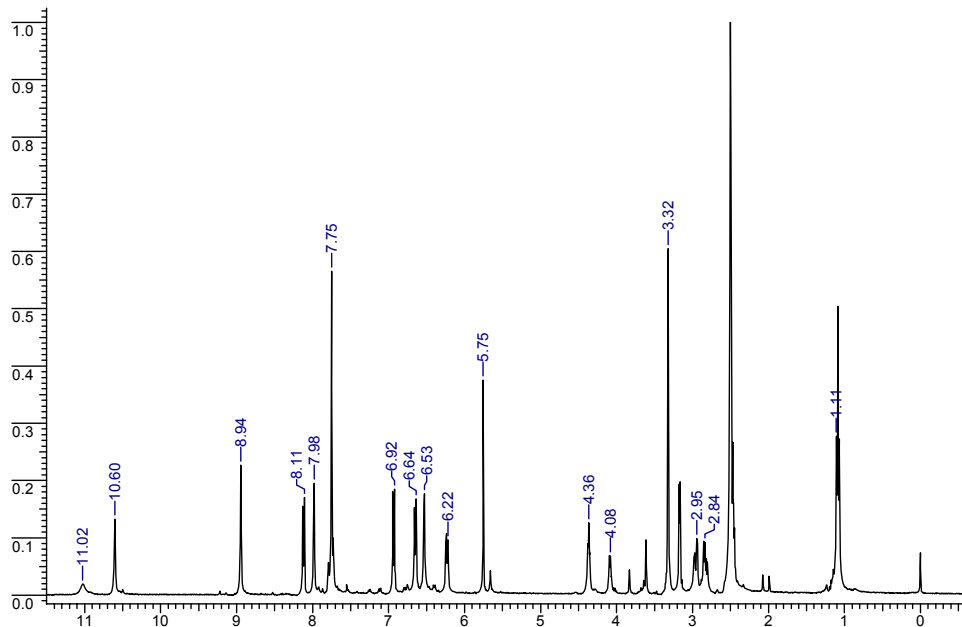
¹H NMR

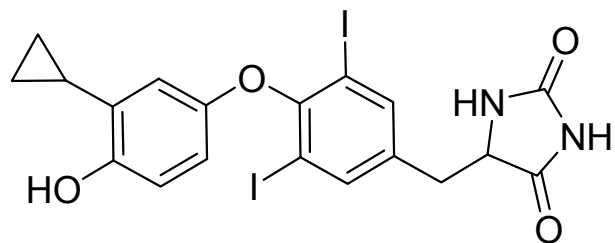




5-(4-(3-Ethyl-4-hydroxyphenoxy)-3,5-diiodobenzyl)imidazolidine-2,4-dione (CO28)

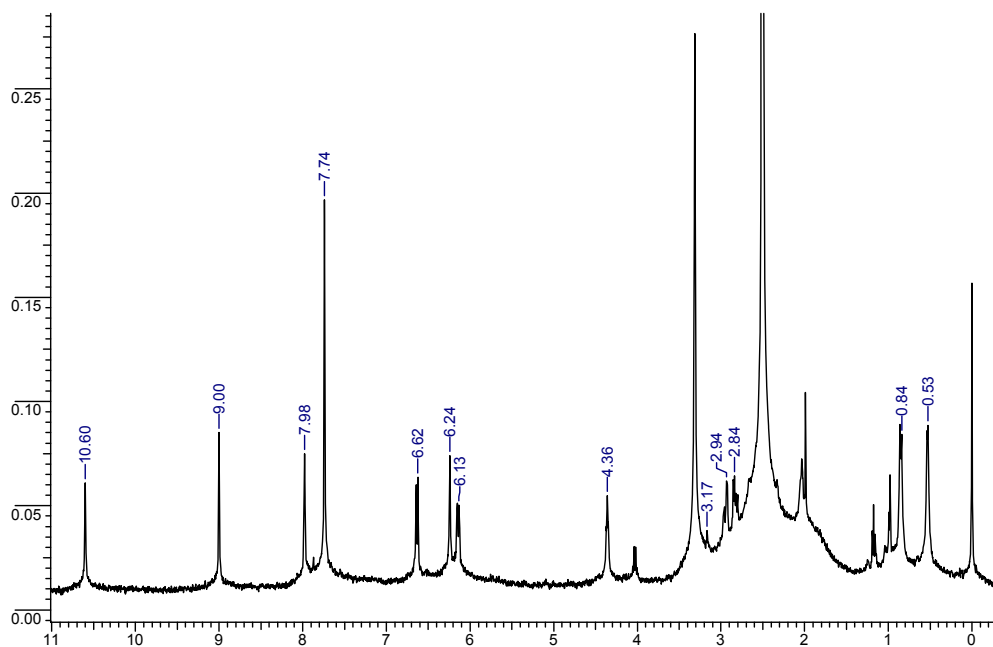
¹H NMR

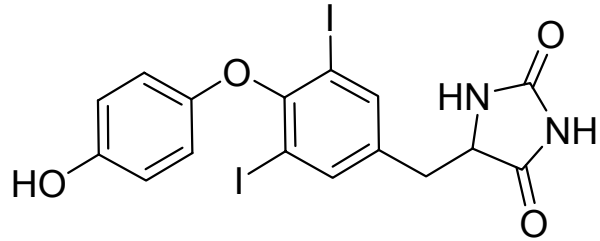




5-(4-(3-Cyclopropyl-4-hydroxyphenoxy)-3,5-diodobenzyl)imidazolidine-2,4-dione (CO29)

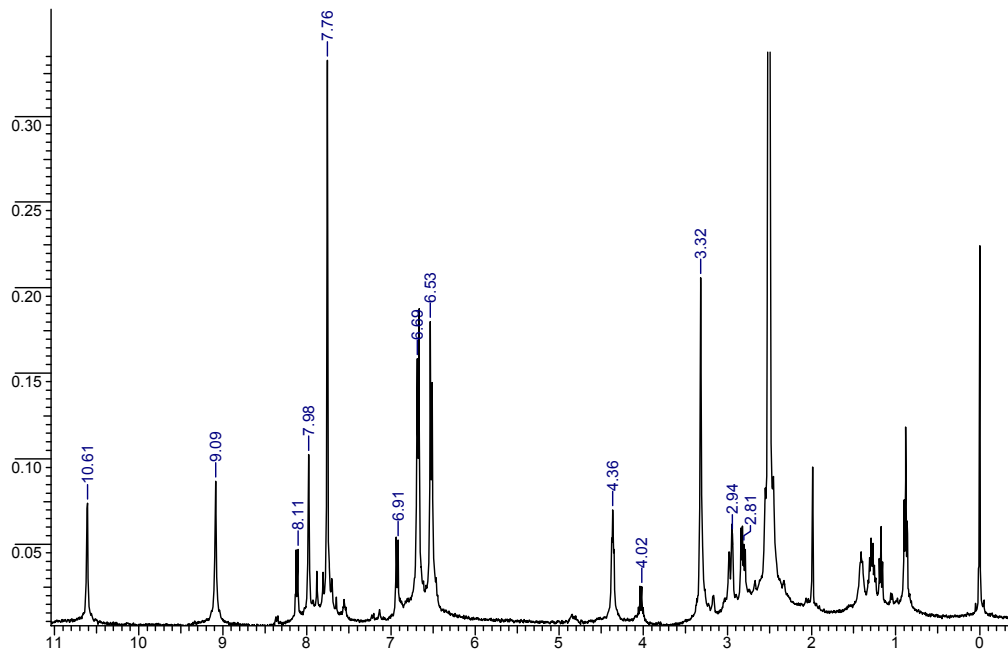
^1H NMR

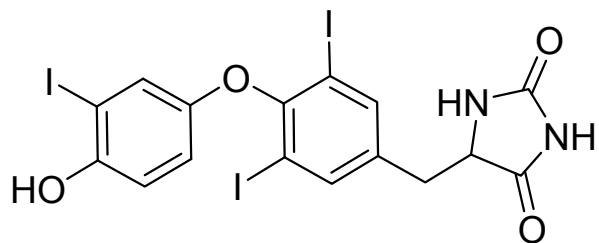




5-(4-(4-Hydroxyphenoxy)-3,5-diodobenzyl)imidazolidine-2,4-dione (CO30)

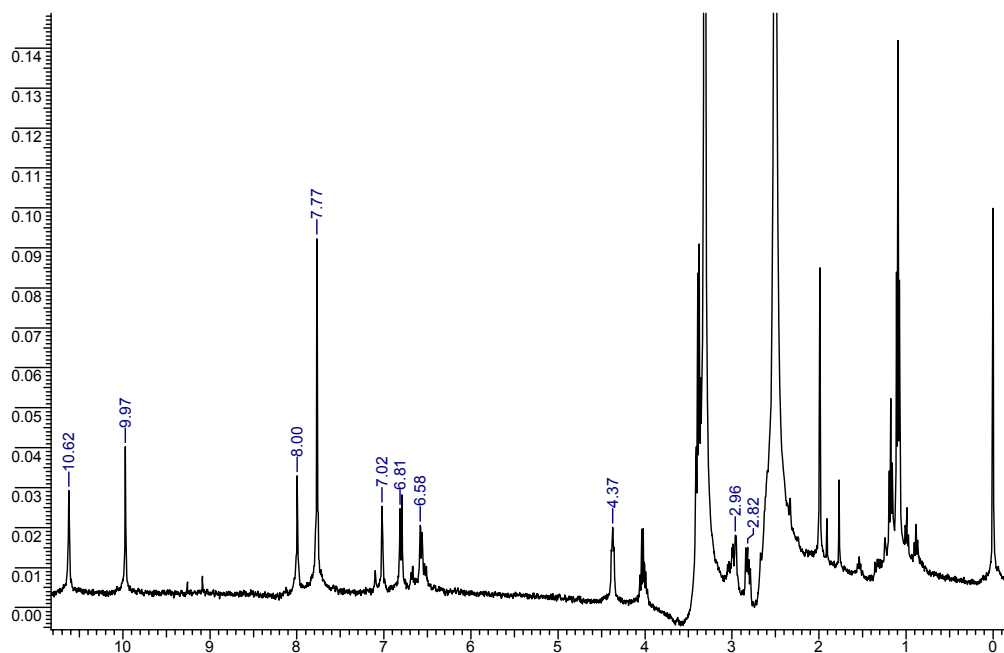
¹H NMR

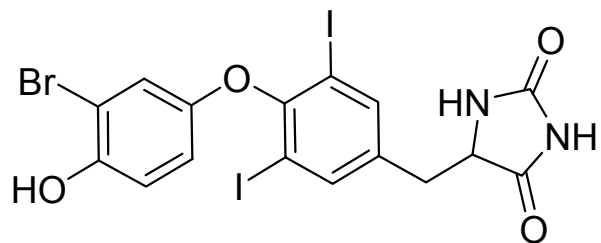




5-(4-(4-Hydroxy-3-iodophenoxy)-3,5-diodobenzyl)imidazolidine-2,4-dione (CO31)

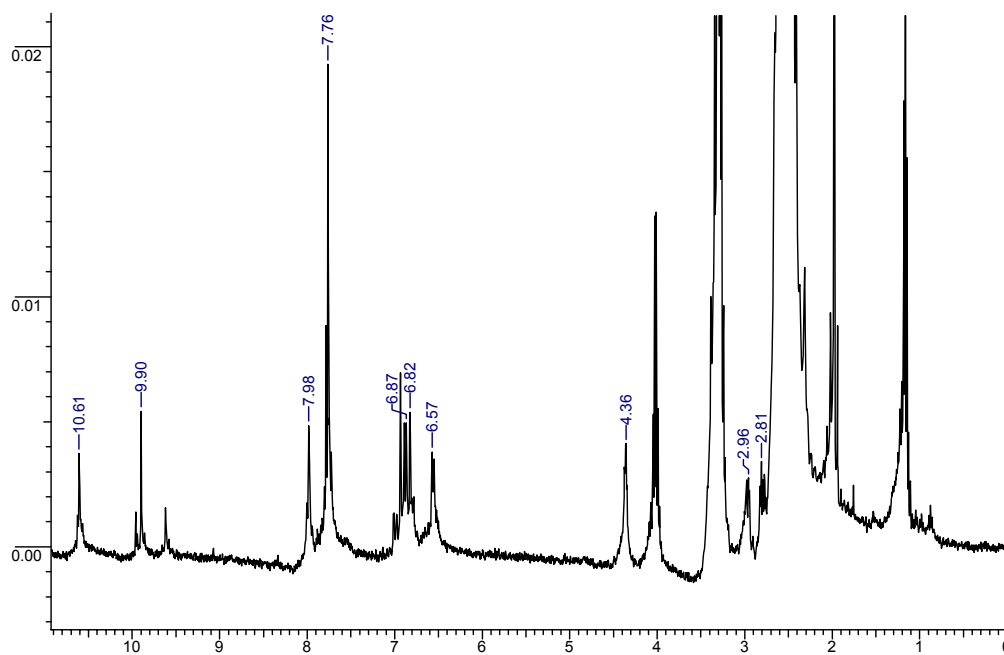
^1H NMR





5-(4-(3-Bromo-4-hydroxyphenoxy)-3,5-diodobenzyl)imidazolidine-2,4-dione (CO32)

^1H NMR



Publishing Agreement

It is the policy of the University to encourage the distribution of all theses and dissertations. Copies of all UCSF theses and dissertations will be routed to the library via the Graduate Division. The library will make all theses and dissertations accessible to the public and will preserve these to the best of their abilities, in perpetuity.

Please sign the following statement:

I hereby grant permission to the Graduate Division of the University of California, San Francisco to release copies of my thesis or dissertation to the Campus Library to provide access and preservation, in whole or in part, in perpetuity.

Cory A. Ocasio

Author Signature

July 20, 2007

Date